

Elucidating Mechanisms of Premature Ovarian Failure using a Transgenic Mouse Model

Heidy Kaune Galaz

Linacre College

Thesis submitted for the Degree of Doctor of Philosophy

University of Oxford

Trinity term

2015

To Agatha…

Conocer el amor de los que amamos es el fuego que alimenta la vida…

Knowing the love of the ones we love is the fire that fuels life…

Pablo Neruda

Acknowledgments

I thank my supervisor Dr Suzannah Williams for her support during the past few years. Thank you for believing in me and for giving me the opportunity to join your group.

I would also like to thank my fellow group members:

- Panayiota Ploutarchou and Sairah Sheikh, thank you for your friendship and for being so generous and kind.

- Dr Patricia Grasa and Anna Deleva, we have not only walked together the path towards elucidating the mysteries of science, but we have also followed the most important and beautiful trail of our lives, our route to motherhood.

I would also like to thank my parents for their unconditional support.

Finally, I thank my family: my beloved husband Dr Juan Montiel and my sweet daughter Agatha Montiel Kaune. Juan, without your help and support this dream would not have come true. Agatha, you made everything more challenging but in the most beautiful and delicious way. I love you both; you are the most important beings in my life.

Abstract

Premature ovarian failure (POF) is a condition that affects around 1% of women of reproductive age. It is idiopathic in 74-90% of cases and the mechanisms involved remain unclear. Several mouse models of POF have been described, however new models are necessary to understand the aetiology of POF and to hopefully identify candidate molecules that can be used as targets for intervention. A mouse model of POF (DM) occurs from oocyte-specific deletion of two glycosyltransferases encoded by *C1galt1* and *Mgat1*, thus oocytes lack core 1-derived *O*-glycans and complex *N*-glycans. DM females have POF by 3 months of age exhibiting follicle depletion, elevated gonadotropins and decreased sex steroids. Female mice are fertile prior to ovarian failure producing a single small litter and thus, the DM model provides an outstanding opportunity to explore the onset of POF. In addition, since ablation of these glycans occurs only in the oocyte generates a progressive ovarian failure and POF, this model provides a unique opportunity to further our understanding of the role of the oocyte in the regulation of ovarian function and fertility. In this thesis, the influence of the abnormal endocrine environment was discarded as the origin of the altered follicle development in DM. *In vitro* and *in vivo* analysis of follicle development using follicle culture and the reaggregated chimeric ovary technique has highlighted intra-ovarian factors as responsible for the onset of POF in DM females. Finally, ovary transcriptomic analysis revealed an accumulation of changes in gene expression with age consistent with the DM phenotype. These results have highlighted potential therapies as well as genes and pathways as candidate molecules to try to reverse POF in the DM mouse model.

Table of Contents

ACKNOWLEDGMENTS **3**

ABSTRACT **4**

CHAPTER 1: INTRODUCTION **12**

1.1 Ovarian function **13**

1.1.1 Follicle development 13

1.1.2 The role of the oocyte in ovarian function 17

1.2 Premature ovarian failure **20**

1.2.1 Overview 20

1.2.2 Clinical presentation 21

1.2.3 Causes 23

1.2.4 Genetically modified animal models for POF 27

1.3 Double mutant mouse model **31**

1.3.1 *N*-glycans 31

1.3.2 *O*-glycans 34

1.3.3 Molecular basis of the double mutant phenotype 36

1.3.4 DM phenotype 38

CHAPTER 2: MATERIAL AND METHODS **43**

2.1 Double mutant mice **44**

2.2 Genotyping **44**

2.2.1 Ear genomic DNA extraction 44

2.2.2 Polymerase chain reaction (PCR) 45

2.2.3 Analysis of PCR products 47

2.3 Histological processing 47

2.3.1 Embedding 47

2.3.2 Sectioning 48

2.3.3 Hematoxylin-eosin staining 48

CHAPTER 3: FERTILITY ASSESSMENT OF DM FEMALES REVEALS A DELAYED PREIMPLANTATION DEVELOPMENT *IN VIVO* 50

3.1 Introduction 51

3.2 Aims 52

3.3 Material and methods 53

3.3.1 Mice 53

3.3.2 Mating 53

3.3.3 Ovulation rate and Oocyte/zygote collection 54

3.3.4 *In vivo* preimplantation embryo development 54

3.3.5 *In vitro* embryo development 54

3.3.6 Implantation analysis 55

3.3.7 Post implantation analysis 55

3.3.8 Statistical analysis 56

3.4 Results 57

3.4.1 Ovulation rate at 6-weeks is normal in DM females 57

3.4.2 Fertilisation rate is not affected in DM females 58

3.4.3 *In* vitro preimplantation embryo development is normal in DM females 60

3.4.4 In vivo preimplantation embryo development is altered in DM females 62

3.4.5 Implantation is delayed in DM females 64

3.4.6 Postimplantation embryo development progressed normally in DM females 65

3.5 Discussion 66

CHAPTER 4: A NORMAL ENDOCRINE ENVIRONMENT IS NOT ABLE TO SUPPORT FOLLICLE DEVELOPMENT AFTER THE ONSET OF POF IN THE DM MOUSE ASSESSED USING OVARIAN TRANSPLANTATION 71

4.1 Introduction 72

4.2 Aims 76

4.3 Materials and methods 77

4.3.1 Ovary transplantation under the kidney capsule 77

4.3.2 Assessment of follicle development 79

4.3.3 Area measurement and follicular density 81

4.3.4 Statistical analysis 81

4.4 Results 82

4.4.1 Establishment of the technique: C57BL/6 females and Control non-sibling females are unable to support growth of the grafted tissue 82

4.4.2 Morphology of the grafted tissues 4 weeks after transplantation 86

4.4.3 Follicle counts revealed the absence of developing follicles after transplantation in DM explants 89

4.4.4 Primary follicle arrest in the DM transplanted tissue cannot be overcome in the presence of a normal endocrine environment 91

4.4.5 Follicle numbers 4 weeks after the transplantation have the same profile as the 9-week ovarian tissue 93

4.5 Discussion **95**

CHAPTER 5: EVALUATION OF DM FOLLICLE GROWTH *IN VITRO* **99**

5.1 Introduction **100**

5.2 Aims **102**

5.3 Material and methods **103**

5.3.1 Mice 103

5.3.2 Follicle culture 103

5.3.3 Morphology assessment 104

5.3.4 Statistical analysis 105

5.4 Results **106**

5.4.1 Standardisation – Human recombinant FSH (h-rFSH) activity 106

5.4.2 DM Follicles have a decreased survival rate *in vitro* 107

5.4.3 DM follicles that survive the end of follicle culture reach the same size as Control follicles. 109

5.4.4 *In vitro* antrum development of DM follicles is different from Controls 111

5.5 Discussion **112**

CHAPTER 6: ASSESSING THE ROLE OF THE OOCYTE AND SOMATIC CELLS IN DM FOLLICLE DEVELOPMENT USING REAGGREGATED CHIMERIC OVARIES **115**

6.1 Introduction **116**

6.2 Aims **119**

6.3 Material and Methods **120**

6.3.1 Mice 120

6.3.2 X-gal staining for genotyping 122

6.3.3 Preparation of reaggregated chimeric pellets 123

6.3.4 Transplant of reaggregated chimeric pellets under the kidney capsule 127

6.3.5 Assessment of cell separation and efficiency of the exchange of germ-somatic cells to produce reaggregated chimeric pellets 128

6.3.6 Histological processing 129

6.4 Results 132

6.4.1 Validation of the reaggregated chimeric pellet technique 132

6.4.2 Total follicle counts: 3- and 9-week DM germ cells are able to generate follicles in a reaggregated chimeric ovary 134

6.5 Discussion 140

CHAPTER 7: OVARIAN DM TRANSCRIPTOMIC PROFILE USING MICROARRAY ANALYSIS BEFORE, DURING AND AFTER THE ONSET OF POF 143

7.1 Introduction 144

7.2 Aims 146

7.3 Material and Methods 147

7.3.1 Sample collection 147

7.3.2 RNA extraction 148

7.3.3 Integrity assessment of RNA 149

7.3.4 Microarrays 150

7.3.5 Microarray data analysis 150

7.4 Results 159

7.4.1 RNA extraction and integrity 159

7.4.2 Microarray analysis 160

7.5 Discussion **185**

CHAPTER 8: CONCLUSIONS **195**

REFERENCES **200**

APPENDIX A: ARTICLES PUBLISHED **221**

Article 1: Embryos generated from oocytes lacking complex *N*- and *O*-glycans have compromised development and implantation **222**

Article 2: Oocyte-derived Smad4 is not required for development of the oocyte or the preimplantation embryo **233**

APPENDIX B: DIFFERENTIALLY EXPRESSED GENES IN 9-WEEK DM OVARIES **241**

APPENDIX C: FUNCTIONAL ANNOTATION CLUSTER FOR 9-WEEK UP-REGULATED GENES **288**

APPENDIX D: FUNCTIONAL ANNOTATION CLUSTER FOR 9-WEEK DOWN-REGULATED GENES **301**

Chapter 1: Introduction

1.1 Ovarian function

1.1.1 Follicle development

The ovarian follicles are the functional units of the ovary and determine ovarian function and fertility. A follicle is constituted of a central oocyte surrounded by layers of somatic cells, granulosa and theca cells. Normal follicle development relies on complex endocrine, paracrine and autocrine mechanisms that mediate the interaction between the oocyte and the somatic cells allowing normal follicle growth.

Primordial follicles are formed by immature oocytes, arrested at the diplotene stage (dictyate) of prophase I of meiosis, each surrounded by a single layer of squamous granulosa cells externally limited by the basal lamina. Primordial follicles constitute the resting pool of follicles in the ovary and remain inactive until follicles are recruited and begin to grow. In rodents, oocytes initiate meiosis at the end of foetal life and follicle growth is first observed early in the post-natal period (*1*). The initiation of follicle growth is characterized by oocyte growth and activation of granulosa cells from flattened squamous cells to cuboidal cells. In this way, primordial follicles develop to primary follicles, formed by the growing oocyte surrounded by 1 layer of cuboidal granulosa cells. Shortly after the initiation of follicular growth, the zona pellucida (ZP) is secreted by the oocyte into the periviteline space from the primary stage of follicle development onwards(*2*). In the mouse, the zona pellucida (ZP) is composed by three highly glycosylated proteins designated ZP1, ZP2 and ZP3, which associate with each other to form

long filaments of ZP2-ZP3 dimers cross-linked by ZP1 dimers (*3*). The ZP has many important functions such as, providing a protective coating for the oocyte, facilitating the passage of molecules towards and from the oocyte, participating as an essential modulator during fertilization and supporting preimplantation embryo development (*3-5*). In this way, ZP generation is one of the most important changes that occur during follicle development. Primary follicles become secondary follicles with 2 or more layers of granulosa cells surrounding the oocyte. A complex network of blood vessels also formed outside the basal lamina, which determine exposure of the follicle to systemic circulating factors (*6*). At this stage some stromal cells outside the basal lamina are recruited to form the theca cell layer. As the follicle enlarges, the theca differentiates into two lineages: the theca externa and the theca interna. Morphologically, the theca externa cells do not differ from outer somatic cells, meanwhile the theca interna cells display morphological and physiological features typical of steroid secreting-cells (*7*). When the theca interna is well formed, the secondary follicle becomes known as a preantral follicle. It has been established that follicles are unresponsive to gonadotropins when they initiate growth, however gonadotropins are critical to complete follicle development (*8*). FSH receptors (FSHR) are absent in primordial follicles whereas they are detectable from the primary stage of follicle development, with expression increasing at the preantral stage (*9-12*). Combined action of FSH and LH is fundamental to ensure follicle development. LH stimulates theca cells to produce androgens, which are aromatized in granulosa cells under

FSH stimuli. This is known as the two-cell two-gonadotropin hypothesis for ovarian estrogen synthesis (*13*) (Figure 1.1).

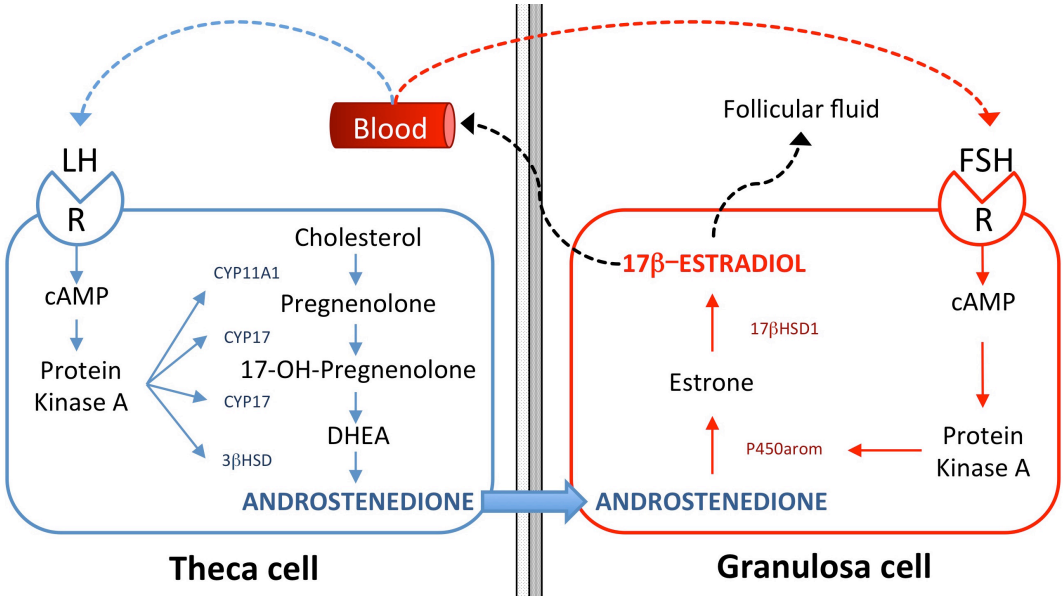


Figure 1.1: Two-cell two-gonadotropin hypothesis for the ovarian estrogen synthesis. Androstenedione produced in theca cells under LH stimuli is transported to the granulosa cells. Under FSH induction, granulosa cells transform androstenedione into 17β-estradiol. Modified from Craig, 2011 (*14*).

As follicle development progresses, follicular fluid is produced by the follicle and contained in the antral cavity, a distinctive feature of antral follicles. As the antral cavity enlarges, the granulosa cells begin to differentiate according to their location inside the follicle. The population of cells in direct contact with the oocyte becomes the cumulus oophorus and the granulosa cells surrounding the

antrum and in contact with the basal lamina become the mural granulosa cells. The cumulus oophorus and the oocyte form the cumulus-oocyte complex that will be ovulated. In mouse follicle development from primary stage to ovulation takes approximately 19 days (*15*).

A classification for mouse follicles has been used since 1968 (*16*). This classification comprises 10 categories of follicles based on the number of granulosa cells surrounding a central section of an oocyte. In this regard, type 1 and 2 follicles constitute primordial follicles, type 3a and 3b are primary follicles, type 4 are secondary, type 5a and 5b are preantral and type 6, 7 and 8 comprise antral follicles (Figure 1.2). This classification will be use in this thesis.

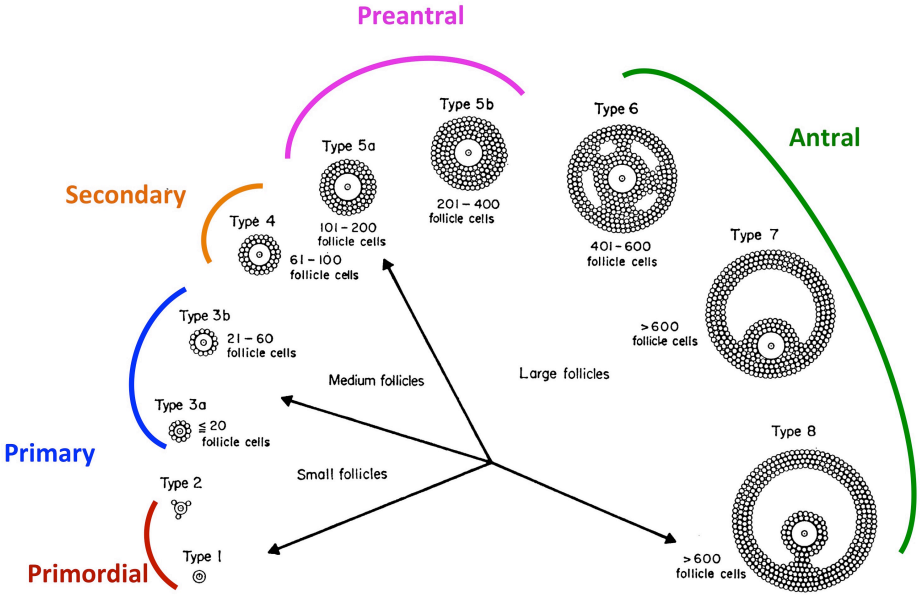


Figure 1.2: Classification of mouse follicles according to Pedersen and Peters criteria (*16*).

1.1.2 The role of the oocyte in ovarian function

Early studies demonstrated that gap junctions formed between granulosa cells, and between granulosa cells and the oocyte are essential to maintain communication between the two compartments and to facilitate transferring of mediator molecules (*17*, *18*). Cumulus cells form transzonal cytoplasmic processes that penetrate the ZP contacting the oocyte cytoplasmic membrane (*19*). This direct contact between the oocyte and granulosa cells are essential for follicle development (*20*, *21*).

In the last 20 years, it has become clear that the oocyte has a critical role in the regulation of ovarian function other than simply carrying the maternal genome or supporting the early stages of embryo development. Considerable effort has been carried out to try to elucidate the role of the oocyte in follicle development and fertility (*22-26*).

In mice, studies demonstrated that oocyte-secreted factors, such as GDF9 and BMP15 were essential in cumulus cell differentiation and expansion, supporting a direct role of the oocyte in the normal development of cumulus cells (*27*, *28*). Using reaggregated ovaries technique, it has also been demonstrated that oocytes seems to be ruling follicle development. Reaggregated ovaries from newborn mice oocytes and newborn rat somatic cells were generated and allowed to grow beneath the kidney capsule of bilaterally ovariectomized SCID mice (*29*). This study demonstrated that mouse germ cells are able to support

follicle development and oocytes retain their species-specific morphological features when growing in rat follicles. Even more, oocytes recovered after grafting were fertilized and developed to term after transfer to pseudopregnant foster mothers (*29*). Using the same technique, the effect of the age of the oocyte on follicle development was also assessed in mouse. Reaggregated ovaries generated with 12-day or newborn germ cells and newborn somatic cells demonstrated an accelerated follicle development in reaggregated ovaries containing older germ cells (*30*). Moreover, oocytes recovered 9 days after grafting revealed normal competence to resume and complete meiosis, undergo fertilization and support preimplantation development. This work demonstrated that the intrinsic developmental program of the oocytes is orchestrating and coordinating follicle development (*30*).

The most important oocyte-secreted factors, that have been studied in the last 20 years, are GDF9 and BMP15 (*31-33*). These TGF-β family members are essential for fertility synergistically regulating follicle development and oocyte competence (*22*, *34*, *35*). It was also established that their effect varies depending on the species (*36*). GDF9 deficient female mouse exhibited block of follicle development beyond the primary stage and therefore females are infertile (*22*). In sheep, BMP15 is essential for female fertility and natural mutations can cause both, increased ovulation rate and infertility phenotypes in a dosage-sensitive manner (*37*). Altered levels of GDF9 and BMP15 has been also linked with pathological conditions in women. Oocytes from patients with polycystic ovary syndrome have decreased expression of GDF9 and BMP15 that could be related

with the impaired oocyte quality and developmental competence observed in women with PCOS (*38*).

Others oocyte-secreted factors that have been proved to be essential for fertility are spermatogenesis and oogenesis specific basic helix-loop-helix 1 (Sohlh1) and Fibroblast growth factor 10 (FGF10). *Sohlh1* knockout mice lead to disrupted folliculogenesis (*39*), moreover the presence of genomic variants of *Sohlh1* in women with non-syndromic premature ovarian insufficiency (POI) and non-syndromic hypergonadotropic hypogonadism (*40*, *41*) highlighted this gene as a candidate for ovarian dysfunction in humans. FGF10 has been proved to regulate fertility in cows (*42*). Supplementation of culture medium with FGF10 during in vitro oocyte-maturation in cattle enhanced cumulus expansion and embryo development (*43*) and increased glucose uptake and expression of genes in the ovulatory cascade (*44*).

Despite the evidence presented above, our understanding on how the oocyte regulates ovarian function is still very limited. The complex intraovarian environment could be deregulated in pathological conditions leading to infertility, such as premature ovarian failure. In this regard, models of this pathology could help us to expand our knowledge about how the cross- talk between the oocyte and other ovarian cell components are ruling the fate of fertility.

1.2 Premature ovarian failure

1.2.1 Overview

Premature ovarian failure (POF) is a clinical condition characterised by hypergonadotropic hypogonadism and amenorrhea that affects 1% to 3% of women under 40 years of age (*45-47*). POF affects the ability of ovaries to maintain follicle development and ovulation. The ovarian manifestation varies from a complete depletion of follicles (afollicular POF) to the presence of a variable population of follicles (follicular POF) that fail to develop (*45*, *48*). The proportion of women with afollicular and follicular POF has been a matter of debate for several years between clinicians, and empirical studies have failed to provide reliable data. However, some studies indicate that the proportion of afollicular and follicular POF is fairly equal indicating that an important number of women with follicular POF could benefit from therapies focusing on reactivation of follicle development. Evaluation of POF women with normal karyotypes demonstrated that 50% of the patients present an intermittent ovarian function due to the presence of ovarian follicles (*49*). Moreover, a recent study analysed ovarian cortical tissue histology and demonstrated that 54% of women with POF have residual follicles that can potentially be reactivated to resume fertility (*50*). Unfortunately, the numbers of the residual follicles were not reported in this study.

Even though the probability is low, some women with POF can become pregnant spontaneously. For that reason some authors proposed the term

"primary ovarian insufficiency" (POI) to replace POF in the attempt to use a clinical term that reflect the transient ovarian function displayed by some women with POF (*51*, *52*). Recently, it has been proposed that the use of POI as a clinical term has introduced confusion in the literature. Moreover, authors suggested that the use of the term POI along with POF may lead to phenotypic heterogeneity and may prevent finding of significant disorder-genotype associations in translational studies and therefore the term POF should be maintained (*53*). Following that rationale, the term POF will be used in this thesis.

1.2.2 Clinical presentation

In women the clinical diagnosis of ovarian failure is based on FSH levels greater than 40 mIU/ml and presence of secondary oligomenorrhea (irregular menstrual cycles) or amenorrhea (absence of menstrual cycles) lasting more than 4 months in women under 40 years of age. In POF, the lack of growing follicles in the ovary generate decreased levels of inhibin resulting in decreased negative feedback on the pituitary with consequently higher levels of FSH. In women with POF, the lack of growing follicles and therefore graafian follicles in the ovary generates lower levels of estradiol. This is the main cause of the clinical manifestations displayed by women with POF, such as decreased bone mineral density, increased cardiovascular morbidity and increased risk of neurological diseases (*54*) (Figure 1.3).

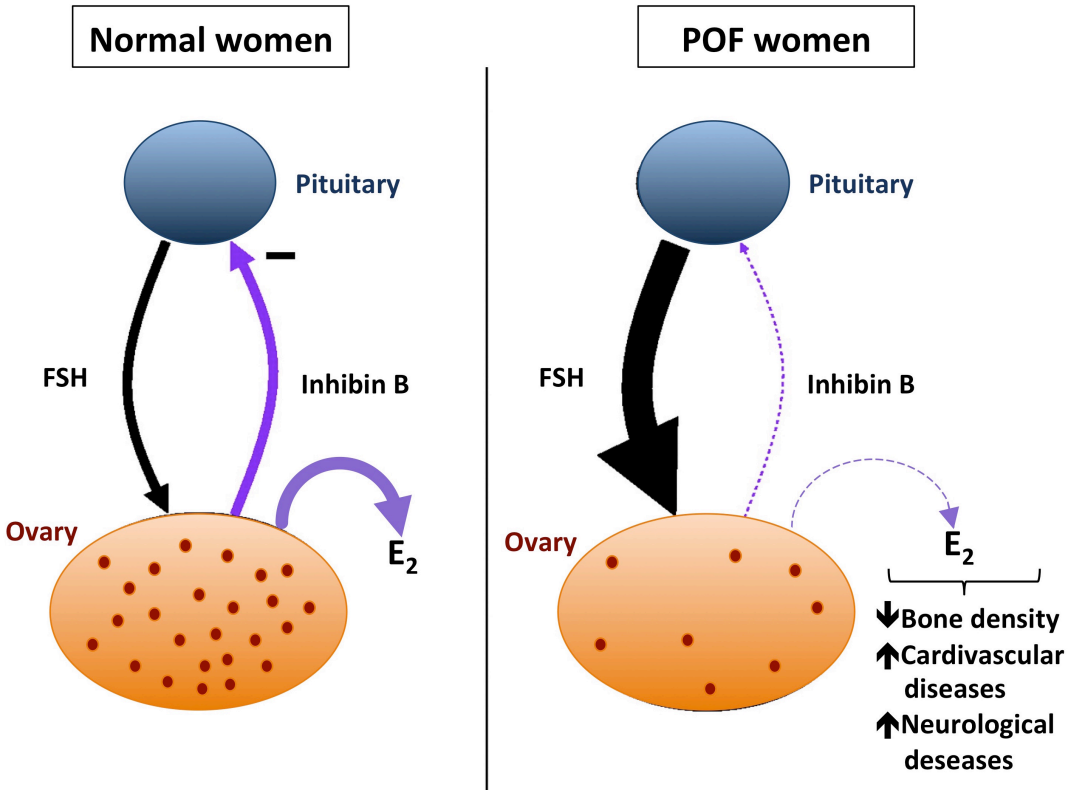


Figure 1.3: Ovarian function observed in normal and POF women. In POF the follicular dysfunction causes lower production of inhibin leading to increased levels of FSH compared with normal women. Ovarian production of estradiol (E_2) is also decreased in women with POF causing higher risk of lower bone density, cardiovascular and neurological diseases. Adapted from Shelling, 2010 (*46*).

Out of the fertility and reproductive fields, the diagnosis of POF is emotionally challenging for women. Psychological evaluation demonstrated that women with POF scored significantly higher for shyness, social anxiety and depression, and lower on self-esteem compared with controls (*55*). Another study carried out on 154 women with POF (POI in the article) also revealed lower self-

esteem along with lower perceived social support compared with Control women (*56*). A questionnaire to evaluate quality of life applied to Control and POF women revealed that although the quality of life was in general not different between the groups, having POF led to a 2.5-fold increased risk of low score in the psychological domain of the questionnaire (*57*). Moreover, women with POF had higher sexual dysfunction than premenopausal Control women indicating potential negative consequences for the couple and overall family life (*58*).

Both physiological and psychological aspects related with POF indicate that is necessary to provide women with adequate psychosocial and clinical support in order to minimize the deep repercussion of the diagnosis on the patients quality of life. This involves not only complex clinical management of the pathology, but also exerts considerable pressure over the health services.

1.2.3 Causes

Several factors have been identified related with the generation of POF. Unfortunately, due to the highly heterogeneous nature of the disease, a direct causal relation between the possible cause and the pathology cannot be established in most of the cases and therefore in around 70% of the cases the cause is considered as idiopathic (*45*, *46*, *59-61*).

1.2.3.1 Genetic causes

The most prevalent genetic causes of POF are related with abnormalities of the X chromosome (*46*, *62*) of which Turner syndrome (45, X) is the most common cause of POF. Women with Turner syndrome display normal early ovary development, followed by rapid follicular depletion and oocyte atresia before birth, leading to the absence of puberty in many affected girls and infertility in adult life (*63*). Just a small percentage of females with Turner syndrome retain some follicular activity throughout early adulthood, however there are several ethical and safety issues regarding fertility preservation in young women with Turner syndrome. For instance, pregnancy in women with Turner syndrome is associated with increased risk of maternal mortality, foetal loss, foetal congenital abnormality and abnormal karyotype (*64-66*).

POF has also been associated with other genes of the X chromosome like premutations of *FMR1* (Fragile X mental retardation 1) (*67*) and mutations of BMP15 (Bone morphogenetic protein 15) (*68*, *69*). The *FMR1* gene is responsible for the fragile X syndrome, a form of X-linked mental retardation. When the CGG trinucleotide in the 5'-untranslated region of the *FMR1* gene is expanded over 200 repeats, a full mutation is produced whereas the premutated allele contains expansions between 55 and 199 (*70*). There is evidence that repeats between 55 and 79 may lead to an increased translation of the protein (FMRP), which is a RNA-binding protein that inhibit translation of other mRNAs (*71*, *72*). The possible association between *FMR1* and POF is that *FMR1* is highly expressed in the germ

cell population throughout folliculogenesis in rat (*73*) and mouse (*74*) and therefore the overexpression of the protein could be negatively affecting the expression of genes required for normal oocyte and follicle development.

As described above, BMP15 is an oocyte-secreted factor and is fundamental for normal follicle and oocyte development. Mutations in the *BMP15* gene have also been associated with POF with a variable prevalence between 1.5% to 12% (*75*). Even though several *BMP15* variants have been detected in POF patients, the mechanism underling the association between the *BMP15* variant and the altered BMP15 function remains unknown. However, some of the *BMP15* variants have been associated with defective production of bioactive products due to haploinsufficiency and generation of aberrant protein products by a dominant negative effect (*76-78*).

Mutations in genes located in autosomal chromosomes have also been detected in patients with POF like, *FOXL2* (Forkhead box L2), *FSHR* (FSH receptor) and *FIGLA* (Folliculogenesis specific basic helix-loop-helix). Nonetheless, the frequency of mutations in these genes is very low or associated with complex syndromes. *FOXL2* gene encodes a forkhead transcription factor that contains a fork-head DNA-binding domain and may play a role in ovarian development and function (*79*, *80*). Mutations in *FOXL2* are mainly associated with Blepharophimosis ptosis epicanthus-inversus syndrome (BPES) which has POF as one of the clinical manifestations (*81*). FSHR belongs to family 1 of G protein-coupled receptors and have an essential function in gonad development and

ovarian steroidogenesis (*82-84*). Several mutations leading to single amino acid substitutions of the *FSHR* gene have been described in patients with POF, however meta-analyses have failed to link these variants with POF (*85*, *86*). FIGLA is an oocyte-specific transcription factor involved in folliculogenesis, fertilization and pre-implantation development (*87*). A strong association between two *FIGLA* variants and POF has been identified in Chinese (*88*) and Indian (*89*) populations. Association of POF and *FIGLA* in other ethnic groups are currently unknown.

1.2.3.2 Autoimmune causes

Approximately 10-20% of the patients with POF have also organ-specific autoimmune disease such Addison's disease, myasthenia gravis or hypothyroidism (*46*). However, the direct association between the two conditions is still unclear and has proven to be controversial.

Approximately 2%–10% of POF cases are associated with adrenal failure or autoimmunity and therefore would result from autoimmune oophoritis (*90-92*). In women with POF, a higher risk of autoimmune adrenal insufficiency has been described (*91*) . POF could also be associated with inflammatory autoimmunity targeted to ovarian-specific germline antigens, however only experimental immunization against ZP and inhibin-α proteins have been proved to cause POF (*90*).

1.2.3.3 Iatrogenic causes

POF can be induced after chemotherapy and radiotherapy in patients with cancer. The severity of the clinical features of POF will depend on dose, interval, age and type of drug used for treatment (*93*). Extended exposure to toxic agents can also result in POF. Industrial exposure to 2-bromopropane, a cleaning solvent, in Korean women was associated with POF (*94*). On the other hand, smoking has been suggested as a significant risk factor for POF (*95*).

Due to the high heterogeneity of causes leading to POF, the understanding of the etiology underlying the onset of POF remains poorly understood and mechanistic studies are complex and challenging. In the attempt to provide clues about what mechanisms may be involved in the development of POF in humans, several mouse models have been developed.

1.2.4 Genetically modified animal models for POF

Jagarlamudi *et al.,* in 2010 reviewed and classified in 4 groups all mouse models available for POF (*96*): (1) Mouse models resulting from defects in primordial germ cells development, (2) Mouse models with mutations in meiosis-specific genes, (3) Mouse models with defects in the formation, survival, and activation of primordial follicles, and (4) Mutant mouse models with defects in follicular development. Some relevant examples by group are presented as follow (the complete list of mouse models can be found in Jagarlamudi *et al.,* 2010):

1. Mouse models resulting from defects in primordial germ cells (PGCs) development.

POU class 5 homeobox 1 (POU5F1 or Oct4) is a transcription factor that participates in multiple important processes during embryonic development, stem cell pluripotency and oocyte competence (*97-99*). Germ cell-specific deletion of *Oct4* leads to massive embryonic PGCs apoptosis and lack of oocyte in the adult ovary (*100*).

T-cell intracellular antigen-1-related (TIAR), which belongs to a family of RNA binding proteins, has been implicated in apoptosis (*101*). *Tiar*$^{-/-}$ mice displayed fewer PGCs by E11.5 and complete lack of oogonia by E13.5 due to apoptosis or reduced survival of PGCs (*102*).

BMPs are important members of the TGF-β family. *Bmp4*$^{-/-}$ embryos lacks PGCs and therefore it has been established that BMP4 is required for PGCs migration (*103*). *Bmp8b*$^{-/-}$ and *Bmp2*$^{-/-}$ mice have reduced numbers or are completely lacking PGCs, leading to a lack of follicle development (*104*, *105*).

2. Mouse models with mutations in meiosis-specific genes

SPO11 (SPO11 meiotic protein covalently bound to DSB [double strand break]) is an enzyme required for the introduction of double-strand breaks during meiosis (*106*). Females *Spo11*$^{-/-}$ are completely infertile due to a lack of mature follicles (*107*).

Disrupted meiotic cDNA 1 homolog (DMC1) is a DNA strand exchange protein that acts on double-strand breaks in meiosis (*108*). *Dmc1*$^{-/-}$ ovaries lack follicles due to meiotic arrest of oogonia at early prophase I (*109*).

MutS homolog 4 (MSH4) and MutS homolog 5 (MSH5) are meiosis-specific proteins important for the formation of primordial follicles (*109*). Studies have shown that by postnatal day 4, *Msh4*$^{-/-}$ ovaries completely lack of oogonia (*110*), whereas in *Msh5*$^{-/-}$ ovaries displayed lack of oocytes at 2–3 months of age due to meiotic failure (*111*).

3. Mouse models with defects in the formation, survival, and activation of primordial follicles

Folliculogenesis specific basic helix-loop-helix (FIGLA) is an oocyte-specific gene (*87*). *Figla*$^{-/-}$ mice displayed an apparently normal gonadogenesis during embryo development, however, at birth primordial follicles are absent (*112*).

NOBOX oogenesis homeobox gene (NOBOX) is also an oocyte-specific factor. *Nobox*$^{-/-}$ mice exhibited postnatal oocyte loss, prolonged meiosis at the oogonia stage and impaired primordial to primary follicle transition (*113*).

Forkhead box L2 (*Foxl2*) is a single-exon gene, belonging to the family of winged-helix/forkhead transcription factors. In *Foxl2*$^{-/-}$ ovaries, granulosa cell differentiation is blocked, and the transition from primordial to primary follicles is thus blocked; the mice are infertile due to impaired follicular development (*114*).

4. Mutant mouse models with defects in follicular development

Growth differentiation factor 9 (GDF9) and bone morphogenetic protein 15 (BMP15) are oocyte-specific members of the TGF-β family. *Gdf9*$^{-/-}$ female mice are infertile due to arrest of follicular development (*22*), while *Bmp15*$^{-/-}$ female mice are subfertile, with reduced ovulation, fertilization and litter size (*34*, *35*).

Connexin 37 is an important mediator of the communication between oocytes and granulosa cells and is essential for follicular development. Mice lacking connexin 37 are infertile due to a lack of mature follicles (*115*).

FSH is essential for follicular development and therefore disruption of its signal in mutant mice impairs follicle development and fertility (*116-118*).

Even though these mouse models have provided valuable information on possible candidate genes or pathways involved in the development of POF, their role in the etiology of POF is still unclear. In this regard, more studies are needed not only to elucidate mechanisms underlying the onset of POF and provide possible treatments to women, but also to contribute to a deeper understanding of how fertility is regulated.

1.3 Double mutant mouse model

Using *Cre-LoxP* technology a mouse model with oocyte-specific deletion of two glycosyltransferases has been described (*119*). The double mutant (DM) female mouse has an oocyte-specific deletion of *Mgat1* and *C1galt1* genes, which encode for *N*-acetylglucosaminyltransferase 1 (GlcNAcT-1) and core 1 β1,3-galactosyltransferase (T-synthase) enzymes, respectively. These enzymes are required for the generation of hybrid *N*-glycans and complex *O*-glycans (core 1 and 2 *O*-glycans).

1.3.1 *N*-glycans

The *N*-glycans are attached to the protein backbone by linkage to the asparagine amino acid in the sequon (amino acid sequence) Asn-X-Ser/Thr by an *N*-glycosidic bond. All *N*-glycans share a common core sugar sequence, Manα1–6(Manα1–3)Manβ1–4GlcNAcβ1–4GlcNAcβ1-Asn-X-Ser/Thr, and are classified into three types (Figure 1.4).

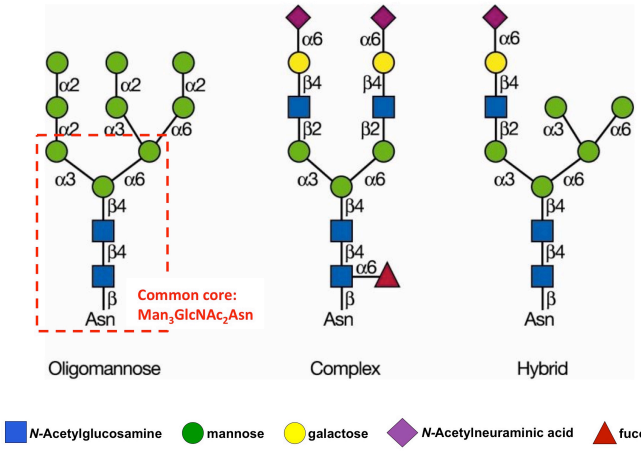


Figure 1.4: Oligomannose, complex and hybrid *N*-glycans. *N*-glycans added to protein Asn-X-Ser/Thr sequons are of three general types in a mature glycoprotein: (1) oligomannose: only mannose residues are attached to the core, (2) complex: sugar projections initiated by *N*-acetylglucosaminyltranferases (GlcNAcTs) are attached to the core and (3) hybrid: only mannose residues are attached to the Manα1-6 arm of the core and 1 or 2 sugar projections are on the Manα1-3 arm. Enclosed by the red dotted line is the common core $Man_3GlcNAc_2Asn$ present in each *N*-glycan. Modified from Varki et al, 2009 (*120*).

The biosynthesis of all *N*-glycans begins on the cytoplasmic face of the endoplasmic reticulum (ER) membrane with the transfer of GlcNAc-P from Uridine diphosphate *N*-acetylglucosamine (UDP-GlcNAc) to the lipid-like precursor dolichol phosphate (Dol-P) to generate dolichol pyrophosphate *N*-acetylglucosamine (Dol-P-P-GlcNAc) (Figure 1.5). Fourteen sugars are sequentially added to Dol-P before transfer of the glycan to an Asn-X-Ser/Thr sequon of a protein that is being synthesized at the ER membrane. This is a highly organized and regulated stepwise process and each phase requires a specific enzyme. The protein-bound *N*-glycan is then modified in the ER and Golgi by a complex series

of reactions catalyzed by membrane-bound glycosidases and glycosyltransferases. Many of these enzymes are sensitive to the physiological and biochemical state of the cell in which the glycoprotein is expressed. Consequently, the sugars attached to the glycosylated asparagine in a mature glycoprotein will depend on the physiological status of the cell in which the glycoprotein is expressed (*120*).

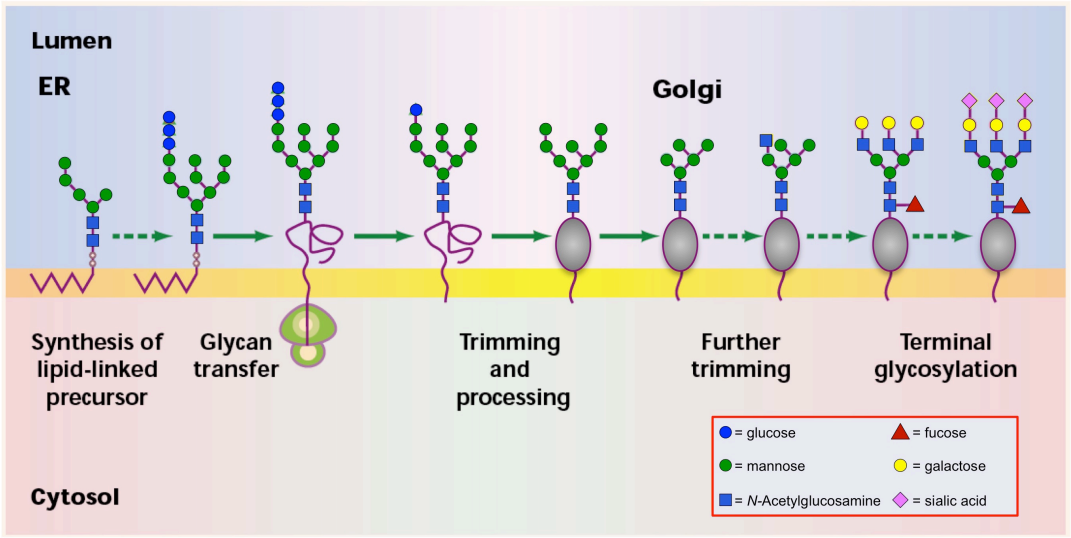


Figure 1.5: Simplified diagram of *N*-glycan synthesis. In the cytosol, sugars are linked onto a lipid precursor, which is then transferred into the lumen of the endoplasmic reticulum (ER) to complete the generation of the core oligosaccharide. The glycan is then transferred to the polypeptide. Sugars are trimmed off, and the glycoprotein is then folded (grey oval) before being moved to the Golgi complex. The glycoprotein can go through a series of further modifications, ending with the capping of the oligosaccharide branches with sialic acid and fucose. Adapted from Dove A., 2001 (*121*).

N-glycans can directly influence fundamental properties of glycoproteins including, conformation, solubility, antigenicity, and recognition by glycan-binding proteins. Absence of complex and hybrid *N*-glycans is embryonically lethal and mice with deletion of the *Mgat1* gene that encodes GlcNAcT-I enzyme (required for the generation of complex and hybrid *N*-glycans), results in death at approximately embryonic day 9.5 (*122*).

1.3.2 *O*-glycans

The *O*-glycans are generally covalently attached to the protein through *N*-acetylgalactosamine (GalNAc) to serine or threonine residues by an *O*-glycosidic bond. The resulting glycans are often named mucin *O*-glycans or *O*-GalNAc glycans.

The simplest mucin *O*-glycan is a single *N*-acetylgalactosamine sugar linked to serine or threonine (Figure 1.6). The most common mucin *O*-glycan is core 1 *O*-GalNAc glycan and it forms the core of many longer, more complex structures. Core 2 *O*-GalNAc glycans contains a branching *N*-acetylglucosamine attached to core 1 and are found in both glycoproteins and mucins from a variety of cells and tissues. Linear core 3 and branched core 4 *O*-GalNAc glycans have been found only in secreted mucins of certain mucin-secreting tissues, such as bronchi, colon, and salivary glands (Figure 1.6). There are also core structures 5–8 but they have an extremely restricted occurrence.

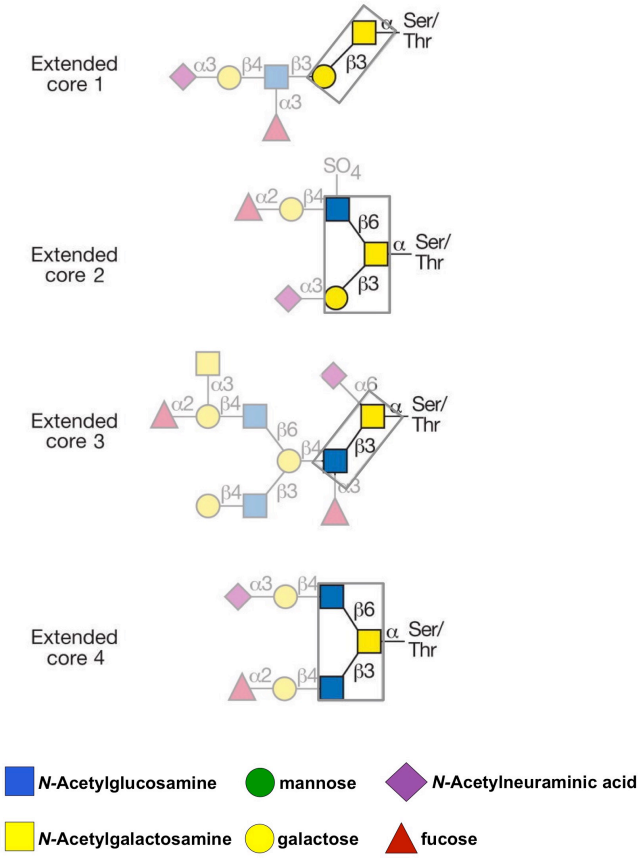


Figure 1.6: Representative examples of complex *O*-GalNAc glycans extended core 1-4. All core structures (in grey boxes) can be extended and branched. Adapted from Varki et al, 2009 (*123*).

O-glycans are important in receptor signalling (*124*), cell-cell interaction (*125*), cell-extracellular matrix interaction (*126*) and provide protection against proteolytic degradation (*127*). Absence of core 1–derived *O*-glycans achieved by deletion of *C1galt1* gene (previously known as *T-syn*) is embryonically lethal in mice after day 12.5 of gestation (*128*).

1.3.3 Molecular basis of the double mutant phenotype

Since absence of both complex and hybrid *N*-glycans and core 1-derived *O*-glycans is incompatible with life, to study the function of these glycans *in vivo*, cell specific ablation of the *Mgat1* and *C1galt1* genes is required. To achieve deletion only in the oocyte, *Cre-LoxP* technology has been used, which allows deletion of a gene flanked by *loxP* sites in the presence of the *Cre* recombinase enzyme. In the DM mouse the *Cre* recombinase transgene is controlled by the promoter region of the oocyte-specific ZP3 gene. As a result, *Cre* recombinase is expressed only in the oocyte, when the expression of ZP3 begins, from the primary stage of development onwards (*2*) and the genes flanked by *loxP* sites are thus deleted.

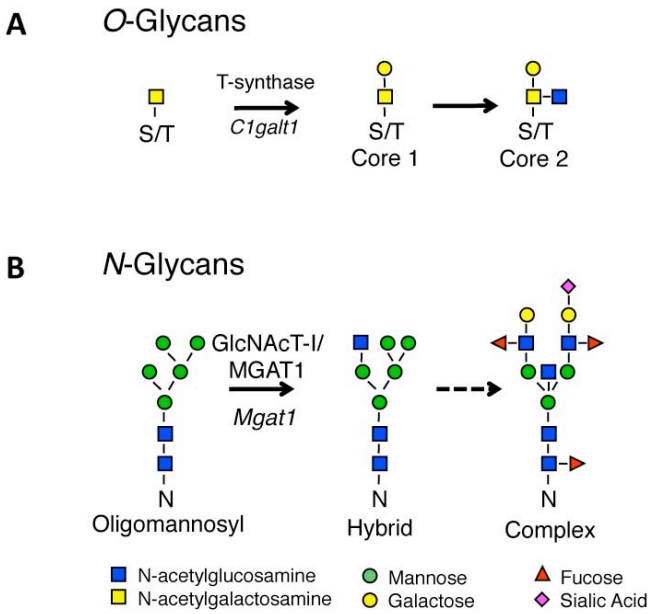


Figure 1.7: *O*- and *N*-glycans generation. (A) T-synthase enzyme encoded by *C1galt1* gene required for the synthesis of core 1 *O*-glycans by transferring galactose to N-acetylgalactosamine on serine/threonine residues (S/T). (B) N-acetylglucosaminyltransferase 1 (GlcNAcT-1) enzyme encoded by *Mgat1* gene is necessary to generate hybrid and complex *N*-glycans from the oligomannosyl structure.

The T-synthase enzyme mediates the synthesis of core 1 *O*-glycans by the addition of galactose to *N*-acetylgalactosamine (GalNAc). Then, core 2 *O*-glycans are generated by the addition of *N*-acetylglucosamine (GlcNAc) to the core 1 structure. On the other hand, GlcNAcT-1 mediates the production of hybrid and complex *N*-glycans by modification and extension of the oligomannosyl structure (Figure 1.7).

Previous to the generation of the DM mice, both oocyte-specific mutations carried by DMs were studied individually. The oocyte-specific deletion of *Mgat1* was firstly reported 11 years (*129*). The lack of GlcNAcT-1 and therefore the absence of hybrid and complex *N*-glycans in the oocyte, leads to decreased fertility due to a reduced number of ovulated eggs after hormonal stimulation and fewer pups per litter. In addition, all Mutant oocytes had an altered ZP. The study revealed that complex and hybrid *N*-glycans are required at some extent for the generation of a developmentally competent oocyte, but fertilization, blastogenesis, and implantation may proceed normally in their absence (*129*). Following studies demonstrated that the ovulation rate of Mutant females is decreased due to aberrant development of preovulatory follicles (*130*).

A mouse with oocyte-specific deletion of *C1galt1* was also reported (*119*). The authors determined that absence of complex *O*-glycans was not required for blastogenesis, implantation, or development prior to midgestation (*119*). Interestingly, the reproductive phenotype was opposite to that presented by the

Mgat1 Mutant mouse. *C1galt1* Mutant mice had an increased ovulation rate due to an increased number of mature follicles at ovulation and a consistently increased fertility due to an increased number of pups per litter. In addition, females carrying an oocyte-specific mutation of *C1galt1* exhibited some abnormalities of the ovarian morphology, such as an altered ZP structure and the presence of multiple-oocyte follicles (MOFs), although these MOFs do not contribute to the increased ovulation rate observed in these females (*131*, *132*).

1.3.4 DM phenotype

An evident feature of DM oocytes is that the ZP is morphologically altered, which is concordant with the fact that ZP proteins are highly glycosylated and therefore their structure is affected by the absence of complex *N*- and *O*-glycans in the oocyte. However DM females are fertile indicating that complex *N*- and *O*-glycans are not required for fertilization (*119*, *129*, *130*). DM females are fertile at 6 weeks of age, but produce a smaller litter of around 50% of Controls. In addition, DM females were unable to produce subsequent litters even though they were exposed to males up to 6 months of age (*119*). Ovarian morphology was analysed at 3 and 6 weeks and at 3 months of age and follicle development became increasingly aberrant with age (Figure 1.8). By 3 months of age, DM ovaries contained reduced numbers of follicles at later stages of development. However, ovaries had an increased number of follicles at the primary 3a stage, which may suggest a block at the primary stage of follicle development.

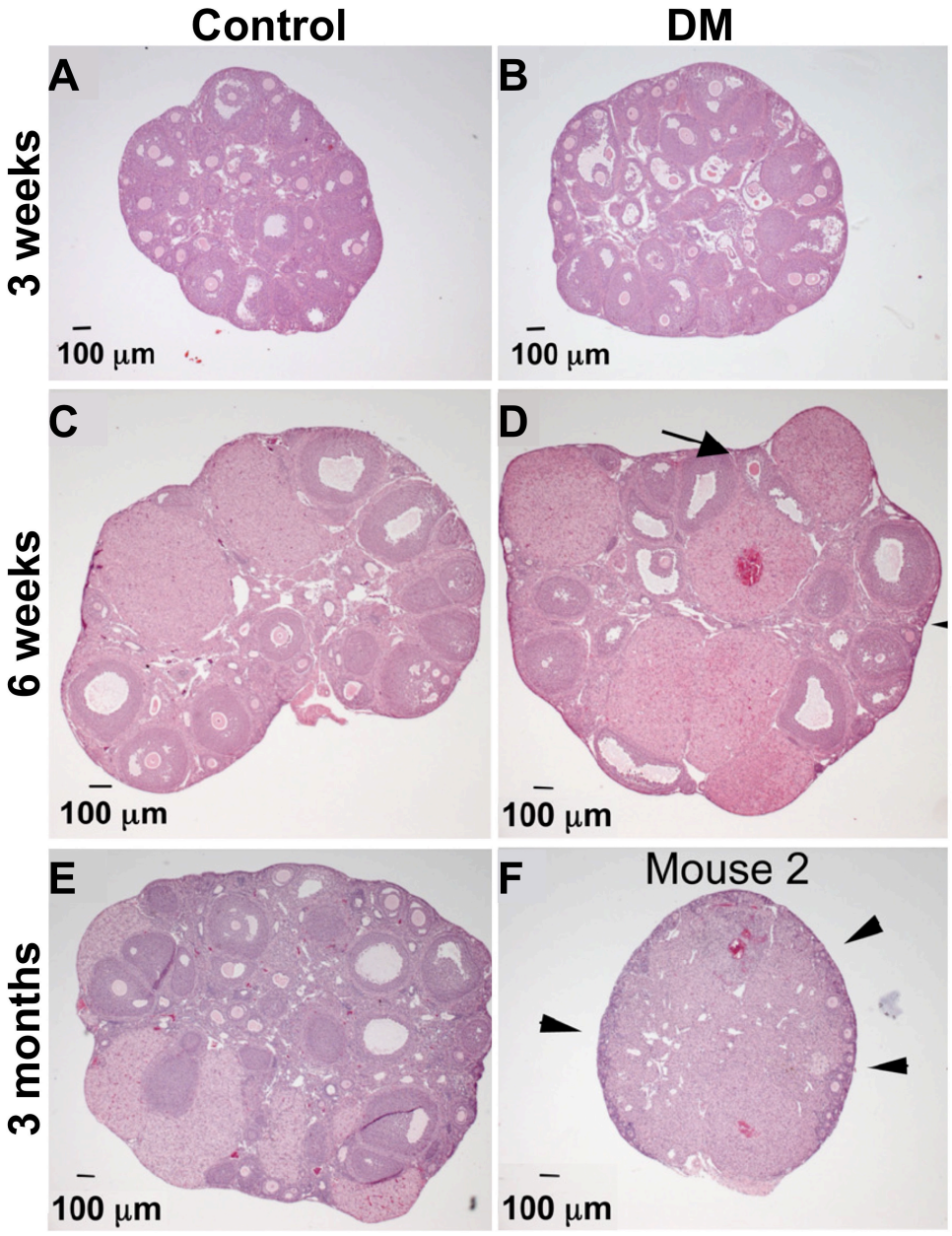


Figure 1.8: Morphology of DM and Control ovaries. Representative ovary sections of Control (A,C,E) and DM (B,D,F) at 3 weeks (A,B), 6 weeks (C,D) and 3 months (E,F). Ovaries at 3 and 6 weeks contain numerous follicles at all stages of follicle development in both control and DM. Some abnormalities were also described in DM ovaries, such as oocytes lacking ZP (arrow in D) and the presence of empty follicles in 3 month-ovaries (arrowheads in F). Adapted from Williams, and Stanley, 2011 (*133*).

The ovarian failure observed in DM females by 3 months was also consistent with an altered endocrine profile displayed by the females at the same age, characterized by elevated gonadotropins and decreased sex steroids confirming the DM mouse as a model of POF (Figure 1.9) (*133*).

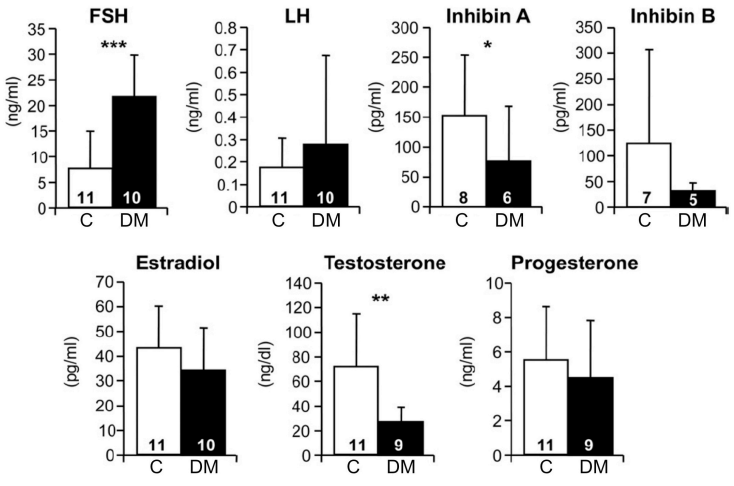


Figure 1.9: Serum gonadotropin and ovarian steroids of Control (C) and DM 3-month mice. The number in the bar is the number of animals evaluated. *P<0.05; **P<0.005; ***P =0.001. Adapted from Williams, and Stanley, 2011 (*133*).

There are two main aspects of the DM mouse that make it very attractive as a research model for POF. Firstly, the DM phenotype is concordant with clinical features of POF in women, which is a devastating diagnosis for many women. In this sense, the DM model represents an opportunity to study and explore possible mechanisms underlying the onset of POF that could potentially highlight candidate targets to re-establish follicle development.

Secondly, emphasizing that the double deletion in the DM mouse is oocyte-specific, the model provides an opportunity to study the mechanisms through which the oocyte is regulating ovarian physiology and ultimately, fertility. The fact that DM females switch their phenotype from fertile to infertile in a very short timeframe constitutes a remarkable opportunity to study the dynamics behind the regulation of fertility by the oocyte.

Based on the evidence presented above, the overarching hypotheses and aims of this thesis are:

Hypotheses:

- The small litter size observed in DM females at 6 weeks is due to a decreased ovulation rate compared with Controls.
- The presence of a normal endocrine environment reverts POF phenotype in DM females.
- Intrinsic ovarian factors are preventing progress of follicle development in DM females.
- DM germ cells form POF mice are able to resume normal follicle development when reaggregated with WT somatic cells.
- The gene expression profile of DM ovaries reflects the phenotype previous, during and after the onset of POF.

Aims:

- To determine the cause of the small litter size in DM females.
- To evaluate if the presence of a normal endocrine environment could overcome the block on follicle development observed in DM females.
- To determine if DM follicle growth can be restored to Control levels in a controlled *in vitro* environment.
- To evaluate if DM oocytes preserve the potential to restore follicle development.
- To characterize the gene expression profile of DM ovaries from prepuberal, fertile and infertile females.

Chapter 2: Material and Methods

2.1 Double mutant mice

Oocyte-specific deletion of *Mgat1* and *C1galt1* genes was achieved using *Cre*-lox technology. As described previously (*119*), mice carrying floxed *Mgat1* and *C1galt1* alleles and a ZP3*Cre* transgene generate oocytes deficient in complex and hybrid *N*-glycans and core 1-derived *O*-glycans. The deletion occurs from the primary stage of follicle development when ZP3*Cre* transgene is expressed (*2*, *134*). The ZP3*Cre* transgene does not affect fertility and floxed *C1galt1* and *Mgat1* alleles function as wild-type genes (*119*, *129*). Female mice carrying floxed *Mgat1* and *C1galt1* alleles and a ZP3*Cre* transgene were used as Mutant females (DM) whereas females carrying the floxed *Mgat1* and *C1galt1* alleles but not the ZP3*Cre* transgene were used as Controls. Mice were kept under controlled conditions in 12 h light:12 h darkness cycles and with water and food *ad libitum*. All the experiments involving mice were done with permission from the Home Office and the Local Ethical Review Committee.

2.2 Genotyping

2.2.1 Ear genomic DNA extraction

Ear biopsies were digested overnight with 1.5% of proteinase K (Roche diagnostics, Mannheim, Germany) in 51 μl of buffer (100mM Tris-HCl, 5mM EDTA, 0.2M NaCl and 0.2% SDS) at 55°C. Next morning digested tissue was centrifuged at

13,200 rpm for 8 min and 40 μl of supernatant heated at 99°C in order to deactivate proteinase K. Finally the sample was diluted with 100 μl of distilled water (Gibco, life technologies, UK) and stored at 4°C.

2.2.2 Polymerase chain reaction (PCR)

In order to verify floxed *Mgat1* and *C1galt1* alleles and the presence of the ZP3*Cre* transgene, individual PCR genotyping was carried out using ear genomic DNA. Primers PS585 and PS586 detected the *Mgat1* floxed allele, primers FB33 and FB34 detected *C1galt1* floxed allele and primers PS502 and PS607 detected ZP3*Cre* transgene (Table 2-1). The final PCR reaction mix contained ultrapure distilled water, 10X PCR buffer (Bioline Reagents, London, UK), 50 mM MgCl2 (Bioline Reagents, London, UK), 10 mM dNTPs(Roche diagnostics, Mannheim, Germany), primers (Eurogentec, Seraing, Belgium), Taq polymerase (Bioline Reagents, London, UK) and 1μl of genomic DNA with a total volume of 25 μl. Specific amounts of the reagents used for *Mgat1*, *C1galt1* and ZP3*Cre* reaction PCR mix are detailed in Table 2-2.

PCR for *C1galt1* was performed with an initialization step of 2 min at 94°C followed for 35 cycles of: 30 sec at 94°C (denaturation), 30 sec at 66°C (annealing) and 1 min at 72°C (extension). PCR conditions for *Mgat1* and *ZP3Cre* were the same except that annealing temperature for *Mgat1* was 56°C. Female mice with floxed C*1galt1* and *Mgat1* alleles and no ZP3*Cre* transgene were used as Controls

and female mice carrying floxed C*1galt1* and *Mgat1* alleles and the ZP3*Cre* transgene were used as Mutant females (DM).

Table 2-1: Primer sequences used to amplify *Mgat1*, *C1galt1* and *Cre*.

Gene	Primer	Sequence	PCR product length
Mgat1	PS585 PS586	5'-TGCAAGCCAACACTTGTCTC-3' 5'-GAGACCTGCTTACTGCAGCC-3'	561 bp
C1galt1	FB33 FB34	5'-GTCCACAGAGGGCCATTAGA-3' 5' TGCTGATCCACAGAGGAAGA-3'	384 bp
ZP3*Cre*	PS502 PS607	5'-GGACATGTTCAGGGATCGCCAGGCG-3' 5'-CCATGAGTGAACGAACCTGG-3'	350 bp

Table 2-2: PCR reaction mix for *Mgat1*, *C1galt1* and ZP3*Cre* genotyping

Reagents (μl)	**PCR reaction mix**		
	Mgat1	***C1galt1***	**Zp3*Cre***
Distilled H_2O	19.3	19.05	18.75
10x PCR buffer	2.5	2.5	2.5
10 mM MgCl2	0.5	0.75	0.75
dNTP (10 mM)	0.5	0.5	0.5
Primer 1	0.5 (PS 585)	0.5 (FB 33)	0.5 (PS 502)
Primer2	0.5 (PS 586)	0.5 (FB 34)	0.5 (PS 607)
Taq polymerase (5 U/μl)	0.2	0.2	0.5
DNA	1	1	1
Final volume	**25**	**25**	**25**

2.2.3 Analysis of PCR products

One percent agarose gels were prepared by adding agarose in TAE buffer and then heating the mixture in a microwave to dissolve the agarose powder. Once the gel had cooled slightly, ethidium bromide (Fisher Scientific, Loughborough, UK) was added to a final concentration of 0.01% in order to allow DNA visualization. The agarose mixture was then poured into an electrophoresis chamber fitted with a well comb insert and left to set. TAE buffer was added until the gel was complete covered and the well comb removed.

PCR products were spun down for a couple of seconds and mixed with 5 μl of loading buffer. Six microliters of PCR products for *Cre* genotyping and 15 μl for *Mgat1* and *C1galt1* genotyping were loaded into different wells along with molecular weight markers. Samples were run at 90-100 millivolts for approximately 40 min and gel was visualized in a UV transilluminator.

2.3 Histological processing

2.3.1 Embedding

Fixed tissue was passed through increasing concentrations of ethanol from 70% to 100% before immersion in xylene. Then tissue was embedded in melted paraffin wax, placed into plastic moulds and left to cool until the paraffin block was set.

2.3.2 Sectioning

Paraffin blocks were removed from the mould and excess of wax trimmed around the sample. Blocks were then placed on a microtome (Leica, Nussloch, Germany) and serially sectioned at 5μm. Wax ribbons were floated in a water bath at ~45°C and collected on positive charged microscope slides (SuperFrost® Plus, VWR international, Leuven, Belgium), which allow electrostatic adhesion of the sections to the slide. Slides were placed in an oven at 62°C for 1 h until dry.

2.3.3 Hematoxylin-eosin staining

Slides were dewaxed in three steps of xylene and then rehydrated in decreasing concentrations of ethanol (from 100% to 50%) and then water. Nuclear staining was carried out by immersion of slides in hematoxylin for 2 min before slides were washed in tap water. In order to reduce hematoxylin intensity of the hematoxylin staining, slides were dipped for 5 sec in acid alcohol (1% HCl in 70% ethanol) followed by a tap water wash. Slides were submerged in 80% ethanol before proceeding with cytoplasmic staining with alcoholic eosin. Slides were then dehydrated by immersion into sequential steps of ascending concentrations of ethanol and finalizing with 2 steps of xylene. Slides were mounted with DPX (Fisher Scientific, Loughborough, UK)and left to dry overnight. Protocol is detailed in Table 2-3.

Table 2-3: Hematoxylin-eosin staining protocol for paraffin embedded sections

Step	Reagent	Time
Dewaxing	Xylene	3 steps: 8, 4 and 4 min
Rehydration	100% ethanol	2 steps: 3 min each
	90% ethanol	2 min
	70% ethanol	2 min
	50% ethanol	3 min
	Tap water	3 min
Staining	Harris hematoxylin	2 min
	Tap water (running)	5 min
	Acid alcohol	5 sec
	Tap water (running)	5 min
	Tap water	5 min
	80% ethanol	1 min
	Alcoholic eosin	1 sec
Dehydration	95% ethanol	30 sec
	100% ethanol	3 steps: 45 sec, 1 and 2 min
	Xylene	2 steps: 8 min each

Chapter 3: Fertility assessment of DM females reveals a delayed preimplantation development *in vivo*

3.1 Introduction

Oocytes from DM females have an altered zona pellucida (ZP), however DM females are fertile indicating that these glycans are not required for sperm-ZP binding (*119*, *129*, *130*). DM females are fertile at 6 weeks of age, yet they only produce one litter and the size of the litter is reduced around 50%. Just 6 weeks later, by 12 weeks of age, fertility is seriously compromised and DM females undergo failure of ovarian function evidenced by depletion of developing follicles, elevated gonadotropins and decreased sex steroid (*133*). Since the DM phenotype is consistent with clinical features of POF in women, this model presents an opportunity to study the onset of follicular POF.

The mechanisms underlying the abrupt change of phenotype in DM females from fertile at 6 weeks of age to POF at 12 weeks of age have not previously been studied. The fact that the deletion is restricted only to the oocyte makes the understanding of possible mechanisms even more challenging due to the fact that the oocyte is equally affected in 6 and 9 week old DM females. On the other hand, DM females have a smaller litter size when fertile at 6 weeks, which needs to be studied to understand the effect of the oocyte-specific deletion of *Mgat1* and *C1galt1* on the decreased number of pups observed in DM females.

3.2 Aims

- To analyse the fertility profile of DM females when fertile at 6 weeks and infertile at 9 weeks.
- To investigate the origin of the small litter size in DM females.
- To evaluate *in vivo* and *in vitro* preimplantation embryo development in DM females.
- To evaluate implantation capacity of embryos up to mid-gestation (9.5dpc).

3.3 Material and methods

3.3.1 Mice

Female mice with floxed *C1galt1* and *Mgat1* alleles and no ZP3*Cre* transgene (*C1galt1*$^{F/F}$ *Mgat1*$^{F/F}$) were used as Controls and females carrying floxed *C1galt1* and *Mgat1* alleles along with the ZP3*Cre* transgene (*C1galt1*$^{F/F}$ *Mgat1*$^{F/F}$:ZP3*Cre)* were used as Mutants. The protocols involving mice were in compliance with the Animals (Scientific Procedures) Act 1986, UK. Animals were maintained in a 12-12 light-darkness conditions and provided with food and water *ad libitum*.

3.3.2 Mating

Control and DM females aged 6 and 9 weeks were housed with fertile males for up to 2 weeks. Females were evaluated daily for presence of a vaginal plug, which was considered as evidence of mating. Females with vaginal plug present were removed from the mating cage and that morning was designated as 0.5 days post coitus (dpc). Females mated at 6 weeks of age were named as “6-week group” and females mated at 9 weeks of age were designated as “9-week group”.

3.3.3 Ovulation rate and Oocyte/zygote collection

Females were killed at 0.5 dpc and dissected oviducts were collected into warmed M2 medium (Sigma-Aldrich, Dorset UK). Oviducts were either opened or flushed and the zygotes and oocytes were counted.

3.3.4 *In vivo* preimplantation embryo development

To collect preimplantation embryos, the oviducts from 6-week females were dissected at 3.5 dpc and embryos were flushed with warm M2 medium. Embryos were morphologically evaluated using a Leica M125 microscope (Leica microsystems, Germany) and MicroPublisher 5.0 RTV camera (Qimaging, London, UK) and classified as blastocysts, morulae, and arrested or fragmented embryos.

3.3.5 *In vitro* embryo development

Zygotes at 0.5 dpc were obtained from 6-week females as described above (section 3.3.3) and cultured for 4 days in 50 μl drops of KSOM media (Millipore, MA, USA) supplemented with essential and non-essential amino acids (Gibco, Fisher Scientific, UK). Drops were covered with mineral oil (Sigma-Aldrich) to avoid evaporation during culture and incubated at 37°C in air with 5% CO_2. Fertilization rate was evaluated at 1.5 dpc by examining the number of 2-cell embryos and development was evaluated every 24h until the end of culture at 4.5 dpc. *In vitro* embryo culture was for 1 day longer than *in vivo* because embryo development *in*

vitro takes longer than *in vivo* (*135*). Morphological evaluation and classification of embryos was done as described for *in vivo* preimplantation development (section 3.3.4).

3.3.6 Implantation analysis

Implantation was evaluated in 6-week females at 5.5 dpc and 6.5 dpc. To support visualization of implantation sites at 5.5 dpc, females were injected into the heart with 100 μl of 1% Chicago Sky Blue (Sigma-Aldrich) in ddH_2O, and sacrificed 5 min later. Pentobarbitone was used as non-recovery anaesthesia during procedure. The uterine horns were removed and the number of implantation sites visible as blue dots recorded. Afterwards, uterine horns were flushed to recover non-implanted embryos. Implantation sites at 6.5 dpc were visualized directly without Chicago Sky Blue stain. At both time points, ovaries were dissected to determine the number of CL. Dr. Patricia Grasa collaborated on this experiment.

3.3.7 Post implantation analysis

Plugged 6-week females were sacrificed at 9.5 dpc and the number of deciduae counted. Deciduae were dissected and a morphological analysis of embryo development was performed. Ovaries were collected and dissected to determine the number of CL. Dr. Patricia Grasa mainly carried out this experiment.

3.3.8 Statistical analysis

Analysis was carried out using Prism software version 4.0b (GraphPad Software, Inc., version 4.0b, 2004. La Jolla, CA, USA). The Mann–Whitney U test was performed to detect differences between groups and the Pearson test was used to assess correlation.

The results described in this chapter were published (Appendix A) in collaboration with Dr. Patricia Grasa (*136*). For this study she carried out the ovulation rate and post-implantation experiments and analysis and I carried out the fertilization rate, *in vitro* and *in vivo* preimplantation development experiments and analysis. We also collaborated for some of the post-implantation experiments.

3.4 Results

3.4.1 Ovulation rate at 6-weeks is normal in DM females

It has been previously demonstrated that DM females have a small litter of around 4 pups when mated at 6-weeks but they are unable to produce a second litter (*119*, *133*). To assess if this small litter size is due to a diminished number of ovulated eggs, ovulation rate was evaluated at 0.5 dpc using 6- and 9-week DM females. Surprisingly, average ovulation rate at 6-weeks was not different between DM and Control females (7.5±0.8 and 8.3±0.2, Figure 3.1A). However, 3 weeks later, at 9-week, DM females exhibited a marked decreased in the ovulation rate compared with Control females (1.3±0.5 and 8.2±0.9, $P<0.0001$) meanwhile in the Control group, the ovulation rate remained constant (Figure 3.1B). There is a strong and significant negative correlation between age and ovulation rate in DM females ($r=-0.87$, $P<0.0001$, Figure 3.1C). This dramatic decrease in the ovulation rate showed by DM females at 9 weeks of age is most likely the single biggest factor contributing to the lack of a second litter in these females.

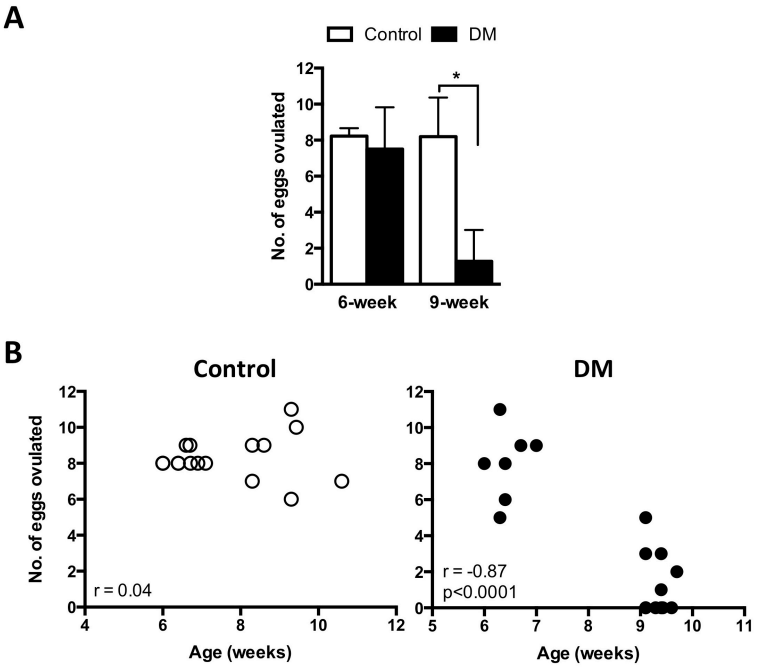


Figure 3.1: Ovulation rate of DM and Control females. (A) Ovulation rate in 6-week groups (results are expressed as mean ± SEM). (B) Correlation between ovulation rate and mice age in Control (n=16) and DM (n=18) groups. The ovulation rate was assessed as the number of zygotes/eggs collected from the oviduct at 0.5 dpc of DM and Control females mated at 6 (6-week group) and 9 weeks (9-week group). * *P*<0.001.

3.4.2 Fertilisation rate is not affected in DM females

Since DM females have a normal ovulation rate at 6 weeks compared with Controls, fertilisation rate was investigated in order to address the cause for the small size of the first litter. Zygotes from DM and Control females at 6 weeks of age were collected from the oviduct at 0.5 dpc and cultured. Fertilisation rate was confirmed and evaluated 24 h later by the presence of two-cell embryos. All

eggs/embryos in the DM group had an abnormal thinner ZP. Moreover, 30% of the DM zygotes lacked a ZP (Figure 3.2).

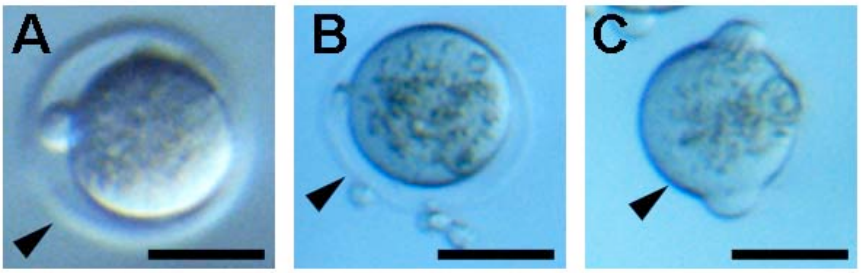


Figure 3.2: Zygotes at 0.5 dpc collected from (A) Control and (B-C) DM females. Arrowhead indicates (A) normal ZP, (B) thinner and abnormal ZP and (C) complete absence of ZP. Bar scale 50 μm.

Despite the abnormal ZP present in these zygotes, the percentage that developed to two-cell stage was the same as Controls (Figure 3.3).

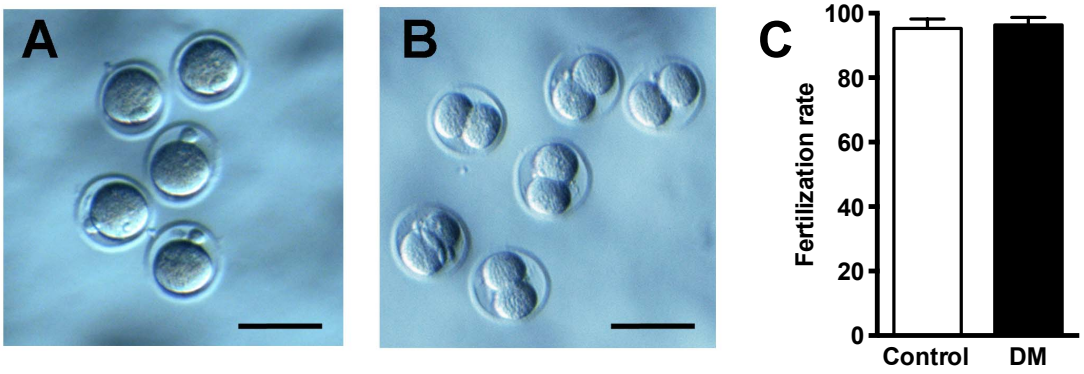


Figure 3.3: Fertilisation rate. Zygotes collected from Control (n=12 females, 91 zygotes) and DM (n=6 females, 40 zygotes) females at 0.5 dpc were cultured *in vitro* and fertilization rate assessed at 1.5 dpc by evaluating the number of two-cell embryos. Representative images of (A) Control zygotes collected at 0.5 dpc and (B) two-cell embryos after 1 day of culture. Results are expressed as mean ± SEM. Bar scale 100 μm.

3.4.3 *In* vitro preimplantation embryo development is normal in DM females

Since fertilisation rate was not the cause for the decreased litter size in DM females, preimplantation embryo development was evaluated. The number of embryos collected and the proportion of embryos at each stage at the end of culture were similar between DM and Control females despite the abnormal ZP found in embryos from DM females (Figure 3.4).

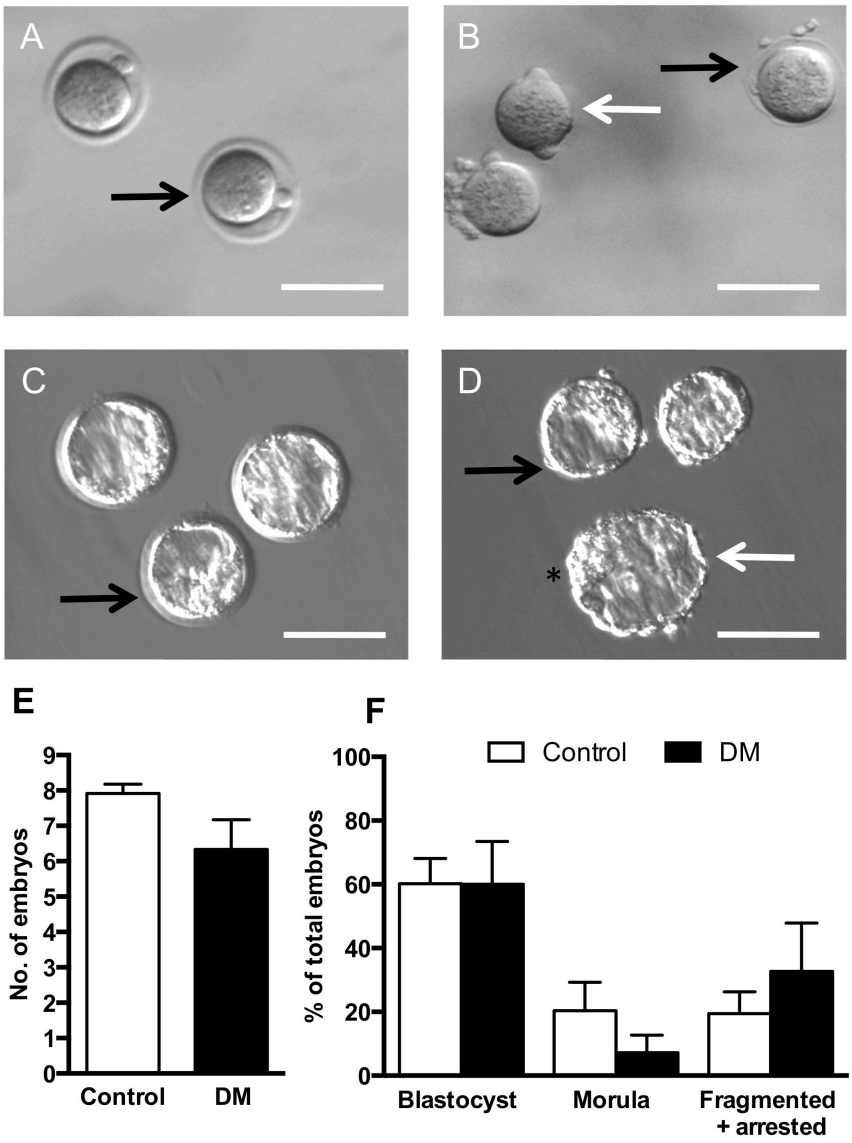


Figure 3.4: Preimplantation embryo development *in vitro*. Embryos cultured *in vitro* from Control (A and C, n=12 females, 91 zygotes) and DM females (B and D, n=6 females, 40 zygotes). Zygotes/eggs collected at 0.5 dpc (A and B) and blastocyst at the end of culture at 4.5 dpc (C and D). Asterisk in (D) indicates a bigger blastocyst that seems to have resulted from the fusion of two embryos because the number of embryos presented in this dish was reduced by one at the end of the culture. (E) Number of embryos collected from Control and DM females at 0.5 dpc. (F) Proportion of blastocysts, morulae and fragmented and arrested embryos at the end of culture. Results are expressed as mean ± SEM. Bar scale 100 μm.

3.4.4 In vivo preimplantation embryo development is altered in DM females

In vitro culture offers a controlled environment that could support preimplantation embryo development better than *in vivo* embryo development. The altered ZP observed in embryos from DM females could lead to an abnormal development and/or transport of the embryos from the oviduct to the uterus and ultimately embryo loss. This may be an explanation for the small litter size in DM females. To assess this hypothesis, embryos were collected from 6-week plugged females at 3.5 dpc. The first remarkable finding was that only 45.5% of plugged DM females contained embryos when dissected compared with 100% of Control females, despite the fact that DM females have a normal ovulation rate. The number of embryos recovered from DM females that did have embryos, was lower than Controls (3.2±1.3 and 7.0±0.6, respectively) as well as the number of blastocysts (DM=1.2±0.5 and Control=5.8±0.8). The percentage of embryos that were at the blastocyst stage in the Control group was 81.2% whereas in the DM group the percentage of blastocyst was 42.5%. However, 40 % of the embryos from the DM group were morulae compared with 11.7% in the Controls, indicating delayed embryo development in the DM group (Figure 3.5).

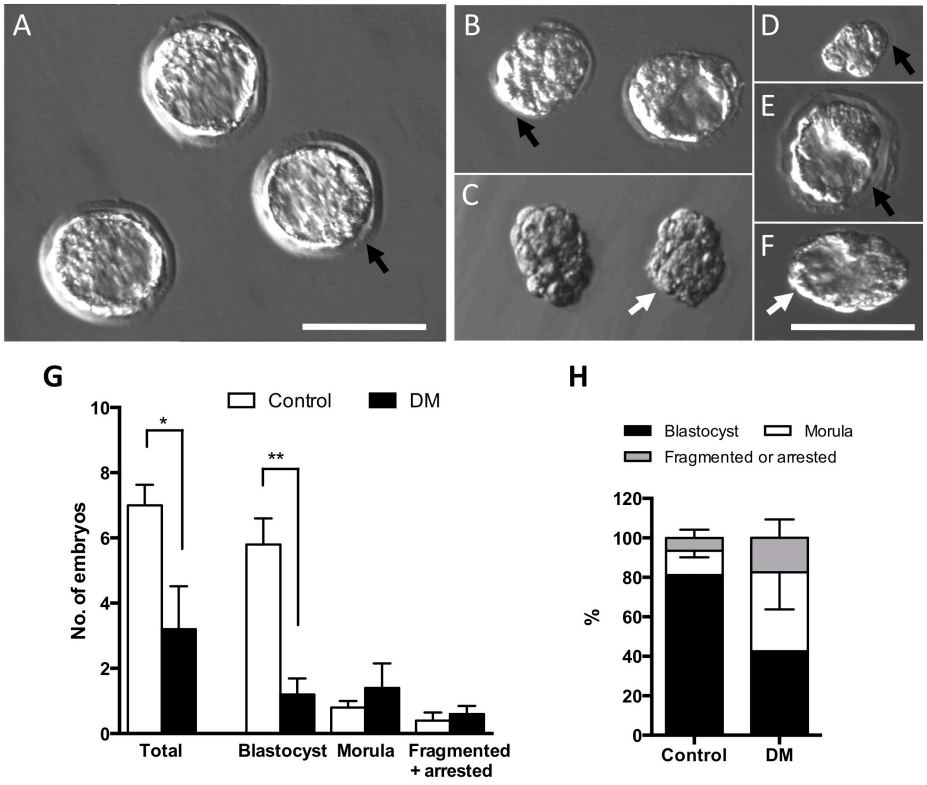


Figure 3.5: *In vivo* preimplantation development at 3.5 dpc. Embryos collected at 3.5 dpc from the uterus of (A) Control (n=5 females, 46 embryos) and (B-F) DM (n=5 females, 32 embryos) females. (A) Normal blastocysts, (B) blastocyst and morula, (C) morulae, (D) arrested four-cell stage embryo, (E) blastocyst with abnormal ZP and (F) blastocyst without ZP. Black arrow indicates ZP; white arrow indicates absence of ZP. (G) Number of embryos collected from Control and DM females at 3.5 dpc. (H) Proportion of blastocysts, morulae and fragmented and arrested embryos from Control and DM females at 3.5 dpc. Results are expressed as mean ± SEM. Bar scale 100 μm. *P=0.05; **P<0.01.

3.4.5 Implantation is delayed in DM females

The delayed development of embryos from DM group revealed by the increased percentage of morulae was investigated further in order to evaluate the implantation capability. Females dissected at 5.5 dpc had a decreased number of implantation sites, 1.3±0.4; around half the embryos collected at 3.5 dpc. To evaluate this apparent delay in the implantation process, females were dissected 24 h later at 6.5 dpc. Interestingly, the number of implantation sites were 3.2±1.0, more than double that at 5.5 dpc and consistent with the number of embryos recovered at 3.5 dpc (Table 3-1).

Table 3-1: Implantation sites at 5.5 and 6.5 dpc.

		CONTROL	DM
5.5 dpc	**n**	8	4
	Age of females (wks)	6.5 ± 0.1	6.4 ± 0.0
	Implantation sites	7.3 ± 0.6	**1.3 ± 0.4 ****
6.5 dpc	**n**	4	5
	Age of females (wks)	6.7 ± 0.2	6.3 ± 0.1
	Implantation sites	7.8 ± 0.3	**3.2 ± 1.0 ****

** *P*<0.01 compared with Control

3.4.6 Postimplantation embryo development progressed normally in DM females

To evaluate the progress of the delayed embryo development until mid-gestation, 6-week females were dissected at 9.5 dpc. DM females contained less implantation sites than Control females (3.0±0.6 and 7.6±0.5. *P*<0.05; Figure 3.6A) and this number was consistent with the number of embryos recovered at 3.5 dpc (3.2±1.3; Figure 3.5G) and the number of implanted embryos at 6.5 dpc (3.2±1.0; Table 3-1). Embryos in the deciduae were also evaluated and classified as normal or abnormal according to the gross morphology (Figure 3.6B-C). No significant differences were found between the proportion of normal and abnormal embryos between Control and DM females (Figure 3.6C).

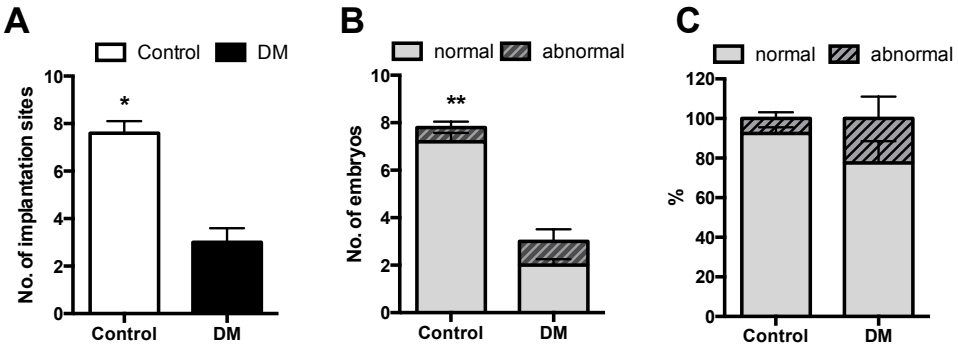


Figure 3.6: Post-implantation embryos at 9.5 dpc. Control (n=5 females) and DM (n=6 females) females were dissected at 9.5 dpc and deciduae were counted and dissected. (A) Number of implantation sites evaluated in the Control and DM groups. (B) Number of normal and abnormal embryos obtained from Control and DM females. (C) Proportion of normal and abnormal embryos obtained from Control and DM females. Results are expressed as mean ± SEM. **P*<0.05, ***P*<0.001.

3.5 Discussion

Previous studies have demonstrated that oocyte-specific deletion of *Mgat1* and *C1galt1* in the DM mouse produce a POF phenotype by 12 weeks of age (*119*, *133*). Although these females are fertile when they reach puberty at 6 weeks of age, they produce only one small litter (*119*). To determine the origin of the small litter size, ovulation rate and embryo development were analysed. Unexpectedly, the 6-week DM female group have a normal ovulation rate compared with Controls however, ovulation rate decreased dramatically 3 weeks later, at 9-week, demonstrating that the onset of POF could be even earlier than previously published (*119*, *133*). When DM females were mated at 6 weeks of age, they produce only a single small litter (*119*) although, on average they ovulate normal numbers of eggs, the number of eggs ovulated per female is highly variable. This finding is consistent with the presence of morphologically normal follicles in 6-week DM ovaries, although ovaries also contain some follicular abnormalities such as follicles containing oocytes lacking ZP and cumulus cells or empty follicles (*133*). Therefore, the most likely explanation for the severe decline in ovulation rate from 6 to 9 weeks observed in DM females, is an accumulative defect in follicle development that gets more severe with age, explaining the lack of a second litter in these females.

Since the cause for the smaller litter size observed in 6-week DM females is not a decreased ovulation rate, preimplantation development was studied. Analysis of *in vitro* preimplantation development revealed that eggs from 6-week

DM females have a normal fertilisation rate compared with Controls and their embryos develop normally until the blastocyst stage. On the other hand, when *in vivo* preimplantation embryo development was evaluated at 3.5 dpc, only 45.5% of mated DM females contained embryos, despite the fact that ovulation rate is normal in DM 6-week females. Surprisingly, the number of embryos at 3.5 dpc was around half the ovulation rate 3 days earlier, revealing a considerable loss of embryos surviving during early embryogenesis. Furthermore, embryo development in those embryos that did survive in DM females was delayed, with an increased proportion of embryos at the morula stage while the majority of embryos from Control females had reached blastocyst stage. These data indicate that the lack of complex *N*- and *O*-glycans during oocyte development results in a substantial decrease in embryo viability *in vivo* with an associated decrease in female fertility. This delayed development of embryos from DM females was not unexpected as embryos generated from oocytes lacking only complex *N*-glycans are also retarded (*129*). Since, *in vitro* development is normal in embryos from DM females with the same proportion of blastocysts as embryos from Controls, it can be inferred that *in vivo* development in embryos from DM females is affected by factors not present *in vitro.* These factors can be either intrinsic to the embryo or resulting from a modified environment of the reproductive tract of DM females, since embryo development can be affected by both, oocyte quality and the environment in which the embryo develops (*26*, *135*, *137*). During the transit through the oviduct, embryos within the protective coat of the ZP undergo cleavage, compaction and cavitation before developing into a blastocyst.

Blastocysts then hatch from the ZP and implant in the endometrial lining of the uterus (*138*). In the mouse, the ZP consists of three proteins: ZP1, ZP2 and ZP3, which are glycosylated with complex *N*- and *O*-glycans (*5*). The lack of *N*- and *O*-glycans in DM oocytes, results in a defective ZP structure and thus DM ZP is thinner and more fragile than Control ZP (*119*). All embryos from DM females analysed in this study exhibited an altered or absent ZP. The absence of ZP was most likely due to a loss of the ZP either during ovulation or whilst in transit to the uterus. A critical role for the ZP in preventing adherence of developing embryos to the oviduct has been demonstrated by analyzing ZP-free eggs and embryos that were reintroduced to the oviduct (*4*). Furthermore, removal of the ZP from 8-cell and blastocyst embryos has a detrimental effect in their developmental potential (*139*). In addition, the ZP has been demonstrated to be essential to maintain embryo competency before and after morula compaction (*140*, *141*), to contribute to DNA methylation (*142*) and has been used as a marker of implantation success of human embryos (*143-145*). Finally, embryo lethality induced by shear stress (caused by the movement of fluid over the surface of cells) is accelerated by ZP removal (*146*). Based on these studies, it is likely that the altered thickness or absence of a functional ZP in DM embryos has a role in the aberrant early embryogenesis *in vivo* and could be the cause of the early embryonic loss. Accordingly, the normal *in vitro* preimplantation development exhibited by embryos from DM females, may be because the weak ZP remains intact around the embryo during the controlled culture conditions, allowing progress of embryo development.

In vitro analysis revealed one unexpected occurrence of embryo fusion in embryos from DM females. Although five DM zygotes were present at the beginning of the culture, at the end, only four embryos were present including one abnormally large blastocyst (Figure 3.4D). Fusion of two of the ZP-free embryos is the only logical conclusion in the absence of a degenerating embryo. The formation of natural chimeras has been described in mammals, including humans (*147*). Although chimeric embryos can be generated by injection of stem cells into blastocysts, they can also be generated *in vitro* by aggregation of embryonic stem cells with denuded morulae (*148*, *149*) or by aggregation of ZP free cleavage embryos (*150*) . Although our data indicate that this phenomenon can occur in ZP-free DM embryos *in vitro*, its occurrence *in vivo* is unknown. However, it is unlikely to be involved in the decreased number of embryos and pups observed in DM females, as none of the embryos collected at 3.5 dpc were abnormally large.

In this study a delay in embryo development was observed *in vivo* at 3.5 dpc in embryos from DM females, revealed by the high proportion of morula-stage embryos compared with Controls. As a result, a delay in implantation was also observed in DM females. At 5.5 dpc an equivalent to a third of the number of the embryos recovered at 3.5 dpc were implanted (Table 3-1). However, 1 day later at 6.5 dpc, the number of embryos implanted was equivalent to the number found at 3.5 dpc, consistent with a delay implantation in DM females. In addition, the number of implantation sites by mid-gestation, evaluated at 9.5 dpc, was equivalent to the number of embryos collected at 3.5 dpc, the number of

implantation sites at 6.5 dpc and with the small litter size reported previously on DM females (*119*). Implantation is a complex and highly regulated process and only possible during a limited time frame, named the implantation window, in which the uterus is receptive to a competent embryo. This process requires molecular interactions between the blastocyst and the receptive uterus, which has been described in many species including mice and humans (*151*, *152*). Interestingly, the delay in embryo development observed at 3.5 dpc in this study had no impact on subsequent implantation, since the number of implantation sites at 9.5 dpc was equivalent to the number of preimplantation embryos collected at 3.5 dpc. Ueda *et al* (*153*), transferred both, zygotes and eight-cell embryos simultaneously into the uterus of pseudo-pregnant recipient mice on day 0. Both groups of embryos implanted and had synchronized their development at around 162 h post-transfer, revealing that the "window of implantation" could be expanded. This may explain why all the blastocysts and morulae found at 3.5 dpc in DM females are able to implant over an extended period.

In summary, the results in this chapter reveal that the lack of complex *N*- and *O*-glycans during oocyte development impairs embryo preimplantation development and viability *in vivo*, leading to delayed development, implantation and as a result; a small litter size in DM females. Accordingly, the small litter size observed in DM females is most likely due to the altered ZP displayed by embryos from DM females.

Chapter 4: A normal endocrine environment is not able to support follicle development after the onset of POF in the DM mouse assessed using ovarian transplantation

4.1 Introduction

DM females develop POF by 3 months of age characterized by deletion of developing follicles due to a block in follicle development at the primary stage of follicle development at the 3a-3b transition (*133*). The endocrine profile is also altered in DM females at 3 months of age with DM females displaying elevated FSH and decreased testosterone and inhibin A in sera (*133*). Even though, the altered endocrine profile displayed by DM females is likely to be a consequence rather than a cause of the POF, it could potentially be contributing to the altered follicle development.

In normal physiological conditions, the sexual steroids produced in the ovary support follicle development. The theca cell and the granulosa cell compartments coordinate ovarian steroidogenesis in a synchronized manner to produce estrogen, explained by the two-cell two-gonadotropin model (described in Chapter 1). Androgens (testosterone and androstenedione) are synthetized in the theca cell layer of the follicle stimulated by LH. These androgens cross the basal lamina and diffuse into the granulosa cells that under FSH stimuli produce the enzyme aromatase to convert androgens into estradiol; essential for follicle development (*154*, *155*). At the same time, FSH secretion is downregulated by inhibin A, which is secreted by the granulosa cells and the corpus luteum under FSH stimulation (*156*, *157*).

The endocrine profile of DM females is likely to be produced by an altered ovarian steroidogenesis (Figure 1.9, Chapter 1). Firstly, the elevated FSH levels are consistent with lower levels of inhibin A and B, therefore a reduced negative feedback of the FSH secretion. In addition, testosterone levels were also decreased in DM females, however estradiol levels although decreased were not significant compared to Control. Lower levels of estradiol were expected in DM females since testosterone is a source for estradiol synthesis. A possible explanation for the unaltered levels of estradiol could be that aromatisation in the granulosa cells is less effective for testosterone than for androstenedione (*158*). Another unexpected finding was that progesterone levels showed no differences between DM and Controls despite the fact that by 3 month DM females do not ovulate and therefore ovaries lack corpora lutea (Figure 1.5 Chapter 1). Authors ascribe this finding to the fact that DM ovaries at 3 months occasionally contain some corpora lutea and ovaries display a considerable amount of luteinized tissue that expressed 3β-HSD enzyme (*133*). Even though unexpected, the normal level of progesterone in DM females is consistent with the unchanged level of LH, since progesterone inhibits LH secretion.

In women with POF, there is evidence that hormonal intervention could recover ovarian function in terms of restoring ovulation and achieving of pregnancy. Recently in 2014, a woman with Blepharophimosis, ptosis, epicanthus inversus syndrome type I (BPES type I), a genetic disorder caused by a mutation in the *FOXL2* gene, recovered ovarian function, achieved pregnancy and delivered healthy twin babies after ovarian stimulation with gonadotropins (*159*). BPES type

I is a rare condition characterized by eyes abnormalities and POF, which is consistent with the fact that mutations in the *FOXL2* gene are one of the few known causes of POF in women (*160*). Even though in this case the treatment with gonadotropins successfully reactivated follicle development, authors are cautious with their results, since POF associated with BPES type I may not follow the same clinical course as idiopathic POF.

Another report in 2013 describes successful ovulation and pregnancy after ovarian stimulation of a woman with idiopathic POF and undetectable levels of Anti-Müllerian Hormone (AMH) (*161*). A normal karyotype, normal uterus but undetectable ovaries by ultrasonography and very low levels of AMH supported the diagnosis of idiopathic POF in this woman. AMH is expressed in the granulosa cells of the primary follicles soon after primordial follicles are recruited from the dormant pool (*162*) and therefore its levels are a reflection of follicle development (*163*). The hormone treatment used in this case was an initial estrogen replacement therapy (ERT) plus GnRH agonist followed by human menopausal gonadotropin (hMG) for ovarian induction, which was applied along with the ERT. After detection of one big antral follicle by ultrasound, the patient was injected with human chorionic gonadotropin (hCG) to induce ovulation and advised to have coitus the following day. Pregnancy test was positive 14 days after hCG injection and was confirmed by ultrasonography 2 weeks later. The pregnancy was ongoing when the report was published.

In summary, the altered endocrine profile observed in DM females at 3 months of age is consistent with POF and could potentially be an important factor contributing to the quiescent state of the DM ovaries and lack of follicle development. In this sense, a normal hormonal environment could restore follicle development and ultimately fertility in this mouse model.

4.2 Aims

- To evaluate if the presence of a normal endocrine environment could restore normal follicle development in DM ovarian tissue.
- To assess if the block of follicle development of 3a stage follicles could be released in a normal endocrine environment

4.3 Materials and methods

4.3.1 Ovary transplantation under the kidney capsule

4.3.1.1 Preparation of donor tissue

Nine to 10 week old DM and Control females were selected as ovary tissue donors. Mice were killed by cervical dislocation and ovaries removed and placed in warm sterile L-15 Leibovitz media (Hyclone, Thermo Scientific, Utah, USA) supplemented with 3 mg/ml of BSA. The bursa and any additional non-ovary tissue were carefully removed. Since DM ovaries are about half the size of Control ovaries, ovaries from Control females were cut into quarters and ovaries from DM donors were cut into halves in order to match the size of the transplanted tissue between groups. One of the ovary pieces was selected for transplantation and placed in fresh warm sterile medium meanwhile the recipient was prepared for surgery. A second piece of tissue of the same ovary was fixed and histologically processed to evaluate the transplanted tissue.

4.3.1.2 Recipients for transplantation

Recipients for transplantation were C57BL/6 mice (n=39) or either Control non-sibling females (n=2) or Control sibling females (n=13) of the donor mice. Mice were anesthetised in an induction chamber using 4% isoflurane and 2.5 litres per minute (LPM) of oxygen. Once the animal was under anaesthesia, it was

moved to the anaesthesia mask with 2-2.5% of isoflurane and 1 LPM of oxygen. The surgical area was prepared by removing the fur with clippers and cleaning the area aseptically with a chlorhexidine solution, then the anesthetised animal was placed on a heated pad at 37°C and injected subcutaneously with 0.05 - 0.1 mg/kg of Buprenorphine (Vetergesic, Alstoe Limited, York, UK) to provide analgesia after surgery. Depth of anaesthesia was assessed using the pedal withdrawal reflex. Once the absence of the reflex was confirmed in the anesthetized mouse, the surgical procedure was initiated.

4.3.1.3 Surgical procedure

Under magnification, the left kidney was exteriorised through a dorso-lateral incision and a small opening on the kidney capsule made using a pair of fine tip forceps. A sterile fine tip plastic pipet was used to place the ovary tissue under the capsule and to gently push the ovary tissue away from the capsule opening. The kidney was placed back inside the body cavity and the body wall and skin closed with interrupted suture. The animal was placed in a warm recovery chamber and evaluated constantly until fully recovered from anaesthesia, for approximately 20 minutes. Two hours after surgery animals were returned to the animal house maintenance room and they were evaluated daily for signs of distress and infection for the first week after the surgery. During the first 48 h after surgery, mice had easy access to food pellets, mashed pellets, water and

medicated jelly with meloxicam to provide analgesia (Metacam, Boehringer Ingelheim, Bracknell,UK).

4.3.2 Assessment of follicle development

Mice were killed 2, 3 and 4 weeks after transplantation and the transplanted ovarian tissue retrieved and fixed overnight in 10% buffered formalin (Sigma). After fixation, tissue was placed in 70% ethanol and stored at 4°C until paraffin embedded. Tissue was sectioned and every 10^{th} section collected onto a separate slide, stained with haematoxylin and eosin and follicle numbers determined according to Pedersen and Peters (*16*) (Figure 1.2, Chapter 1). This follicle classification is based on the number of granulosa cells through the central section of a follicle and morphology. The original Pedersen and Peters classification proposed 8 follicle categories that were grouped to the following commonly known groups: primordial follicles: types 1 and 2; primary follicles: types 3a and 3b; secondary follicles: type 4; preantral follicles: types 5a and 5b; antral follicles: types 6, 7 and 8 (Figure 4.1). Some follicles at 5a and 5b stages developed an early antrum in Control and DM grafted tissue. Even though granulosa cell number is consistent with the preantral stage, these follicles were classified as antrals.

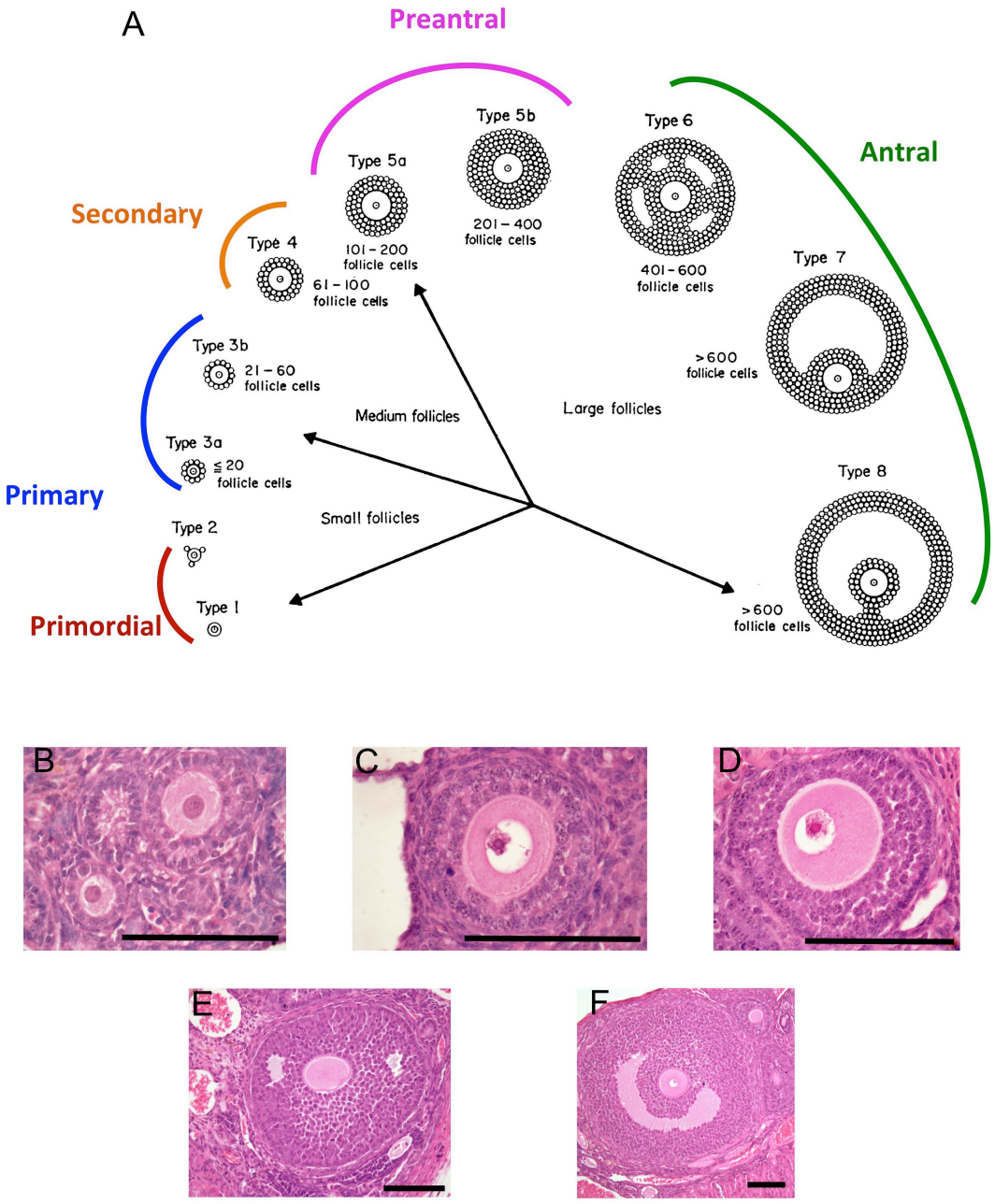


Figure 4.1: Follicle classification. (A) Classification of follicles according to Pedersen and Peters (1968). (B-F) Representative images of different types of follicles obtained from the grafted ovary tissues 4 weeks after transplantation. (B) Primaries, (C) secondary, (D) preantral, (E and F) antral follicles. Bar scale 100 μm.

4.3.3 Area measurement and follicular density

The area in the section of grafted tissue analysed for follicles counts was determined using ImageJ software (version 1.46r, National Institutes of Health, USA). All sections used for follicle counts (one every 10^{th} section) were photographed and images were used to measure the total area of the tissue, using the freehand selection tool of the software. The addition of all area measurements constitutes the total area of the grafted tissue analysed. This variable along with the follicle counts was used to determine the follicular density in all Control and DM grafted tissues.

4.3.4 Statistical analysis

Analysis was carried out using Prism software version 4.0b (GraphPad Software, Inc., version 4.0b, 2004. La Jolla, CA, USA). The Mann–Whitney U test was performed to detect differences between groups with equal variances. Kolmogorov-Smirnov test was carried out when unequal variances were detected.

4.4 Results

4.4.1 Establishment of the technique: C57BL/6 females and Control non-sibling females are unable to support growth of the grafted tissue

Since the strain background of the DM mouse is 129/B6, dominant in C57BL/6, for the first set of experiments 6 to 8 weeks old C57BL/6 mice were used as recipients of the transplanted tissue. The grafted ovaries were retrieved 2, 3 and 4 weeks after transplantation to establish the optimal time frame for the transplant to generate developing follicles. C57BL/6 mice were unable to support the grafted tissue and signs of rejection were present in all of the Control and DM transplants (n=39). Assessment of the Control transplanted tissue before transplantation revealed that all donor Control ovaries were histologically normal and follicles in different stages of follicle development were found (Figure 4.2A). However, grafted ovarian tissue retrieved 2, 3 and 4 weeks after transplantation exhibited evident signs of tissue rejection including, lymphocytic infiltration and abnormal ovarian morphology with absence of normal follicles (Figure 4.2B-F).

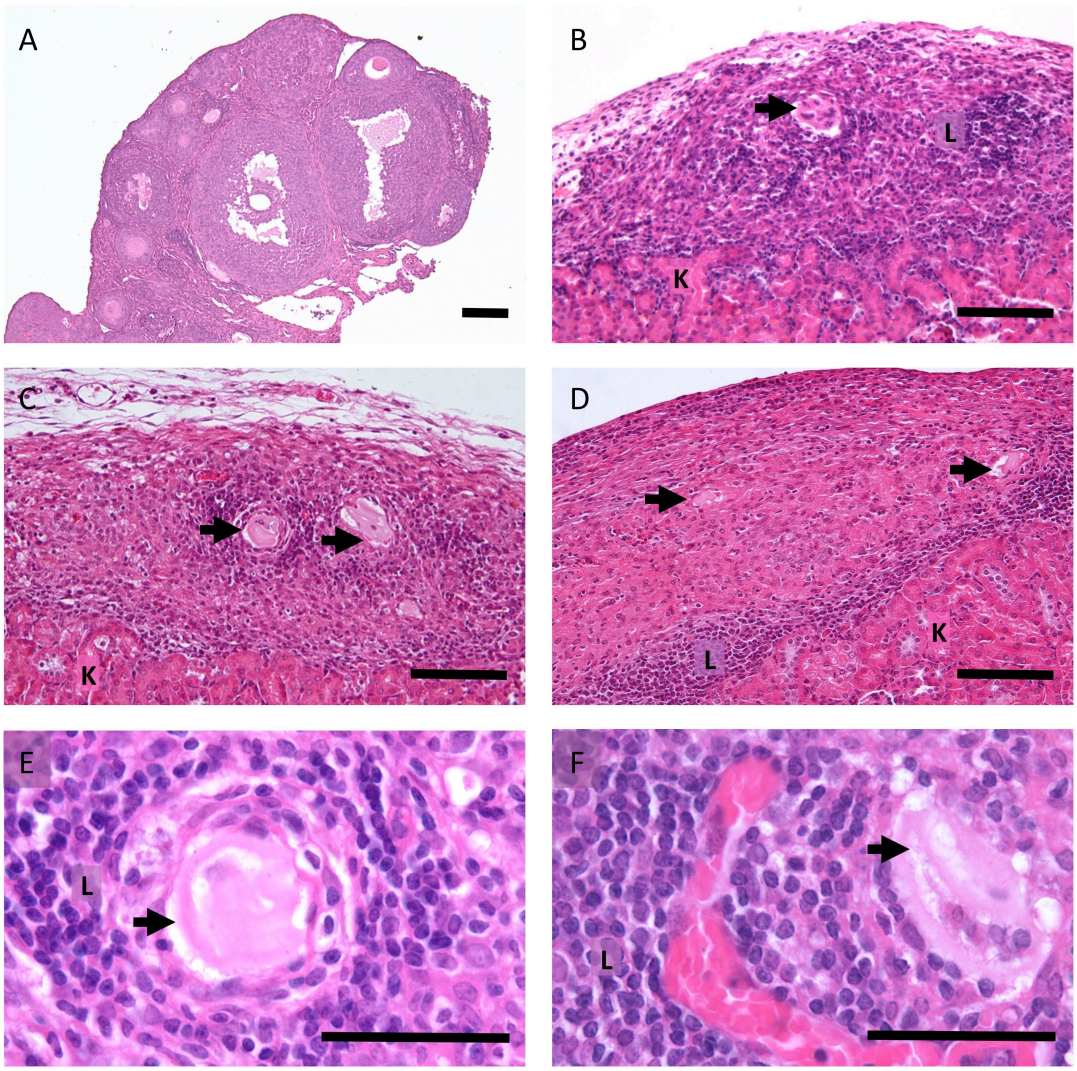


Figure 4.2: C57BL/6 recipients rejected ovary graft from 9-week Control donors. (A) Representative section of Control 9-week donor ovary displaying all types of follicles. Signs of rejection of the Control tissue determined by absence of normal follicles and lymphocyte infiltration were found at (B) 2 weeks, (C) 3 weeks and (D) 4 weeks after the transplantation. Detailed abnormalities of the oocytes and presence of a lymphocytic infiltration can be observed in E and F. Cl: corpus luteum, AF: antral follicle, L: lymphocytic infiltration, K: kidney tissue, asterisk: follicles, arrows: damaged oocytes. Bar scale 100 μm.

Since C57BL/6 females were unable to support the grafted ovarian tissue, a second set of transplants was carried out using Control mice from the DM colony as recipients since these were of the same mixed strain background. To select the best donor, non-siblings (n=2), siblings (n=3) and littermates (n=2) of the donors were tested as recipients. Four weeks after the transplant the tissue was retrieved and analysed as before. Non-sibling Control recipients, did not supported graft development since signs of tissue rejection were found in the grafted tissue. The same signs of rejection observed in the tissue transplanted to C57BL/6 recipients were detected in both, Control and DM donor tissues: lymphocytic infiltration and histological features non-compatible with the morphology of the ovary and follicle-like residual structures (Figure 4.3 A and B). However when Control siblings and littermates of donors were used as recipients, the grafted tissue developed normally and all classical features of the ovary morphology were observed in both, Control (Figure 4.3 C and E) and DM (Figure 4.3 D and F) grafts. For the following experiments, only sibling or littermate Control females were selected as recipients.

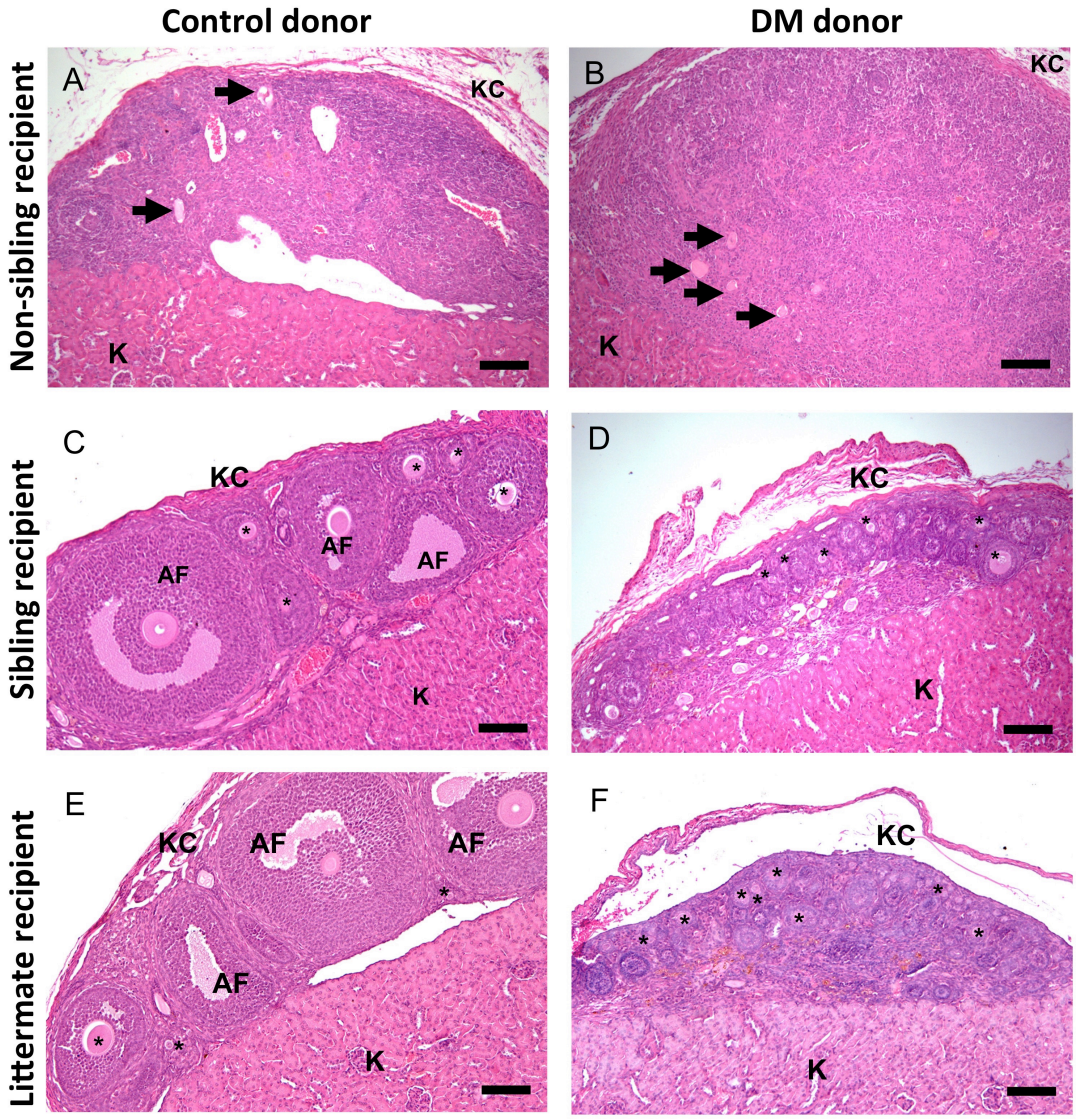


Figure 4.3: Compatibility test between recipients and donors within the DM colony 4 weeks after transplantation. Non-sibling Control recipients of the donors exhibited tissue rejection of the transplanted tissue (A and B). Siblings (C and D) and littermates (E and F) of the donors were able to support the grafted ovarian tissue. (A, C, E) Control donor, (D, E, F) DM donor. AF: antral follicle, KC: kidney capsule, K: kidney tissue, asterisk: follicles, arrows: degenerated oocytes. Bar scale 100 μm.

4.4.2 Morphology of the grafted tissues 4 weeks after transplantation

Analysis of the Control sibling-grafted tissue (n=5) revealed morphology comparable with the 9-week Control tissue when transplanted, 4 weeks earlier (Figure 4.4 A and B). All stages of follicle development were present in the Control tissue, from primordial to large antral follicles (Figure 4.4 B-D), while DM grafted tissues (n=8) exhibited follicles up to primary stage of follicle development with depletion of follicles from secondary stage onwards (Figure 4.5 C and D). Similar to Control grafted tissues, the morphology of DM grafted tissues is equivalent to the 9-week DM ovarian tissue prior to the transplantation (Figure 4.5 A and B). No signs of rejection were found in either Control or DM grafted tissues.

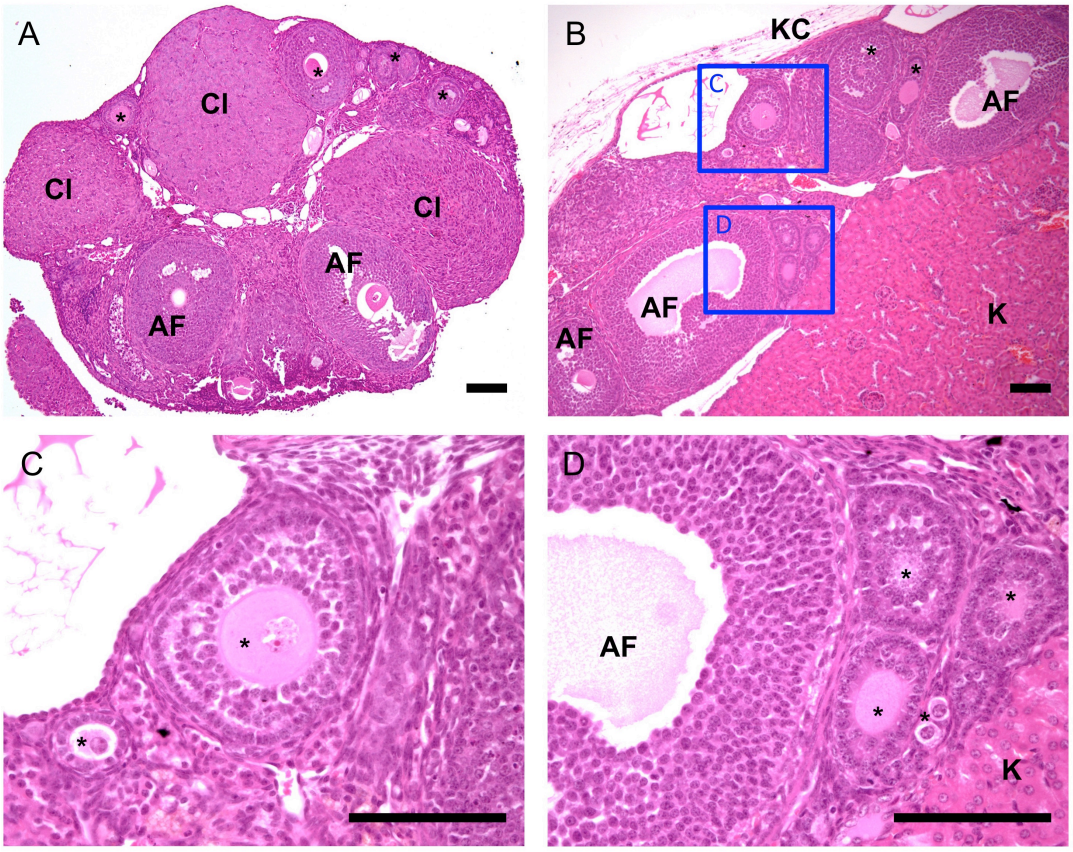


Figure 4.4: Control sibling-grafted tissue. (A) Morphology of a Control ovary before the transplantation displaying classical features of a normal ovary with all types of follicles and corpora lutea present. (B) The grafted tissue 4 weeks after transplantation presented normal morphology and all stages of follicle development. C and D show in detail the different types of follicles observed in B, (C) primary and secondary follicles and (D) primordial, secondary and antral follicles. AF: antral follicle, Cl: corpus luteum, KC: kidney capsule, K: kidney tissue, asterisk: follicles. Bar scale 100 μm.

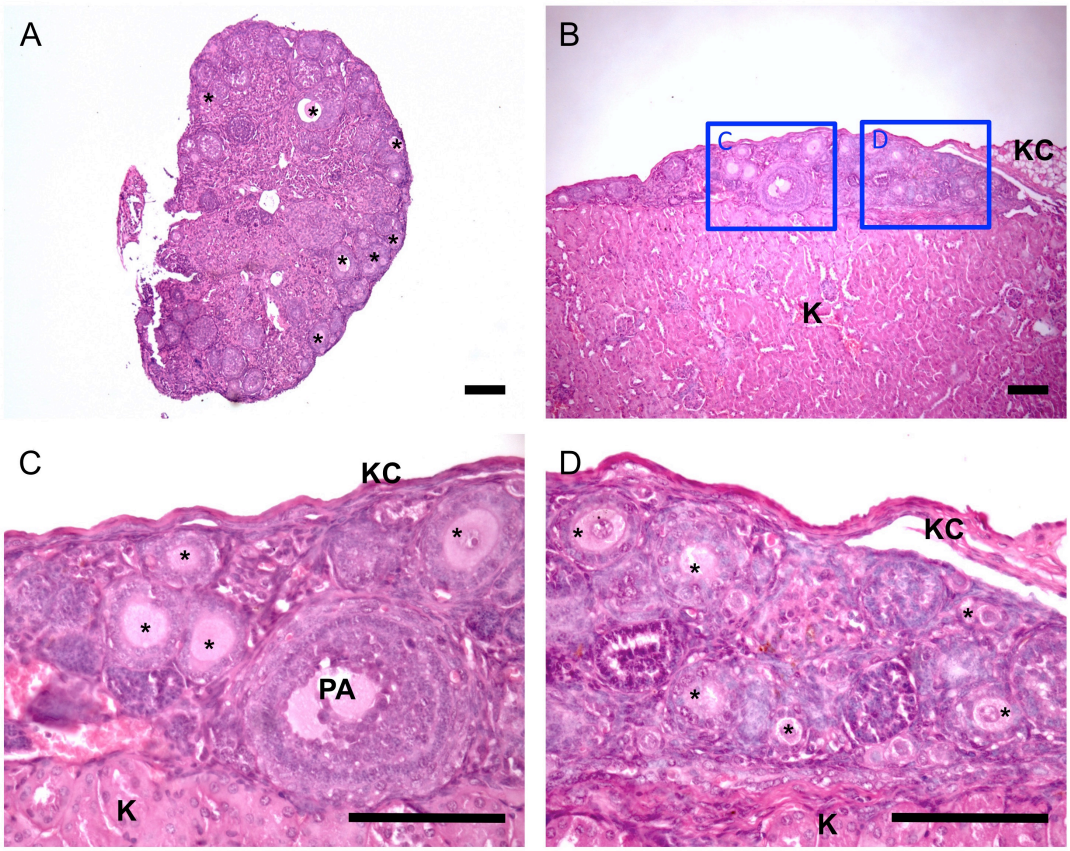


Figure 4.5: DM sibling-grafted tissue. (A) Morphology of DM ovary before the transplantation displaying classical features of a 9-week DM ovary: presence of developing follicles and absence of growing follicles. (B) The grafted tissue 4 weeks after transplantation exhibited morphology comparable with 9-week DM ovaries. C and D show in detail some of the follicles observed in B. The majority of the follicles existing in the grafted tissue were primary (C and D) meanwhile a depletion of the following stages of follicle development was observed with an early preantral follicle observed in C. PA: preantral follicle, KC: kidney capsule, K: kidney tissue, asterisk: follicles. Bar scale 100 μm.

4.4.3 Follicle counts revealed the absence of developing follicles after transplantation in DM explants

No differences in the total number of developing follicles were detected between Control and DM grafted tissues (Figure 4.6A). However, the total tissue area analysed was significantly smaller in DM compared with Controls (Figure 4.6B), consequently the follicular density of the grafted tissue, represented as total number of follicles per mm^2 was significantly bigger in DM than Controls (Figure 4.6C).

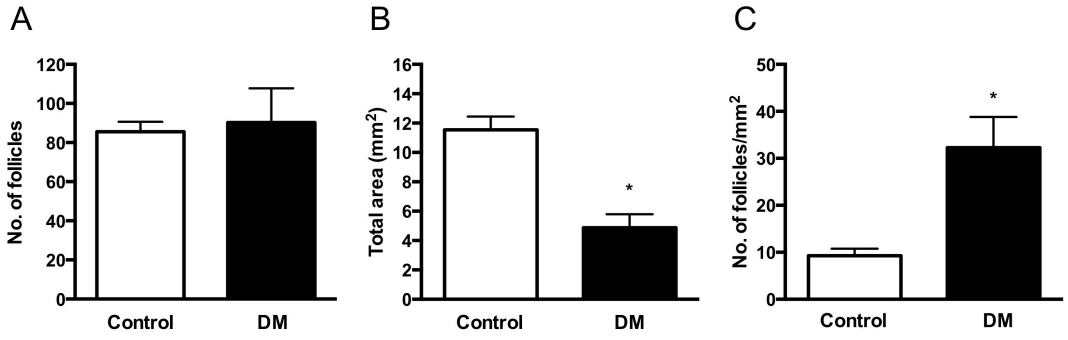


Figure 4.6: Total follicle counts 4 weeks after transplantation. (A) Total number of follicles in Control (n=5) and DM (n=8) grafted ovarian tissue. (B) Total area of the grafted tissue analysed in Control and DM. (C) Density of follicles per mm^2 of grafted ovarian tissue analysed in Control and DM. Results are expressed as mean ± SEM.* $P<0.05$.

Developing ovarian follicles were counted and classified according to Pedersen and Peters criteria (*16*) and then grouped as primary, secondary, preantral and antral (Figure 4.1). The follicle development profile of the Control and DM grafted ovarian tissue was similar, exhibiting an increased number of follicles in primary stage followed by a marked decrease of all later stages of follicle development (Figure 4.7). Even though, Control grafts contained a reduction in follicle numbers from secondary stage onwards, these stages of follicle development were equally represented in the tissue. However, in DM grafted tissue follicle counts from secondary stage onwards were very low with mean counts just above zero. The number of follicles at all stages of follicle development were lower in DM compared with Control, except for primary stage were DM follicle number was higher than Control, however due to the high variability among DM group samples, this difference did not reached statistical significance (P=0.17).

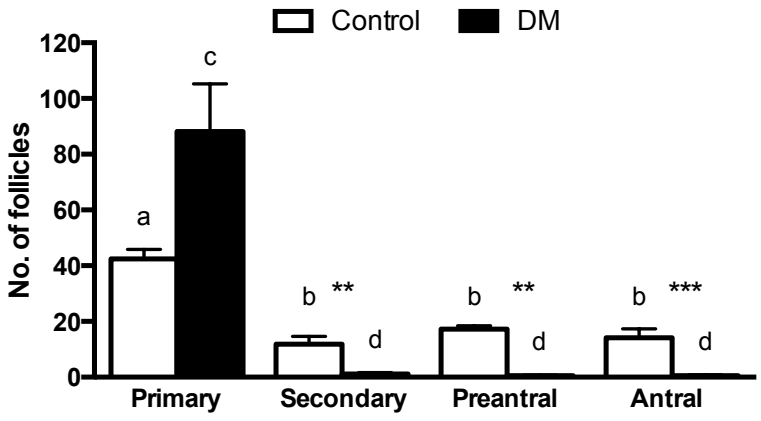


Figure 4.7: Follicle counts. Follicle counts according to the stage of development in Control (n=5) and DM (n=8) grafted ovarian tissue 4 weeks after the transplantation. Results are expressed as mean ± SEM. ***P*<0.01, ****P*<0.001. (a) vs (b) *P*<0.001. (c) vs (d) *P*<0.0001.

4.4.4 Primary follicle arrest in the DM transplanted tissue cannot be overcome in the presence of a normal endocrine environment

Williams and Stanley (*133*) reported that the number of primary follicles in DM ovaries from 3 month old females was increased compared with Control mice and this was due to an increase in the number of 3a type follicles. This suggests that there is a block in the progress of follicle development at the 3a stage. The results obtained from the DM transplanted ovarian tissue reveal that the total number of primary follicles is also increased compared with Control and with the latest stages of follicle development in DM grafted tissue (Figure 4.7). To assess whether this increase was due to an increased number in 3a follicles as observed in 3-month mice, primary follicles at 3a and 3b stages were analysed. Since 9-week-old female mice were used as donors, 9-week follicle counts were used as a reference to analyse primary follicle counts before the transplant. Nine-week follicle counts revealed the same block in follicle development at 3a stage displayed by 3-month females. Moreover, despite the normal hormonal environment of the recipient females, the developmental block remains 4 weeks after the transplant since the number of 3a follicles was increased compared with 3b in the DM grafted tissue (Figure 4.8). In addition, 3a follicle number was higher in DM compared with Control whereas 3b follicle counts were the same in both groups.

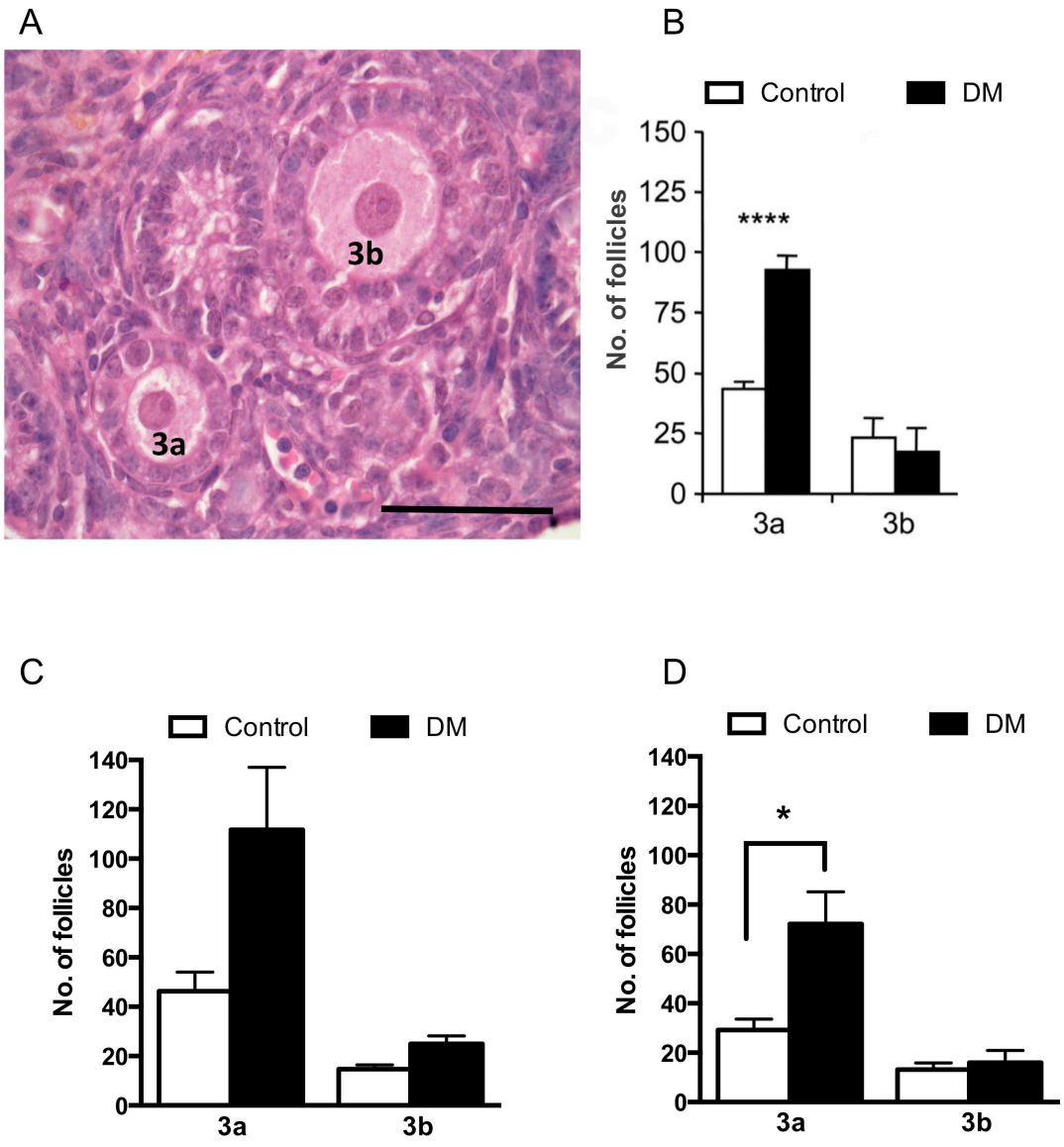


Figure 4.8: Primary follicle counts. (A) Representative images of primary follicles type 3a and 3b according to Pedersen and Petersen classification (*16*). (B) Previously published 3a and 3b follicle counts in 3-month Control and DM ovaries (*133*) . (C) Primary follicle counts in 9-week (Control n=3, DM n=3) ovaries and (D) 4 weeks after transplantation (Control n=5, DM n=8). Results are expressed as mean ± SEM. **P*<0.05, *****P*<0.0005. Bar scale 50 μm.

4.4.5 Follicle numbers 4 weeks after the transplantation have the same profile as the 9-week ovarian tissue

The number of follicles at different stages of follicle development is preserved before and after the transplant, with DM ovaries having an increased number of primary follicles whilst the numbers of secondary, preantral and antral follicles decrease dramatically (Figure 4.9B). The Control transplanted tissue displayed all stages of follicle development and a similar follicle development profile as 9-week Control ovaries (Figure 4.9A). The normal endocrine environment of the Control recipients supported follicle development in the Control tissue, while 9-week DM graft was unable to resume normal follicle development, with less than 1% of the total number of follicles reaching the preantral and antral stages (Figure 4.9B).

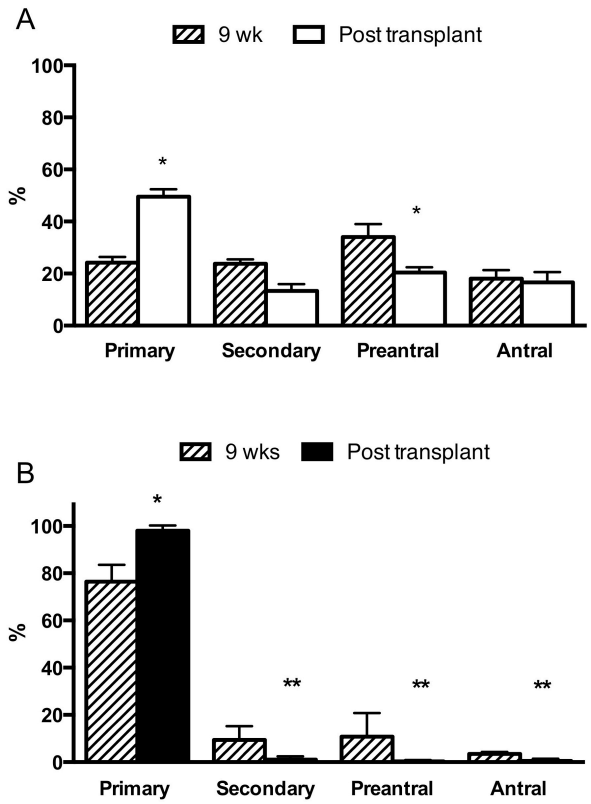


Figure 4.9: Follicle counts before and after transplantation. Ovarian follicle counts in 9-week ovaries (Control n=3 ovaries, DM n=3 ovaries) and in ovarian grafted tissue 4 weeks after transplant (Control n=5, DM n=8) in (A) Control and (B) DM. Results are expressed as mean ± SEM. **P*<0.05, ***P*<0.001.

4.5 Discussion

DM females switch their phenotype very rapidly from fertile at 6-week to POF by 3 months, displaying classical features of the pathology including lack of ovulation, decreased follicle development and altered hormone production (*133*). Elevated FSH and decreased testosterone and inhibin A characterize the altered endocrine profile in DM females. Although, the altered hormonal profile is not the cause of POF in this mouse model, it may be an important factor that contributes to the deterioration of ovarian function in DM females. In this POF model, the altered levels of gonadotropins and sex steroids could potentially maintain the quiescent ovarian state observed in DM females at 3 months of age and prevents follicle development from the secondary stage of follicle development onwards. In this regard, ovaries from DM females have the potential to resume follicle development since primordial and primary follicles are still present in the ovaries after the onset of POF. Even though the origin of the POF phenotype in DM females is the oocyte-specific deletion of *Mgat1* and *C1galt1*, if the modified endocrine environment is contributing to the block of follicle progression, then this is a potential target to attempt to recover follicle development.

There is some evidence that women with POF can recover ovarian function after hormonal therapy (*159*, *161*). However, considering that in around 90% of the POF women the cause of the pathology remains unknown, and the range of

potential causes is huge and very heterogeneous (*48*, *160*), caution is appropriated when considering hormonal intervention as a potential restorative therapy of the ovarian function in women with POF. A systematic review of randomized clinical trials aimed to restore fertility in patients with idiopathic POF using different hormonal treatments schemes, has been recently published (*164*). This review concludes that there is no scientific evidence that any of the treatments used can improve the pregnancy rates in patients with POF. This is due mainly because the lack of a placebo group in the studies and also because there is not a clear difference between ovulation and pregnancy rates for all the treatment tested and the spontaneous pregnancy rate observed in these patients. However, authors agreed that in same cases ovulation and pregnancy has been successfully achieved in women with POF.

To analyse the effect of a normal hormonal environment on DM ovarian follicle growth *in vivo*, ovary transplant under the kidney capsule of Control sibling females was carried out. In Controls, all stages of follicle development were observed 4 weeks after transplantation confirming that the environment provided by the Control sibling host is adequate to maintain ovarian function and thus follicle growth for at least 4 weeks. In stark contrast, analysis of DM grafted ovaries revealed markedly hypotrophy of the tissue compared to Control grafts with a lack of antral follicles. Follicle counts of the grafted tissues 4 weeks after transplantation revealed that total number of follicles were comparable between DM and Control however, the follicular density of the tissue was higher in DM compared to Controls due to the smaller size of the tissue.

Both Control and DM grafted ovaries contained an increased number of primary follicles compared with ovaries at 9 weeks of age. This finding is consistent with previous publications of accelerated follicular activation after grafting in non-ovariectomized recipients (*165*, *166*). During and after transplantation, ischemia induces follicular death and a diminished number of follicles can be observed shortly after transplantation (*166*, *167*). As a result, a reduction in inhibin A and AMH secretion release FSH downregulation and therefore several primordial follicles are recruited (*166*, *167*). Due to the increased number of primary follicles observed in DM and Control grafted tissues, this increased primordial recruitment mechanism seems to be activated. Since massive follicular death occurs after transplantation, the follicle development observed 4 weeks after the transplant is originated from the primordial follicle pool present in the tissue at the time of transplantation. Therefore, the early follicle activation observed in DM grafted tissue demonstrates that the tissue can respond to the normal hormonal environment however, this is not enough to re-establish complete follicle development. In addition, in the DM graft, blocked follicle development at the 3a stage previously described in DM ovaries (*133*) is present 4 weeks after transplantation and could not be overcome with the presence of the normal hormonal profile of the Control donors.

These data indicate that the mechanisms underlying the onset of POF in the DM females is complex and is not restricted to the abnormal endocrine environment observed in these females. The fact that the deletion of *Mgat1* and *C1galt1* genes is restricted to the oocyte, points towards abnormal

communication between the oocyte and the surrounded granulosa cells as the triggering event that impacts deeply on ovarian physiology. Therefore, after the onset of POF and in the presence of a normal endocrine environment, follicles in DM ovaries are not able to restore normal growth.

In conclusion, the normal endocrine environment alone provided by the Control-sibling recipient is not able to support normal follicle development in 9-week DM ovarian tissue. This normal hormonal environment is also incapable of release the block of follicle development at 3a stage.

Chapter 5: Evaluation of DM follicle growth *in vitro*

5.1 Introduction

DM females have only one small litter at 6 weeks and the absence of a second litter is due to a decrease in ovulation rate at 9 weeks (*136*) (Chapter 2). The abnormal endocrine environment in DM females was evaluated as a potential target for recovery of follicle development by transplanting 9-week DM ovarian tissue to a WT host. However, follicle development was not resumed beyond the secondary stage of follicle development 4 weeks after transplantation (Chapter 3). These findings suggest that the DM abnormal hormonal profile alone is not responsible for the altered follicle development.

Since follicle development is highly regulated by intra-ovarian factors, oocyte-specific deletion of *Mgat1* and *C1galt1* is likely to be disturbing intra-ovarian signalling in DM ovaries affecting follicle progression. Co-culture of different sizes follicles determined that follicle-follicle interactions are likely to play an important role determining follicle fate, since the large dominant follicle retarded the growth of smaller follicle (*168*). In cattle, intra-ovarian factors seem to be regulating oocyte competence since location of the dominant preovulatory follicle in relation to the corpus luteum appears to be key in fertility success after artificial insemination. After confirmation of ovulation, development of the preovulatory follicles ipsilateral to the corpus luteum was associated with a decreased conception rate compared with development of the preovulatory follicle contralateral to the corpus luteum (*169*). Spatial analysis of follicles in mice

ovaries 4, 8 and 12 days after birth suggested that primordial follicles inhibit other follicles to initiate growth, since recruited follicles were less likely to be present when 1 or more primordial follicles were within a 10 μm distance (*170*).

Glycans have several important cellular functions, including provide structural components to the extracellular matrix, modify protein properties such as stability and solubility, command protein trafficking and mediate cell signalling (*171*, *172*). Potentially, the absence of complex *N*- and *O*-glycans in the oocyte could be affecting some of these functions in the ovary, leading to a block in follicle development. If intra-follicular mechanisms are still intact in DM follicle after the onset of POF, there is a possibility that follicle growth could be resume if the blocking signalling is evaded.

5.2 Aims

- To evaluate if under controlled *in vitro* conditions, DM follicle development differs from Control.

- To determine if DM follicle growth can be restored to Control levels in a controlled *in vitro* environment.

5.3 Material and methods

5.3.1 Mice

Littermates 6-week DM and Control female pairs were selected for follicle culture. Control females were used initially to test FSH activity and to standardize FSH Concentration.

5.3.2 Follicle culture

Ovaries were dissected and placed in warm Leibovitz L-15 culture medium (HyClone-Thermo Scientific) supplemented with 3mg/ml of bovine serum albumin (BSA fraction V, Fisher Scientific, Loughborough, UK). Preantral follicles were microdissected using 30G needles and acupuncture needles and cultured as previously described (*173*, *174*). For the procedure, follicles were selected for culture according to size, integrity of the basal lamina and the amount of surrounding theca tissue attached after dissection. Selected follicles were ~140 to 200 μm in diameter with undamaged basal lamina and with some theca tissue surrounding the follicle. Follicle were placed individually in a 96-well plate containing 30 μl of minimum essential medium (MEM Alpha Modification, HyClone-Thermo Scientific) supplemented with 140 mM ascorbic acid (Sigma-Aldrich, St Louis, USA), 5% fetal bovine serum (FBS, Biosera, Ringmer, UK) and 2.5

- 7.5 IU/ml recombinant human FSH (r-hFSH, Gonal-F, Merk Serono, Feltham, UK). The culture medium, was filtered using a 22 μm pore syringe filter, placed in the well covered with 75 μl of silicon oil (Dow Corning, BDH, VWR international, Lutterworth, UK) and equilibrated in the incubator at 37°C, 5%CO_2 in air for at least 2 h before use. Follicles were cultured for up to 6 days and transferred daily to a new well with freshly prepared culture medium. Images were taken daily with a Leica M125 microscope (Leica Microsystems, Germany) and MicroPublisher 5.0 RTV camera (Qimaging, London, UK) at 10x magnification to evaluate growth, morphology, survival and antrum formation. Growth was also evaluated daily by measuring the diameter of the follicle with an ocular reticle at 5x magnification. Only viable follicles that grew beyond day 3 were included for the follicular growth curve analysis.

5.3.3 Morphology assessment

Morphology was evaluated daily by observation under the microscope and confirmed by analysing the daily images taken through culture. ImageJ software (version 1.46r, National Institutes of Health, USA) was used to measure follicle diameter.

5.3.4 Statistical analysis

Statistical analysis was carried out using Prism software version 4.0b (GraphPad Software, Inc., version 4.0b, 2004. La Jolla, CA, USA). The Mann–Whitney U test was performed to detect differences between groups with equal variances.

5.4 Results

5.4.1 Standardisation – Human recombinant FSH (h-rFSH) activity

Follicles with a diameter of 195.2±3.8 μm from three 4-6 weeks old Control females were dissected and cultured with 2.5, 5 and 7.5 IU of h-rFSH for up to 6 days. Twelve follicles were cultured from each female and one female was used per condition. Follicles that were unable to grow or stopped their growth anytime by day 3 of culture were classified as unviable and discarded from analysis. Follicle growth was evaluated daily to determine FSH activity (Figure 5.1). All concentrations of FSH were able to support follicle growth and no differences in the final follicle diameter were detected between the 3 conditions. Since standard follicle culture protocols recommend using the minimum amount of FSH required for normal follicle development, a concentration of 2.5 IU of h-rFSH was used for further *in vitro* follicle culture.

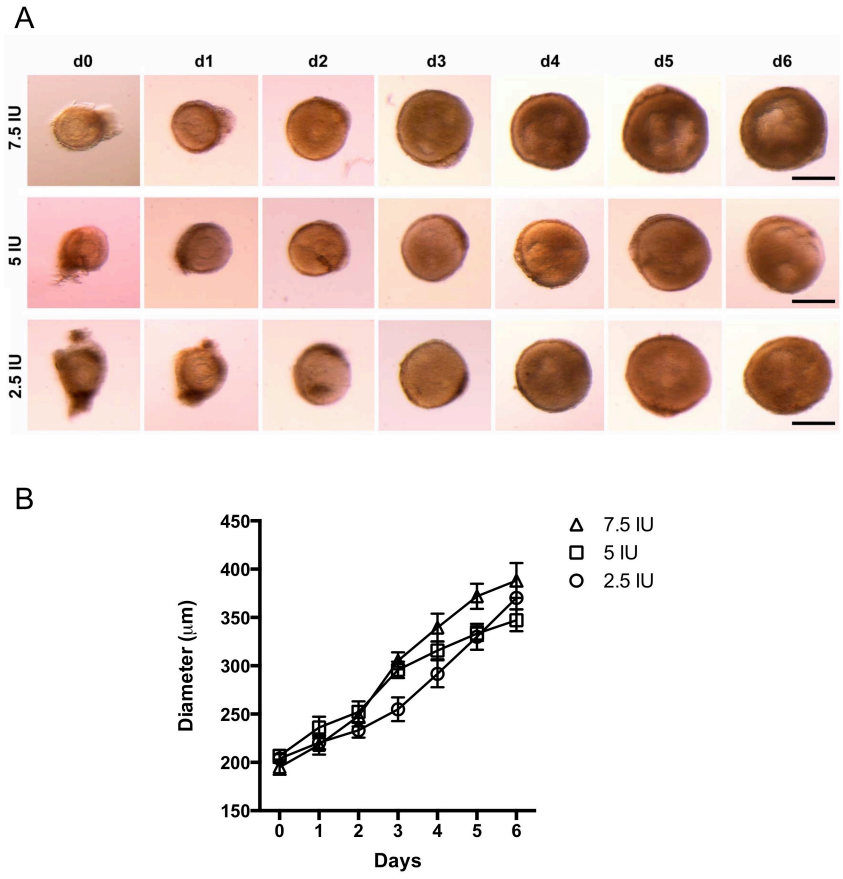


Figure 5.1: h-rFSH activity assay. Ovarian follicles were dissected (d0) from Control females (n=3 females: 36 follicles) and cultured with 2.5, 5 or 7.5 IU of h-rFSH for 6 days. Bar scale 200 μm.

5.4.2 DM Follicles have a decreased survival rate *in vitro*

Twelve ovarian follicles were dissected from each 6-week DM (n=4) and Control female (n=4) and cultured with 2.5 IU of rFSH. Follicles that were unable to grow or stopped growing by day 3 of culture were classified as arrested. The

survival rate of follicles was significantly decreased in DM compared with Controls, 48.5±8.8% and 91.7±3.4%, respectively (Figure 5.2).

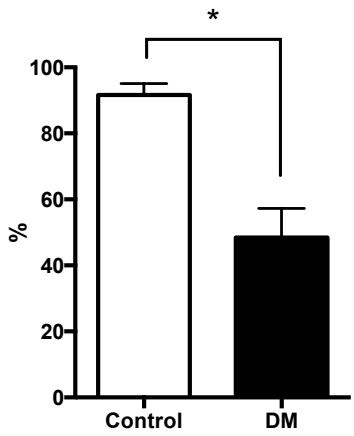


Figure 5.2: Survival rate of Control (n=48 follicles, 4 mice) and DM (n=48 follicles, 4 mice) ovarian follicles cultured *in vitro* with 2.5 IU of h-rFSH. Results are expressed as mean ± SEM. *P<0.05.

The diameter at collection of the unviable follicles was not different from the ones that grew normally in either, the Control or DM group (Table 5-1). However, there was a difference in the day when DM and Control follicles stop growing. DM follicles mainly stopped their growth between day 1 and 2 of culture meanwhile arrest of growth in Control follicles occurred mainly in the first 24h of culture (Figure 5.3).

Table 5-1: Diameter of DM and Control follicles on the day of collection (day 0).

	Follicles growing beyond day 3 of culture		Arrested follicles	
	Control	**DM**	**Control**	**DM**
Diameter day 0 (μm)	185.3 ± 2.0	188 ± 4.8	195.4 ± 8.3	177.7 ± 4.0

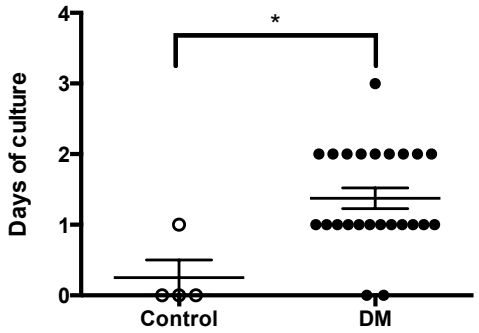


Figure 5.3: Arrest of follicle growth during *in vitro* culture with 2.5 IU of h-rFSH. Results are expressed as mean ± SEM. *P<0.05.

5.4.3 DM follicles that survive the end of follicle culture reach the same size as Control follicles.

Interestingly, the final diameter reached by growing DM follicles, was similar to the Control group, demonstrating that DM follicles are able to grow and

develop *in vitro* (Figure 5.4). However, the growing curve of DM follicles was slightly different. DM follicles grew faster during the first days of culture compared with Controls specially, days 2 and 3 of culture (P<0.05, Figure 5.4B).

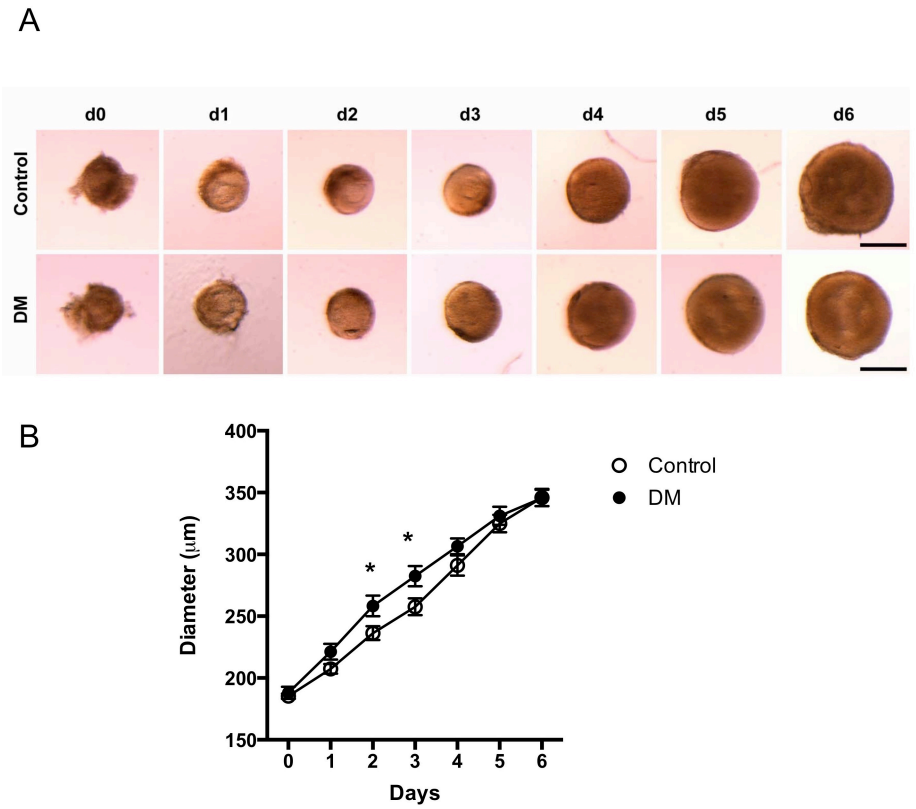


Figure 5.4: Ovarian follicle development *in vitro*. (A) Representatives images of *in vitro* follicle growth of Control (upper panel) and DM (lower panel) follicles. (B) Growth curve of Control (number of mice=4, number of follicles=43) and DM (number of mice=4, number of follicles=23) follicles during *in vitro* culture. Results are expressed as mean ± SEM. **P*<0.05. Bar scale 200 μm.

5.4.4 *In vitro* antrum development of DM follicles is different from Controls

In vitro antrum formation was assessed according to the day when this was first observed under the microscope and to the size of the follicle on the same day. There was no difference in the day that follicular antrum developed between Control and DM follicles (Figure 5.5A), however the diameter of DM follicles when the antrum was visible, was increased compared with Controls (288.6±6.4 μm and 266.7±5.9 μm, respectively) (Figure 5.5B).

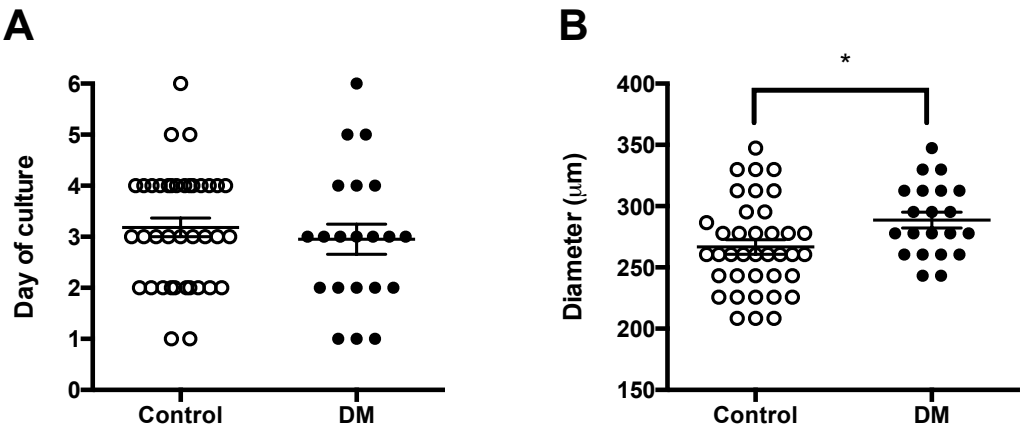


Figure 5.5: Formation of follicular antrum during *in vitro* culture. (A) Day of culture when Control and DM follicles developed antrum. (B) Size of Control and DM follicles the day of antrum development. Results are expressed as mean ± SEM. *P<0.05.

5.5 Discussion

Oocyte-specific deletion of *C1galt1* and *Mgat1* alleles in DM females produce a rapid deterioration of ovarian function from fertile females at 6 weeks to a complete ovarian dysfunction and POF by 3 months (*133*, *136*). The development of POF is characterized by a sharp decrease in ovulation rate from 6 to 9 weeks (*136*), an altered endocrine profile and impaired follicle development by 3 months of age (*133*). Infertility in DM females manifests from 9 weeks onwards and even though the total number of follicles is comparable to 3-month Control ovaries, the majority of the follicles in DM ovaries are arrested at the 3a stage of primary follicle development with ovaries lacking follicles from the secondary stage onwards (*133*). Follicle development was unable to be restored when 9-week DM ovarian tissue was exposed to a normal endocrine environment (Chapter 4). Thus, the abnormal hormonal environment by itself is not responsible for the POF phenotype in DM females.

Given the lack of response of DM ovaries to the normal endocrine profile, intra-ovarian factors could be determining the aberrant follicle development in DM females. Early studies assessed the possibility that follicles could secrete factors that affect directly the development of the adjacent follicles within the ovary. Co-culture of early antral and late preantral follicles *in vitro* has demonstrated that larger follicles retard the growth of smaller follicles (*168*) and therefore mouse follicles secrete factors that can affect the development of other

follicles when cultured from the late preantral to Graafian stages of follicle development (*175*).

Ovarian follicle development is regulated by a balance between extra and intra-ovarian factors (*176*). Several intra-ovarian factors such as epidermal growth factor (EGF), fibroblast growth factors (FGFs), insulin-like growth factors (IGFs) and transforming growth factor (TGF)-β family members, such as GDF-9 and anti-Müllerian hormone (AMH), have been implicated in normal and pathological folliculogenesis, like in women with polycystic ovary syndrome (*177*).

The question of how the intrinsic intra-ovarian factors could be involved in the altered follicle development exhibited by DM females was addressed in this chapter using follicle culture. Preantral follicles were dissected from DM ovaries and cultured *in vitro* in order to isolate follicles from potential suppressing intra-ovarian factors. Under *in vitro* conditions, the survival rate of DM follicles was approximately half of the Controls (91.7±3.4% and 48.5±8.8%, respectively; $P<0.05$). This could indicate that intra-follicular mechanisms preventing follicle development are expressed at the preantral stage of follicle development in 6-weeks DM females and are excluding approximately half of the follicles from reaching further stages of follicle development. However, the DM follicles that did survive were able to reach an equivalent final size as Control follicles. More detailed analyses revealed that the growing curve of DM follicles was slightly different to Controls, since DM follicles grew faster during first days of culture.

The different growing profile of DM follicles was also evident by an altered antrum development. DM follicles developed an antrum when they were larger than Control follicles however, the day the antrum develops was the same between groups. The antrum cavity is filled with follicular fluid mainly composed of mucopolysaccharides produced by granulosa cells, from serum transudate and steroids and hormones (*178-181*). The composition of the follicular fluid is related to the physiological status of the follicle and could reflect the fertility potential of the oocyte inside that follicle in both, humans (*182-184*) and cattle (*185*). Therefore, the abnormal antrum development exhibited by DM follicles *in vitro* could be potentially impairing the developmental potential of the follicles.

In summary, DM follicles are able to growth *in vitro* reaching the same size as Control follicles at 6-week. However, the survival rate is severely compromised, with about half surviving compared to Control. On the other hand, the growing curve of DM follicles that are able to develop *in vitro*, is different from Controls demonstrated by an initial accelerated growing speed and a different pattern in the antrum development. How this could compromise the viability of the oocyte inside the follicle is still unknown.

Chapter 6: Assessing the role of the oocyte and somatic cells in DM follicle development using reaggregated chimeric ovaries

6.1 Introduction

Follicular development, oocyte growth and ultimately fertility is regulated by two-way communication between the oocyte and the somatic cells (granulosa and theca cell layers) that form the follicle (*21*). These highly coordinated interactions can be via direct cell-to-cell contact or paracrine signaling between the follicular compartments (*186*, *187*). The oocyte produces factors that modulates somatic cell development and differentiation inducing follicle development (*25*, *188-190*). In addition, somatic cells secrete factors that regulate oocyte development and provide optimum conditions for the oocyte to develop competence for ovulation and fertility (*191*, *192*).

The interactions between the oocyte and somatic cells will determine the ovarian phenotype and the ultimate capability of the oocyte. On the other hand, changes in the ovarian phenotype could potentially occur if any of the cell layers comprising the follicle is modified inducing changes in the intraovarian molecular signaling.

In bovine, cumulus cells of the cumulus-oocyte complexes (COC) have a high proliferative rate and low progesterone secretion compared with mural granulosa cells (*193*). When oocytes were removed from the complexes, the remaining granulosa cells changed their properties to a mural granulosa cell-like phenotype with a decrease in proliferation rate and higher progesterone secretion. Moreover, when the granulosa cells from oocytectomized complexes were cultured with denuded oocytes, their phenotype changed to a COC

phenotype, indicating that oocyte secreted factors are determining the phenotype of the granulosa cells (*193*).

The ability of oocytes to induce changes in the phenotype of the granulosa cells is restricted by the stage of oocyte development. Oocytes from preantral follicles are capable of inducing preantral granulosa cells to shift their phenotype from preantral to mural granulosa cells, inherent of antral follicles (*194*). However, the effect of the oocyte on the granulosa cells decreases as oocyte development progresses, indicating that the influence of the oocyte over the granulosa cell differentiation depends on the developmental stage of the oocyte (*194*).

Generation of reaggregated chimeric pellet (RCP) is a technique based on the differential separation of ovarian germ and somatic cells followed by the reaggregation of both cellular types allowing the generation of a reaggregated pellet with two different cell sources. The RCP is grafted beneath the kidney capsule of ovariectomized females and left to grow in order to allow follicle development and to generate a reaggregated chimeric ovary (RCO), which resembles the morphology of a normal ovary (*29*, *195*). This technique is a valuable tool to study the roles of germ and somatic cells in follicle development. RCPs were generated from LTXBO and WT newborn mouse ovaries (*195*). LTXBO is a recombinant inbred strain characterized in that the females produce oocytes with a high frequency of MI arrest and parthenogenetic activation (*196*). RCOs from LTXBO and WT ovaries were generated to evaluate the influence of somatic

and germ cells in the defects of LTXBO oocyte. This study demonstrated that complete follicle development in the RCOs is possible when LTXBO germ cells are aggregated with WT somatic cells, however the phenotypes of MI arrest and parthenogenetic activation in LTXBO oocytes are intrinsic to the oocyte since these manifestations occurs regardless the somatic cell genotype (*195*). In another study, RCPs were generated by reaggregation of 12 days old mouse oocytes with newborn somatic cells demonstrated that follicular development rate is accelerated compared to the normal follicular development rate displayed by RCPs generated with newborn germ and somatic cells (*30*). These results indicate that the oocyte is coordinating follicle development, which is based on the intrinsic developmental program of the oocyte.

Using the RCP technique, the role of somatic and germ cells can be investigated in the DM model. Although the mutation of *Mgat1* and *C1galt1* genes is oocyte-specific, DM females switch their phenotype rapidly from fertile at 6 weeks to POF by 3 months, affecting the entire ovarian morphology and physiology. Whether a modification of the oocyte environment could potentially rescue the ability of DM germ cells to coordinate follicle development, will be addressed in this chapter.

6.2 Aims

- To determine if oocytes from prepuberal (3-week) and adult (9-week) DM mice can develop in reaggregated chimeric ovaries.

- To compare follicle development in reaggregated chimeric ovaries generated from DM and Control germ cells and WT somatic cells

6.3 Material and Methods

6.3.1 Mice

6.3.1.1 Mice for validation of the technique and assessment of cell separation

To validate the chimeric ovary technique and to assess the efficiency of the germ-somatic cell exchange, mice from two different lineages were used. Ovaries from B6SJLF1 (WT) and B6;129S-*Gtrosa*26 (ROSA26-lacZ; ubiquity expressing the *LacZ* gene) mice were used to generate RCPs. To produce B6SJLF1/J pups, females C57BL/6 mice were mated with SJL/J males and ovaries from P0 (day of birth)/P1 (day after birth) B6SJLF1/J females were collected and used as a source for somatic cells. P0/P1 ROSA26-lacZ ovaries were used to isolate germ cells. ROSA26-lacZ mice were generously provided by Professor Elizabeth Robertson, Sir William Dunn School of Pathology, University of Oxford. SJL/J and C57BL/6 mice were obtained from Harlan (Bicester, UK).

6.3.1.2 Mice for DM experiments

Ovaries from 3 and 9 weeks old DM and Control females were used to obtain ovarian germ cells and ovaries from P0/P1 B6SJLF1/J mice were used as a source of somatic cells.

To produce RCOs using 9-week germ cells, a total number of 25 DM and 14 P0/P1 B6SJLF1/J ("9-week DM RCO" group) and 25 Control and 17 P0/P1 B6SJLF1/J ("9-week Control RCO" group) female mice were used.

To generate RCOs using 3-week germ cells, a total number of 14 DM and 14 P0/P1 B6SJLF1/J ("3-week DM RCO" group) and 14 Control and 14 P0/P1 B6SJLF1/J ("3-week Control RCO" group) female mice were used.

All experiments were carried out in triplicates. To avoid variability between Control and DM groups regarding the amount of cells used to generate the RCO, experiments were balanced according to the number of mice used to obtain somatic and germ cells.

A summary of the mice used to generate RCPs is presented in Table 6-1.

Table 6-1: Summary of mice used to generate RCOs

Type of RCP		**Germ cells**			**Somatic cells**		
		Mouse strain	**Age**	**Number of mice**	**Mouse strain**	**Age**	**Number of mice**
Validation for cell separation (1 RCP)		ROSA26-lacZ	P0/P1	3	B6SJLF1/J	P0/P1	6
3-week RCOs	**Control (3 RCPs)**	Control (*C1galt1*$^{F/F}$ *Mgat1*$^{F/F}$)	3 wk	14	B6SJLF1/J	P0/P1	14
	DM (3 RCPs)	DM (*C1galt1*$^{F/F}$ *Mgat1*$^{F/F}$:ZP3*Cre*)	3 wk	14	B6SJLF1/J	P0/P1	14
9-week RCOs	**Control (3 RCPs)**	Control (*C1galt1*$^{F/F}$ *Mgat1*$^{F/F}$)	9 wk	25	B6SJLF1/J	P0/P1	17
	DM (3 RCPs)	DM (*C1galt1*$^{F/F}$ *Mgat1*$^{F/F}$:ZP3*Cre*)	9 wk	25	B6SJLF1/J	P0/P1	14

6.3.1.3 Recipient mice for transplantation

In order to avoid rejection of the RCOs, immunocompromised mice (C.B-17 SCID or B6Rag1) were used as recipients for the transplant. C.B-17 SCID mice were obtained from Harlan and B6Rag1 mice were generously provided by Professor Fiona Powrie, Nuffield Department of Medicine, University of Oxford.

6.3.2 X-gal staining for genotyping

Tail tips of P0/P1 pups or ear biopsies for older ROSA26-lacZ mice were fixed for 1 h at RT in in 200 μl of gluteraldehyde solution containing 25% glutaraldehyde, 1M $MgCl_2$ and 0.1M PBS (pH 7.3). The samples were then washed 3 times for 15 min in 200 μl of detergent rinse solution containing 1M MgCl2, 1% sodium deoxycholate, 1% NP-40 and 0.1M PBS (pH 7.3). Finally samples were incubated in 100 μl of X-gal solution at 37°C for 1 hour.

Tissue from mice carrying the *LacZ* gene stained blue at the end of the process. Positive and negative control tissues were included in every X-gal staining procedure.

Details of the components of the solutions are detailed in Table 1.

Table 6-2: Composition of fixation, detergent rinse and X-gal staining solutions used for X-gal staining.

Solution	Reagents	Volume (μl) for 1ml solution
Fixation	25% glutaraldehyde	8
	1M $MgCl_2$	2
	0.1M PBS (pH 7.3)	990
Detergent rinse	1M $MgCl_2$	2
	1% sodium deoxycholate	10
	1% NP-40	20
	0.1M PBS (pH 7.3)	968
X-gal staining	50mg/ml X-gal	20
	250 mM potassium ferricyanide	20
	250 mM potassium ferrocyanide	20
	1M $MgCl_2$	2
	1% sodium deoxycholate	10
	1% NP-40	20
	1M Tris (pH 7.3)	20
	0.1M PBS (pH 7.3)	888

6.3.3 Preparation of reaggregated chimeric pellets

The generation of RCP involved the dissociation of ovaries into germ and somatic cells following by exchange and recombination of both cellular types to form a reaggregated pellet. This technique is based on the different properties of adherence to a culture dish of the germ and somatic cells after dissociation of the ovary; somatic cells attach to the culture dish during culture whereas germ cells do not (*197*).

The procedure has been modified from the original protocol (*195*) which use germ and somatic cells from newborn mice ovaries to form a chimeric pellet. Here the germ cells were obtained from 3- and 9-week DM ovaries while somatic

cells were obtained from newborn ovaries. Therefore, this is the first time that reaggregated chimeric ovaries have been generated from adult cells.

6.3.3.1 Collection of ovaries

Female mice were killed by cervical dislocation (adults) or decapitation (newborns) and ovaries from 4-10 adult females and 4-6 neonates were collected into warm PBS (GIBCO) supplemented with 1mg/ml BSA (BSA fraction V, Fisher Scientific, Loughborough, UK). The bursa and fat were removed under the microscope and the ovaries washed twice in PBS/BSA before being transferred to a new dish.

6.3.3.2 Dissociation of ovaries

Ovaries were enzymatically dissociated into a single cell suspension with 0.05% trypsin and 0.53mM EDTA (GIBCO), supplemented with 0.02% DNase-I (Sigma) for 15 min at 37°C and 5% CO_2 in air. Gentle pipetting of the tissue was carried out at 5 min intervals up to a maximum of 30 min until complete dissociation of the tissue. The single cell suspension was transferred into a 15 ml centrifuge tube and an equal volume of warm Medium 199 (M199, GIBCO) supplemented with 31.3mM sodium lactate (Sigma), 10mg/mL Penicilin-Streptomycin (Sigma P0781) and 10% fetal bovine serum (FBS) was added to the

tube. The sample was centrifuged at 2000× *g* for 5 min, the supernatant discarded and the pellet resuspended in fresh M199/FBS.

6.3.3.3 Differential separation of germ and somatic cells

The cell suspension was transferred to a 10 cm cell culture treated dish for overnight culture. The following morning the non-adhered cell population was separated from the adhered cells. Cells, including germ cells, non-viable somatic cells and red blood cells were collected by swirling the dish carefully to move the non-adhered cells to the centre of the dish. These cells were collected with a pipette without disturbing the monolayer of somatic cells and transferred to a new tissue culture dish with fresh M199/FBS. The remaining somatic cell monolayer was washed three times with PBS/BSA to remove any residual unattached cells. The adhered somatic cells were treated with trypsin for 3 to 5 min at 37°C. Cells were collected, centrifuged at 2000× *g* for 5 min and resuspended in fresh media. Cells were transferred into a new cell culture-treated dish and cultured for further 6 h. This second round of differential adhesion and separation was carried out to ensure complete separation of cell types. The germ cell population were filtered using a 30 μm pre-separation filter (Miltenyi Biotec GmbH, Germany) in order to exclude more developed oocytes and select germ cells from follicles up to the early secondary stage of follicle development. Germ and somatic cells were individually centrifuged and re-suspended in 100μl of

M199/FBS to obtain a highly concentrated cell suspension and cell counts were conducted using a haemocytometer.

6.3.3.4 Generation of reaggregated chimeric pellets (RCP)

Germ and somatic cells were mixed in a microcentrifuge tube with 35 µg/ml of phytohemagglutinin (PHA; Sigma) and the mixture was centrifuged at 10,000 × *g* for 30 s. The tube was then rotated at 180° and centrifuged for a further 30 s to form a compact and rounded pellet. This combined cells is now referred as a RCP (reaggregated chimeric pellet).

RCPs were transferred with a Pasteur pipette to a 24 mm diameter Millicell-PC membrane with a pore size of 4 µm (Millipore) for overnight culture in Waymouth medium MB 752/1 (Sigma) supplemented with 10% FBS. After overnight culture, the RCP was ready to be implanted beneath the renal capsule of bilaterally ovariectomized immunocompromised mice.

The generation of RCPs was conducted by Mrs Anna Deleva and Mrs Sairah Sheikh, Nuffield Department of Obstetrics & Gynaecology, University of Oxford.

6.3.4 Transplant of reaggregated chimeric pellets under the kidney capsule

The preparation of the recipient mice and the surgical procedure of the transplant of the RCP into the kidney capsule of the immunocompromised mouse were performed as described in Chapter 4. In addition, ovariectomy was carried out on the recipient females. After transferring the RCP under the kidney capsule, the kidney was gently placed back into the abdominal cavity and the ipsilateral ovary located and gently held outside the body wall using a bulldog serrefine clamp. Using fine tip forceps the bursa was opened and the ovary completely exposed. The ovarian vasculature was ligated using silk suture and the ovary removed using small spring scissors. The bulldog serrefine clamp was released and the body wall closed with interrupted suture using absorbable suture material. Using the same skin incision the opposite side of the body wall was opened and the contralateral ovariectomy performed, followed by the suturing of the body wall and skin with interrupted suture. Post surgery care and recovery of the mice was carried out as described in Chapter 4.

Surgeries were conducted in collaboration with Mrs Anna Deleva, Nuffield Department of Obstetrics & Gynaecology, University of Oxford.

6.3.5 Assessment of cell separation and efficiency of the exchange of germ-somatic cells to produce reaggregated chimeric pellets

In order to assess the success of somatic and germ cell separation prior to reaggregation of the RCP, ROSA26-lacZ animals and WT C57BL/6 mice were used to provide one of the two cell populations. ROSA26-lacZ animals ubiquitously express the *LacZ* gene, which encodes for the β-galactosidase enzyme. β-galactosidase catalyses the hydrolysis of X-gal and generates a blue colour in cells expressing β-galactosidase that can be readily visualized under the microscope. Based on this principle, RCPs generated from *LacZ* positive and WT cells (LacZ negative) can be differentially observed after histochemical X-gal detection.

6.3.5.1 Reaggregated chimeric ovaries collection

RCPs were grafted in the recipient mice for 21 days to allow enough time for the RCP to develop into a reaggregated chimeric ovary (RCO). Since follicle development in mice takes 21 days, follicles at all stages of follicle development were expected in RCOs. At 21 days after transplantation, mice were killed by cervical dislocation and the kidney exposed and explored under the microscope to identify the RCO. Once the RCO was detected, the kidney capsule containing the transplanted tissue was removed using small spring scissors. The tissue was then collected in pre-chilled PBS (4°C) and placed on ice.

6.3.5.2 X-gal staining for transplanted chimeric reaggregated ovaries

X-gal staining for RCOs was carried out as described in section 1.3.2 with some modifications after the permeabilization step of the protocol. Permeabilized tissue was incubated overnight in 100 µl of X-gal staining solution at 37°C. After staining, the tissue was washed 3 times for 15 min in 200 µl of detergent rinse solution, photographed under the microscope and either kept in PBS at 4°C until embedding or embedded immediately.

6.3.6 Histological processing

6.3.6.1 Embedding

Plastic embedding moulds, cassettes and paraffin wax were placed into an oven at 62°C to allow the melting of the wax and to warm up the moulds and cassettes prior to embedding. Since some of the RCOs were small and handling of the sample throughout the embedding process could compromise the integrity of the tissue, agarose embedding prior to paraffin embedding was carried out for the smallest samples to facilitate further processing.

6.3.6.1.1 Agarose embedding

If embedding was carried out immediately after X-gal staining, RCOs were placed for 2 min in PBS before agarose embedding. If the sample was stored in PBS at 4°C, then the tissue was transferred to RT followed directly by agarose

embedding. Agarose at 2% concentration was dissolved in PBS in a microwave for ~10 sec. The tissue was placed onto parafilm and PBS removed with a pipette. Then, the tissue was covered in the warm agarose, ensuring that the agarose completely covered the tissue. The agarose block was allowed to cool and the excess of agarose cut around the RCO. The tissue was then easily handled and ready to continue with the paraffin wax embedding process.

6.3.6.1.2 Paraffin embedding

The tissue (plus or minus agarose) was dehydrated in increasing concentrations of ethanol as follow: 50%, 70%, 80%, 95% and 3 steps of 100% ethanol, 15 min each. Ovaries were incubated for 20 min in 3 steps of xylene to remove the ethanol from the tissue. The RCOs were then carefully transferred into plastic moulds containing melted paraffin wax and incubated at 62°C for 2 h to allow tissue penetration by the paraffin (embedding). After embedding, the plastic cassettes were placed on top, pressed gently into the moulds and filled with melted wax. Once the positioning of the tissue into the mould was checked, the oven was turned off and the block left to set overnight. The next day moulds were placed in the fridge for 1 h to help loosen the wax block from the mould, and the wax blocks containing embedded tissue removed from the moulds.

6.3.6.2 Sectioning and evaluation

The tissue was serial sectioned at 5 μm and all sections were collected onto positively charged slides. Slides were placed in an oven at 62°C for 1 h to let slides to dry and to adhere sections to the slides. RCO sections generated from *LacZ* positive cells and B6SJLF1/J mice stained for X-gal were dewaxed with 2 consecutives steps of 8 min in xylene followed by a last step of 4 min in xylene prior to mounting DPX mounting medium (Fisher). Slides with RCO sections generated from DM and B6SJLF1/J mice were dewaxed as above and hematoxylin and eosin stained previous to mounting. All sections were evaluated under the microscope and follicles counted according to Pedersen and Peters (*16*) and as described previously in Chapter 4.

6.4 Results

6.4.1 Validation of the reaggregated chimeric pellet technique

6.4.1.1 Formation of reaggregated chimeric pellet can be achieved using newborn BL6SJLF1/J somatic and germ cells.

Previously, the generation of RCPs was successfully achieved by reaggregation of germ and somatic cells from newborn ovaries (*195*) and by reaggregation of newborn somatic cells with prepuberal germ cells (*30*). Since the technique needed to be established in our lab, the protocol was tested, adjusted and evaluated in preliminary experiments. B6SJLF1/J P0-P1 ovaries were dissociated into germ and somatic cells followed by reaggregation of both cell types in order to generate RCPs.

Twenty-one days after the transplant, gross morphology analysis, demonstrated the presence of multiple follicles evidenced by the presence of rounded semi-transparent structures (Figure 6.1A). Histological analysis demonstrated the presence of all stages of follicle development in the grafted RCOs (Figure 6.1B).

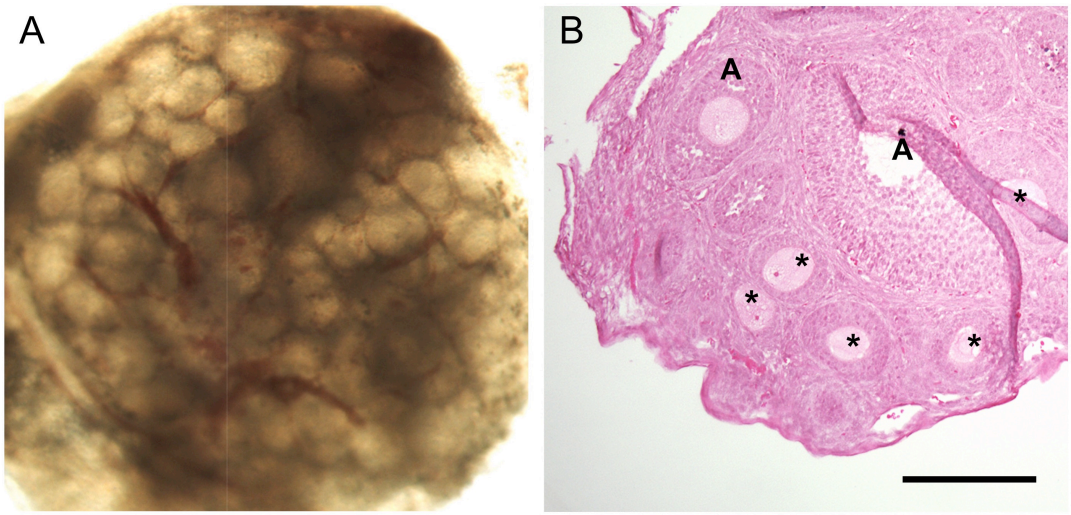


Figure 6.1: Establishment of the RCP technique using newborn B6SJLF1/J somatic and germ cells. Evaluation of RCOs gross morphology retrieved 21 days after transplantation demonstrated the presence of multiple follicles (A). Hematoxylin and eosin stained sections confirmed the presence of multiple follicles in all stages of follicle development (B). Asterisks are indicating follicles in different stages of follicle development. A: antral follicles. Bar scale 200 μm.

6.4.1.2 Successful separation of germ and somatic cells: ROSA26-lacZ germ cells and WT somatic cells.

In order to confirm efficient separation of the somatic and germ cells before re-aggregation, ROSA26-lacZ along with WT ovaries were used to generate RCPs. Twenty-one days after the transplant of the RCO, histological analysis demonstrated a successful separation and exchange of germ and somatic cells. Analysis of X-gal stained tissue revealed the presence of blue stain in all oocytes that were originated from ROSA26-lacZ germ cells, meanwhile a complete

absence of staining was observed in the chimeric stroma originated from WT somatic cells (Figure 6.2).

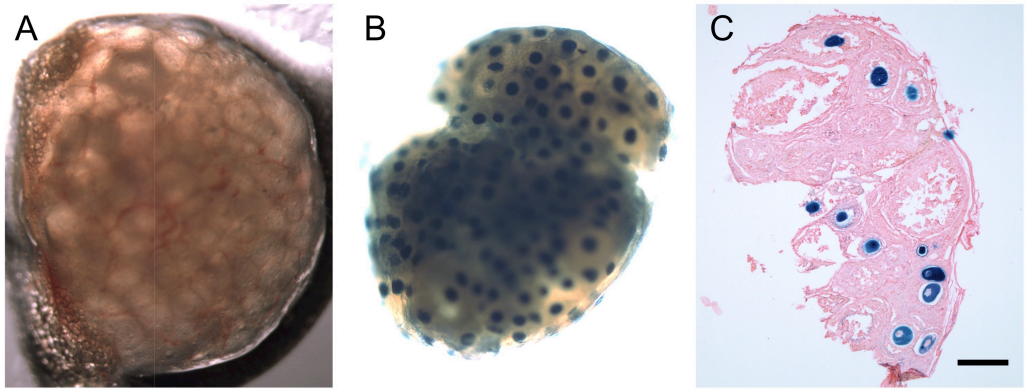


Figure 6.2: Confirmation of the successful separation of the somatic and germ cell prior to the formation of the RCP. (A) Image of a chimeric ovary formed by reagreggation of WT somatic cells and ROSA26-lacZ germ cells retrieved 21 days after the transplantation. (B) X-gal staining of the RCO in (A) showing the expected blue staining for oocytes expressing *LacZ* gene (ROSA26-lacZ mice). (C) Sectioning and eosin counterstain of the RCO after X-gal staining confirmed the success in the separation of the germ and somatic cells. Bar scale 200 μm.

6.4.2 Total follicle counts: 3- and 9-week DM germ cells are able to generate follicles in a reaggregated chimeric ovary

Analysis revealed the presence of follicles in both, 3- and 9-week RCOs (Figure 6.3). Three-week DM RCOs contained a lower number of follicles compared with the Control (3 ± 1.5 and 18 ± 5.2, respectively. Control n=3, DM n=3), however, this difference is not significant. Surprisingly, germ cells from 9-

week ovaries were able to generate follicles to the same extent as Controls (3.3 ± 1.7 and 3.3 ± 0.7, respectively. Control n=3, DM n=3).

In general terms, the number of follicles that developed in both DM and Control RCOs was low compared to previous experiments conducted in our lab using newborn somatic and germ cells.

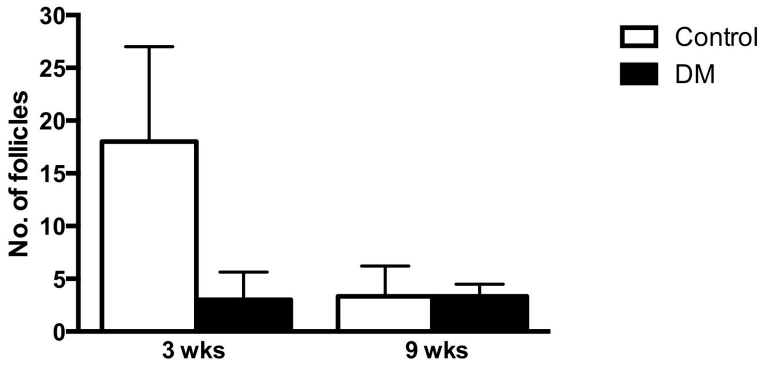


Figure 6.3: Total follicles counts of 3-week Control RCOs (n=3) and DM RCOs (n=3) and 6-week Control RCOs (n=3) and DM RCOs (n=3). Results are expressed as mean ± SEM.

6.4.2.1 Follicle development in 3-week RCOs

RCOs formed by re-aggregation of 3-week germ cells and WT somatic cells (3-week RCOs) were evaluated 21 days after transplantation. Follicle development analysis in 3-week Control RCOs revealed the presence of all stages of follicle development, from primary to antral (Figure 6.4). On the other hand, RCOs

containing 3-week DM germ cells exhibited an absence of primary follicles and therefore contained only secondary to antral follicles. Unexpectedly, follicle numbers were very low especially in RCOs using 3-week DM germ cells, exhibited an average of 1.3 ± 0.8 for secondary follicles and a scarce average of 0.7 ± 0.3 for antral follicles (Figure 6.4A).

The analysis of the proportion of the different types of follicles revealed that Control and DM 3-week RCOs exhibited a high join proportion of secondary and preantral follicles (75.9% and 81.8%, respectively), while in both antral follicles displayed the lowest proportion among follicles (Control: 3.7%, DM: 18.2%) (Figure 6.4B).

The statistical analysis did not support a significant difference between Control and DM RCOs due to the variability of the results and the low number of samples (3 RCOs per group).

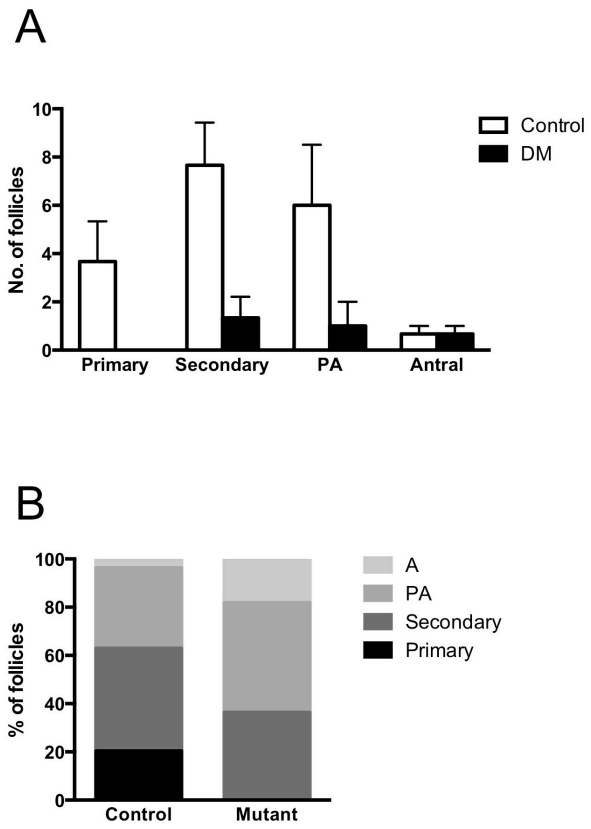


Figure 6.4: Follicle development in 3-week RCOs. (A) number and (B) proportion of follicles according to the stage of follicle development. A: antral, PA: preantral. Results are expressed as mean ± SEM.

6.4.2.2 Follicle development in 9-week RCOs

RCOs formed by re-aggregation of 9-week germ cells and WT somatic cells (9-week RCOs) were evaluated 21 days after transplantation. Unlike the follicle development profile observed in 3-week Control RCOs, 9-week Control RCOs displayed only two stages of follicle development: primary and preantral. Surprisingly, DM RCPOs exhibited all stages of follicle development (Figure 6.5).

However, as in 3-week DM ROCs, the numbers of follicles developed was very low and even lower than follicles numbers observed in 3-week ROCs. Despite the low numbers of follicles observed in the 9-week DM group, the fact that RCOs developed preantral and antral follicles is an unexpected finding.

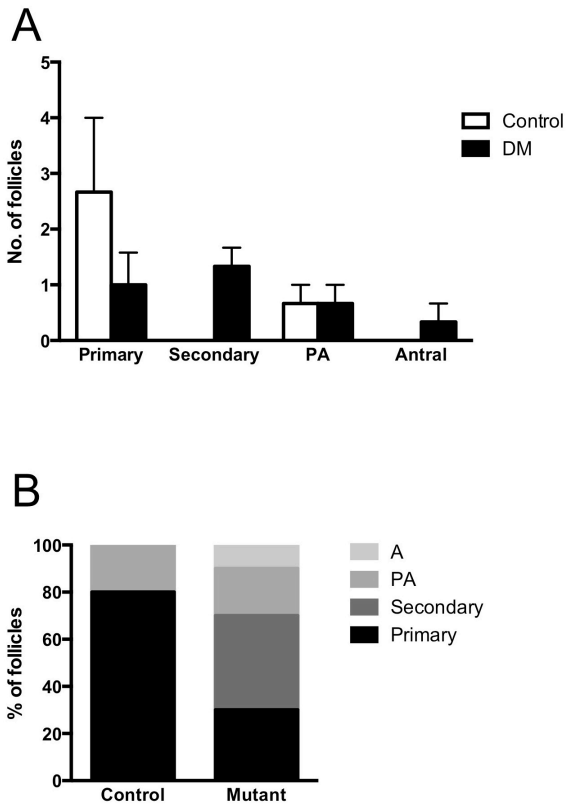


Figure 6.5: Follicle development in 9 weeks RCOs. Number (A) and proportion (B) of follicles according to the stage of follicle development. A: antral, PA: preantral. Results are expressed as mean ± SEM.

A graphical representation of the variation of follicles numbers between 3- and 9-week DM and Control RCOs is shown in Figure 6.6. Surprisingly, a predominant negative variation from Control is observed in 3-week DM group while a predominant positive variation from Control was observed in 9-week DM group, representing larger follicle numbers in DM RCOs at 9 weeks compared with Control.

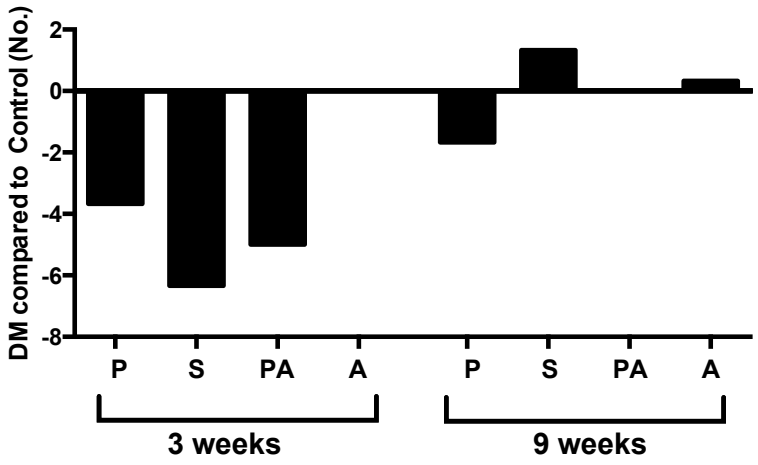


Figure 6.6: Variation from Control of the number of follicles in DM RCOs. (A) Representation of the positive or negative variation from Control of the number of follicles obtained from DM chimeric ovaries. (B) Average numbers of the different types of follicles obtained in 3 weeks DM and Control chimeric ovaries.

6.5 Discussion

DM females are infertile by 9 weeks and develop POF by 3 months of age. As reviewed in Chapter 3, arrest in follicle development at the primary stage of follicle development, at the 3a-3b transition (*133*), is contributing to the infertility and the POF phenotype in DM females. Therefore, the presence of follicles in DM ovaries after the onset of POF, makes the attempts to resume follicle development a feasible target to overcome POF. Even though the deletion of the genes in the oocyte occurs from the primary stage of follicle development onwards (*2*), it is known that mutated oocytes are fertile when females reach puberty and that the oocyte is likely to be impairing ovarian physiology and fertility shortly after females have their first litter (Chapter 3) (*133*, *136*). Whether the oocyte or the follicular somatic cells or both, become unable to support follicle development was addressed in this chapter using RCOs.

Generation and analysis of RCOs allows the study the different influences of the somatic cells and germ cells individually on follicle development. This technique was established using newborn somatic and germ cells up to 12 days of age (*29*, *30*, *195*). In the current study this technique was implemented for the first time using adult 3 and 9 weeks old DM and Control germ cells. DM RCOs with 3-week germ cells were able to generate follicles up to the antral stage of follicle development, yet the total number of follicles was diminished compared with Control 3-week RCOs. When 9-week DM germ cells along with WT newborn

somatic cells were used to generate RCOs, all types of follicles were generated, from primary to antral. This was an unexpected finding since at 9 weeks of age DM females are infertile with ovulation rate just above zero (Chapter 3) and ovarian morphology reveals lack of follicle development (Chapter 4). Surprisingly, no antral follicles developed in 9-week Control RCOs. These findings indicate that DM germ cells preserve the potential to develop follicles when associated with WT somatic cells. This could indicate that the oocyte is affecting somatic cells physiology, imprinting the POF phenotype in this cell compartment and therefore their ability to sustain follicle development.

In DM ovaries it is likely that the genetically altered oocyte is inducing changes in the physiology of the granulosa cells and in turn, the somatic cell compartments of the follicle are inhibiting follicle development and oocyte growth. A potential clinical application of this finding is that granulosa cells could be assessed to evaluate oocyte health and predict outcome when oocytes are used in assisted reproductive techniques. Unfortunately, current studies carried out on human cumulus and granulosa cells have been unable to find biomarkers for prediction of oocyte quality terms of fertility capacity and embryo outcome (*198*).

The generation of RCPs using adult germ cells is a newly established technique and further optimization is needed in order to generate a RCP that can support a better follicle development. One of the factors that can be modified to optimize the technique and is currently being addressed is to adjust of the

number of somatic and granulosa cells and the somatic-granulosa cells ratio used to generate the RCP. Even though optimization is ongoing and the number of follicles obtained in RCOs was low, the fact that DM 9-week oocytes retain the ability to sustain follicle development, when associated with WT somatic cells is a remarkable finding that could open the possibility to use the generation of RCOs as a potential therapeutic tool.

Chapter 7: Ovarian DM transcriptomic profile using microarray analysis before, during and after the onset of POF

7.1 Introduction

Microarrays provide the opportunity to evaluate whole-genomes through functional genomic analyses. Over the last decade genome-wide microarray technology has been used to evaluate signalling pathways involved in both normal and pathological processes. In the reproductive system, transcriptomics of the human endometrium has been essential to analyse endometrial changes through the menstrual cycle with clinical implications in Assisted Reproductive Technologies (ART) making advances towards personalized medicine for women with endometrial factors (*199*).

High throughput gene expression analysis of human cumulus-oocyte complexes has expanded our current knowledge on oocyte biology. For example, microarray analysis has allowed the unprecedented identification of expression patterns of specific genes during oocyte maturation like fibroblastic growth factor 9 (*FGF9*) and *SRY* (sex determining region Y)-box 15 (*SOX15*) (*200*).

Several genes implicated in POF have been identified, like bone morphogenetic protein 15 (*BMP15*), fragile X mental retardation 1 (*FMR1*) and forkhead box L2 (*FOXL2*) (*160*, *201*). Although, these studies have contributed to establishing a list of potential candidate genes responsible for POF, understanding the mechanisms triggering the pathology based on the study of individual genes is highly unlikely since the etiology of POF is highly heterogeneous. A more comprehensive approach identifying pathways and functions rather than individual genes, would be of great benefit to unravel the mechanisms underlying

physiological or pathological processes. In this regard, ovarian transcriptome obtained using microarrays in a rat model of POF (induced by 4-vinylcyclohexene diepoxide - VCD) has recently been published (*202*). The results of the functional enrichment analysis highlighted autoimmunity and cardiomyopathy as potential functions related with POF initiation in this particular experimental model (*202*).

As described in the previous chapters, the DM mouse model provides a remarkable opportunity to carry out wide-genome expression analysis across the different stages of the reproductive life of DM females, including evaluation of the gene expression profile during the onset of POF. In addition, the analysis of transcriptomic changes in the DM ovary will provide insights on how the oocyte is inducing the altered ovarian physiology, which ultimately will trigger the POF phenotype in the DM mouse model.

7.2 Aims

- To characterize the genetic profile of DM ovaries at 3-week (prepuberal), 6-week (when females are fertile) and 9-week of age (when females are infertile) through whole ovaries microarrays.
- To identify possible genetic pathways that could be involved in the onset of POF in DM females.

7.3 Material and Methods

7.3.1 Sample collection

Collection of ovary samples was performed in an RNase-free environment. Working surfaces were treated with RNase cleaning solution (RNaseZap®, Ambion, Applied Biosystems, Inc, USA) and certified RNase-free plastic ware was used and dissection tools sterilized.

Ovaries were collected from DM female mice at 3 weeks, 6 weeks and 9 weeks of age. For 3-week samples, ovaries were dissected from females at exactly 21 d. In order to minimize variability in the ovaries collected at 6- and 9-week of age, samples were collected the day after plugging. To achieve this, females were housed with males and daily checked for the presence of vaginal plugs, which indicates mating. Ovaries were collected at midday of the day when a vaginal plug was found. In this way all 6- and 9-week ovaries were collected at the same stage of the oestrous cycle.

Dissection was carried out under sterile conditions and ovaries were collected in a 1:1 solution of RNAlater®/PBS. Ovaries were quickly and carefully cleaned of extra-ovarian tissue and bursa under a dissection microscope and placed in a new dish with fresh RNAlater®/PBS. Ovaries were then transferred individually to 0.5 ml eppendorf tube with RNAlater®, placed in dry ice to allow quick freezing and stored at -80°C. In all three groups a piece of ear tissue was

collected to confirm genotype (protocol detailed in Chapter 2) before samples were pooled and processed for RNA extraction.

7.3.2 RNA extraction

All bench surfaces, material and tools were either sterilized or cleaned deeply with ethanol 70% and treated with RNaseZap®. Samples were thawed and ovaries from the same age were pooled in groups of 3 to constitute one sample. Triplicate samples (pooled ovaries) for every age (3-, 6- and 9-week) for Control and DM samples were carried out. Samples were weighed and RNA extracted using RiboPure kit (Ambion) according to the manufacturer instructions. Excess of RNAlater® solution was removed with a pipette and tissue was homogenized in 10-20 volumes of *TRI Reagent* (RiboPure kit) using a homogenizer. When fully disrupted, the homogenate was incubated for 5 min at room temperature. After the incubation 5 μl of Bromochloropropane (BPC, a phase separation reagent) for every 50 μl of homogenate was added and the sample agitated in a vortex at maximum speed for 15 sec and incubated for 5 min at room temperature. Samples were then centrifuged at 12,000 x g for 10 min at 4°C. This separated the mixture into three layers: a lower red organic phase, an interphase and an upper colourless aqueous phase, which contained the RNA. Without disturbing the layers underneath, the upper aqueous layer was transferred to a new 1.5 ml microcentrifuge tube and 25 μl of 100% ethanol for every 50 μl of the aqueous phase collected was added to the tube. The sample was agitated immediately in a

vortex at maximum speed for 5 sec to avoid RNA precipitation. Samples were placed into a *Filter-Tube assembly* (RiboPure kit) and centrifuged at 12,000 x g for 30 sec at room temperature until all the liquid passed across the filter. At this stage the RNA is bound to the filter. The liquid that had passed through the filter was discarded, and the filter returned to the collection tube. Samples were washed twice by adding 100 μl of *Wash Solution* (RiboPure kit) to the *Filter-Tube assembly* and centrifuged for 30 sec. After the second wash, the sample was centrifuged again for 30 sec to remove any residual *Wash Solution*. The filter cartridge was transferred into a new collection tube avoiding any contact with the flow-through to prevent residues of ethanol in the eluted RNA. Finally, 20 μl of *Elution Buffer* (RiboPure kit) was added to the *Filter-Tube assembly*, incubated at room temperature for 2 min and centrifuged for 30 sec at room temperature to elute RNA from the filter. The RNA collected in the tube was quantified using a NanoDrop ND-1000 spectrophotometer (ThermoScientific), aliquoted and stored at -80°C.

7.3.3 Integrity assessment of RNA

All samples were normalized to a concentration of 50 ng/μl and integrity of RNA assessed using a BioAnalyzer (Agilent 2100, Agilent Technologies, USA). This was carried out by the High-Throughput Genomics Group at the Wellcome Trust Centre for Human Genetics, University of Oxford.

7.3.4 Microarrays

Based on RNA integrity analysis, microarray analysis was iniciated. Total RNA was sent to the High-Throughput Genomics Group at the Wellcome Trust Centre for Human Genetics, University of Oxford. Whole-genome expression profile was carried out using Illumina MouseWG-6_v2.0 Expression BeadChip (Illumina Inc, USA), which assesses 45,281 mouse transcripts per sample. Three chips were used in total to allocate the 18 samples analysed: 3 DM 3-week, 3 Control 3-week, 3 DM 6-week, 3 Control 6-week, 3 DM 9-week and 3 Control 9-week samples (6 samples per chip). The distribution of the samples in every chip is described in Table 7-1. The samples were distributed randomly within each chip.

Table 7-1: Distribution of the DM and Control ovary RNA samples in the 3 microarrays chips used.

	Chip1			**Chip2**			**Chip3**		
	3 wks	**6 wks**	**9 wks**	**3 wks**	**6 wks**	**9 wks**	**3 wks**	**6 wks**	**9 wks**
DM	Sample A	Sample A	Sample A	Sample B	Sample B	Sample B	Sample C	Sample C	Sample C
Control	Sample A	Sample A	Sample A	Sample B	Sample B	Sample B	Sample C	Sample C	Sample C

7.3.5 Microarray data analysis

The data output files generated by the Illumina arrays were generated using Illumina GenomeStudio® data analysis software (Illumina, Inc, USA). Two

different sets of files were obtained with the results of the level of expression per sample. The first one contained the levels of expression per probe and a second set which contained the level of expression per gene. Illumina beadarray chips contain different probes designed to target specific transcripts in the genome, thereby different probes can be targeting the same gene. When microarray results are analysed using the gene files, level of expression of different probes profiling the same gene are averaged and any relevant information regarding differences in expression per transcripts is lost. In order to take advantage of this extra information, the analysis was carried out using the expression per gene probe.

Probe profiles microarray results from Control and DM samples at 3-, 6- and 9-week were analysed using RStudio (version 0.98.1079, RStudio, Inc.) statistical software. RStudio platform was loaded with a series of packages required to analyse microarray data (Table 7-2).

Table 7-2: R packages used for microarray analysis

R Package	Description	Version
Lumi	BeadArray Specific Methods for Illumina Methylation and Expression Microarrays	2.18.0
Limma	Data analysis, linear models and differential expression for microarray data	3.22.6
Annotate	Using R environments for annotation	1.44.0
lumiMouseAll.db	Mouse Illumina expression annotation data (chip lumiMouseAll) assembled using data from public repositories	1.22.0

Lumi (*203*), a specific package for Illumina expression microarrays was used to data input, quality control, variance stabilization, normalization and gene annotation of probe expression profiles. Taking advantage of the technical replicates available on Illumina microarray, a variance-stabilizing transformation (VST) algorithm (*204*) was applied to normalize raw data. Subsequent quantile normalization was carried out to remove technical noise due to different hybridization patterns between the Illumina chips.

Annotated Illumina probe identifiers were replaced using nucleotide universal identifier (nuID) (*205*), this step allows elimination of inconsistencies of Illumina identifiers, e.g. identifiers annotation modified between chip versions. Since universal, nuID is used as a source-independent naming convention for oligomers (*205*).

Once non-annotated and unexpressed genes were filtered, differential expression analysis was carried out using linear models for microarray data contained in limma package (*206*). First, a design matrix was created, which includes separate coefficients for Control and DM mice, then the difference was extracted as a contrast. Limma fits a linear model to the expression data for each probe and a moderated t-, F-statistics and log-odds of differential expression is computed by empirical Bayes moderation of the standard errors towards a common value. The output of this analysis is a list of differentially expressed transcripts and the following summary statistics:

- Adj.P.Val : P-value after adjustment for multiple testing
- P.Value : Raw P-value
- t : Moderated t-statistic
- B : B-statistic or log-odds that the gene is differentially expressed
- logFC : Log2-fold change
- F : Moderated F-statistic combines the t-statistics for all the pair-wise comparisons into an overall test of significance for that gene

Once analysed, gene official symbols and names were matched with the nuIDs of the differentially expressed transcripts.

Results visualization was carried out using volcano plots and heatmaps generated by limma and heatmap.plus (version 1.3) packages, respectively.

A functional enrichment analysis was carried out in order to identify possible biological functions/pathways to account for the onset of POF in DM females. In addition, candidates for potential alternative splicing were identified.

A flowchart summarising the analysis design for microarray results is presented in Figure 7.1.

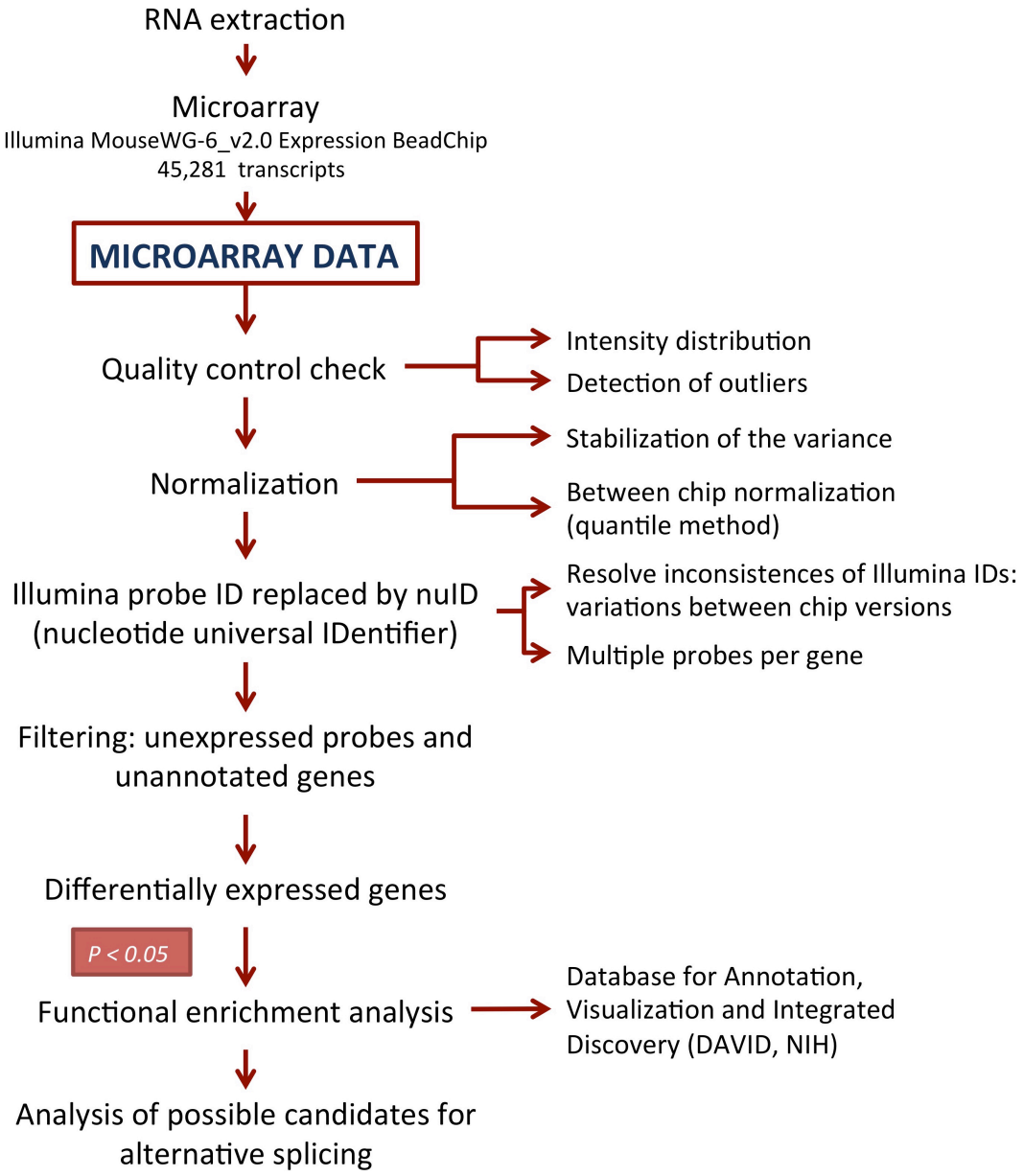


Figure 7.1: Flowchart of microarray analysis.

7.3.5.1 Functional enrichment analysis

The Database for Annotation, Visualization and Integrated Discovery (DAVID Bioinformatics Resources v6.7, National Institute of Allergy and Infectious Diseases, NIH, USA) was used to identify functionally enriched gene modules (*207*, *208*) . This database matches and clusters gene sets to establish their biological significance based on the Gene Ontology (GO) Consortium (http://geneontology.org).

Differentially expressed genes in DM samples were divided into "up-regulated" and "down-regulated" from Control, according to the fold-change value. The up-regulated and down-regulated list of genes were uploaded into DAVID environment and analysed by calling Functional Annotation Clustering. This DAVID environment reports clusters of similar annotations, allowing easier interpretation of the results and focalization on the biological relevance. Genes that are highly associated with certain terms are clustered together and the level of association is statistically measured by Fisher Exact test. As an output, functional enrichment clusters, grouping several genes were identified and values of group Enrichment Score, the geometric mean of member's P values (in negative log scale) and the Benjamini-Hochberg corrected P-Value (P-value corrected for multiple hypothesis testing) were obtained. The top ranked annotations groups based on the Enrichment Score most likely have lower P values for their annotation members.

7.3.5.2 Quantitative real time polymerase chain reaction (RT-qPCR)

In order to validate differential expression of *Ctsk* gene, complementary DNA (cDNA) was synthesized and amplified using RT-qPCR from an adapted version of Echevarria Vargas and Vivas-Mejía, 2013 (*209*). To allow quantification, RT-qPCR of *Ctsk* was carried out along with the housekeeping gene beta-actin (*Actb*). In a nuclease-free 0.2 ml thin-walled PCR tube 4 ng of total RNA per sample was used to prepare the poly(A) mix (Table 7-3). In order to hybridize the oligo-dT primer to the poly(A) tail of mRNA molecules, samples were incubated at 72 °C for 3 min. The tubes were spun down (700*g* for 10 seconds at room temperature) and immediately put back on ice.

Table 7-3: Poly(A) mix

Volume (μl)	Reagent
1 μl	Oligo-dT (10 μM)
2 μl	RNA (2 ng/μl)
1 μl	dNTP mix (10 mM; Invitrogen™)
0.3 μl	Nuclease-free water (Ambion®)

The reverse transcription mix (Table 7-4) was added to the samples and incubated for 90 min at 42 °C, followed by 10 cycles of 2 min 50°C, 2 min 42°C. The reverse transcription reaction was stopped (enzyme inactivation) by heating the sample to 70 °C for 15 min and samples stored at 4°C.

Table 7-4: Reverse transcription mix

Volume (μl)	Reagent
2 μl	Superscript II first strand buffer (5X; Invitrogen™)
0.5 μl	DTT (100 mM; Invitrogen™)
2 μl	Betaine (5M; Sigma-Aldrich)
0.06 μl	$MgCl_2$ (1M; Sigma-Aldrich)
0.25 μl	RNase Inhibitor (40 U/μl; Clontech®)
0.5 μl	SuperScript® II Reverse Transcriptase (Invitrogen™)
0.3 μl	Nuclease-free water (Ambion®)

Quantitative RT-PCR reactions for the first strand of cDNA obtained from the previous step were subsequently carried out using one-step SYBR Green PCR master mix (Applied Biosystems) with primers and cDNA added in optimized concentrations to minimize primer-dimer generation (Table 7-5).

Table 7-5: PCR mix

Volume (μl)	Reagent
10 μl	Fast SYBR® Green Master Mix (2X)
0.8 μl	Forward and Reverse primers (200nM each)
9.2 μl	cDNA template (4μl) + RNase free water (5.2 μl)

The PCR reaction was run in a StepOne Plus real-time PCR system (Applied Biosystems®) with cycling conditions at 95°C for 20 s, followed by 40 cycles of

95°C for 15 s, 60°C for 30 s. Gene amplification specificity was verified by melting curve analyses.

Primer sequences

Ctsk-F 5'-CTTTCCAGTTTTACAGCAGAG-3' (oligo: 8018904178-10/0, Sigma-Aldrich)

Ctsk-R 5'-GAGAGCATATCCTTTGTTTCC -3'(oligo: 8018904178-10/1, Sigma-Aldrich)

Actb-F 5'-CCTCCCTGGAGAAGAGCTATG-3' (*210*)

Actb-R 5'-TTACGGATGTCAACGTCACAC-3' (*210*)

All values obtained were normalized with respect to mRNA levels of *Actb* using *the* ΔΔCt method (*211*).

The average Ct (threshold of cycle) of *Ctsk* was normalized to the *Actb* for each sample

ΔCt = Ct (Total *Ctsk*) − Ct (*Actb*).

The difference between the ΔCt of each DM sample and the ΔCt of the control sample was calculated as follows:

ΔΔCt = ΔCt(DM) – ΔCt (Control)

RT-qPCR was carried out by Dr Juan Montiel, MRC, Functional Genomics Unit, University of Oxford.

7.4 Results

7.4.1 RNA extraction and integrity

RNA extraction was successfully carried out in all samples and sufficient amounts of RNA obtained to proceed with microarray analysis. Analysis of the samples confirmed that high quality RNA was obtained as evidenced by the high RNA Integrity Number (RIN). RIN is an algorithm based on the entire electrophoretic trace of the RNA sample and used to determine the integrity of the RNA. Integrity values from 1 to 10 are the output values, with 10 representing perfect RNA sample with zero degradation, whereas 1 represents a completely degraded RNA sample (*212*). All Control and DM samples displayed an exceptionally high RINs (Control RIN=9.74±0.06, DM RIN= 9.80±0.11, Table 7-6).

Table 7-6: Quantity and integrity of RNA obtained per sample

Sample			RNA concentration (ng/μl)	28S/18S	A260/A280	A260/A230	RIN
Control	3W	A	429.4	1.4	2.04	2.05	9.8
		B	181.5	1.1	2.06	2.11	10
		C	293.4	1.1	2.06	2.1	10
	6W	A	464.9	1.4	2.04	2.16	9.8
		B	401.7	1.1	2.04	2.12	9.6
		C	470	1.3	2.05	2.18	9.8
	9W	A	567.6	1.1	2.09	1.95	9.5
		B	861	1.5	2.12	2.21	9.7
		C	408.8	1.3	2.04	2.16	9.5
DM	3W	A	216.3	1.2	2.08	2.19	10
		B	105.7	1.4	2.04	1.95	10
		C	200.5	1.5	2.12	2.17	10
	6W	A	432.5	1.8	2.08	2.16	9
		B	456.8	1.4	2.06	1.95	9.9
		C	571.2	1.7	2.13	2.17	9.9
	9W	A	580.2	1.9	2.14	2.13	9.8
		B	408.8	1.5	2.08	2.17	9.8
		C	575.9	1.5	2.12	2.16	9.5

7.4.2 Microarray analysis

7.4.2.1 Quality control check

To analyse general features of the microarray results the data was plotted, as average signal intensity per chip and per sample. The quality control metrics displayed in Figure 7.2 demonstrate that the sample-independent control probes for biotin and hybridization had a high signal, indicating that the experimental procedure was successful. However, one of the chips (Chip No. 9853741028) had a lower hybridization signal. The three chips used in this study were from the same batch, have the same expiration date and were processed together. After consulting with Illumina technical support the reason why this chip had a lower signal is unclear. However, the signal of this chip was suitable to generate good quality data and therefore the data was not excluded from the analysis. Normalization steps specifically designed to eliminate the chip effect were carried out to allow further analysis. The sample-dependent plots are displayed in C and D of Figure 7.2. Variability between samples can be attributed to several factors such as labelling efficiency and loading variations, and can be largely corrected by normalization of the data. The high intensity observed in all samples and across chips indicated that the quality of the data obtained was high and no sample proved to be a cause of concern.

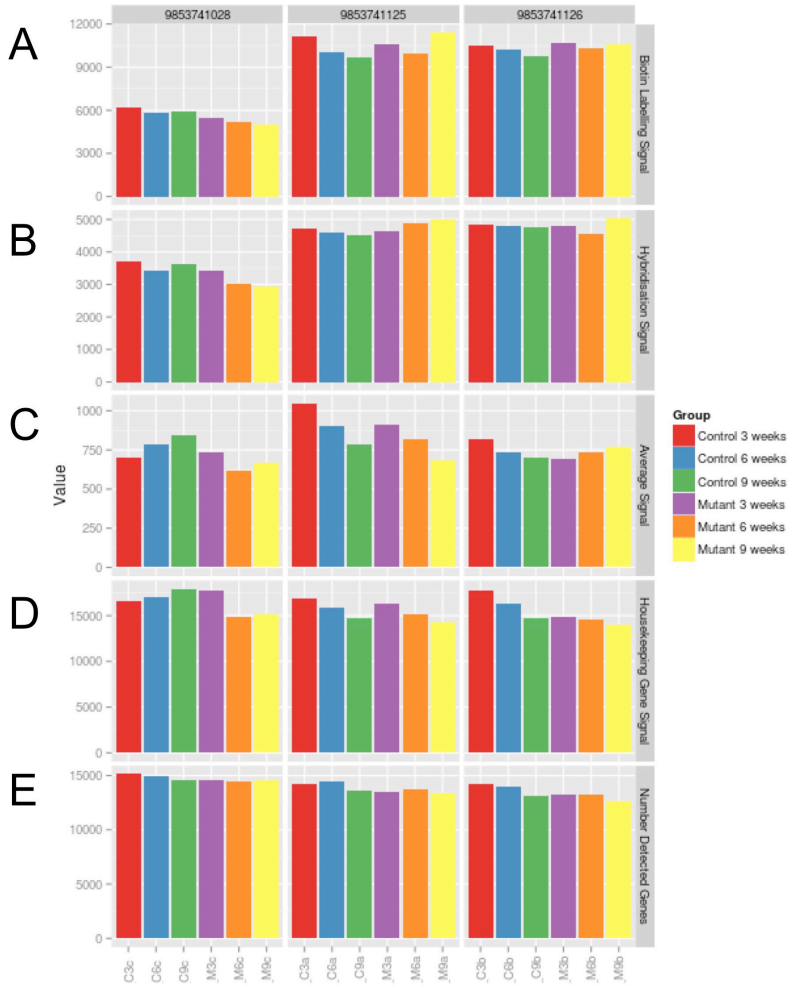


Figure 7.2: Quality control metrics for raw microarray data. The numbers at the top represents the three different chips used and samples are coloured according to their group. (A) and (B) correspond to the sample-independent control probes for biotin and hybridization. (C) and (D) correspond to the sample-dependent plots. (E) number of genes detected per sample On the bottom (X axis) capital “C” and “M” stands for Control and DM respectively, the numbers “3”, “6” and “9” represents the age of the sample and lower case “a”, “b” and “c” represent the 3 sample replicates.

The probe intensity distribution (for all 45,281 probes) has been plotted in boxplots to check overall data quality, possible outliers samples and the main source of variation (Figure 7.3).

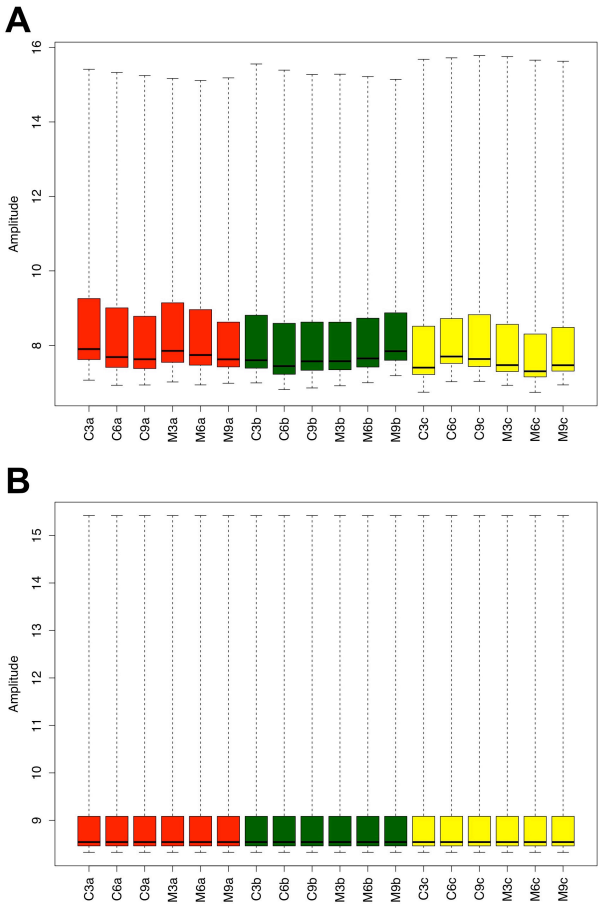


Figure 7.3: Boxplot graphs of intensity distribution of the raw data previous (A) and after normalization (B). Colours represent the three different chips used in the experiment. Capital "C" and "M" stands for Control and DM respectively, the numbers "3", "6" and "9" represents the age of the sample and lower case "a", "b" and "c" represent the 3 sample replicates.

The probe intensity distribution can also be displayed as density plots. This analysis demonstrated high quality data and absence of outlier samples indicated by the characteristic profile for the probe intensity distribution (Figure 7.4)

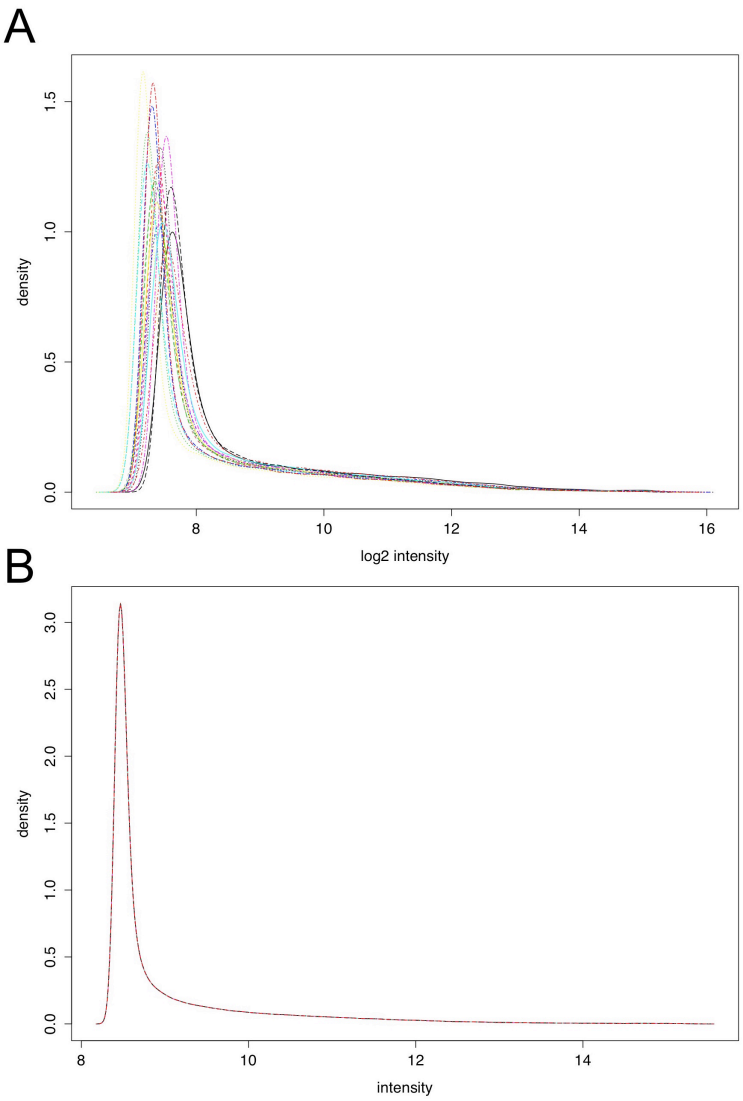


Figure 7.4: Density plots of signal distribution before (A) and after (B) normalization for all 18 samples analysed. Each colour represents one sample.

7.4.2.2 Hierarchical clustering analysis

Hierarchical clustering and principal components analysis (PCA) are useful tools to identify outlier samples and the main factors that could be affecting the gene expression profile, like technical or experimental conditions.

Clustering of the normalized data shows two main clusters separating the 3-week samples (on the left) from the 6- and 9-week samples. In addition, a subcluster of 9-weeks DM samples can also be observed on the right (Figure 7.5).

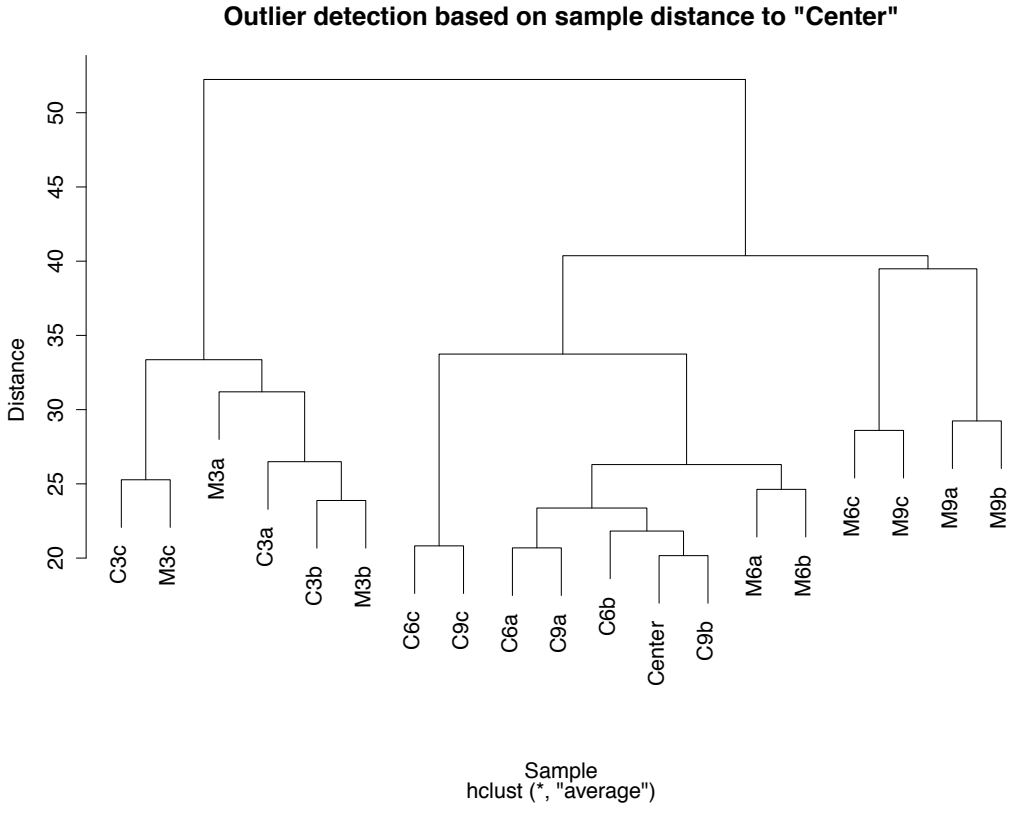


Figure 7.5: Hierarchical clustering for outlier detection of normalized samples.

7.4.2.3 Principal component analysis (PCA)

The PCA determines statistically the key variables in a multidimensional data set that explain the major sources of variance in the samples. If multiple major sources of variance are detected, PCA can be used to identify dimensions that can be eliminated from the data in order to simplify the analysis. In the microarray analysis of the DM and Control ovary samples, PCA was used to determine if important sources of variance are affecting the results and could bias the interpretation of the data. In this case the major sources of variation should be derived from the intrinsic origin of the samples: phenotype and age.

PCA for DM and Control ovary samples at 3-, 6- and 9-week revealed that the major source of variance detected between samples could be explained by the first and second component, from which ~60% corresponds to the first component and ~15% corresponds to the second component (Figure 7.6A). When all samples were plotted according to the first and second components (Figure 7.6B) a clear separation of the samples is observed according to the age. In addition samples were clustered according to the genotype (DM or Control) in 9-week samples. The clustering of the samples according to age and genotype is detected by the first component plotted in the X-axis. A first cluster can be observed to the left of the graph (Figure 7.6B) containing Control and DM 3-week samples. A second cluster is grouping the majority of 6-week Control and DM

samples and 9-week Control samples, while a third cluster to the right of the graph, was formed only by DM 9-week samples.

All the samples loaded in the Illumina chip that exhibited a lower signal (samples with a lower case “c”) formed a cluster detected by the second component (samples outlined by the red circle in Figure 7.6B). Since the second component only explained ~15% of the variance detected in the samples, and the quality control check of the data carried out previously revealed that these samples are not outliers and not a source of concern in order to generate good quality data, the decision was made to use all three replicates in the analysis. However, a PCA of the samples removing the potentially conflictive replicates was carried out to determine how the source of variance is distributed among the components.

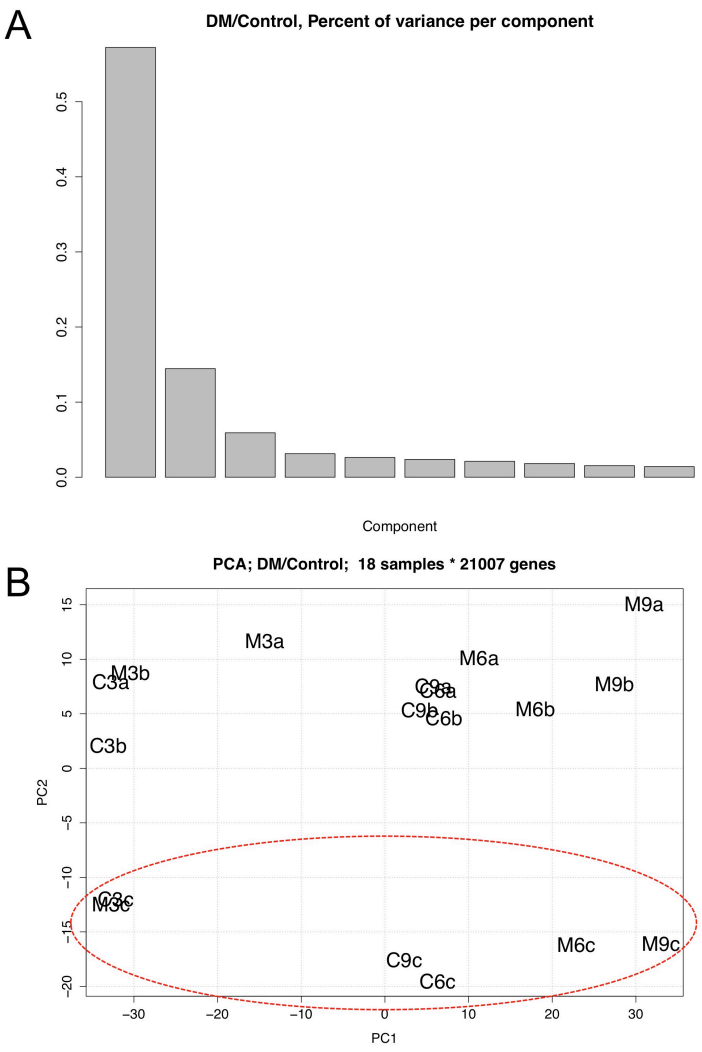


Figure 7.6: PCA of DM and Control samples. (A) Bar plot representing the proportion of variance explained by all 10 components analysed. (B) Samples plotted according to the first (X-axis) and second (Y-axis) components, which detected ~75% of the sample variability. Samples within the red circle are clustered by the second component and correspond to samples loaded in the same Illumina chips. Capital "C" and "M" stands for Control and DM respectively, the numbers "3", "6" and "9" represent the age of the sample and lower case "a", "b" and "c" represent the 3 sample replicates and correspond also to the 3 Illumina chips used.

7.4.2.4 Testing the exclusion of the replicates with lower hybridization signal

To test the effect on the analysis of the data, normalization and quality control check was carried out excluding the replicates with lower hybridization signal. The initial normalization of the 12 samples (2 replicates) was carried out as previously described for all 18 samples (3 replicates). The boxplots and the density graphs of the samples prior and after the normalization are represented in Figure 7.7 and Figure 7.8, respectively.

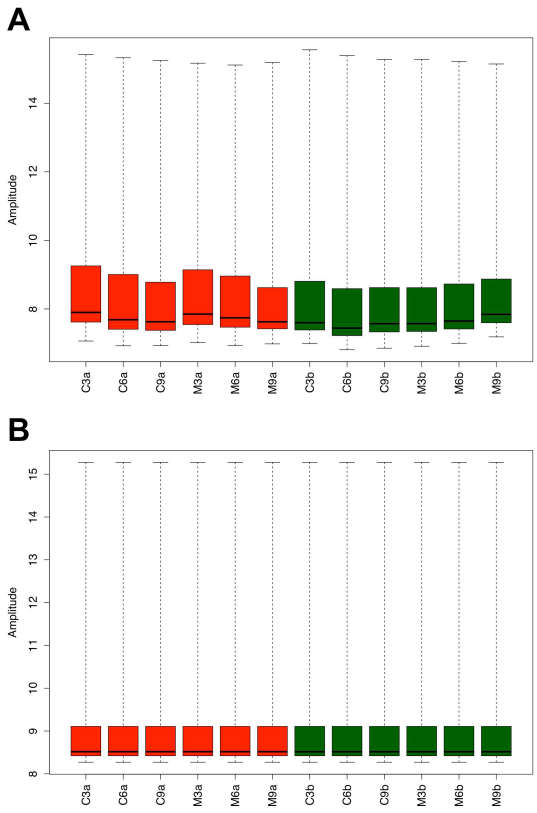


Figure 7.7: Boxplot graphs of intensity distribution of the raw data previous (A) and after normalization (B). Colours represent the two different chips used in the experiment. Capital "C" and "M" states for Control and DM respectively, the numbers "3", "6" and "9" represents the age of the sample and lower case "a" and "b" represent the two replicates included in the analysis.

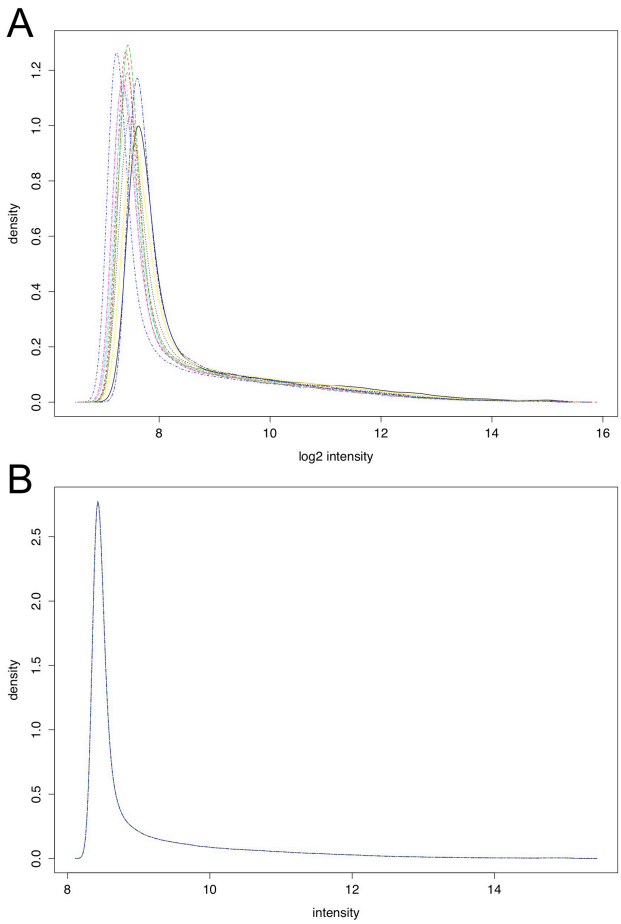


Figure 7.8: Density plots of signal distribution before (A) and after (B) normalization for the 12 samples analysed. Every colour represents one sample.

Finally, PCA of the two sets of replicates revealed only a slight increased of ~5% of the variation explained by the first component when compared with the PCA analysis using the three replicates. The same minor variation was observed for the second component (Figure 7.9A). The visualization of the samples when plotted according to the first and second components, revealed no clustering of the samples according to the chip (Figure 7.9B).

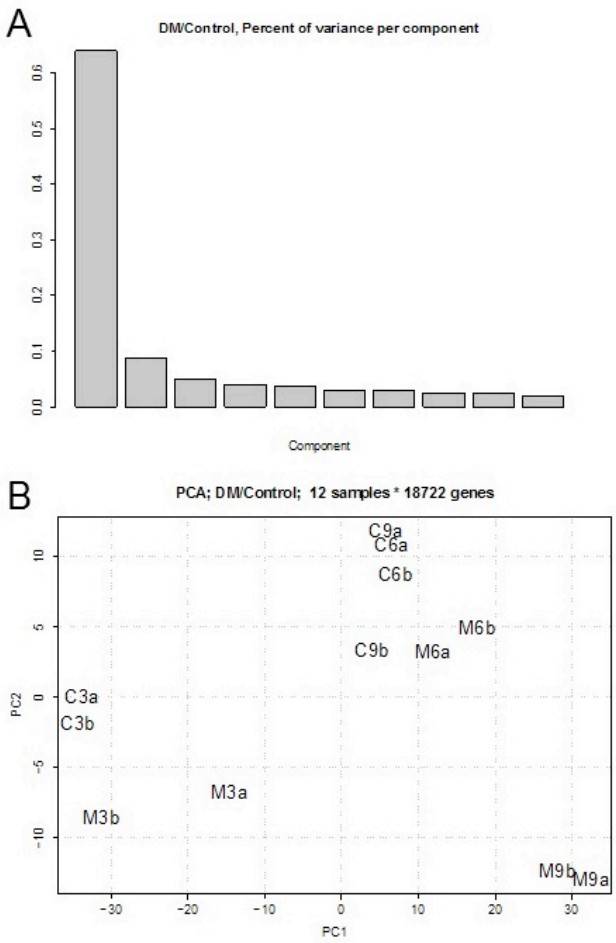


Figure 7.9: PCA of DM and Control samples. (A) Bar plot representing the proportion of variance explained by all 10 components analysed. (B) Samples plotted according to the first (X-axis) and second (Y-axis) components. Capital "C" and "M" stands for Control and DM respectively, the numbers "3", "6" and "9" represent the age of the sample and lower case "a" and "b" represent the 2 sample replicates and correspond also to one of the 2 Illumina chips analysed.

These results supported the initial decision to include data from all 3 chips in the analysis, since the robustness of the analysis may be compromised if only two replicates are used.

7.4.2.5 Differentially expressed genes/probes between Control and DM samples

The number of genes/probes differentially expressed between Control and DM samples at 3-, 6- and 9-week, is presented in Figure 7.10.

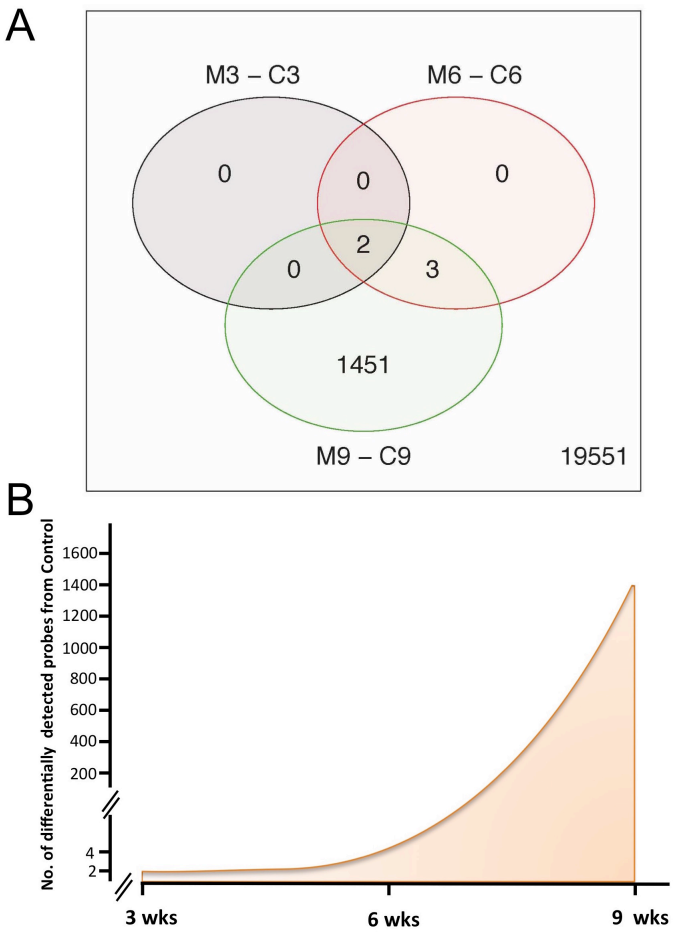


Figure 7.10: Differentially expressed transcripts between Control and DM ovary samples. (A) Venn diagram representing all differentially expressed transcripts between Control and DM samples at 3- (M3-C3), 6- (M6-C6) and 9-week (M9-C9). (B) Diagram illustrating a hypothetical curve that represents the dramatic change in gene expression of DM ovaries from Control.

After normalization and filtering of the data, a total number of 21,007 probes were analysed. Control and DM ovaries at 3- and 6-week differ in only 2 and 5 genes, respectively. However, this difference triggers dramatically just 3 weeks later, at 9-week, where the number of probes differentially expressed is 1,456 corresponding to 1,253 genes (Figure 7.10A). A Diagram illustrating a hypothetical curve that represents the prominent and sudden change in gene expression detected in 9-week DM samples can be observed in Figure 7.10B.

In order to visualize the gene expression profiles observed in DM ovaries, volcano plots were made for 3-, 6- and 9-week samples (Figure 7.11). All probes analysed (21,007) were plotted according to the $\log_2$FC (X-axis) and the P value (Y-axis). At 3-week, the vast majority of the genes/probes are below the significance level of 0.05 and around the "Zero" of fold of change (FC) given a flatten "V" shape to the volcano plot (Figure 7.11A). This implies a great grade of similarity between Control and DM samples. At 6-week the volcano "V" shape begins to open up from the central "0" in terms of FC and more genes/probes becomes increasingly significant (Figure 7.11B). At this stage it can be clearly visualized that from the 5 differentially expressed genes, *Ctsk* is the only gene that is overexpressed in DM samples. A completely different scenario can be observed in the volcano plot at 9-week (Figure 7.11C). The differentially expressed genes/probes, represented by the purple and green dots (total number of 1,456) are widely represented and a significant number of them are above or below 1.5 FC from Control.

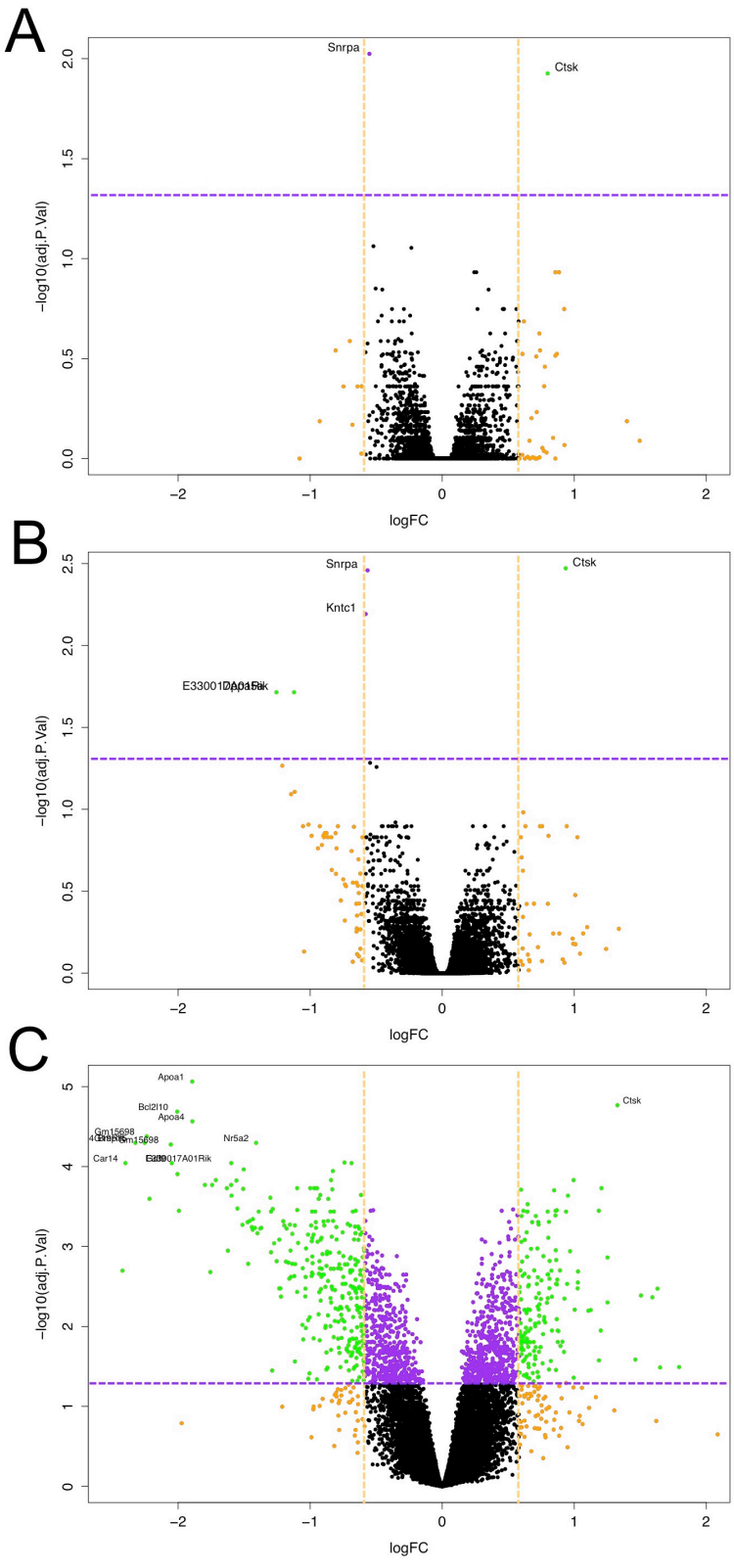


Figure 7.11: Volcano plots of DM ovaries gene expression. All transcripts analysed were plotted according to the significance and fold-change (FC) on the Y- and X-axes, respectively at 3-week (A), 6-week (B) and 9-week (C). Purple dotted lines mark the significance level of 0.05. Orange dotted lines mark 1.5 FC compared to Control samples.

The list of genes differentially expressed at 3-, 6- and 9-week (only top 10, the complete list of genes differentially expressed at 9-week is in Appendix B) in DM ovaries is presented in Table 7-7. The table presents the results according to the logarithm base 2 of fold change (log_2FC) from Control samples and adjusted P value (Adj.P.Val).

At 3-week, DM ovaries differentially expressed Small nuclear ribonucleoprotein polypeptide A (*Snrpa*), which is down-regulated compared with Control (log_2FC= -0.55, Adj.P.Val=0.009). Cathepsin K (*Ctsk*) is also differentially expressed at 3-week and unlike *Snrpa*, *Ctsk* is up-regulated in DM samples (log_2FC= 0.79, Adj.P.Val=0.01).

At 6-week, 3 additional genes are added to those differentially expressed at 3-week: Kinetochore associated 1 (*Kntc1*), Developmental pluripotency associated 5A (*Dppa5a*) and RIKENcDNA E330017A01 gene (*E330017A01Rik*). From the five genes differentially expressed at 6-weeks just *Ctsk* is up-regulated in DM samples; the other 4 genes are down-regulated, being *Dppa5a* and *E330017A01Rik* that displayed the lower expression from Control (log_2FC= -1.25 and -1.12, respectively).

Table 7-7: Significant differentially expressed genes (Adj.P.val <0.05) between Control and DM samples at 3-, 6- and 9-week. The fold of changes are represented by logarithm base 2 (Log_2FC). The complete list of genes differentially expressed at 9-week is in Appendix B.

Age	Gene symbol	Gene name	Log_2FC	Adj.P.val
3-wk	*Snrpa*	Small nuclear ribonucleoprotein polypeptide A	-0.5508	0.0094
	Ctsk	Cathepsin K	0.7989	0.0118
6-wk	*Ctsk*	Cathepsin K	0.9355	0.0033
	Snrpa	Small nuclear ribonucleoprotein polypeptide A	-0.5646	0.0034
	Kntc1	Kinetochore associated 1	-0.5790	0.0064
	Dppa5a	Developmental pluripotency associated 5A	-1.2547	0.0193
	E330017A01Rik	RIKEN cDNA E330017A01 gene	-1.12147	0.0193
9-wk (top ten)	*Apoa1*	Apolipoprotein A-I	-1.8921	8.63E-06
	Ctsk	Cathepsin K	1.3272	1.71E-05
	Bcl2l10	Bcl2-like 10	-2.0058	2.05E-05
	Apoa4	Apolipoprotein A-IV	-1.8910	2.72E-05
	Gm15698	Transcription elongation factor B (SIII) polypeptide 2 pseudogene	-2.2373	4.19E-05
	Nr5a2	Nuclear receptor subfamily 5 group A member 2	-1.4089	5.05E-05
	E330034G19Rik	RIKEN cDNA E330034G19 gene	-2.2523	5.05E-05
	Bmp15	Bone morphogenetic protein 15	-2.3228	5.05E-05
	Gm15698	Transcription elongation factor B (SIII) polypeptide 2 pseudogene	-2.0546	5.29E-05
	Kntc1	Kinetochore associated 1	-0.7397	8.90E-05

At 9-week 1,456 genes/probes are differentially expressed in DM samples. The first 10 probes are described in Table 7-7. Transcription elongation factor B (SIII) polypeptide 2 pseudogene (*Gm15698*) is represented by 2 probes that

consistently displayed a highly down-regulated gene expression profile (Log_2FC -2.23 and -2.05). *Ctsk* exhibited constant up-regulation in all 3 stages evaluated.

To visualize how the samples are clustered according gene expression, the top 100 differentially expressed genes at 9-week were represented in a heatmap (Figure 7.12). This heatmap plots the level of gene expression (gene probes in this case) per sample and clusters both, genes and samples, in a dendrogram. Four groups of samples are clearly distinguished: DM 9-week, DM and Control 3-week, DM 6-week and Control 6- and 9-week.

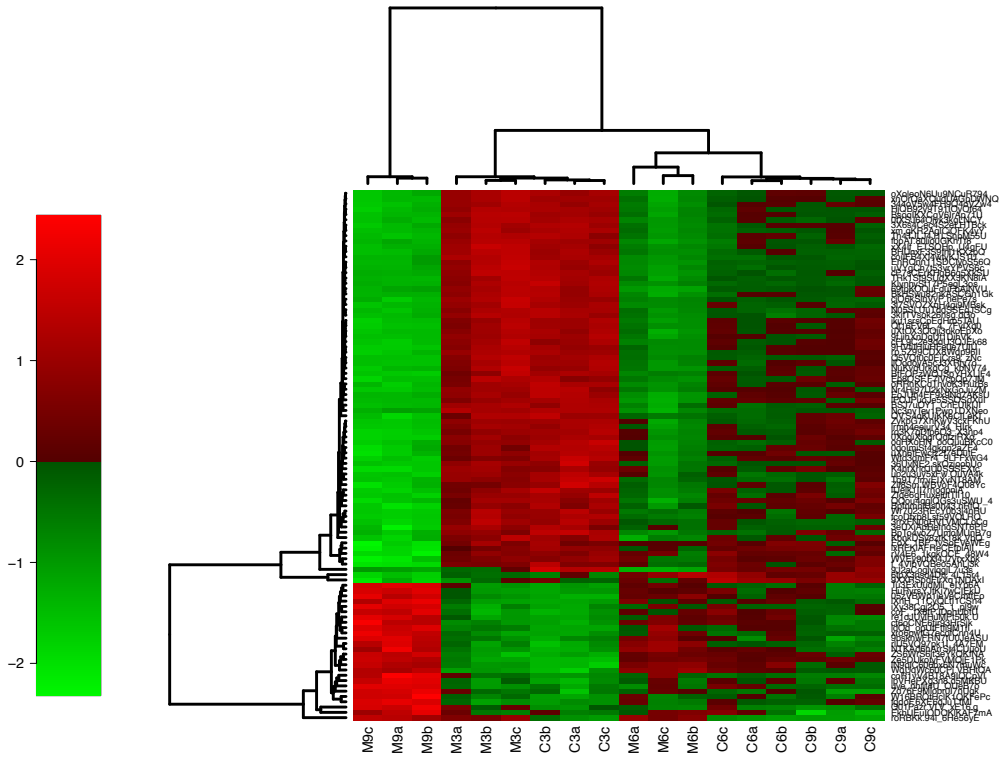


Figure 7.12: Heatmap of top 100 differentially expressed genes between Control and DM 9-week ovaries. Colours represent the level of gene expression per individual gene probe. The list of the 100 gene probes analysed is at the right and individual samples are at the bottom of the plot. Clustering of the samples and the gene probes are represented by the cladograms at the top and the left of the heatmap.

7.4.2.6 Functional enrichment analysis

The list of the 1,253 differentially expressed genes detected in ovaries at 9-week was divided in up-regulated and down-regulated according to their positive or negative FC value, respectively. Then, both set of genes were uploaded and analysed separately in DAVID.

Interestingly, the top five functional enrichment clusters for up-regulated and down-regulated genes are related with completely different cellular functions with highly significant enrichment scores. The enrichment scores ranks the biological significance of gene groups based on overall P-values.

The top five functional enrichment clusters of up-regulated genes in 9-week DM ovaries are presented in Table 7-8. Interestingly, the first cluster is related with signal peptide and glycosylation with 210 genes grouped in this cluster and a high enrichment score of 5.95. The following clusters are extracellular matrix, immune response, LPA (lipoprotein, propeptides and anchored to membrane) and cell adhesion.

Table 7-8: Top five functional enrichment clusters of up-regulated genes in 9-week DM ovaries

Functional annotation	No. of genes	Enrichment score
Signal peptide, glycosylation	210	5.95
Extracellular matrix	52	5.83
Immune response	61	3.26
LPA: Lipoprotein, Propeptide: removed in mature form, Anchored to membrane	40	2.83
Cell adhesion	31	2.75

The top five functional enrichment clusters for down-regulated genes in 9-week DM ovaries are related with non-membrane bound organelles, cell cycle, DNA replication, chromosome structure, and nuclei and organelle lumen (Table

7-9), all of these clusters account for a diminished cellular replication in 9-week DM ovaries compared with Control.

Table 7-9: Top five functional enrichment clusters of down-regulated genes in 9-week DM ovaries.

Functional annotation	No. of genes	Enrichment score
Non-membrane-bounded organelle	134	22.04
Cell cycle	86	19.47
DNA replication	59	17.91
Chromosome structure	54	12.57
Nuclei and organelle lumen	82	10.53

7.4.2.7 Validation of Cathepsin K expression with real-time polymerase chain reaction (RT-qPCR)

Since *Ctsk* is one of the genes that exhibited an altered gene expression compared with Controls in all three stages of DM ovaries analysed (3-, 6- and 9-week), further validation of this finding was carried out with quantitative real-time polymerase chain reaction (RT-qPCR).

Up-regulation of *Ctsk* in DM ovaries at 3-, 6- and 9-week was confirmed by RT-qPCR and the pattern of gene expression is consistent with microarrays results (Figure 7.13).

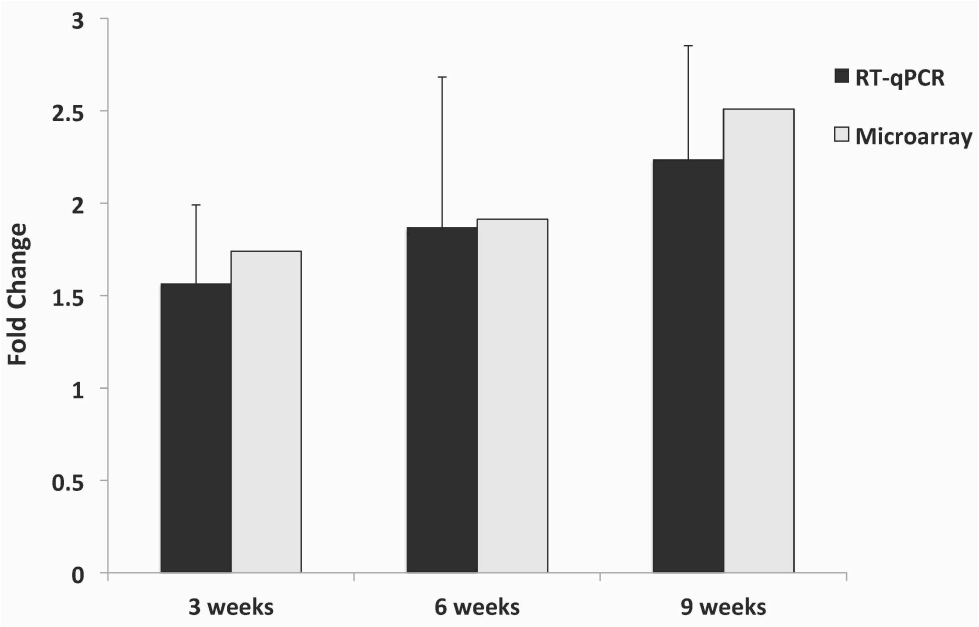


Figure 7.13: Comparison between RT-qPCR (black bars) and microarray (grey bars) results for *Ctsk* expression in DM ovaries at 3-, 6- and 9-week. Error bars correspond to S.E.M. Data generated by Dr Juan Montiel, MRC, Functional Genomics Unit, University of Oxford.

7.4.2.8 Profile of Oocyte-secreted genes

A subset of 14 oocyte-secreted genes were selected from differentially expressed genes at 9-week and plotted in Figure 7.14. Only Spermatogenesis and Oogenesis Specific Basic Helix-loop-Helix 1 gene (*Sohlh1*) displayed overexpression

in DM ovaries compared with Control, the remaining 13 genes are down-regulated in DM ovaries.

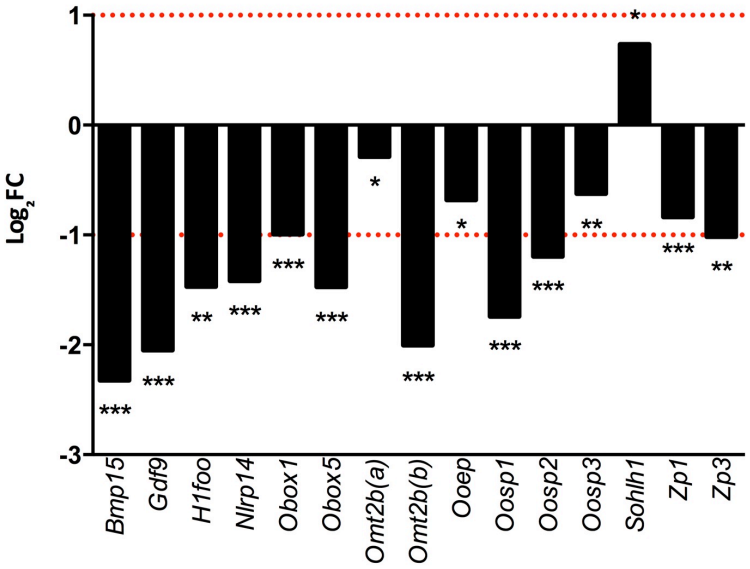


Figure 7.14: Expression profile of oocyte-secreted genes in 9-week DM ovaries. Results are expressed as Log_2FC of DM ovaries compared to Control. Two probes tested Omt2b gene expression: *Omt2b(a)* corresponds to probe ID clDeCN,5Kgq447dB9E and *Omt2b(b)* corresponds to probe ID Qf16FV6L_4_7FyIXq0. Dotted red lines are indicating 2 and -2 FC from Control. Asterisks represent adjusted P-value of gene expression compared with Controls. * $P \leq 0.05$, ** $P \leq 0.01$ *** $P \leq 0.001$.

7.4.2.9 Analysis of alternative splicing candidate genes

The Illumina chips used for this study have the advantage that multiple probes would target the same gene, meaning that multiple regions of the gene are tested at the same time. This feature provides an opportunity to detect possible candidates for alternative splicing. Differentially expressed genes

detected at 9-week targeted by more than one probe were tested. A first set of genes were selected according whether one of the probes have a FC greater than 1.5 or lower than -1.5 (equivalent to $Log_2FC = 0.58$ and -0.58, respectively, Figure 7.15).

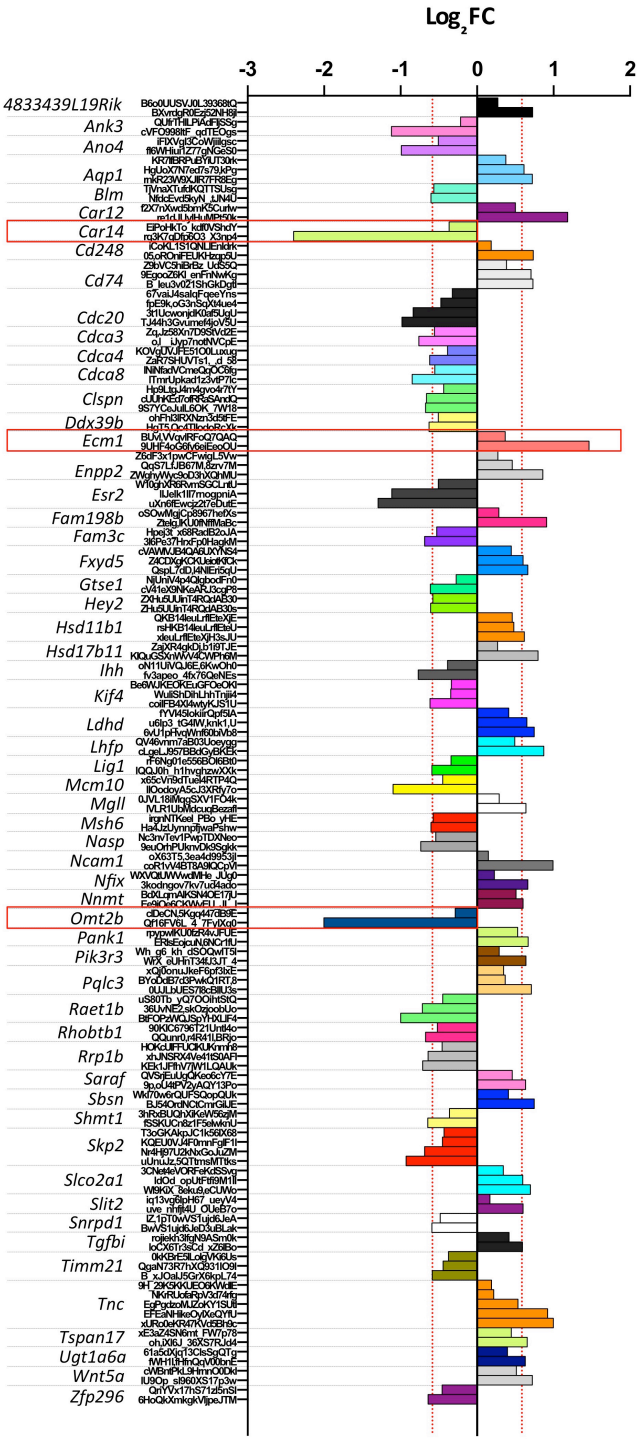


Figure 7.15: Analysis of possible splicing variants of differentially expressed genes on 9-week DM samples. Probes detecting transcripts of the same gene were clustered. Using a cut-off of 1.5 FC the probes with discordant levels of expression were selected. Bars of the same colours represent probes for the same gene. Red dotted lines mark positive or negative 1.5 FC of expression compared with Control. Solid red lined are enclosing *Car14*, *Ecm1* and *Omt2b* transcripts which with the higher levels of discordance and therefore, candidates for alternative splicing.

The genes with the greatest expression discrepancy between the probes were carbonic anhydrase 14 (*Car14*), extracellular matrix protein 1 (*Ecm1*) and oocyte maturation beta (*Omt2b*). However, all the probes profiling the same gene follow the same direction of expression; down-regulation for *Car14* and *Omt2b* and up-regulation for *Ecm1*. The genes with FC lower than 1.5 or greater than -1.5 were also analysed (Figure 7.16).

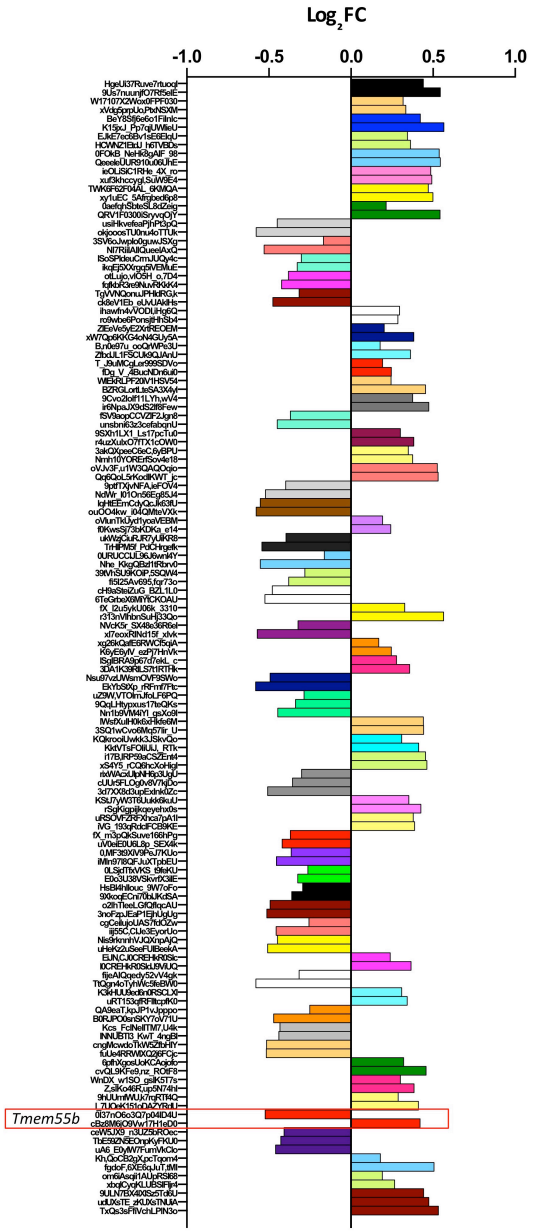


Figure 7.16: Analysis of possible splicing variants of differentially expressed genes on 9-week DM samples. All probes with expression level below or above 1.5 and -1.5 FC were included in the analysis. Probes detecting transcripts of the same gene were clustered. Colours represent different probes for the same gene. *Tmem55b* gene was assessed by 2 probes that have apposite levels of expression.

This analysis revealed that the two probes for transmembrane protein 55B gene (*Tmem55b*) exhibited a completely opposite behaviour in terms of expression, one is down-regulated (probe 0l37nO6o3Q7p04ID4U , Log_2FC= -0.52) and the other one is up-regulated (probe cBz8M6jO9Vw17H1eD0, Log_2FC=0.42). This finding positions *Tmem55b* as a gene candidate for alternative splicing with differential regulation of variants.

7.5 Discussion

Understanding the mechanisms underlying the rapid onset of POF in DM females would provide an opportunity to understand how the oocyte is regulating fertility within the ovary and could potentially contribute to the understanding of the pathology in women (*136*). In this chapter, whole genome gene expression analysis was carried out on ovaries from prepuberal (3-week), fertile (6-week) and infertile (9-week) DM and Control females. Gene expression analysis revealed that at 3 weeks just two genes, small nuclear ribonucleoprotein polypeptide A (*Snrpa*) and cathepsin k (*Ctsk*) are differentially expressed in DM ovaries compared with Controls. At 6-week three more genes are added: kinetochore associated 1 (*Kntc1*), developmental pluripotency associated 5A (*Dppa5a*) and RIKEN cDNA E330017A01 (*E330017A01Rik*). Interestingly, just 3 weeks later at 9-week, differentially expressed genes in DM ovaries dramatically increased reaching a total number of 1,253 genes. This finding is consistent with the accelerated phenotype shift from fertile to infertile in DM ovaries presented in previous chapters (*136*).

Interestingly, prepuberal DM ovaries (3-week) displayed a subtle change in gene expression compared with Control with only two genes being differentially expressed: *Snrpa* and *Ctsk*. Previously, functional and morphological analysis of 3-week DM ovaries has been reported (*133*). Prepuberal DM ovaries displayed a normal response to superovulation with comparable number of eggs ovulated in DM and Control females however, slightly alterations of ovary morphology were

reported like: presence of multiple-oocyte follicles (MOFs), ZP changes and presence of granulosa cells beneath the ZP in some oocytes. Whether down-regulation of *Snrpa* and up-regulation of *Ctsk* could be triggering these changes in 3-week DM ovaries or if these genes are involve directly or indirectly in DM ovarian phenotype is still unclear and further studies are needed to address this question.

Ctsk encodes cathepsin K, a cysteine protease expressed primarily in osteoclasts. Once secreted cathepsin K degrades collagen and other matrix proteins during bone resorption therefore, its role it has been largely studied in bone formation (*213-215*). In this regard, cathepsin K is currently an important target for osteoporosis therapy (*216*). Only one report has being published studying *Ctsk* expression in the ovary (*217*). In this study, northern blot analysis revealed changes in *Ctsk* mRNA during the oestrous cycle in mice, with maximum mRNA levels from late pro-oestrus until meta-oestrus. Immunohistochemistry revealed that cathepsin K staining is present in the ovary germinal epithelium with staining being especially strong in the contact points with secondary and Graafian follicles. Granulosa cells become immunopositives for cathepsin K upon follicle maturation and can be detected in oocytes in all stages of follicle development. On the other hand, theca cells displayed a weak immunostaining meanwhile the ovarian stroma exhibited negative immunostaining for Ctsk (*217*). Since Ctsk degrades extracellular matrix and it is expressed in the germinal epithelium contacting secondary and Graafian follicles, it can be inferred that Ctsk could play an active role in the ovulation process. The microarray analysis presented in this

chapter revealed that *Ctsk* is up-regulated in DM ovaries in all stages analysed (3-, 6- and 9-week). This overexpression has also been confirmed by RT-qPCR (Figure 7.13).

The second differentially expressed gene in 3-week DM samples was *Snrpa.* This gene encodes the small nuclear ribonucleoprotein polypeptide A protein, which has been implicated in the coupling of splicing and polyadenylation and it is capable of autoregulates its own synthesis inhibiting polyadenylation of the *Snrpa* pre-mRNA (*218*). The presence of this protein has not been described in the ovary.

At 6-week, 3 more genes are differentially expressed in DM ovaries: *Kntc1*, *Dppa5a* and *E330017A01Rik*. *Kntc1* encodes a protein that, along with many other proteins, is involved in mechanisms that ensure proper chromosome segregation during cell division. *Dppa5a* (also known as *Dppa5, Esg1* and *Ecat2*) encodes developmental pluripotency-associated protein 5A, which is involved in the control of cell pluripotency and early embryogenesis. Moreover, expression of *Dppa5a* has been indicated as a specific marker for pluripotent stem cells (*219-223*). Gene expression profile analysis in sows myometrium and ovary during pregnancy linked *Dppa5* with litter size and litter birth weight in pigs (*224*). Strong expression of *Dppa5* gene was detected in primordial germ cells at the transcriptional level in humans and mice (*225*) and single cell transcriptomic analysis using mRNA-Seq revealed expression of *Dppa5a* in mouse oocytes (*226*). *E330017A01Rik* gene function is currently unknown however its presence has been previously identified in the ovary. Quantitative RT-PCR analysis revealed that

E330017A01Rik is predominantly expressed in newborn mouse ovaries compared with other tissues. *In situ* hybridization carried out in adult mice showed strong expression in oocytes with only background staining in the rest of the ovarian tissue (*87*). The transcriptomic analysis carried out in 3- and 6-week DM ovaries is indicating these 5 genes as potential key candidates for the initiation of ovarian dysfunction and ultimately, the POF phenotype displayed by DM females. However, participation of other genes in the onset of POF in the DM model cannot be discarded and further analysis will be needed to address this question.

The sudden increase of differentially expressed genes observed in 9-week DM ovaries was analysed using gene ontology (GO) approach and therefore functional enrichment analysis was carried out. All up-regulated and down-regulated genes were analysed independently using DAVID platform. Interestingly, the top 5 annotation clusters of up-regulated genes are related with glycosylation, extracellular matrix, immune response, propeptides and cell adhesion (Table 7-8). Meanwhile the top 5 annotation clusters for down-regulated genes are related with non-membrane-bounded organelles, cell cycle, DNA replication, chromosome structure and nuclei and organelle lumen (Table 7-9). Down-regulation of cell cycle-related function was expected due to the marked reduction in ovarian function observed in 9-week DM females. On the other hand and considering that DM females produce oocytes lacking complex and hybrid *N*-glycans and core 1-derived *O*-glycans and that glycans are important regulators of cellular communication, the fact that this stimuli is inducing an up-regulation in cell signalling and glycosylation activity is both intriguing and fascinating and could

be indicating a compensatory mechanism. This finding is indicating the oocyte as a regulator of fertility and ovarian function through direct protein-protein molecular interactions between oocyte and somatic cell secreted factors. These results identify post-translational processing as a new area towards the understanding of infertility-related pathologies adding new information to the classical gene expression approach. Functional studies, like testing the effect of cathepsin K on follicle development *in vitro* using cathepsin K inhibitors to attempt recovering of follicle development, would be valuable to get a comprehensive understanding of how the oocyte-somatic cells communication is taking place in the DM ovary and to contribute to our knowledge of the molecular mechanisms involved in fertility regulation by the oocyte.

Since the DM female mouse has an oocyte-specific deletion a subset of 15 genes encoding oocyte-secreted proteins were extracted from the list of differentially expressed genes at 9-week and analysed in terms of fold of change from Control samples (Figure 7.14). DM females display arrest of follicle development but the total number of follicles (and therefore oocytes) remain unchanged between DM and Controls. Therefore, possible changes in levels of expression of oocyte-secreted proteins is not related to a decreased number of oocytes in the DM ovary.

Fourteen genes were down-regulated of which 71.4% (10 genes) displayed an expression level below 2-fold compared with Control samples. From these, *Bmp15* and *Gdf9* displayed the higher decrease in gene expression. Reduced

expression of *BMP15* and *GDF9* has been reported in ovaries from women with PCOS (*38*, *227-229*) and these studies agree that this is directly related with the aberrant follicle development and infertility observed in these women, which is consistent with the arrest of follicle development and infertility observed in 9-week DM ovaries. From the 15 oocyte-expressed genes analysed, *Sohlh1* (spermatogenesis and oogenesis specific basic helix-loop-helix 1) is the only gene that was up-regulated in DM ovaries. Analysis of *Sohlh1* in mouse ovaries showed that the protein is expressed preferentially in the oocyte and its disruption in *Sohlh1* knockout mice lead to disrupted folliculogenesis and therefore it is critical for normal fertility (*39*). Its function when up-regulated is unknown. Targeting gene sequencing of *SOHLH1* in Han Chinese and Serbian women with nonsyndromic premature ovarian insufficiency (POI) revealed the presence of 10 heterozygous variants that may suggest a role of *SOHLH1* in POI (*40*). Moreover, exome sequencing analysis performed in two pairs of sisters with non-syndromic hypergonadotropic hypogonadism from two unrelated families revealed the presence of mutations in *SOHLH1* (*41*). These studies (*40*, *41*) targeted this gene as a candidate for ovarian dysfunction for the first time in humans.

A meta-analysis carried out on data extracted from 59 publications (5333 patients and 9399 controls) found an association between 5 genes (*BMP15*, *ESR1*, *FMR1*, *FSHR* and *INHA*) polymorphisms and the risk of POF (*86*). From these five genes only bone morphogenetic protein 15 (*Bmp15*) and inhibin alpha (*Inha*) were differentially expressed in DM ovaries, being both genes down-regulated in 9-week DM ovaries compared with Controls (log_2FC=-2.32, AdjPVal=5.05e-05 and

log_2FC=-1.02, AdjPVal=0.0007, respectively). *Bmp15* encodes a protein that is a member of the transforming growth factor-beta superfamily and along with *Gdf9* it is involved in oocyte maturation and follicular development (*34*, *35*, *190*, *230*). Defects in *Bmp15* have been related with ovarian pathologies and infertility including altered ovulation (*231*), PCOS (*227*) and POF (*86*). *Inha* encodes the alpha subunit of inhibins A and inhibin B proteins complexes. In the ovary inhibin A is implicated in granulosa cell proliferation and differentiation, androgen synthesis and oocyte development (*232*) and constitute a candidate gene for POF (*233*).

The analysis of microarray gene expression carried out in this chapter based on the analysis of the expression profile per probe instead of per gene provided the opportunity to analyse potential gene candidates for alternative splicing for those genes targeted by more than one probe. Using a 1.5-fold increase or decrease expression change as a cut-off point to determine discordant expression of probes per gene, probes for the same gene were clustered and plotted. This analysis revealed that only 3 genes exhibited considerable differences on the expression levels: *Car14*, *Ecm1* and *Omt2b* (Figure 7.15). However, the changes in all cases followed the same direction of change; up-regulation for the two probes targeting *Car14* and *Omt2b* genes and down-regulation for the two probes targeting *Ecm1*. A second analysis was carried out on the multiple-probes genes with levels of expression lower than 1.5 and higher than -1.5-fold of change. Interestingly, one gene exhibited opposite direction of change for its 2 probes transmembrane protein 55B gene (*Tmem55b*). *Tmem55b*

(also known as type I phosphatidylinositol 4,5-bisphosphate 4-phosphatase) was identified and characterized for the first time in humans for Ungewickell *et al* in 2005 (*234*). The enzyme was described as a catalyser of the hydrolysis of phosphatidylinositol-4,5-bisphosphate to phosphatidylinositol-5- phosphate.

Phosphatidylinositides regulate intracellular membrane traffic by controlling the timing and localization of endocytic membrane trafficking, recruiting components of the intracellular transport machinery. The study revealed that the enzyme was ubiquitously expressed and localized on late endosomal/lysosomal membranes in epithelial cells. Overexpression in HeLa cells demonstrated increased EGF-receptor degradation after EGF stimulation (*234*). Recently, a new role for *Tmem55b* as a regulator for cholesterol metabolism has been reported (*235*). Using a combined gene expression profiling and functional studies approach carried out in lymphoblastoid cell lines from patients, *TMEM55B* was highly correlated with 3-hydroxy-3-methylglutaryl-CoA reductase (*HMGCR*), which encodes the rate-limiting enzyme for cholesterol synthesis. In hepatoma cell lines *TMEM55B* appears to modulate the activity of low-density lipoprotein receptor regulating cellular levels of cholesterol and the low-density lipoprotein receptor (LDLR) (*235*). Given the high demand for cholesterol by steroidogenic cells, four sources for cholesterol intake can be used: de novo synthesis in the endoplasmic reticulum, cholesterol stored in lipid droplets, uptake of circulating HDL via scavenger receptor B1 (SR-B1) and uptake of low-density lipoproteins (LDLs) via receptor-mediated endocytosis (*236*). As described before, this last mechanism for cholesterol cellular intake has been related with *TMEM55b* through

modulation of LDLR. In the ovary, cholesterol is used for theca cells to generate androgens, which in turn are converted to estrogen by granulosa cells (*237*). Based on this evidence and by the fact that *Tmem55b* is differentially expressed in 9-week DM ovaries, a role of *Tmem55b* in ovarian steroid production in mice is highly probable.

Twelve *Tmem55b* mRNA variants have been reported in the mRNA catalogue AceView, from the National Center for Biotechnology Information (NCBI) at the National Library of Medicine (NLM) (*238*), which support *Tmem55b* as a candidate for alternative splicing in 9-week DM ovaries. The finding that two *Tmem55b* probes displayed opposite gene expression changes suggests a complex regulatory gene control deserving further analysis.

Transcriptomic analysis of DM ovaries demonstrated a sharp change in gene expression compared with Controls from 6-week, when females are fertile, to 9-week, when DM females undergoes infertility. According to the results, only 2 genes at 3-week and 5 genes at 6-week were detected as differentially expressed in DM ovaries compared with Controls, which could represent candidate gene regulators for the onset of POF in the DM model. Remarkably, differentially expressed genes at 9-week in the DM ovaries are, among others, functionally enriched for cell communication and extracellular matrix, representing potential pathways affecting ovarian function and impairing fertility capacity. These candidate genes and pathways should be explored in depth to understand how the oocyte is triggering these events. In addition to the current study, which has

used high RNA quality samples, replicates and accurate computational analysis, further studies are necessary to validate the findings presented in this chapter. These results are fascinating and, as in any genome-wide analysis, substantial and valuable information can still be extracted from the data. Undoubtedly, these results will provide a solid foundation for future studies to contribute to our understanding of how the oocyte is orchestrating ovarian physiology and fertility.

Chapter 8: Conclusions

The oocyte-specific deletion of *Mgat1* and *C1galt1* in the DM mouse produces a POF phenotype by 3 months of age even though the females are fertile when reach puberty (*119*, *133*). The DM model provides an exciting opportunity to explore in depth the potential causes of this early ovary dysfunction.

In this thesis a decrease in ovulation rate has been excluded as the cause of the small litter size observed in DM females at 6 weeks of age (*119*). Instead it was found that the small litter size observed is most likely due to the altered ZP displayed by embryos from DM females during the preimplantation period, probably leading to delayed development and implantation. Interestingly, the onset of ovarian failure is even earlier than previously published (*133*). This work established a sharp decrease in the ovulation rate at 9 weeks, which explains the absence of a second litter in DM females.

The work conducted in this thesis also determine that the altered hormone profile of DM females is not the cause of follicle development arrest, since follicle development could not be resumed when DM ovarian tissue was transplanted into a host with a normal hormonal environment. However, the transplanted DM tissue exhibited an increase in the number of primary follicles compared with 9-week DM ovaries. This finding is consistent with previous publications of accelerated follicular activation after grafting (*165*, *166*) and demonstrate that the tissue can respond to the normal hormonal environment, however this is not enough to restore normal follicle development.

As the endocrine environment seems not to be the cause of POF in the DM model, the question of how intrinsic intra-ovarian factors could be involved in the altered follicle development was addressed. *In vitro* culture of preantral follicles was carried out to assess the possible influence of ovarian factors on the impaired follicle development observed in DM ovaries. Interestingly, the survival rate of DM follicles was about half of the survival rate exhibited by Control follicles, suggesting that there are intrinsic follicular factors that are interfering with DM follicle development. This hypothesis is supported by the finding that although, DM follicles that did survive were able to reach an equivalent final size to Controls, their growing curve was differed. How this could compromise the viability of the oocyte inside the follicle is still unknown.

The possibility that altered intra-follicular signaling in DM follicles could be preventing follicle development was also explored. Insight was obtained when DM germ cells were reaggregated with WT somatic cells to generate reaggregated chimeric ovaries (RCOs). This study demonstrated that 3- and 9- week DM oocytes are able to form follicles when associated with WT somatic cells. Amazingly, RCOs generated with 9-week oocytes, which come from infertile females with ovarian failure, produced follicles in equivalent numbers and at more advanced stages of follicle development than Control. These findings suggest that: i) DM oocytes from ovaries that have undergone POF retain the ability to support follicle development, ii) the 3a-3b follicle development block displayed by DM ovaries from 9 weeks onwards (discussed in Chapter 4) could be overcome using the RCO techniques. As the *Mgat1* and *C1galt1* deletions exist only in the oocyte of DM females from the

primary stage of follicle development onwards (*2*), and the phenotype of DM females changes from fertile (6 weeks) to infertile (9 weeks) and finally POF (3 month), it is clear that the oocyte is inducing changes on the somatic cell compartment. These changes could be accumulating over time and could be affecting not only the somatic cell compartments of the ovary but also the oocyte itself due to signalling feedback from the granulosa cells. Even though the RCO technique is still being optimised, the results presented in this thesis indicate the RCO technique as a promising therapeutic tool to re-establish follicle development in the DM and potentially other manifestations of POF.

Finally, the genetic profile of DM ovaries as the females transit from fertile to infertile was investigated using microarray. Consistent with the DM phenotype, the genetic profile of DM ovaries changes dramatically from 3 to 9 weeks. At 3 weeks just 2 genes are differentially expressed in DM ovaries: cathepsin K (*Ctsk*) and small nuclear ribonucleoprotein polypeptide A (*Snrpa*). Even though, Control and DM mice are essentially the same in terms of phenotype (*133*), *Cstk* and *Snrpa* could be potentially the main activators/mediators of the phenotypic changes observed later on in DM fertility. Both genes continued to be differentially expressed at 6 and 9 weeks, however 3 more genes are added to the list at 6 weeks: kinetochore associated 1 (*Kntc1*), developmental pluripotency associated 5A (*Dppa5a*) and RIKEN cDNA E330017A01 (*E330017A01Rik*). Interestingly, just 3 weeks later at 9 weeks, DM ovaries exhibited a dramatic change in gene expression, with 1,253 genes differentially expressed from Controls. *Ctsk* expression has been validated in this study but further validation is

needed. In addition, functional enrichment analysis revealed that functions related with glycosylation and extracellular matrix are altered in DM ovaries. This finding support previous results in this thesis that indicate intra-ovarian factors as responsible for the onset of POF in DM females. Is likely that in DM ovaries, altered glycosylation of oocyte-secreted proteins is impairing ovarian structure and normal communication between the oocyte and the somatic cell compartments, accumulating damage very rapidly over time. This accumulated damage could explain that despite the fact that DM females express the oocyte-specific mutation during all their reproductive life, their phenotype changes abruptly from fertile at 6 weeks to infertile just 3 weeks later. The microarrays results are very promising in terms of identifying genes and their pathways as possible candidates to explore mechanistic roles in POF develop. However, further validation is essential.

In summary, the work presented in this thesis explores in depth the origin of the fertility profile displayed by DM females and has highlighted intra-ovarian factors as responsible for the onset of POF. The expression analysis revealed progressive transcriptomic changes, and potential genes and pathways responsible for the POF phenotype in the DM mouse model highlighting target molecules to try to reverse POF**.**

References

1. M. E. Pepling, From primordial germ cell to primordial follicle: Mammalian female germ cell development. *genesis*. **44**, 622–632 (2006).

2. C. C. Philpott, M. J. Ringuette, J. Dean, Oocyte-specific expression and developmental regulation of ZP3, the sperm receptor of the mouse zona pellucida. *Developmental Biology*. **121**, 568–575 (1987).

3. P. M. Wassarman, C. Liu, E. S. Litscher, Constructing the mammalian egg zona pellucida: some new pieces of an old puzzle. *Journal of Cell Science*. **109 (Pt 8)**, 2001–2004 (1996).

4. J. A. Modliński, The role of the zona pellucida in the development of mouse eggs in vivo. *J Embryol Exp Morph*. **23**, 539–547 (1970).

5. P. M. Wassarman, E. S. Litscher, Influence of the zona pellucida of the mouse egg on folliculogenesis and fertility. *Int. J. Dev. Biol.* **56**, 833–839 (2012).

6. A. N. Hirshfield, Development of follicles in the mammalian ovary. *Int. Rev. Cytol.* **124**, 43–101 (1991).

7. G. Pelletier *et al.*, Immunoelectron microscopic localization of three key steroidogenic enzymes (cytochrome P450(scc), 3 beta-hydroxysteroid dehydrogenase and cytochrome P450(c17)) in rat adrenal cortex and gonads. *J. Endocrinol.* **171**, 373–383 (2001).

8. S. Cecconi, Growth and Differentiation of Small Ovarian Follicles in Mammals: Problems and Future Perspectives. *Journal of Reproduction and Development*. **48**, 431–445 (2002).

9. S. S. Smith, S. R. Ojeda, Neonatal release of gonadotropins is essential for development of ovarian follicle-stimulating hormone receptors. *Biology of Reproduction*. **34**, 219–227 (1986).

10. S. G. Hillier, Current concepts of the roles of follicle stimulating hormone and luteinizing hormone in folliculogenesis. *Hum Reprod*. **9**, 188–191 (1994).

11. A. Mayerhofer, G. A. Dissen, M. E. Costa, S. R. Ojeda, A role for neurotransmitters in early follicular development: induction of functional follicle-stimulating hormone receptors in newly formed follicles of the rat ovary. *Endocrinology*. **138**, 3320–3329 (1997).

12. E. A. McGee, A. J. Hsueh, Initial and cyclic recruitment of ovarian follicles. *Endocrine Reviews*. **21**, 200–214 (2000).

13. Y. S. MOON, B. K. TSANG, C. SIMPSON, D. T. Armstrong, 17 beta-Estradiol biosynthesis in cultured granulosa and thecal cells of human ovarian follicles: stimulation by follicle-stimulating hormone. *Journal of Clinical Endocrinology & Metabolism*. **47**, 263–267 (1978).

14. Z. R. Craig, W. Wang, J. A. Flaws, Endocrine-disrupting chemicals in ovarian function: effects on steroidogenesis, metabolism and nuclear receptor signaling. *Reproduction*. **142**, 633–646 (2011).

15. T. Pedersen, Follicle kinetics in the ovary of the cyclic mouse. *Acta Endocrinol.* **64**, 304–323 (1970).

16. T. Pedersen, H. Peters, Proposal for a classification of oocytes and follicles in the mouse ovary. *J. Reprod. Fertil.* **17**, 555–557 (1968).

17. E. Anderson, D. F. Albertini, Gap junctions between the oocyte and companion follicle cells in the mammalian ovary. *J. Cell Biol.* **71**, 680–686 (1976).

18. P. T. Brower, R. M. Schultz, Intercellular communication between granulosa cells and mouse oocytes: existence and possible nutritional role during oocyte growth. *Developmental Biology*. **90**, 144–153 (1982).

19. D. F. Albertini, C. M. Combelles, E. Benecchi, M. J. Carabatsos, Cellular basis for paracrine regulation of ovarian follicle development. *Reproduction*. **121**, 647–653 (2001).

20. R. Canipari, Oocyte--granulosa cell interactions. *Human Reproduction Update*. **6**, 279–289 (2000).

21. R. B. Gilchrist, L. J. Ritter, D. T. Armstrong, Oocyte-somatic cell interactions during follicle development in mammals. *Animal Reproduction Science*. **82-3**, 431–446 (2004).

22. J. Dong *et al.*, Growth differentiation factor-9 is required during early ovarian folliculogenesis. *Nature*. **383**, 531–535 (1996).

23. M. M. Matzuk, K. H. Burns, M. M. Viveiros, J. J. Eppig, Intercellular communication in the mammalian ovary: oocytes carry the conversation. *Science*. **296**, 2178–2180 (2002).

24. K. J. Hutt, D. F. Albertini, An oocentric view of folliculogenesis and embryogenesis. *REPRODUCTIVE BIOMEDICINE ONLINE*. **14**, 758–764 (2007).

25. R. B. Gilchrist, M. Lane, J. G. Thompson, Oocyte-secreted factors: regulators of cumulus cell function and oocyte quality. *Human Reproduction Update*. **14**, 159–177 (2008).

26. G. M. Kidder, B. C. Vanderhyden, Bidirectional communication between oocytes and follicle cells: ensuring oocyte developmental competence. *Can. J. Physiol. Pharmacol.* **88**, 399–413 (2010).

27. F. J. Diaz, K. Wigglesworth, J. J. Eppig, Oocytes are required for the preantral granulosa cell to cumulus cell transition in mice. *Developmental Biology*. **305**, 300–311 (2007).

28. K. Sugiura *et al.*, Estrogen promotes the development of mouse cumulus cells in coordination with oocyte-derived GDF9 and BMP15. *Mol Endocrinol*. **24**, 2303–2314 (2010).

29. J. J. Eppig, K. Wigglesworth, Development of mouse and rat oocytes in chimeric reaggregated ovaries after interspecific exchange of somatic and germ cell components. *Biology of Reproduction*. **63**, 1014–1023 (2000).

30. J. J. Eppig, K. Wigglesworth, F. L. Pendola, The mammalian oocyte orchestrates the rate of ovarian follicular development. *Proc. Natl. Acad. Sci. U.S.A.* **99**, 2890–2894 (2002).

31. S. A. McGrath, A. F. Esquela, S. J. Lee, Oocyte-specific expression of growth/differentiation factor-9. *Mol Endocrinol*. **9**, 131–136 (1995).

32. M. Laitinen *et al.*, A novel growth differentiation factor-9 (GDF-9) related factor is co-expressed with GDF-9 in mouse oocytes during folliculogenesis. *Mech. Dev.* **78**, 135–140 (1998).

33. J. L. Dube *et al.*, The bone morphogenetic protein 15 gene is X-linked and expressed in oocytes. *Mol Endocrinol*. **12**, 1809–1817 (1998).

34. Y.-Q. Su *et al.*, Synergistic roles of BMP15 and GDF9 in the development and function of the oocyte–cumulus cell complex in mice: genetic evidence for an oocyte–granulosa cell regulatory loop. *Developmental Biology*. **276**, 64–73 (2004).

35. C. Yan *et al.*, Synergistic roles of bone morphogenetic protein 15 and growth differentiation factor 9 in ovarian function. *Mol Endocrinol*. **15**, 854–866 (2001).

36. J. Y. Lin *et al.*, Effects of species differences on oocyte regulation of granulosa cell function. *Reproduction*. **144**, 557–567 (2012).

37. S. M. Galloway *et al.*, Mutations in an oocyte-derived growth factor gene (BMP15) cause increased ovulation rate and infertility in a dosage-sensitive manner. *Nat. Genet.* **25**, 279–283 (2000).

38. L.-N. Wei, X.-Y. Liang, C. Fang, M.-F. Zhang, Abnormal expression of growth differentiation factor 9 and bone morphogenetic protein 15 in stimulated oocytes during maturation from women with polycystic ovary syndrome. *Fertility and Sterility*. **96**, 464–468 (2011).

39. S. A. Pangas *et al.*, Oogenesis requires germ cell-specific transcriptional regulators Sohlh1 and Lhx8. *Proc. Natl. Acad. Sci. U.S.A.* **103**, 8090–8095 (2006).

40. S. Zhao *et al.*, Transcription factor SOHLH1 potentially associated with primary ovarian insufficiency. *Fertility and Sterility*. **103**, 548–553.e5 (2015).

41. Y. Bayram *et al.*, Homozygous loss-of-function mutations in SOHLH1 in patients with non-syndromic hypergonadotropic hypogonadism. *The Journal of clinical endocrinology and metabolism*, jc20151150 (2015).

42. J. Buratini *et al.*, Expression and function of fibroblast growth factor 10 and its receptor, fibroblast growth factor receptor 2B, in bovine follicles. *Biology of Reproduction*. **77**, 743–750 (2007).

43. K. Zhang, P. J. Hansen, A. D. Ealy, Fibroblast growth factor 10 enhances bovine oocyte maturation and developmental competence in vitro. *Reproduction*. **140**, 815–826 (2010).

44. E. S. Caixeta *et al.*, Bone morphogenetic protein 15 and fibroblast growth factor 10 enhance cumulus expansion, glucose uptake, and expression of genes in the ovulatory cascade during in vitro maturation of bovine cumulus-oocyte complexes. *Reproduction*. **146**, 27–35 (2013).

45. A. Meskhi, M. W. Seif, Premature ovarian failure. *Curr. Opin. Obstet. Gynecol.* **18**, 418–426 (2006).

46. A. N. Shelling, Premature ovarian failure. *Reproduction*. **140**, 633–641 (2010).

47. C. B. Coulam, S. C. Adamson, J. F. Annegers, Incidence of premature ovarian failure. *Obstet Gynecol*. **67**, 604–606 (1986).

48. L. M. Nelson, Clinical practice. Primary ovarian insufficiency. *N. Engl. J. Med.* **360**, 606–614 (2009).

49. L. M. NELSON *et al.*, Development of luteinized graafian follicles in patients with karyotypically normal spontaneous premature ovarian failure. *Journal of Clinical Endocrinology & Metabolism*. **79**, 1470–1475 (1994).

50. N. Suzuki *et al.*, Successful fertility preservation following ovarian tissue vitrification in patients with primary ovarian insufficiency. *Hum Reprod*. **30**, 608–615 (2015).

51. J. L. Simpson, Genetic and phenotypic heterogeneity in ovarian failure: overview of selected candidate genes. *Annals of the New York Academy of Sciences*. **1135**, 146–154 (2008).

52. C. K. Welt, Primary ovarian insufficiency: a more accurate term for premature ovarian failure. *Clin. Endocrinol. (Oxf)*. **68**, 499–509 (2008).

53. E. Kovanci, A. K. Schutt, Premature ovarian failure: clinical presentation and treatment. *Obstetrics and gynecology clinics of North America*. **42**, 153–161 (2015).

54. L. T. Shuster, D. J. Rhodes, B. S. Gostout, B. R. Grossardt, W. A. Rocca, Premature menopause or early menopause: Long-term health consequences. *Maturitas*. **65**, 161–166 (2010).

55. P. J. Schmidt *et al.*, Shyness, social anxiety, and impaired self-esteem in Turner syndrome and premature ovarian failure. *JAMA*. **295**, 1374–1376 (2006).

56. S. A. Orshan *et al.*, Women with spontaneous 46,XX primary ovarian insufficiency (hypergonadotropic hypogonadism) have lower perceived social support than control women. *Fertility and Sterility*. **92**, 688–693 (2009).

57. C. L. Benetti-Pinto, D. M. B. de Almeida, M. Y. Makuch, Quality of life in women with premature ovarian failure. *http://dx.doi.org/10.3109/09513590.2010.520374*. **27**, 645–649 (2011).

58. A. A. Deeks, M. Gibson-Helm, H. Teede, A. Vincent, Premature menopause: a comprehensive understanding of psychosocial aspects. *Climacteric*. **14**, 565–572 (2011).

59. R. W. Rebar, Premature ovarian failure. *Obstet Gynecol*. **113**, 1355–1363 (2009).

60. S. Vujovic, Aetiology of premature ovarian failure. *Menopause Int*. **15**, 72–75 (2009).

61. P. Laissue, G. Vinci, R. A. Veitia, M. Fellous, Recent advances in the study of genes involved in non-syndromic premature ovarian failure. *Molecular and Cellular Endocrinology*. **282**, 101–111 (2008).

62. N. Mendoza *et al.*, Spanish consensus on premature menopause. *Maturitas*. **80**, 220–225 (2015).

63. J. K. Hewitt *et al.*, Fertility in Turner syndrome. *Clin. Endocrinol. (Oxf)*. **79**, 606–614 (2013).

64. Practice Committee of American Society For Reproductive Medicine, Increased maternal cardiovascular mortality associated with pregnancy in women with Turner syndrome. *Fertility and Sterility*. **97**, 282–284 (2012).

65. N. Chevalier *et al.*, Materno-Fetal Cardiovascular Complications in Turner Syndrome after Oocyte Donation: Insufficient Prepregnancy Screening and Pregnancy Follow-Up Are Associated with Poor Outcome. *The Journal of clinical endocrinology and metabolism*. **96**, E260–E267 (2010).

66. L. Tarani *et al.*, Pregnancy in patients with Turner's syndrome: six new cases and review of literature. *Gynecol. Endocrinol.* **12**, 83–87 (1998).

67. M. D. Wittenberger *et al.*, The FMR1 premutation and reproduction. *Fertility and Sterility*. **87**, 456–465 (2007).

68. B. Wang *et al.*, Analyses of growth differentiation factor 9 (GDF9) and bone morphogenetic protein 15 (BMP15) mutation in Chinese women with premature ovarian failure. *Clin. Endocrinol. (Oxf)*. **72**, 135–136 (2010).

69. D. Tiotiu *et al.*, Variants of the BMP15 gene in a cohort of patients with premature ovarian failure. *Hum Reprod*. **25**, 1581–1587 (2010).

70. E. G. Allen *et al.*, Examination of reproductive aging milestones among women who carry the FMR1 premutation. *Hum Reprod*. **22**, 2142–2152 (2007).

71. D. Z. Loesch *et al.*, Transcript levels of the intermediate size or grey zone fragile X mental retardation 1 alleles are raised, and correlate with the number of CGG repeats. *J. Med. Genet.* **44**, 200–204 (2007).

72. P. Jin, S. T. Warren, Understanding the molecular basis of fragile X syndrome. *Hum. Mol. Genet.* **9**, 901–908 (2000).

73. I. Ferder *et al.*, Expression of fragile X mental retardation protein and Fmr1 mRNA during folliculogenesis in the rat. *Reproduction*. **145**, 335–343 (2013).

74. C. Lu *et al.*, Fragile X premutation RNA is sufficient to cause primary ovarian insufficiency in mice. *Hum. Mol. Genet.* **21**, 5039–5047 (2012).

75. L. Persani, R. Rossetti, C. Cacciatore, Genes involved in human premature ovarian failure. *J Mol Endocrinol*. **45**, 257–279 (2010).

76. E. Di Pasquale, P. Beck-Peccoz, L. Persani, Hypergonadotropic ovarian failure associated with an inherited mutation of human bone morphogenetic protein-15 (BMP15) gene. *Am. J. Hum. Genet.* **75**, 106–111 (2004).

77. E. Di Pasquale *et al.*, Identification of new variants of human BMP15 gene in a large cohort of women with premature ovarian failure. *Journal of Clinical Endocrinology & Metabolism*. **91**, 1976–1979 (2006).

78. R. Rossetti *et al.*, BMP15 mutations associated with primary ovarian insufficiency cause a defective production of bioactive protein. *Hum. Mutat.* **30**, 804–810 (2009).

79. L. Crisponi *et al.*, The putative forkhead transcription factor FOXL2 is mutated in blepharophimosis/ptosis/epicanthus inversus syndrome. *Nat. Genet.* **27**, 159–166 (2001).

80. J. Cocquet *et al.*, Evolution and expression of FOXL2. *J. Med. Genet.* **39**, 916–921 (2002).

81. E. De Baere, M. Fellous, R. A. Veitia, The transcription factor FOXL2 in ovarian function and dysfunction. *Folia Histochemica et Cytobiologica*. **47**, S43–S49 (2010).

82. L. Dunkel, J. L. Tilly, T. Shikone, K. Nishimori, A. J. Hsueh, Follicle-stimulating hormone receptor expression in the rat ovary: increases during prepubertal development and regulation by the opposing actions of transforming growth factors beta and alpha. *Biology of Reproduction*. **50**, 940–948 (1994).

83. P. J. O'Shaughnessy, P. Marsh, K. Dudley, Follicle-stimulating hormone receptor mRNA in the mouse ovary during post-natal development in the normal mouse and in the adult hypogonadal (hpg) mouse: structure of alternate transcripts. *Molecular and Cellular Endocrinology*. **101**, 197–201 (1994).

84. S. G. Hillier, Gonadotropic control of ovarian follicular growth and development. *Molecular and Cellular Endocrinology*. **179**, 39–46 (2001).

85. J. Du *et al.*, Two FSHR variants, haplotypes and meta-analysis in Chinese women with premature ovarian failure and polycystic ovary syndrome. *Mol. Genet. Metab.* **100**, 292–295 (2010).

86. D. Pu, Y. Xing, Y. Gao, L. Gu, J. Wu, Gene variation and premature ovarian failure: a meta-analysis. *Eur. J. Obstet. Gynecol. Reprod. Biol.* **182**, 226–237 (2014).

87. S. Joshi, H. Davies, L. P. Sims, S. E. Levy, J. Dean, Ovarian gene expression in the absence of FIGLA, an oocyte-specific transcription factor. *BMC Dev. Biol.* **7**, 67 (2007).

88. H. Zhao *et al.*, Transcription Factor FIGLA is Mutated in Patients with Premature Ovarian Failure. *The American Journal of Human Genetics*. **82**, 1342–1348 (2008).

89. D. Tosh, H. S. Rani, U. S. Murty, A. Deenadayal, P. Grover, Mutational analysis of the FIGLA gene in women with idiopathic premature ovarian failure. *Menopause*. **22**, 1–7 (2015).

90. V. K. Tuohy, C. Z. Altuntas, Autoimmunity and premature ovarian failure. *Curr. Opin. Obstet. Gynecol.* **19**, 366–369 (2007).

91. V. K. Bakalov, V. H. Vanderhoof, C. A. Bondy, L. M. NELSON, Adrenal antibodies detect asymptomatic auto-immune adrenal insufficiency in young women with spontaneous premature ovarian failure. *Hum Reprod*. **17**, 2096–2100 (2002).

92. C. BETTERLE *et al.*, Premature Ovarian Failure - Autoimmunity and Natural-History. *Clin. Endocrinol. (Oxf)*. **39**, 35–43 (1993).

93. E.-D. Kreuser, W.-D. Hetzel, D. O. Billia, E. Thiel, Gonadal toxicity following cancer therapy in adults: significance, diagnosis, prevention and treatment. *Cancer Treatment Reviews*. **17**, 169–175 (1990).

94. J. M. Koh *et al.*, Primary ovarian failure caused by a solvent containing 2-bromopropane. *Eur. J. Endocrinol.* **138**, 554–556 (1998).

95. B. L. Harlow, L. B. Signorello, Factors associated with early menopause. *Maturitas*. **35**, 3–9 (2000).

96. K. Jagarlamudi, P. Reddy, D. Adhikari, K. Liu, Genetically modified mouse models for premature ovarian failure (POF). *Molecular and Cellular Endocrinology*. **315**, 1–10 (2010).

97. H. R. S. Guangming Wu, Role of Oct4 in the early embryo development. *Cell Regeneration*. **3**, 7 (2014).

98. S. Jerabek, F. Merino, H. R. Schöler, V. Cojocaru, OCT4: dynamic DNA binding pioneers stem cell pluripotency. *Biochim. Biophys. Acta*. **1839**, 138–154 (2014).

99. M. Zuccotti *et al.*, OCT4 and the acquisition of oocyte developmental competence during folliculogenesis. *Int. J. Dev. Biol.* **56**, 853–858 (2012).

100. J. Kehler *et al.*, Oct4 is required for primordial germ cell survival. *EMBO Rep.* **5**, 1078–1083 (2004).

101. J. L. Taupin, Q. Tian, N. Kedersha, M. Robertson, P. Anderson, The RNA-binding protein TIAR is translocated from the nucleus to the cytoplasm during Fas-mediated apoptotic cell death. *Proc. Natl. Acad. Sci. U.S.A.* **92**, 1629–1633 (1995).

102. A. R. Beck, I. J. Miller, P. Anderson, M. Streuli, RNA-binding protein TIAR is essential for primordial germ cell development. *Proc. Natl. Acad. Sci. U.S.A.* **95**, 2331–2336 (1998).

103. K. A. Lawson *et al.*, Bmp4 is required for the generation of primordial germ cells in the mouse embryo. *Genes & Development*. **13**, 424–436 (1999).

104. Y. Ying, X. M. Liu, A. Marble, K. A. Lawson, G. Q. Zhao, Requirement of Bmp8b for the generation of primordial germ cells in the mouse. *Mol Endocrinol*. **14**, 1053–1063 (2000).

105. Y. Ying, G. Q. Zhao, Cooperation of endoderm-derived BMP2 and extraembryonic ectoderm-derived BMP4 in primordial germ cell generation in the mouse. *Developmental Biology*. **232**, 484–492 (2001).

106. S. Keeney, C. N. Giroux, N. Kleckner, Meiosis-Specific DNA Double-Strand Breaks Are Catalyzed by Spo11, a Member of a Widely Conserved Protein Family. *Cell*. **88**, 375–384 (1997).

107. P. J. Romanienko, R. D. Camerini-Otero, The mouse Spo11 gene is required for meiotic chromosome synapsis. *Mol. Cell*. **6**, 975–987 (2000).

108. D. K. Bishop, D. Park, L. Xu, N. Kleckner, DMC1: a meiosis-specific yeast homolog of E. coli recA required for recombination, synaptonemal complex formation, and cell cycle progression. *Cell*. **69**, 439–456 (1992).

109. M. Di Giacomo *et al.*, Distinct DNA-damage-dependent and -independent responses drive the loss of oocytes in recombination-defective mouse mutants. *Proc. Natl. Acad. Sci. U.S.A.* **102**, 737–742 (2005).

110. B. Kneitz *et al.*, MutS homolog 4 localization to meiotic chromosomes is required for chromosome pairing during meiosis in male and female mice. *Genes & Development*. **14**, 1085–1097 (2000).

111. S. S. de Vries *et al.*, Mouse MutS-like protein Msh5 is required for proper chromosome synapsis in male and female meiosis. *Genes & Development*. **13**, 523–531 (1999).

112. S. M. Soyal, A. Amleh, J. Dean, FIGalpha, a germ cell-specific transcription factor required for ovarian follicle formation. *Development*. **127**, 4645–4654 (2000).

113. A. Rajkovic, S. A. Pangas, D. Ballow, N. Suzumori, M. M. Matzuk, NOBOX deficiency disrupts early folliculogenesis and oocyte-specific gene expression. *Science*. **305**, 1157–1159 (2004).

114. D. Schmidt *et al.*, The murine winged-helix transcription factor Foxl2 is required for granulosa cell differentiation and ovary maintenance. *Development*. **131**, 933–942 (2004).

115. A. M. Simon, D. A. Goodenough, E. Li, D. L. Paul, Female infertility in mice lacking connexin 37. *Nature*. **385**, 525–529 (1997).

116. M. H. Abel, I. Huhtaniemi, P. Pakarinen, T. R. Kumar, H. M. Charlton, Age-related uterine and ovarian hypertrophy in FSH receptor knockout and FSHbeta subunit knockout mice. *Reproduction*. **125**, 165–173 (2003).

117. M. H. Abel *et al.*, The effect of a null mutation in the follicle-stimulating hormone receptor gene on mouse reproduction. *Endocrinology*. **141**, 1795–1803 (2000).

118. A. Dierich *et al.*, Impairing follicle-stimulating hormone (FSH) signaling in vivo: targeted disruption of the FSH receptor leads to aberrant gametogenesis and hormonal imbalance. *Proc. Natl. Acad. Sci. U.S.A.* **95**, 13612–13617 (1998).

119. S. A. Williams, L. Xia, R. D. Cummings, R. P. McEver, P. Stanley, Fertilization in mouse does not require terminal galactose or N-acetylglucosamine on the zona pellucida glycans. *Journal of Cell Science*. **120**, 1341–1349 (2007).

120. A. Varki *et al.*, *N-Glycans* (Cold Spring Harbor Laboratory Press, Cold Spring Harbor (NY), ed. 2, 2009).

121. A. Dove, The bittersweet promise of glycobiology. *Nature Biotechnology*. **19**, 913–917 (2001).

122. Mice lacking N-acetylglucosaminyltransferase I activity die at mid-gestation, revealing an essential role for complex or hybrid N-linked carbohydrates. *Proc. Natl. Acad. Sci. U.S.A.* **91**, 728–732 (1994).

123. A. Varki *et al.*, *O-GalNAc Glycans* (Cold Spring Harbor Laboratory Press, Cold Spring Harbor (NY), ed. 2, 2009).

124. P. Stanley, Golgi Glycosylation. *Cold Spring Harbor Perspectives in Biology*. **3**, –a005199 (2011).

125. T. Yago *et al.*, Core 1-derived O-glycans are essential E-selectin ligands on neutrophils. *Proceedings of the National Academy of Sciences*. **107**, 9204–9209 (2010).

126. O-glycosylation modulates integrin and FGF signalling by influencing the secretion of basement membrane components. *Nat Commun*. **3** (2012), doi:10.1038/ncomms1874.

127. Podoplanin requires sialylated O-glycans for stable expression on lymphatic endothelial cells and for interaction with platelets. *Blood*. **124**, 3656–3665 (2014).

128. L. Xia, Defective angiogenesis and fatal embryonic hemorrhage in mice lacking core 1-derived O-glycans. *J. Cell Biol.* **164**, 451–459 (2004).

129. S. Shi *et al.*, Inactivation of the Mgat1 gene in oocytes impairs oogenesis, but embryos lacking complex and hybrid N-glycans develop and implant. *Molecular and Cellular Biology*. **24**, 9920–9929 (2004).

130. S. A. Williams, P. Stanley, Oocyte-specific deletion of complex and hybrid N-glycans leads to defects in preovulatory follicle and cumulus mass development. *Reproduction*. **137**, 321–331 (2009).

131. S. A. Williams, P. Stanley, Mouse fertility is enhanced by oocyte-specific loss of core 1-derived O-glycans. *FASEB J.* **22**, 2273–2284 (2008).

132. A. P. Christensen, S. H. Patel, P. Grasa, H. C. Christian, S. A. Williams, Oocyte glycoproteins regulate the form and function of the follicle basal lamina and theca cells. - PubMed - NCBI. *Developmental Biology* (2014), doi:10.1016/j.ydbio.2014.12.024.

133. S. A. Williams, P. Stanley, Premature ovarian failure in mice with oocytes lacking core 1-derived O-glycans and complex N-glycans. *Endocrinology*. **152**, 1057–1066 (2011).

134. M. Lewandoski, K. M. Wassarman, G. R. Martin, Zp3-cre, a transgenic mouse line for the activation or inactivation of loxP-flanked target genes specifically in the female germ line. *Curr. Biol.* **7**, 148–151 (1997).

135. I. Van der Auwera, T. D'Hooghe, Superovulation of female mice delays embryonic and fetal development. *Hum Reprod*. **16**, 1237–1243 (2001).

136. P. Grasa, H. Kaune, S. A. Williams, Embryos generated from oocytes lacking complex N- and O-glycans have compromised development and implantation. *Reproduction*. **144**, 455–465 (2012).

137. G. E. Mann, G. E. Lamming, Relationship between maternal endocrine environment, early embryo development and inhibition of the luteolytic mechanism in cows. *Reproduction*. **121**, 175–180 (2001).

138. A. Nagy, M. Gertsenstein, K. Vintersten, *Manipulating the mouse embryo: a laboratory manual* (2003).

139. R. A. Bronson, A. McLaren, Transfer to the mouse oviduct of eggs with and without the zona pellucida. *J. Reprod. Fertil.* **22**, 129–137 (1970).

140. H. Suzuki, M. Togashi, J. Adachi, Y. Toyoda, Developmental ability of zona-free mouse embryos is influenced by cell association at the 4-cell stage. *Biology of Reproduction*. **53**, 78–83 (1995).

141. R. Ribas *et al.*, Development of a zona-free method of nuclear transfer in the mouse. *Cloning Stem Cells*. **7**, 126–138 (2005).

142. R. C. Ribas *et al.*, Effect of zona pellucida removal on DNA methylation in early mouse embryos. *Biology of Reproduction*. **74**, 307–313 (2006).

143. W. T. Garside, J. R. Loret de Mola, J. A. Bucci, R. W. Tureck, S. Heyner, Sequential analysis of zona thickness during in vitro culture of human zygotes: correlation with embryo quality, age, and implantation. *Mol. Reprod. Dev.* **47**, 99–104 (1997).

144. A. Gabrielsen, S. Lindenberg, K. Petersen, The impact of the zona pellucida thickness variation of human embryos on pregnancy outcome in relation to suboptimal embryo development. A prospective randomized controlled study. *Hum Reprod*. **16**, 2166–2170 (2001).

145. Y. Shen, T. Stalf, C. Mehnert, U. Eichenlaub-Ritter, H.-R. Tinneberg, High magnitude of light retardation by the zona pellucida is associated with conception cycles. *Hum Reprod*. **20**, 1596–1606 (2005).

146. Y. Xie *et al.*, Shear stress induces preimplantation embryo death that is delayed by the zona pellucida and associated with stress-activated protein kinase-mediated apoptosis. *Biology of Reproduction*. **75**, 45–55 (2006).

147. L. Strain, J. Dean, M. Hamilton, D. T. Bonthron, A true hermaphrodite chimera resulting from embryo amalgamation after in vitro fertilization. *N. Engl. J. Med.* **338**, 166–169 (1998).

148. R. S. PRATHER, L. J. HAGEMANN, N. L. FIRST, Preimplantation Mammalian Aggregation and Injection Chimeras. *Gamete Res*. **22**, 233–247 (1989).

149. G. S. Eakin, A.-K. Hadjantonakis, Production of chimeras by aggregation of embryonic stem cells with diploid or tetraploid mouse embryos. *Nat Protoc*. **1**, 1145–1153 (2006).

150. C. J. Epstein *et al.*, Production of viable adult trisomy 17 reversible diploid mouse chimeras. *Proc. Natl. Acad. Sci. U.S.A.* **79**, 4376–80 (1982).

151. C. Simón, J. C. Martín, A. Pellicer, Paracrine regulators of implantation. *Baillieres Best Pract Res Clin Obstet Gynaecol*. **14**, 815–826 (2000).

152. S. K. Dey *et al.*, Molecular cues to implantation. *Endocrine Reviews*. **25**, 341–373 (2004).

153. O. Ueda *et al.*, Possible expansion of "Window of Implantation" in pseudopregnant mice: time of implantation of embryos at different stages of development transferred into the same recipient. *Biology of Reproduction*. **69**, 1085–1090 (2003).

154. B. Falck, Site of Production of Oestrogen in Rat Ovary as Studied in Micro-Transplants. *Acta Physiol Scand Suppl*. **47**, 1–101 (1959).

155. D. T. Baird, Evidence in vivo for the two-cell hypothesis of oestrogen synthesis by the sheep Graafian follicle. *J. Reprod. Fertil.* **50**, 183–185 (1977).

156. S. Luisi, P. Florio, F. M. Reis, F. Petraglia, Inhibins in female and male reproductive physiology: role in gametogenesis, conception, implantation and early pregnancy. *Human Reproduction Update*. **11**, 123–135 (2005).

157. J. K. Findlay *et al.*, The roles of activins, inhibins and estrogen in early committed follicles. *Molecular and Cellular Endocrinology*. **163**, 81–87 (2000).

158. C. J. Corbin, J. M. Trant, K. W. Walters, A. J. Conley, Changes in testosterone metabolism associated with the evolution of placental and gonadal isozymes of porcine aromatase cytochrome P450. *Endocrinology*. **140**, 5202–5210 (1999).

159. L. W. Roth, R. Alvero, Pregnancy in a woman with premature ovarian insufficiency associated with blepharophimosis, ptosis, epicanthus inversus syndrome type I. A case report. *J Reprod Med*. **59**, 87–89 (2014).

160. F. Pouresmaeili, Z. Fazeli, Premature ovarian failure: a critical condition in the reproductive potential with various genetic causes. *Int J Fertil Steril*. **8**, 1–12 (2014).

161. I. Tsuji, K. Ami, N. Fujinami, Pregnancy following ovarian induction in a patient with premature ovarian failure and undetectable serum anti-Müllerian hormone. *J. Obstet. Gynaecol. Res.* **39**, 1070–1072 (2013).

162. J. A. Visser, I. Schipper, J. S. E. Laven, A. P. N. Themmen, Anti-Müllerian hormone: an ovarian reserve marker in primary ovarian insufficiency. *Nat Rev Endocrinol*. **8**, 331–341 (2012).

163. S. L. Broer, F. J. M. Broekmans, J. S. E. Laven, B. C. J. M. Fauser, Anti-Müllerian hormone: ovarian reserve testing and its potential clinical implications. *Human Reproduction Update*. **20**, 688–701 (2014).

164. A. Robles, M. A. Checa, M. Prat, R. Carreras, Medical alternatives to oocyte donation in women with premature ovarian failure: a systematic review. *Gynecol. Endocrinol.* **29**, 632–637 (2013).

165. M.-M. Dolmans *et al.*, Short-term transplantation of isolated human ovarian follicles and cortical tissue into nude mice. *Reproduction*. **134**, 253–262 (2007).

166. D. T. Baird, B. Campbell, C. de Souza, E. Telfer, Long-term ovarian function in sheep after ovariectomy and autotransplantation of cryopreserved cortical strips. *Eur. J. Obstet. Gynecol. Reprod. Biol.* **113 Suppl 1**, S55–9 (2004).

167. J. Donnez, Ovarian tissue cryopreservation and transplantation: a review. *Human Reproduction Update*. **12**, 519–535 (2006).

168. S. J. Baker, V. Srsen, R. Lapping, N. Spears, Combined effect of follicle-follicle interactions and declining follicle-stimulating hormone on murine follicle health in vitro. *Biology of Reproduction*. **65**, 1304–1310 (2001).

169. R. Miura, S. Haneda, K. Kayano, M. Matsui, Short communication: Development of the first follicular wave dominant follicle on the ovary ipsilateral to the corpus luteum is associated with decreased conception rate in dairy cattle. *J. Dairy Sci.* (2014), doi:10.3168/jds.2014-8388.

170. P. Da Silva-Buttkus, G. Marcelli, S. Franks, J. Stark, K. Hardy, Inferring biological mechanisms from spatial analysis: prediction of a local inhibitor in the ovary. *Proceedings of the National Academy of Sciences*. **106**, 456–461 (2009).

171. J. Axford, The impact of glycobiology on medicine. *Trends in Immunology*. **22**, 237–239 (2001).

172. A. M. Sinclair, S. Elliott, Glycoengineering: the effect of glycosylation on the properties of therapeutic proteins. *J Pharm Sci*. **94**, 1626–1635 (2005).

173. A. A. Murray *et al.*, Follicular growth and oocyte competence in the in vitro cultured mouse follicle: effects of gonadotrophins and steroids. *Molecular Human Reproduction*. **14**, 75–83 (2008).

174. A. A. Murray *et al.*, Role of ascorbic acid in promoting follicle integrity and survival in intact mouse ovarian follicles in vitro. *Reproduction*. **121**, 89–96 (2001).

175. N. Spears *et al.*, Mouse ovarian follicles secrete factors affecting the growth and development of like-sized ovarian follicles in vitro. *Biology of Reproduction*. **67**, 1726–1733 (2002).

176. P. G. Artini *et al.*, Growth factors and folliculogenesis in polycystic ovary patients. *Expert Review of Endocrinology & Metabolism*. **2**, 215–223 (2007).

177. J. Qiao, H. L. Feng, Extra- and intra-ovarian factors in polycystic ovary syndrome: impact on oocyte maturation and embryo developmental competence. *Human Reproduction Update*. **17**, 17–33 (2011).

178. M. M. Andersen, J. Kroll, A. G. Byskov, M. Faber, Protein composition in the fluid of individual bovine follicles. *J. Reprod. Fertil.* **48**, 109–118 (1976).

179. H. J. GRIMEK, M. E. BELLIN, R. L. AX, Characteristics of Proteoglycans Isolated From Small and Large Bovine Ovarian Follicles. *Biology of Reproduction*. **30**, 397–409 (1984).

180. P. Cristol *et al.*, [Pregnancies by fertilization in vitro. Biochemistry of the follicular fluid]. *Pathol. Biol.* **33**, 155–161 (1985).

181. K. P. MCNATTY, D. T. Baird, Relationship Between Follicle-Stimulating-Hormone, Androstenedione and Estradiol in Human Follicular-Fluid. *J. Endocrinol.* **76**, 527–531 (1978).

182. C. Mendoza *et al.*, Follicular fluid markers of oocyte developmental potential. *Hum Reprod*. **17**, 1017–1022 (2002).

183. M. Das, D. J. Gillott, E. Saridogan, O. Djahanbakhch, Anti-Mullerian hormone is increased in follicular fluid from unstimulated ovaries in women with polycystic ovary syndrome. *Hum Reprod*. **23**, 2122–2126 (2008).

184. P. Piomboni *et al.*, Protein modification as oxidative stress marker in follicular fluid from women with polycystic ovary syndrome: the effect of inositol and metformin. *J Assist Reprod Genet*. **31**, 1269–1276 (2014).

185. K. Bender, S. Walsh, A. C. O. Evans, T. Fair, L. Brennan, Metabolite concentrations in follicular fluid may explain differences in fertility between heifers and lactating cows. *Reproduction*. **139**, 1047–1055 (2010).

186. J. D. O'Shea, Structure-function relationships in the wall of the ovarian follicle. *Aust. J. Biol. Sci.* **34**, 379–394 (1981).

187. J. E. Fortune, The early stages of follicular development: activation of primordial follicles and growth of preantral follicles. *Animal Reproduction Science*. **78**, 135–163 (2003).

188. J. J. Eppig, Oocyte control of ovarian follicular development and function in mammals. *Reproduction*. **122**, 829–838 (2001).

189. F. Otsuka, K. J. McTavish, S. Shimasaki, Integral role of GDF-9 and BMP-15 in ovarian function. *Mol. Reprod. Dev.* **78**, 9–21 (2011).

190. J. Peng *et al.*, Growth differentiation factor 9:bone morphogenetic protein 15 heterodimers are potent regulators of ovarian functions. *Proc. Natl. Acad. Sci. U.S.A.* **110**, E776–E785 (2013).

191. J. A. Parrott, M. K. Skinner, Kit-ligand/stem cell factor induces primordial follicle development and initiates folliculogenesis. *Endocrinology*. **140**, 4262–4271 (1999).

192. A. L. L. Durlinger, J. A. Visser, A. P. N. Themmen, Regulation of ovarian function: the role of anti-Müllerian hormone. *Reproduction*. **124**, 601–609 (2002).

193. R. Li, R. J. Norman, D. T. Armstrong, R. B. Gilchrist, Oocyte-secreted factor(s) determine functional differences between bovine mural granulosa cells and cumulus cells. *Biology of Reproduction*. **63**, 839–845 (2000).

194. K. E. Latham, K. Wigglesworth, M. McMenamin, J. J. Eppig, Stage-dependent effects of oocytes and growth differentiation factor 9 on mouse granulosa cell development: advance programming and subsequent control of the transition from preantral secondary follicles to early antral tertiary follicles. *Biology of Reproduction*. **70**, 1253–1262 (2004).

195. J. J. Eppig, K. Wigglesworth, Y. Hirao, Metaphase I arrest and spontaneous parthenogenetic activation of strain LTXBO oocytes: chimeric reaggregated ovaries establish primary lesion in oocytes. *Developmental Biology*. **224**, 60–68 (2000).

196. J. J. Eppig, K. Wigglesworth, D. S. Varnum, J. H. Nadeau, Genetic regulation of traits essential for spontaneous ovarian teratocarcinogenesis in strain LT/Sv mice: aberrant meiotic cell cycle, oocyte activation, and parthenogenetic development. *Cancer Research*. **56**, 5047–5054 (1996).

197. A. Steinberger, E. Steinberger, In vitro culture of rat testicular cells. *Exp. Cell Res.* **44**, 443–452 (1966).

198. T. Burnik Papler, E. Vrtacnik Bokal, L. Lovrecic, A. N. Kopitar, A. Maver, No Specific Gene Expression Signature in Human Granulosa and Cumulus Cells for Prediction of Oocyte Fertilisation and Embryo Implantation. *PLoS ONE*. **10**, e0115865 (2015).

199. P. Díaz-Gimeno, M. Ruíz-Alonso, D. Blesa, C. Simón, Transcriptomics of the human endometrium. *Int. J. Dev. Biol.* **58**, 127–137 (2014).

200. S. Assou *et al.*, The human cumulus--oocyte complex gene-expression profile. *Hum Reprod*. **21**, 1705–1719 (2006).

201. E. B. Cordts, D. M. Christofolini, A. A. dos Santos, B. Bianco, C. P. Barbosa, Genetic aspects of premature ovarian failure: a literature review. *Arch Gynecol Obstet*. **283**, 635–643 (2010).

202. J. Li *et al.*, Microarray gene expression profiling and bioinformatics analysis of premature ovarian failure in a rat model. *Experimental and Molecular Pathology*. **97**, 535–541 (2014).

203. P. Du, W. A. Kibbe, S. M. Lin, lumi: a pipeline for processing Illumina microarray. *Bioinformatics*. **24**, 1547–1548 (2008).

204. S. M. Lin, P. Du, W. Huber, W. A. Kibbe, Model-based variance-stabilizing transformation for Illumina microarray data. *Nucleic Acids Research*. **36**, e11–e11 (2008).

205. P. Du, W. A. Kibbe, S. M. Lin, nuID: a universal naming scheme of oligonucleotides for illumina, affymetrix, and other microarrays. *Biology Direct*. **2**, 16 (2007).

206. G. K. Smyth, Linear models and empirical bayes methods for assessing differential expression in microarray experiments. *Stat Appl Genet Mol Biol*. **3**, Article3 (2004).

207. D. W. Huang, B. T. Sherman, R. A. Lempicki, Bioinformatics enrichment tools: paths toward the comprehensive functional analysis of large gene lists. *Nucleic Acids Research*. **37**, 1–13 (2009).

208. D. W. Huang, B. T. Sherman, R. A. Lempicki, Systematic and integrative analysis of large gene lists using DAVID bioinformatics resources. *Nat Protoc*. **4**, 44–57 (2009).

209. I. M. E. Vargas, P. E. Vivas-Mejía, Assessment of mRNA splice variants by qRT-PCR. *Methods Mol. Biol.* **1049**, 171–186 (2013).

210. K. C. Thomas *et al.*, Evidence based selection of commonly used RT-qPCR reference genes for the analysis of mouse skeletal muscle. *PLoS ONE*. **9**, e88653 (2014).

211. K. J. Livak, T. D. Schmittgen, Analysis of relative gene expression data using real-time quantitative PCR and the 2− ΔΔCT method. *Methods*. **25**, 402–408 (2001).

212. A. Schroeder *et al.*, BMC Molecular Biology | Full text | The RIN: an RNA integrity number for assigning integrity values to RNA measurements. *BMC Mol Biol*. **7**, 3 (2006).

213. M. A. Gentile *et al.*, Increased fracture callus mineralization and strength in cathepsin K knockout mice. *Bone*. **66**, 72–81 (2014).

214. C. Jacome-Galarza *et al.*, Altered hematopoietic stem cell and osteoclast precursor frequency in cathepsin K null mice. *J. Cell. Biochem.* **115**, 1449–1457 (2014).

215. S. Lotinun *et al.*, Osteoclast-specific cathepsin K deletion stimulates S1P-dependent bone formation. *J. Clin. Invest.* **123**, 666–681 (2013).

216. E. Cairoli, V. V. Zhukouskaya, C. Eller-Vainicher, I. Chiodini, Perspectives on osteoporosis therapies. *J. Endocrinol. Invest.* **38**, 303–311 (2015).

217. S. Oksjoki, M. Söderström, E. Vuorio, L. Anttila, Differential expression patterns of cathepsins B, H, K, L and S in the mouse ovary. *Molecular Human Reproduction*. **7**, 27–34 (2001).

218. J. M. Klein Gunnewiek *et al.*, Fourteen residues of the U1 snRNP-specific U1A protein are required for homodimerization, cooperative RNA binding, and inhibition of polyadenylation. *Molecular and Cellular Biology*. **20**, 2209–2217 (2000).

219. J. Adjaye *et al.*, Primary differentiation in the human blastocyst: comparative molecular portraits of inner cell mass and trophectoderm cells. *Stem Cells*. **23**, 1514–1525 (2005).

220. T. Dansranjavin *et al.*, The role of promoter CpG methylation in the epigenetic control of stem cell related genes during differentiation. *Cell Cycle*. **8**, 916–924 (2009).

221. M. A. Lagarkova, P. Y. Volchkov, A. V. Lyakisheva, E. S. Philonenko, S. L. Kiselev, Diverse epigenetic profile of novel human embryonic stem cell lines. *Cell Cycle*. **5**, 416–420 (2006).

222. T. Aoki *et al.*, Generation of induced pluripotent stem cells from human adipose-derived stem cells without c-MYC. *Tissue Engineering Part A*. **16**, 2197–2206 (2010).

223. K. Miharada, V. Sigurdsson, S. Karlsson, Dppa5 improves hematopoietic stem cell activity by reducing endoplasmic reticulum stress. *Cell Rep*. **7**, 1381–1392 (2014).

224. L. Wang *et al.*, Data mining in networks of differentially expressed genes during sow pregnancy. *Int. J. Biol. Sci.* **8**, 548–560 (2012).

225. S. K. Kim *et al.*, Identification of developmental pluripotency associated 5 expression in human pluripotent stem cells. *Stem Cells*. **23**, 458–462 (2005).

226. F. Tang *et al.*, mRNA-Seq whole-transcriptome analysis of a single cell. *Nat. Methods*. **6**, 377–382 (2009).

227. L.-N. Wei *et al.*, Reduced and delayed expression of GDF9 and BMP15 in ovarian tissues from women with polycystic ovary syndrome. *J Assist Reprod Genet*. **31**, 1483–1490 (2014).

228. F. L. Teixeira Filho *et al.*, Aberrant expression of growth differentiation factor-9 in oocytes of women with polycystic ovary syndrome. *Journal of Clinical Endocrinology & Metabolism*. **87**, 1337–1344 (2002).

229. S.-Y. Zhao *et al.*, Expression of growth differentiation factor-9 and bone morphogenetic protein-15 in oocytes and cumulus granulosa cells of patients with polycystic ovary syndrome. *Fertility and Sterility*. **94**, 261–267 (2010).

230. M. A. Fenwick *et al.*, Investigations of TGF-β signaling in preantral follicles of female mice reveal differential roles for bone morphogenetic protein 15. *Endocrinology*. **154**, 3423–3436 (2013).

231. C. J. McIntosh, S. Lawrence, P. Smith, J. L. Juengel, K. P. McNatty, Active immunization against the proregions of GDF9 or BMP15 alters ovulation rate and litter size in mice. *Reproduction*. **143**, 195–201 (2012).

232. P. G. Knight, C. Glister, TGF-beta superfamily members and ovarian follicle development. *Reproduction*. **132**, 191–206 (2006).

233. A. L. Chand, C. A. Harrison, A. N. Shelling, Inhibin and premature ovarian failure. *Human Reproduction Update*. **16**, 39–50 (2009).

234. A. Ungewickell *et al.*, The identification and characterization of two phosphatidylinositol-4,5-bisphosphate 4-phosphatases. *Proc. Natl. Acad. Sci. U.S.A.* **102**, 18854–18859 (2005).

235. M. W. Medina *et al.*, Transmembrane protein 55B is a novel regulator of cellular cholesterol metabolism. *Arterioscler. Thromb. Vasc. Biol.* **34**, 1917–1923 (2014).

236. W. L. Miller, H. S. Bose, Early steps in steroidogenesis: intracellular cholesterol trafficking. *J. Lipid Res.* **52**, 2111–2135 (2011).

237. S. G. Hillier, P. F. Whitelaw, C. D. Smyth, Follicular oestrogen synthesis: the “two-cell, two-gonadotrophin” model revisited. *Molecular and Cellular Endocrinology*. **100**, 51–54 (1994).

238. D. Thierry-Mieg, J. Thierry-Mieg, AceView: a comprehensive cDNA-supported gene and transcripts annotation. *Genome Biology*. **7**, S12–14 (2006).

Appendix A: Articles published

Article 1: Embryos generated from oocytes lacking complex *N*- and *O*-glycans have compromised development and implantation

REPRODUCTION
RESEARCH

Embryos generated from oocytes lacking complex *N*- and *O*-glycans have compromised development and implantation

Patricia Grasa[1], Heidy Kaune[1,2] and Suzannah A Williams[1]

[1]*Nuffield Department of Obstetrics and Gynaecology, Women's Centre, Level 3, John Radcliffe Hospital, University of Oxford, Oxford OX3 9DU, UK and* [2]*Faculty of Medicine, Diego Portales University, Santiago 8370068, Chile*

Correspondence should be addressed to S A Williams; Email: suzannah.williams@obs-gyn.ox.ac.uk

Abstract

Female mice generating oocytes lacking complex *N*- and *O*-glycans (double mutants (DM)) produce only one small litter before undergoing premature ovarian failure (POF) by 3 months. Here we investigate the basis of the small litter by evaluating ovulation rate and embryo development in DM (*Mgat1*$^{F/F}$*C1galt1*$^{F/F}$:ZP3*Cre*) and Control (*Mgat1*$^{F/F}$*C1galt1*$^{F/F}$) females. Surprisingly, DM ovulation rate was normal at 6 weeks, but declined dramatically by 9 weeks. *In vitro* development of zygotes to blastocysts was equivalent to Controls although all embryos from DM females lacked a normal zona pellucida (ZP) and ~30% lacked a ZP entirely. In contrast, *in vivo* preimplantation development resulted in less embryos recovered from DM females compared with Controls at 3.5 days post coitum (dpc) (3.2±1.3 vs 7.0±0.6). Furthermore, only 45% of mated DM females contained embryos at 3.5 dpc. Of the preimplantation embryos collected from DM females, approximately half were morulae unlike Controls where the majority were blastocysts, indicating delayed embryo development in DM females. Post-implantation development in DM females was analysed to determine whether delayed preimplantation development affected subsequent development. In DM females at 5.5 dpc, only ~40% of embryos found at 3.5 dpc had implanted. However, at 6.5 dpc, implantation sites in DM females corresponded to embryo numbers at 3.5 dpc indicating delayed implantation. At 9.5 dpc, the number of decidua corresponded to embryo numbers 6 days earlier indicating that all implanted embryos progress to midgestation. Therefore, a lack of complex *N*- and *O*-glycans in oocytes during development impairs early embryo development and viability *in vivo* leading to delayed implantation and a small litter.

Reproduction (2012) **144** 455–465

Introduction

The fertility of an individual female is a reflection of the number of eggs ovulated and their competence. The development of each oocyte occurs within a follicle which can be considered as the functional unit of the ovary. The development and growth of follicles requires complex endocrine, paracrine and autocrine regulations, as well as bidirectional signals between the oocyte and follicular cells. Each follicle consists of a central oocyte that is surrounded by layers of granulosa cells that are separated from the outer surrounding theca cells by a basal lamina. Upon antrum formation, granulosa cells differentiate into mural granulosa cells that line the follicle wall and cumulus cells that surround the oocyte. Since 1996 when the critical role of the oocyte in follicle development was revealed, elucidating the various functions of the oocyte has been the focus of much research (Dong *et al.* 1996, Matzuk *et al.* 2002, Hutt & Albertini 2007, Gilchrist *et al.* 2008, Kidder & Vanderhyden 2010). Indeed, differentiation of the cumulus cells and their subsequent expansion before ovulation requires oocyte-secreted factors (Diaz *et al.* 2007, Sugiura *et al.* 2010).

Essential cell-to-cell signalling between the oocyte and the surrounding granulosa cells occurs via transzonal processes (TZPs). TZPs penetrate from the granulosa cells through the extracellular matrix coat that surrounds the oocyte. This extracellular matrix coat known as the zona pellucida (ZP) is composed of three glycoproteins, ZP1, ZP2 and ZP3 (Bleil & Wassarman 1980*b*, Wassarman 2005) in the mouse, all of which are expressed exclusively by the oocyte from the primary stage of follicle development onwards (Philpott *et al.* 1987). Glycans on ZP proteins had been postulated as sperm receptors for many years (Bleil & Wassarman 1980*a*, van Duin *et al.* 1994, Litscher *et al.* 2009, Han *et al.* 2010). However, mutant mice generating oocytes lacking complex *N*- and/or *O*-glycans are fertile demonstrating that these glycans are not required for zona–sperm binding in mice although

© 2012 Society for Reproduction and Fertility
ISSN 1470–1626 (paper) 1741–7899 (online)
DOI: 10.1530/REP-12-0084
Online version via www.reproduction-online.org
This is an Open Access article distributed under the terms of the Society for Reproduction and Fertility's Re-use Licence which permits unrestricted non-commercial use, distribution, and reproduction in any medium, provided the original work is properly cited.

the ZP is thinner and more fragile if it lacks *O*-glycans, *N*-glycans or both (Shi *et al.* 2004, Williams *et al.* 2007, Williams & Stanley 2008).

The generation of both core 1 and 2 *O*-glycans (also referred to as complex *O*-glycans) and complex and hybrid *N*-glycans occurs on glycoproteins at specific motifs in a highly regulated manner (Fig. 1). The generation of core 1 and 2 *O*-glycans requires the glycosyltransferase T-synthase encoded by the *C1galt1* gene (previously known as *T-syn*). Core 1 *O*-glycans are synthesized by the addition of galactose to the *N*-acetylgalactosamine (GalNAc) attached via O-linkage to serine or threonine residues. Core 2 *O*-glycans are generated by the attachment of *N*-acetylglucosamine (GlcNAc) to the core 1 structure. Mice lacking *C1galt1* die during gestation at ~E14 due to defective angiogenesis (Xia *et al.* 2004, Williams *et al.* 2007). Mice lacking complex and hybrid *N*-glycans also die *in utero* at E9.5 (Ioffe & Stanley 1994, Metzler *et al.* 1994). Complex and hybrid *N*-glycans are generated by modification and extension of oligomannosyl structures which is initiated by the enzyme *N*-acetylglucosaminyltransferase 1 (GlcNAcT-1, encoded by the *Mgat1* gene). Therefore, to study biological functions of these glycans in the oocyte *Cre-loxP* technology has been used to eliminate the enzymes required for their generation. *Cre-loxP* technology allows a gene flanked by *loxP* sites to be deleted upon exposure to the enzyme *Cre* recombinase.

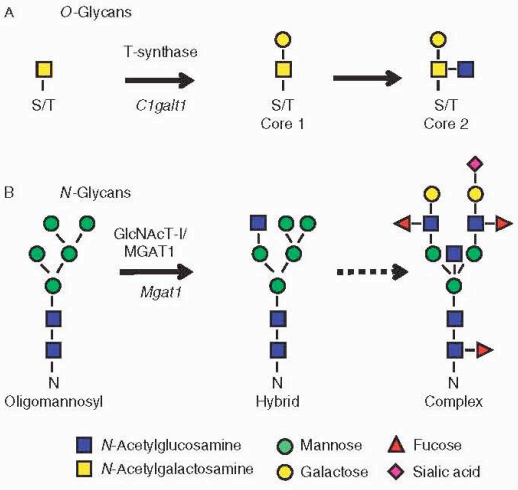


Figure 1 The generation of complex *O*- and *N*-glycans. (A) T-synthase (encoded by *C1galt1*) is required to initiate the synthesis of core 1 *O*-glycans by transferring galactose (Gal) to *N*-acetylgalactosamine (GalNAc) on serine/threonine residues (S/T). Core 2 *O*-glycans are generated by the addition of *N*-acetylglucosamine (GlcNAc) to the GalNAc of core 1 structure. (B) *N*-Acetyl-glucosaminyltransferase 1 (GlcNAcT-1, encoded by *Mgat1*) is required to generate complex and hybrid *N*-glycans from the oligomannosyl structure.

Therefore, by flanking the coding exons of *C1galt1* and/or *Mgat1* with *loxP* sites, and using a *Cre* recombinase transgene under the control of the oocyte-specific ZP3 promoter, mice can be generated which lack these enzymes specifically in the oocyte (Shi *et al.* 2004, Williams & Stanley 2008, 2011).

Females with oocyte-specific deletion of *C1galt1* generate oocytes lacking core 1 and 2 *O*-glycans and exhibit an increase in fertility, revealing a role for these glycans in the regulation of ovulation rate (Williams & Stanley 2008). Oocyte-specific deletion of *Mgat1* results in the generation of oocytes lacking complex and hybrid *N*-glycans. These glycans have a role in generating developmentally competent oocytes, and once fertilised, in embryo implantation and development (Shi *et al.* 2004). $Mgat1^{F/F}$:ZP3*Cre* females have reduced fertility producing smaller litters (Shi *et al.* 2004). Follicle development is also modified in these mice with considerable abnormalities evident in preovulatory follicles (Williams & Stanley 2009). Moreover, oocyte-specific deletion of both *Mgat1* and *C1galt1* in double mutant (DM) females results in ovarian dysfunction leading to an altered endocrine profile and premature ovarian failure (POF) by 3 months of age (Williams & Stanley 2011). However, embryonic development and fertility are normal for mice heterozygous for either *Mgat1* or *C1galt1* generated by crossing $Mgat1^{del/+}$ or $C1galt1^{del/+}$ mice (Ioffe & Stanley 1994, Xia *et al.* 2004). Furthermore, fertility is also normal in mice generating oocytes heterozygous for either *Mgat1* or *C1galt1* using oocyte-specific deletion (Williams *et al.* 2007). In addition, females generating oocytes heterozygous for both *Mgat1* and *C1galt1* have normal fertility (Williams *et al.* 2007).

The aim of this study was to determine the stage(s) at which the decrease in fertility occurs in DM females. We reveal that the decrease in fertility is not due to a reduced ovulation rate but due to modified embryo development.

Results

Ovulation rate

We have previously demonstrated that DM females mated at 6 weeks have decreased fertility producing only a single small litter of ~4 pups (Williams *et al.* 2007, Williams & Stanley 2011). To determine whether the smaller litter size was due to a decrease in the number of eggs ovulated, ovulation rate was assessed by analysis of the number of eggs and/or presumptive zygotes recovered at 0.5 days post coitum (dpc) in females joined with males, at either 6 weeks or 9 weeks of age (termed the '6-week group' and '9-week group' respectively) (Fig. 2).

Most surprisingly, the ovulation rate did not differ between Control and DM females in the 6-week group (Control: 8.3 ± 0.2, $n=9$; DM: 7.5 ± 0.8, $n=8$), although ovulation rate of DM females was considerably more

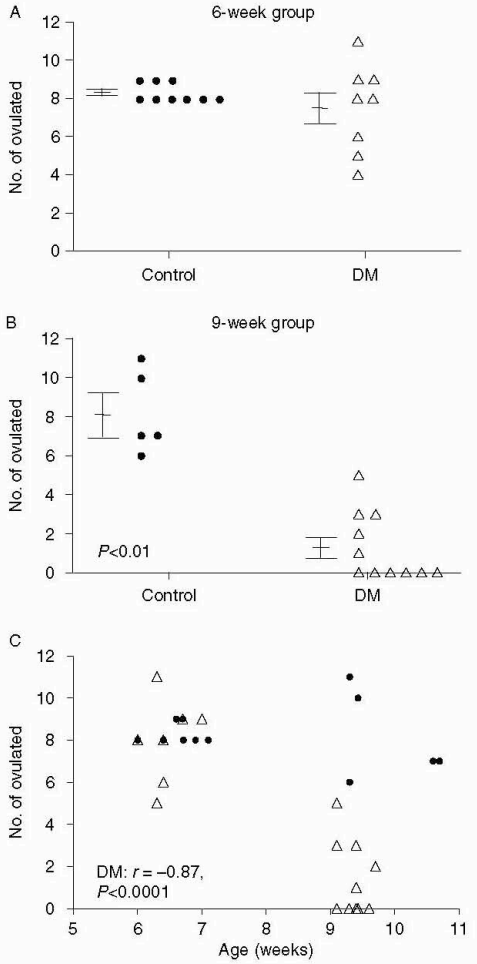


Figure 2 Ovulation rate determined as the number of presumptive zygotes collected from the oviducts 0.5 dpc from Control and DM females joined with males at (A) 6 weeks old (6-week group) and (B) 9 weeks old (9-week group). (C) Correlation between age and number of eggs collected from (closed circle) Control and (open triangle) DM females. Note: some data points overlap and therefore not all are visible. Results are expressed as mean ± S.E.M.

variable than that of Controls (Fig. 2A). Importantly, the age at which Control and DM females ovulated also did not differ (Control: 6.5 ± 0.1 week; DM: 6.3 ± 0.2 week). However, 3 weeks later in the 9-week group DM females exhibited a marked decrease in ovulation rate (Control: 8.2 ± 0.9, $n=5$; DM: 1.3 ± 0.5, $n=11$; $P<0.01$), revealing a rapid loss of function by DM ovaries (Fig. 2B). Analysis of all ovulation rate data reveals a negative correlation in DM females between age and the number of eggs ovulated (Fig. 2C; $r=-0.87$, $P<0.0001$), in contrast to Control females whose ovulation rate remained constant. The sharp drop in DM ovulation rate from the 6- to 9-week group is most likely the main reason DM females do not produce a second litter (Williams & Stanley 2011).

Fertilisation rate and in vitro *embryo development*

Since, unlike litter size, the ovulation rate of DM females was not decreased in the 6-week group, fertilisation rate was investigated to determine whether the thin fragile ZP of DM eggs (Williams *et al.* 2007) was affecting fertilisation *in vivo*. Eggs collected from 6-week group DM and Control females at 0.5 dpc were assumed to have been fertilised and were termed 'presumptive zygotes' (Fig. 3A and B, Control: 7.0 ± 0.3 week, DM: 6.1 ± 0.2 week). When collected, the ZP of presumptive zygotes from DM females was either thin or absent compared with the thick ZP around zygotes from Control females (Fig. 3A and B). Thirty percent of DM presumptive zygotes lacked a ZP (Table 1). However, despite the lack of a normal ZP on all presumptive zygotes collected from DM females the percentage that developed to two-cell embryos after culture was not decreased compared with those from Controls (Fig. 3E; Controls: 95.3 ± 2.9%, DM: 96.4 ± 2.3%).

Since a decrease in fertilisation efficiency was not contributing to the decrease in DM litter size (Fig. 3E and F), *in vitro* embryo development was analysed. Embryos from DM females developed to the blastocyst stage in similar proportions to Controls despite lacking a normal ZP (Table 1 and Fig. 3C, D and G), although they appeared slightly smaller, consistent with other studies of ZP-free blastocysts in mice (Ribas *et al.* 2006). A unique phenomenon occurred during the culture of embryos from one DM female: two ZP-free morulae fused overnight giving rise to one abnormally large blastocyst (Fig. 3D; asterisk).

In vivo *preimplantation embryo development*

As mentioned above, development of embryos from DM females *in vitro* did not differ from Controls and therefore the reason for the decrease in litter size in 6-week females remained undefined. However, the *in vitro* environment may be more beneficial to development of embryos from DM females, which have a thin fragile ZP, as development occurs in a dish with no movement. In contrast, *in vivo* development requires the developing embryos to pass through the oviduct. Therefore, we next evaluated preimplantation development *in vivo* using embryos collected from plugged females at 3.5 dpc (Fig. 4A, B, C, D, E and F). In stark contrast to plugged Control and DM females dissected at 0.5 dpc, all of which contained embryos (Fig. 2A), less than half of all DM females contained embryos at 3.5 dpc (Fig. 4G).

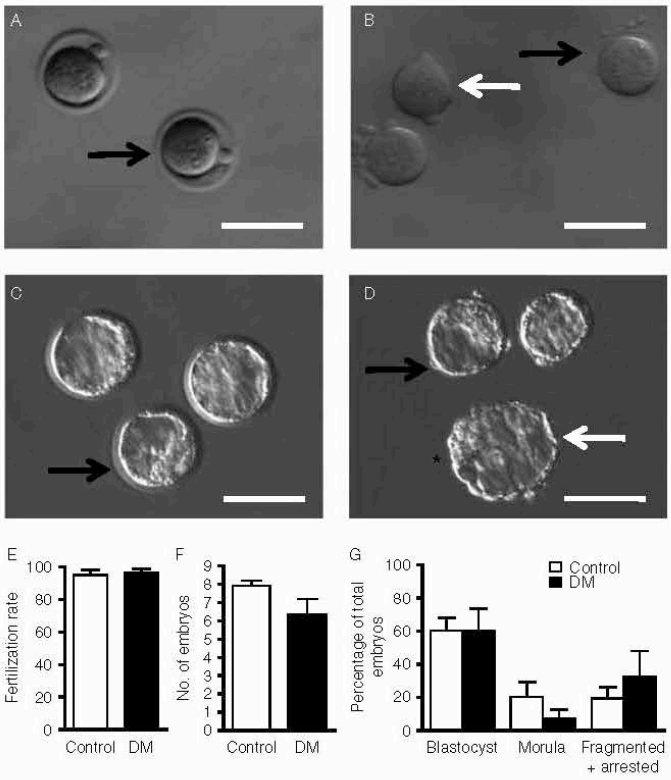


Figure 3 *In vitro* development of preimplantation embryos. Images of embryos collected and cultured *in vitro* from Control (A and C) and DM (B and D) 6-week group females. (A and B) Presumptive zygotes collected at 0.5 dpc. (C and D) Blastocyst after 4 days in culture. Black arrow indicates ZP; white arrows indicate DM embryos without ZP; asterisk indicates a bigger blastocyst that seems to have resulted from the fusion of two embryos because the number of embryos present in this dish was reduced by one. (E) Fertilisation rate of Control ($n=12$) and DM ($n=6$) females. (F) Total number of embryos at the end of the culture period from Control and DM females. (G) Percentage of blastocysts, morulae, fragmented and arrested embryos in Control and DM females at 4.5 dpc. Results are expressed as mean±S.E.M. Bar scale=100 μm.

The very high proportion of mated DM females that lack embryos at 3.5 dpc is most likely contributing significantly to the 70% of DM females that fail to produce a litter (Williams *et al.* 2007).

Of the DM females containing embryos, the number of embryos recovered was lower than Controls (Control: 7.0±0.6, DM: 3.2±1.3, $P=0.05$; Fig. 4H) and only 35% still possessed a ZP (Table 1). Moreover, DM females contained fewer blastocysts than Control females (Control: 5.8±0.8, DM: 1.2±0.5, $P<0.01$). When expressed as a proportion of total embryos, blastocysts and morulae were equally represented in the embryos from DM females whereas embryos from Control females were 80% blastocysts (Fig. 4I).

In light of these observations, *in vivo* and *in vitro* embryonic developments was compared revealing unexpected and striking differences in embryos collected from DM females (Table 2). The total number of *in vivo* developed embryos from DM females collected at 3.5 dpc was half of that obtained after culture ($P=0.08$). Furthermore, the number of blastocysts recovered *in vivo* from DM females was lower than the number obtained *in vitro* ($P=0.05$). Conversely, the number of morulae collected from DM females at 3.5 dpc (1.4±0.7) was almost three times higher than the number obtained in culture (0.5±0.3) although this did not reach significance. In stark contrast to embryos developed *in vivo* from DM females, embryos developed *in vivo* from Control females collected at 3.5 dpc did not differ from those cultured. However, although the *in vitro* conditions were better for development of embryos from DM females, the number of fragmented and/or arrested embryos obtained from *in vitro* culture was three times higher than *in vivo* for embryos collected from both Control and DM females (although this did not reach significance; Table 2).

Implantation analysis

The high proportion of morulae collected from DM females at 3.5 dpc compared with Controls (Fig. 4I and Table 2 although significance was not reached) may indicate a delay in early development of embryos from DM females that could affect implantation. To evaluate whether these morulae are able to progress further and implant, the 6-week group of Control and DM females

Table 1 Number of presumptive zygotes and embryos lacking ZP in both *in vitro* and *in vivo* conditions.

	Collected (0.5 dpc)		***In vitro*** (4.5 dpc)		***In vivo*** (3.5 dpc)	
	No. of presumptive zygotes	No. of ZP-free presumptive zygotes (%)	No. of embryos	No. of ZP-free embryos (%)	No. of embryos	No. of ZP-free embryos (%)
Control	8.3±0.2 (*n*=12)	0.2±0.2[b] (1.9±1.9[#]) (*n*=12)	7.9±0.3 (*n*=12)	0.2±0.2[a] (3.3±3.3[*]) (*n*=12)	7.0±0.6 (*n*=5)	0 (*n*=5)
DM	7.0±1.3 (*n*=6)	1.7±0.7[b] (30.0±12.0[#]) (*n*=6)	6.3±0.8 (*n*=6)	1.3±0.5[a] (29.0±10.3[*]) (*n*=6)	3.2±1.3 (*n*=5)	1.2±0.5 (65.0±19.0) (*n*=5)

Mean±S.E.M. Values with the same superscript are significantly different. $P=0.05$ ([a], [*]); $P<0.05$ ([b], [#]).

was mated and embryo development was analysed at 5.5 dpc. The number of implantation sites was unsurprisingly lower in DM females at 5.5 dpc (1.3±0.4) than in Control females (7.3±0.6, $P<0.01$; Table 3). However, the number of implantation sites at 5.5 dpc in DM females was around half the number of embryos recovered at 3.5 dpc (3.5 dpc: 3.2±1.3, 5.5 dpc: 1.3±0.4, Tables 2 and 3). Furthermore, unfertilised eggs and non-implanted embryos were recovered in DM females in contrast to Control females, indicating that this process is aberrant in DM females.

To determine whether there was a delay in implantation in DM females thus explaining the lower number of implantation sites at 5.5 dpc compared with the mean litter size of 4.0±2.7 (Williams *et al.* 2007), we analysed implantation 24 h later at 6.5 dpc (Table 4). Interestingly, the number of implantation sites in DM females at 6.5 dpc (Table 4) was more than double that at 5.5 dpc (Table 3) and is consistent with the number of embryos at 3.5 dpc (Table 2).

Postimplantation embryo development

Analysis of embryos implanted at 5.5 and 6.5 dpc revealed a delay in implantation. To determine whether development of the implanted embryos was altered due to a difference in the timing of implantation, we analysed embryos at 9.5 dpc in females of the 6-week group. Uterine horns of DM females contained less deciduae and healthy embryos than those of Control females ($P<0.05$ and $P<0.001$ respectively; Table 5). The number of decidua in DM females (3.0±0.6) did not differ from the number of embryos recovered at 3.5 dpc (3.2±1.3), nor the number of implantations at 6.5 dpc (3.2±1.0), and is consistent with a litter size of 4.0±2.7 when DM females are mated at 6 weeks of age (Williams *et al.* 2007). However, not all deciduae in both, Control and DM females contained normal healthy embryos (Table 5), demonstrating that not all implanted embryos generated from either normal or mutant eggs are able to develop to term. Consistent with this, the number of healthy embryos in DM females at 9.5 dpc (2.0±0.3)

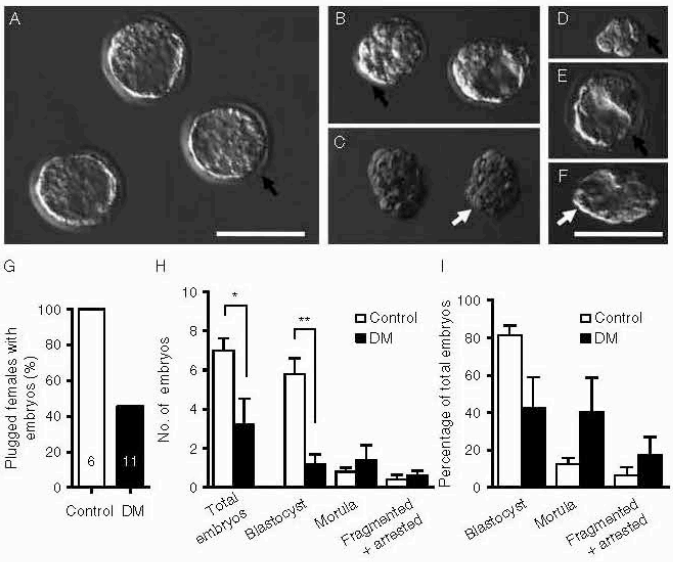


Figure 4 *In vivo* developed embryos at 3.5 dpc. Images of embryos from Control (A) and DM (B, C, D, E and F) females in the 6-week group. (A) Blastocysts, (B) blastocyst and morula, (C) morula, (D) arrested embryo at four-cell stage, (E) blastocyst with abnormal ZP and (F) blastocyst without ZP. Black arrow indicates ZP; white arrow indicates a DM morula without ZP. (G) Percentage of mated females, confirmed by presence of vaginal plug, with embryos recovered after flushing. (H) Number of embryos and distribution of embryonic developmental stages in Control ($n=5$) and DM ($n=5$) females containing embryos. (I) Proportions of blastocysts, morulae and fragmented and arrested embryos as a percentage of the total number of embryos recovered at 3.5 dpc from Control and DM females. Results are expressed as mean±S.E.M. Bar scale=100 μm. *$P=0.05$; **$P<0.01$.

Table 2 *In vitro* (4.5 dpc) and *in vivo* (3.5 dpc) development of embryos from 6-week group Control and DM females.

	Control			DM		
Total number	*In vitro*	*In vivo*	*In vivo*:*in vitro*	*In vitro*	*In vivo*	*In vivo*:*in vitro*
Females with embryos	12	5	–	6[a]	5[b]	–
Embryos per female	7.9±0.3	7.0±0.6	0.9	6.3±0.8	3.2±1.3	0.5
Blastocysts per female	4.8±0.7	5.8±0.8	1.2	3.8±0.9*	1.2±0.5*	0.3
Morulae per female	1.7±0.7	0.8±0.2	0.5	0.5±0.3	1.4±0.7	2.8
Fragmented+arrested embryos per female	1.5±0.5	0.4±0.2	0.3	2.0±0.8	0.6±0.2	0.3
Blastocysts+morulae per female	6.4±0.6	6.6±0.8	1.0	4.3±1.1	2.6±1.0	0.6

Mean±S.E.M. Values with the same superscript are significantly different, *P=0.05.
[a]Data are presented for females whose zygotes were cultured. [b]Eleven DM females were evaluated; however, only five contained embryos.

was similar to the number of morphologically normal embryos (blastocyst+morula) recovered before implantation (2.6±1.0; Table 2).

Embryo and implantation site comparison at the five developmental stages

The number of preimplantation embryos, implanted embryos and deciduae at the five different developmental stages are compared in Fig. 5. At each stage of development, the number of implantations in DM females was markedly lower than that of Controls which was consistently between seven and eight. However, the number of presumptive zygotes recovered in DM at 0.5 dpc was significantly higher than the number of embryos found at any other stage. Therefore, the number of deciduae in DM females at 5.5 dpc is markedly lower than at any of the other time points analysed.

Corpora lutea observations

At all of the developmental stages studied, the number of corpora lutea (CL) was comparable with the number of deciduae in Controls, but in DM ovaries, the number of CL was significantly higher than the number of deciduae (Tables 3, 4 and 5). However, the CL in DM ovaries were not consistent in size or colour compared with Control CL. Some DM CL were smaller than control CL and pale (abnormal CL) compared with the bright red Control CL (normal CL). Despite the low number of implantations, the number of normal CL in DM ovaries was similar to the number of CL in Control females, consistent with a normal ovulation rate of DM females at 6 weeks (Tables 3, 4 and 5). However, at all stages of development, the number of implantation sites or decidua in DM females was lower than the number of normal CL (P<0.05).

Discussion

DM females generating oocytes lacking complex *N*- and *O*-glycans produce only one small litter from mating at 6 weeks before undergoing POF by 3 months of age (Williams *et al.* 2007, Williams & Stanley 2011). To determine the basis of the small litter size we investigated ovulation rate and embryo development. Ovulation rate was unexpectedly normal in the DM females in the 6-week group, but decreased dramatically by 9 weeks, consistent with our previous findings (Williams *et al.* 2007, Williams & Stanley 2011). However, since ovulation rate was normal in the 6-week group, further analyses were required to reveal the basis for the decrease in litter size. Surprisingly, the number of embryos at 3.5 dpc was around half the ovulation rate 3 days earlier, revealing a considerable loss of embryos surviving during blastogenesis. Furthermore, embryo development in those embryos that did survive in DM females was delayed resulting in delayed implantation.

When mated at 6 weeks of age, DM females produce only a single small litter (Williams *et al.* 2007) yet, on average, they ovulate normal numbers of eggs, although the number of eggs ovulated per female is highly variable. This is consistent with the presence of morphologically normal follicles in 6-week DM ovaries, although ovaries also contain some follicular abnormalities such as oocytes lacking cumulus cells or empty follicles (Williams & Stanley 2011). Therefore, the most likely explanation for the precipitous decline in

Table 3 Implantation sites, CL, eggs and non-implanted embryos in Control and DM females at 5.5 dpc.

	No. of females (age plugged; weeks)	**Implantation sites**	**Eggs**	**Non-implanted embryos**	**CL**		
					Total	Normal	Abnormal
Control	8 (6.5±0.1)	7.3±0.6[b]	0	0	8.3±0.3[c]	8.1±0.3	0.1±0.1[a]
DM	4 (6.4±0.0)	1.3±0.4[b,#,*,§]	1.3±0.7	1.3±0.9	11.8±1.0[c,#]	7.8±1.1*	4.0±0.9[a,§]

Mean±S.E.M. Values with the same superscript are significantly different: P<0.05 ([a], [#], * and [§]); P<0.01 ([b] and [c]).

Table 4 Implantation sites and CL in control and DM females at 6.5 dpc.

	No. of females (age plugged; weeks)	**Implantation sites**	**CL**		
			Total	Normal	Abnormal
Control	4 (6.7±0.2)	7.8±0.3[a]	8.3±0.6	8.0±0.4	0.3±0.3
DM	5 (6.3±0.1)	3.2±1.0[a,#,*]	11.5±1.6[#]	9.3±0.7*	2.3±0.9

Mean±S.E.M. Values with the same superscript are significantly different: $P<0.05$ ([#] and *); $P<0.01$ ([a]).

ovulation rate in DM females from 6 to 9 weeks is defective follicle development that gets more severe with age, explaining the lack of a second litter in these females (Williams *et al.* 2007, Williams & Stanley 2011).

Despite the fact that ovulation rate is normal at 6 weeks in DM females, only 45% of mated DM females contained embryos at 3.5 dpc. The very high proportion of mated DM females that lack embryos at 3.5 dpc is most likely contributing significantly to the 70% of DM females that fail to produce a litter (Williams *et al.* 2007). Furthermore, in those DM females that did contain embryos, the number was significantly lower than Controls. This was in stark contrast to just 3 days earlier when ovulation rate in DM females was normal and eggs were fertilised equivalently to those from Control females. These data indicate that the lack of complex *N*- and *O*-glycans during oocyte development results in a substantial decrease in embryo viability *in vivo* with an associated decrease in female fertility. In addition, around half of the morphologically normal embryos recovered from DM females at 3.5 dpc were morulae compared with ~11% in Controls, indicating a delay in development. Delayed development of embryos from DM females was not unexpected as embryos generated from oocytes lacking only complex *N*-glycans are also retarded (Shi *et al.* 2004). However, the development of embryos from DM females was supported *in vitro*, with the same proportion of embryos developing to the blastocyst stage as embryos from Controls. This demonstrates that *in vivo* development of embryos from DM females is affected by factors not present *in vitro*. Furthermore, these factors can either be intrinsic to the developing embryo or result from a modified environment within DM females as embryo development is affected by both oocyte quality and the environment in which the embryo develops (Mann & Lamming 2001, Van der Auwera & D'Hooghe 2001, Kidder & Vanderhyden 2010).

Focusing first on the embryo, as a consequence of the lack of *N*- and *O*-glycans, the ZP of DM oocytes is thinner and more fragile (Williams *et al.* 2007, Williams & Stanley 2009). During the transit through the oviduct, embryos develop within the protective coat of the ZP undergoing cleavage, compaction and cavitation before developing into a blastocyst. Blastocysts hatch from the ZP and implant in the endometrial lining of the uterus (Nagy *et al.* 2003). We have observed that eggs and preimplantation embryos from DM females often lack a ZP which is most likely removed either during ovulation or whilst in transit from the oviduct to the uterus. Analysis of ZP-free eggs and embryos that were reintroduced to the oviduct illustrated a critical role for the ZP in preventing adherence of developing embryos to the oviduct (Modlinski 1970). These data indicate that the dramatic reduction in DM embryos flushed from 3.5 dpc as opposed to the number found at 0.5 dpc may be attributed to adherence of naked DM pre-blastocyst embryos to the oviduct. Furthermore, embryos with the ZP removed early in development have reduced developmental potential (Bronson & McLaren 1970). In addition, embryo lethality induced by shear stress (caused by the movement of fluid over the surface of cells) is hastened by ZP removal (Xie *et al.* 2006) which may also contribute to embryo loss in DM females. The ZP has also a role maintaining embryo morphology including the connections between blastomeres which can influence embryo development in mice (Suzuki *et al.* 1995, Ribas *et al.* 2005). Moreover, removal of the ZP in mice results in reduced DNA methylation at the two-cell and four-cell stages (Ribas *et al.* 2006). In addition, the thickness of the ZP or its variation has been used as a marker of successful implantation of human embryos (Garside *et al.* 1997, Gabrielsen *et al.* 2001, Shen *et al.* 2005). Based on these observations it is likely that the altered thickness or absence of a functional ZP in DM embryos has a role in the aberrant early embryogenesis in embryos from DM females that is not observed *in vitro*.

In vitro analysis revealed one unexpected occurrence of embryo fusion in embryos from DM female. Observations of *in vitro* cultured embryos revealed that

Table 5 Number of decidua, embryos and CL in Control and DM females at 9.5 dpc.

	No. of females (age plugged; weeks)	**Decidua**	**Healthy embryos**	**Unhealthy embryos and reabsorptions**	**CL**		
					Total	Normal	Abnormal
Control	5 (6.6±0.3)	7.6±0.5[a]	7.2±0.4[d]	0.6±0.2	8.2±0.6[c]	7.6±0.5	0.6±0.4[b]
DM	6 (6.3±0.1)	3.0±0.6[a,#,*]	2.0±0.3[d]	1.0±0.5	11.3±0.6[c,#]	8.3±0.5*	3.0±0.7[b]

Mean±S.E.M. Values with same superscript are significantly different: $P<0.05$ ([a] and [b]); $P<0.01$ ([c], [#] and *); $P<0.001$ ([d]).

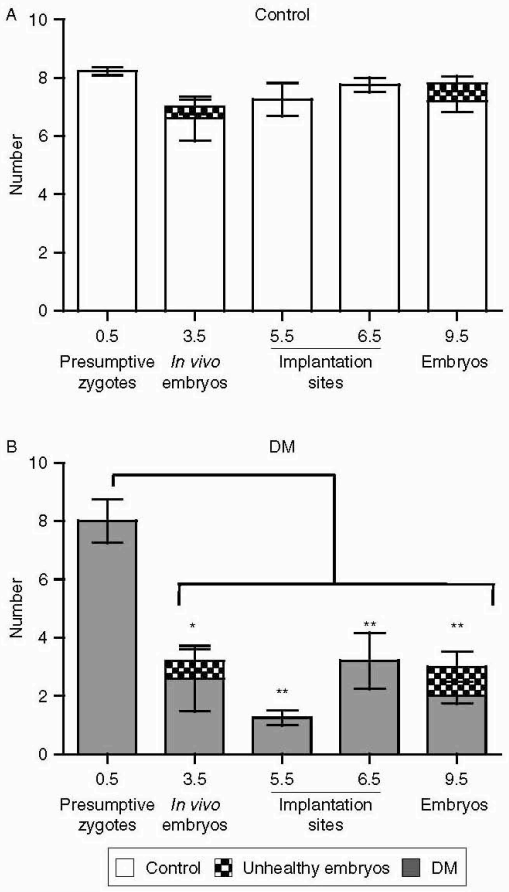


Figure 5 Numbers of eggs ovulated and pre- and post-implantation embryos in Control and DM females at four developmental stages. The graph shows the number of eggs ovulated (0.5 dpc; presumptive zygotes), preimplantation embryos (3.5 dpc) and implanted embryos (5.5, 6.5 and 9.5 dpc) in Control (A) and DM (B) females. $^{*}P<0.05$; $^{**}P<0.01$, with regard to the zygotes collected at 0.5 dpc. Results are expressed as mean ± S.E.M.

although five DM zygotes were present at the beginning of the culture, at the end, only four embryos were present including one abnormally large blastocyst (Fig. 3D). Fusion of two of the ZP-free embryos is the only logical conclusion in the absence of a degenerating embryo. The formation of natural chimeras has been described in mammals, including in humans (Strain *et al.* 1998). Although chimeric embryos can be generated by injection of stem cells into blastocysts, they can also be generated by culture of embryonic stem cells which aggregate with denuded morulae *in vitro* which develop normally upon transfer to a pseudo-pregnant recipient (Prather *et al.* 1989, Eakin & Hadjantonakis 2006). Although our data indicate that this phenomena can occur in ZP-free DM embryos *in vitro*, its occurrence *in vivo* is unknown. However, it is unlikely to be involved in decreasing the number of embryos and pups as none of the embryos collected at 3.5 dpc were abnormally large.

The delay in *in vivo* embryo development in DM females, revealed by the high proportion of embryos at the morula stage, was reflected in a delay in implantation. At 5.5 dpc, only around a third of the number of the preimplantation embryos recovered at 3.5 dpc were implanted (Fig. 5). However, 1 day later at 6.5 dpc, the number of embryos implanted was equivalent to the number found at 3.5 dpc (Fig. 5). In addition, the number of deciduae found at 9.5 dpc in DM females was similar to the number of embryos recovered at 3.5 dpc and to the number of implantations at 6.5 dpc. However, not all deciduae in DM females contained normal healthy embryos with a number of healthy embryos equal to the number of morphologically normal embryos recovered before implantation. The difference between the number of healthy embryos found in this study and the litter size previously published (4.2 ± 2.7) (Williams *et al.* 2007), could be explained by the low sample size (only three of ten mated produced a litter) and the high variability of the fertility data in DM females. Recent studies reveal an active role of the embryo in regulating the expression of uterine genes involved in implantation and decidualization (Kashiwagi *et al.* 2007, Park & Dufort 2011). It is possible that embryos generated from oocytes lacking complex *N*- and *O*-glycans do not induce the appropriate expression of required genes for timely implantation. Implantation is a complex process, ovarian steroid-dependant and only possible during a limited period in which the uterus is receptive to the competent embryo. This process requires complex interactions between the blastocyst and the receptive uterus in many species including mice and humans (Simon *et al.* 2000, Dey *et al.* 2004). Interestingly, the delay in embryo development and implantation was not uniformly deleterious to subsequent development of embryos as some embryos that implanted at 6.5 dpc remained healthy at 9.5 dpc (Fig. 5). Transferring embryos at different stages of development (zygotes and eight-cell embryos) into the uterus of pseudo-pregnant mice revealed that the 'window of implantation' could be expanded (Ueda *et al.* 2003). This may explain why all the blastocysts and morulae found at 3.5 dpc in DM females are able to implant over an extended period.

In addition to modified embryo competence, the maternal endocrine environment may also have a role in modifying embryo development. Maternal ovarian steroids including estradiol and progesterone regulate embryo development and uterus receptivity to implantation (Dey *et al.* 2004, Mohamed *et al.* 2004, 2005). However, although the endocrine profile in DM females is modified by 3 months of age with mice exhibiting elevated FSH, and decreased Inhibin A and testosterone,

this is in association with a severe lack of ovarian follicles and ovarian dysfunction (Williams & Stanley 2011). Most importantly, estradiol and progesterone concentrations were normal in DM females at 3 months (Williams & Stanley 2011) and therefore, it is likely that estradiol and progesterone concentrations are also normal in the 6-week old mice used in these studies. We therefore conclude that modified maternal estradiol and progesterone are unlikely to be involved in modifying embryo development in DM females.

The increased number of CL in DM females was unexpected. We have previously shown in DM females that at 3 weeks follicle development is vastly normal; however, by 6 weeks, ovaries contained fewer follicles and more follicular abnormalities (Williams & Stanley 2011). CL in postpubertal females (6 weeks and 3 months) were not counted or measured in these analyses and therefore the increased number of CL was not revealed. Interestingly, the number of normal CL in DM females corresponds to the ovulation rate of DM (and Control females) at 6 weeks. Therefore, the abnormal CL may be present due to abnormal CL regression as DM females do not exhibit an increased ovulation rate. However, how oocyte-specific deletion of glycosyltransferases results in modified CL regression is intriguing and is under further investigation.

Female mice heterozygous for both *Mgat1* and *C1galt1* exhibit normal fertility (Williams *et al.* 2007), demonstrating that aberrant embryo development in DM females results from oocyte glycoproteins lacking complex *O*- and *N*-glycans during oocyte development and early embryogenesis before activation of the paternal genome. Furthermore, it is clear that activation of the paternal genome during preimplantation embryo development (De Vries *et al.* 2004) cannot rescue later development as the proportion of embryos dying from 6.5 to 9.5 dpc is considerably higher in DM females than in Controls.

In summary, our results reveal that a lack of complex *N*- and *O*-glycans during oocyte development impairs early embryo development and viability *in vivo*, which could lead to delayed implantation and reduced final litter size. Moreover, these data demonstrate that oocyte glycoproteins have a role in early embryo development and the interaction of the embryo with the maternal environment before implantation.

Materials and Methods

Mice

Female mice carrying floxed *Mgat1* and *C1galt1* alleles and a ZP3*Cre* transgene were used as experimental females whereas females carrying the floxed *Mgat1* and *C1galt1* alleles but not the ZP3*Cre* transgene were used as controls because the floxed alleles function as wild-type genes (Shi *et al.* 2004, Williams *et al.* 2007). Mice were kept under controlled conditions in 12 h light:12 h darkness cycles. All the experiments involving mice were done with permission from the Home Office and the Local Ethical Review Committee.

Timed mating

Control and DM female mice aged either 6 or 9 weeks were joined with fertile males ($C1galt1^{F/F}Mgat1^{F/F} \pm$ZP3*Cre*) for mating for up to a maximum of 2 weeks. Embryos generated from $C1galt1^{F/F}Mgat1^{F/F}$ females will be $C1galt1^{F/F}Mgat1^{F/F} \pm$ZP3*Cre* and embryos generated from $C1galt1^{F/F}Mgat1^{F/F}$:ZP3*Cre* females will be $Mgat1^{del/F}C1galt1^{del/F} \pm$ZP3*Cre* with the deleted genes (del) originating from oocyte-specific deletion in the mother and the floxed genes from the sperm of the father. Those joined with males at 6 weeks are herein termed the 6-week group, and those joined with males at 9 weeks are herein termed the 9-week group. Females were examined in the morning daily for evidence of mating by the presence of a vaginal plug and if present, removed from the cage. Midday of the day a plug was visible was deemed 0.5 dpc.

Ovulated egg, presumptive zygote and embryo analysis

For collection of eggs and presumptive zygote, females joined with males at 6 and 9 weeks of age were killed at 0.5 dpc and oviducts were collected in warmed M2 medium (Sigma–Aldrich) and examined. Eggs collected from Control and DM females at 0.5 dpc were assumed to have been fertilised and were termed 'presumptive zygotes'. If they were visible in the oviduct, the oviducts were ripped open to release the presumptive zygotes. Cumulus cells were disaggregated with 0.3 mg/ml of hyaluronidase (Sigma–Aldrich) in M2 media for up to 3 min and the number of presumptive zygotes was recorded. If no presumptive zygotes were visible, the oviducts were flushed with M2 media to collect them and the number was recorded.

In vivo preimplantation embryo development was analysed at 3.5 dpc from female mice joined with males at 6 weeks. Females were killed and the uterus and oviduct collected and placed in warmed M2 media. Embryos were flushed from the oviduct and uterus with warmed M2 media and classified as blastocysts, morulae, and arrested or fragmented embryos, based on morphology.

In vitro *embryo development*

Presumptive zygotes obtained as described above at 0.5 dpc from the 6-week female group were cultured for 4 days in 50 µl drops of KSOM media (Millipore, Billerica, MA, USA) supplemented with essential and non-essential amino acids (Gibco), covered with mineral oil (Sigma–Aldrich) and incubated at 37 °C in air with 5% CO_2. The fertilisation rate was determined after 24 h of culture by analysing the number that had developed into two-cell embryos. Development was analysed and images were collected using a Leica M125 microscope (Leica Microsystems, Germany) and MicroPublisher 5.0 RTV camera (Qimaging, London, UK) every 24 h during the 4-day culture period until 4.5 dpc. *In vitro* embryo culture was for 1 day longer than *in vivo* because embryo development *in vitro* takes longer than *in vivo* (Van der Auwera

& D'Hooghe 2001). Embryos were classified as either blastocysts, morulae, fragmented or arrested based on morphology.

Implantation analysis

Implantation was evaluated in females in the 6-week group at 5.5 and 6.5 dpc. To assist visualisation of implantation sites at 5.5 dpc, females were injected intravenously under anaesthesia with 100 μl of 1% Chicago Sky Blue (Sigma–Aldrich) in ddH_2O, and killed 5 min later. The uterine horns were removed and the number of implantation sites visible as blue dots recorded. Uterine horns were also flushed at 5.5 dpc to recover any non-implanted embryos. Implantation sites at 6.5 dpc were easily identified. At both time points, ovaries were dissected to determine the number of CL.

Post-implantation embryo development

Post-implantation embryo development was assessed in the 6-week group. Plugged females were killed at 9.5 dpc and the number of deciduae (each developing around an implanted embryo) determined. To analyse embryonic development, the deciduae were dissected, embryos extracted and morphology evaluated. Embryos classified as healthy had normal gross morphology and were alive determined by the presence of a beating heart. Ovaries were collected and dissected to determine the number of CL.

Statistical analysis

Results are presented as mean ± S.E.M. The Mann–Whitney *U* test was performed for all statistical analyses with the exception of the Pearson test, which was used to assess the correlation between the age and the number of eggs ovulated. All analyses were performed using Prism software version 4.0b (GraphPad Software, Inc., version 4.0b, 2004. La Jolla, CA, USA).

Declaration of interest

The authors declare that there is no conflict of interest that could be perceived as prejudicing the impartiality of the research reported.

Funding

This work was supported by a grant awarded from the Medical Research Council to S A Williams. H Kaune is a recipient of Becas Chile PhD scholarship from the Government of Chile and PhD scholarship for Academics from Diego Portales University, Chile.

Acknowledgements

We thank Brad Joyce and Dr Shankar Srinivas for their help and advice with the embryo experiments. We also thank members of the animal house facility, in particular, Denise Jelfs and James Ward for their technical assistance with the mice.

References

Bleil JD & Wassarman PM 1980*a* Mammalian sperm–egg interaction: identification of a glycoprotein in mouse egg zonae pellucidae possessing receptor activity for sperm. *Cell* **20** 873–882. (doi:10.1016/0092-8674(80)90334-7)

Bleil JD & Wassarman PM 1980*b* Structure and function of the zona pellucida: identification and characterization of the proteins of the mouse oocyte's zona pellucida. *Developmental Biology* **76** 185–202. (doi:10.1016/0012-1606(80)90371-1)

Bronson RA & McLaren A 1970 Transfer to the mouse oviduct of eggs with and without the zona pellucida. *Journal of Reproduction and Fertility* **22** 129–137. (doi:10.1530/jrf.0.0220129)

De Vries WN, Evsikov AV, Haac BE, Fancher KS, Holbrook AE, Kemler R, Solter D & Knowles BB 2004 Maternal β-catenin and E-cadherin in mouse development. *Development* **131** 4435–4445. (doi:10.1242/dev.01316)

Dey SK, Lim H, Das SK, Reese J, Paria BC, Daikoku T & Wang H 2004 Molecular cues to implantation. *Endocrine Reviews* **25** 341–373. (doi:10.1210/er.2003-0020)

Diaz FJ, Wigglesworth K & Eppig JJ 2007 Oocytes are required for the preantral granulosa cell to cumulus cell transition in mice. *Developmental Biology* **305** 300–311. (doi:10.1016/j.ydbio.2007.02.019)

Dong J, Albertini DF, Nishimori K, Kumar TR, Lu N & Matzuk MM 1996 Growth differentiation factor-9 is required during early ovarian folliculogenesis. *Nature* **383** 531–535. (doi:10.1038/383531a0)

van Duin M, Polman JE, De Breet IT, van Ginneken K, Bunschoten H, Grootenhuis A, Brindle J & Aitken RJ 1994 Recombinant human zona pellucida protein ZP3 produced by chinese hamster ovary cells induces the human sperm acrosome reaction and promotes sperm–egg fusion. *Biology of Reproduction* **51** 607–617. (doi:10.1095/biolreprod51.4.607)

Eakin GS & Hadjantonakis AK 2006 Production of chimeras by aggregation of embryonic stem cells with diploid or tetraploid mouse embryos. *Nature Protocols* **1** 1145–1153. (doi:10.1038/nprot.2006.173)

Gabrielsen A, Lindenberg S & Petersen K 2001 The impact of the zona pellucida thickness variation of human embryos on pregnancy outcome in relation to suboptimal embryo development. A prospective randomized controlled study. *Human Reproduction* **16** 2166–2170. (doi:10.1093/humrep/16.10.2166)

Garside WT, Loret de Mola JR, Bucci JA, Tureck RW & Heyner S 1997 Sequential analysis of zona thickness during *in vitro* culture of human zygotes: correlation with embryo quality, age, and implantation. *Molecular Reproduction and Development* **47** 99–104. (doi:10.1002/(SICI)1098-2795(199705)47:1<99::AID-MRD13>3.0.CO;2-V)

Gilchrist RB, Lane M & Thompson JG 2008 Oocyte-secreted factors: regulators of cumulus cell function and oocyte quality. *Human Reproduction Update* **14** 159–177. (doi:10.1093/humupd/dmm040)

Han L, Monne M, Okumura H, Schwend T, Cherry AL, Flot D, Matsuda T & Jovine L 2010 Insights into egg coat assembly and egg–sperm interaction from the X-ray structure of full-length ZP3. *Cell* **143** 404–415. (doi:10.1016/j.cell.2010.09.041)

Hutt KJ & Albertini DF 2007 An oocentric view of folliculogenesis and embryogenesis. *Reproductive BioMedicine Online* **14** 758–764. (doi:10.1016/S1472-6483(10)60679-7)

Ioffe E & Stanley P 1994 Mice lacking *N*-acetylglucosaminyltransferase I activity die at mid-gestation, revealing an essential role for complex or hybrid N-linked carbohydrates. *PNAS* **91** 728–732. (doi:10.1073/pnas.91.2.728)

Kashiwagi A, DiGirolamo CM, Kanda Y, Niikura Y, Esmon CT, Hansen TR, Shioda T & Pru JK 2007 The postimplantation embryo differentially regulates endometrial gene expression and decidualization. *Endocrinology* **148** 4173–4184. (doi:10.1210/en.2007-0268)

Kidder GM & Vanderhyden BC 2010 Bidirectional communication between oocytes and follicle cells: ensuring oocyte developmental competence. *Canadian Journal of Physiology and Pharmacology* **88** 399–413. (doi:10.1139/Y10-009)

Litscher ES, Williams Z & Wassarman PM 2009 Zona pellucida glycoprotein ZP3 and fertilization in mammals. *Molecular Reproduction and Development* **76** 933–941. (doi:10.1002/mrd.21046)

Mann GE & Lamming GE 2001 Relationship between maternal endocrine environment, early embryo development and inhibition of the luteolytic mechanism in cows. *Reproduction* **121** 175–180. (doi:10.1530/rep.0.1210175)

Matzuk MM, Burns KH, Viveiros MM & Eppig JJ 2002 Intercellular communication in the mammalian ovary: oocytes carry the conversation. *Science* **296** 2178–2180. (doi:10.1126/science.1071965)

Metzler M, Gertz A, Sarkar M, Schachter H, Schrader JW & Marth JD 1994 Complex asparagine-linked oligosaccharides are required for morphogenic events during post-implantation development. *EMBO Journal* **13** 2056–2065.

Modlinski JA 1970 The role of the zona pellucida in the development of mouse eggs *in vivo*. *Journal of Embryology and Experimental Morphology* **23** 539–547.

Mohamed OA, Dufort D & Clarke HJ 2004 Expression and estradiol regulation of Wnt genes in the mouse blastocyst identify a candidate pathway for embryo-maternal signaling at implantation. *Biology of Reproduction* **71** 417–424. (doi:10.1095/biolreprod.103.025692)

Mohamed OA, Jonnaert M, Labelle-Dumais C, Kuroda K, Clarke HJ & Dufort D 2005 Uterine Wnt/β-catenin signaling is required for implantation. *PNAS* **102** 8579–8584. (doi:10.1073/pnas.0500612102)

Nagy A, Gertsenstein M, Vintersten K & Behringer R 2003 *Manipulating the Mouse Embryo. A Laboratory Manual*. 3rd Edn. New York, NY, USA: Cold Spring Harbor Laboratory Press.

Park CB & Dufort D 2011 Nodal expression in the uterus of the mouse is regulated by the embryo and correlates with implantation. *Biology of Reproduction* **84** 1103–1110. (doi:10.1095/biolreprod.110.087239)

Philpott CC, Ringuette MJ & Dean J 1987 Oocyte-specific expression and developmental regulation of ZP3, the sperm receptor of the mouse zona pellucida. *Developmental Biology* **121** 568–575. (doi:10.1016/0012-1606(87)90192-8)

Prather RS, Hagemann LJ & First NL 1989 Preimplantation mammalian aggregation and injection chimeras. *Gamete Research* **22** 233–247. (doi:10.1002/mrd.1120220210)

Ribas R, Oback B, Ritchie W, Chebotareva T, Ferrier P, Clarke C, Taylor J, Gallagher EJ, Mauricio AC, Sousa M *et al.* 2005 Development of a zona-free method of nuclear transfer in the mouse. *Cloning and Stem Cells* **7** 126–138. (doi:10.1089/clo.2005.7.126)

Ribas RC, Taylor JE, McCorquodale C, Mauricio AC, Sousa M & Wilmut I 2006 Effect of zona pellucida removal on DNA methylation in early mouse embryos. *Biology of Reproduction* **74** 307–313. (doi:10.1095/biolreprod.105.046284)

Shen Y, Stalf T, Mehnert C, Eichenlaub-Ritter U & Tinneberg HR 2005 High magnitude of light retardation by the zona pellucida is associated with conception cycles. *Human Reproduction* **20** 1596–1606. (doi:10.1093/humrep/deh811)

Shi S, Williams SA, Seppo A, Kurniawan H, Chen W, Ye Z, Marth JD & Stanley P 2004 Inactivation of the Mgat1 gene in oocytes impairs oogenesis, but embryos lacking complex and hybrid *N*-glycans develop and implant. *Molecular and Cellular Biology* **24** 9920–9929. (doi:10.1128/MCB.24.22.9920-9929.2004)

Simon C, Martin JC & Pellicer A 2000 Paracrine regulators of implantation. *Baillière's Best Practice & Research. Clinical Obstetrics & Gynaecology* **14** 815–826. (doi:10.1053/beog.2000.0121)

Strain L, Dean JC, Hamilton MP & Bonthron DT 1998 A true hermaphrodite chimera resulting from embryo amalgamation after *in vitro* fertilization. *New England Journal of Medicine* **338** 166–169. (doi:10.1056/NEJM199801153380305)

Sugiura K, Su YQ, Li Q, Wigglesworth K, Matzuk MM & Eppig JJ 2010 Estrogen promotes the development of mouse cumulus cells in coordination with oocyte-derived GDF9 and BMP15. *Molecular Endocrinology* **24** 2303–2314. (doi:10.1210/me.2010-0260)

Suzuki H, Togashi M, Adachi J & Toyoda Y 1995 Developmental ability of zona-free mouse embryos is influenced by cell association at the 4-cell stage. *Biology of Reproduction* **53** 78–83. (doi:10.1095/biolreprod53.1.78)

Ueda O, Yorozu K, Kamada N, Jishage K, Kawase Y, Toyoda Y & Suzuki H 2003 Possible expansion of "Window of Implantation" in pseudopregnant mice: time of implantation of embryos at different stages of development transferred into the same recipient. *Biology of Reproduction* **69** 1085–1090. (doi:10.1095/biolreprod.103.017608)

Van der Auwera I & D'Hooghe T 2001 Superovulation of female mice delays embryonic and fetal development. *Human Reproduction* **16** 1237–1243. (doi:10.1093/humrep/16.6.1237)

Wassarman PM 2005 Contribution of mouse egg zona pellucida glycoproteins to gamete recognition during fertilization. *Journal of Cellular Physiology* **204** 388–391. (doi:10.1002/jcp.20389)

Williams SA & Stanley P 2008 Mouse fertility is enhanced by oocyte-specific loss of core 1-derived *O*-glycans. *FASEB Journal* **22** 2273–2284. (doi:10.1096/fj.07-101709)

Williams SA & Stanley P 2009 Oocyte-specific deletion of complex and hybrid *N*-glycans leads to defects in preovulatory follicle and cumulus mass development. *Reproduction* **137** 321–331. (doi:10.1530/REP-07-0469)

Williams SA & Stanley P 2011 Premature ovarian failure in mice with oocytes lacking core 1-derived *O*-glycans and complex *N*-glycans. *Endocrinology* **152** 1057–1066. (doi:10.1210/en.2010-0917)

Williams SA, Xia L, Cummings RD, McEver RP & Stanley P 2007 Fertilization in mouse does not require terminal galactose or *N*-acetylglucosamine on the zona pellucida glycans. *Journal of Cell Science* **120** 1341–1349. (doi:10.1242/jcs.004291)

Xia L, Ju T, Westmuckett A, An G, Ivanciu L, McDaniel JM, Lupu F, Cummings RD & McEver RP 2004 Defective angiogenesis and fatal embryonic hemorrhage in mice lacking core 1-derived *O*-glycans. *Journal of Cell Biology* **164** 451–459. (doi:10.1083/jcb.200311112)

Xie Y, Wang F, Zhong W, Puscheck E, Shen H & Rappolee DA 2006 Shear stress induces preimplantation embryo death that is delayed by the zona pellucida and associated with stress-activated protein kinase-mediated apoptosis. *Biology of Reproduction* **75** 45–55. (doi:10.1095/biolreprod.105.049791)

Received 10 March 2012
First decision 23 April 2012
Revised manuscript received 1 August 2012
Accepted 23 August 2012

Article 2: Oocyte-derived Smad4 is not required for development of the oocyte or the preimplantation embryo

The first study that I conducted in the context of my DPhil studies was carried out in a mouse with an oocyte-specific deletion of *Smad4*. The work in this Mutant mouse allowed me to obtain the required training to develop my DPhil research project based on the DM mouse model. Some of the skills acquired during my work with the *Smad4* Mutant mouse were mouse colony management, fertility assessment and 6.5dpc embryo dissection. In addition, the results of this study were recently published and the article is presented below.

Theriogenology 83 (2015) 897–903

Contents lists available at ScienceDirect

Theriogenology

journal homepage: www.theriojournal.com

Oocyte-derived Smad4 is not required for development of the oocyte or the preimplantation embryo

Heidy Kaune [a,b], Emeline Peyrache [a], Suzannah A. Williams [a,*]

[a] Nuffield Department of Obstetrics and Gynaecology, Women's Centre, Level 3, John Radcliffe Hospital, University of Oxford, Oxford, UK
[b] Faculty of Medicine, Diego Portales University, Santiago, Chile

ARTICLE INFO

Article history:
Received 24 July 2014
Received in revised form 4 November 2014
Accepted 21 November 2014

Keywords:
Smad4
Oocyte
Embryo
Development

ABSTRACT

The generation of a competent egg requires complex molecular interactions between the oocyte and the ovary, and transforming growth factor β (TGF-β) is a major signaling pathway. Smad4 is a central regulator of the TGF-β signaling pathway as it mediates gene expression triggered by activation of TGF-β receptors. Deletion of *Smad4* in granulosa cells disrupts follicle development; however, the role of Smad4 in the oocyte has not been confirmed. Furthermore, the role of Smad4 in embryo development has not been confirmed because previous studies of $Smad4^{del/del}$ embryos were generated from heterozygous parents, and thus it is possible that maternal transcripts rescue development before embryonic day 6.5 (E6.5) when $Smad4^{del/del}$ embryos die. To determine the role of TGF-β signaling in oocyte and embryo development, mice with oocyte-specific deletion of *Smad4* were studied. Fertility was evaluated in Mutant ($Smad4^{F/F}$:ZP3*Cre*) and Control ($Smad4^{F/F}$) females mated continuously with control males during a 6-month period. Surprisingly, Mutant females were fertile with the same litter size (Mutants, 9.23 ± 0.4; Controls, 9.42 ± 0.4) and interlitter period as Controls. Ovulation rate induced using a superovulation regime did not differ between Controls and Mutants at both 6 weeks and 6 months. Embryo development was assessed at E6.5 using Control and Mutant females mated with heterozygous males. Development of $Smad4^{del/del}$ embryos at E6.5 was retarded consistent with previous studies of embryos generated from heterozygous parents indicating that there is no rescue of preimplantation development by maternal transcripts. The numbers of implanted embryos at 6.5 dpc also did not differ (Control: 9.1 ± 0.4; Mutant: 7.0 ± 0.9). However, only 26.3% of E6.5 embryos carried by Mutant females were $Smad4^{del/del}$ compared with the expected ratio of 50%. Since litter size was not decreased, this indicates that either the number of $Smad4^{del}$ sperm fertilizing the oocytes is reduced or implantation of $Smad4^{del/del}$ embryos is suboptimal. In summary, we have shown that *Smad4* in the oocyte, and thus TGF-β signaling, is not required for oocyte or follicle development, ovulation, fertilization, preimplantation development, or implantation.

© 2015 Elsevier Inc. All rights reserved.

1. Introduction

The ovarian follicle is the functional unit within the ovary. It comprises the oocyte, centrally located and surrounded by two types of somatic cells: granulosa cells that enclose the oocyte and theca cells that form the outer layers of the follicle. Follicle development and ultimately fertility rely on paracrine crosstalk between the cellular components of the follicle. These interactions allow granulosa cells to proliferate and differentiate to support oocyte development and competence for fertilization [1,2]. Several of the factors involved in this communication belong to

* Corresponding author. Tel.: +44 (0) 1865 221014; fax: +44 (0) 1865 769141.
E-mail address: suzannah.williams@obs-gyn.ox.ac.uk (S.A. Williams).

0093-691X/$ – see front matter © 2015 Elsevier Inc. All rights reserved.
http://dx.doi.org/10.1016/j.theriogenology.2014.11.024

Table 1
Efficiency of oocyte *Smad4* deletion.

	Control females (*Smad4*$^{F/F}$; n = 4)		Mutant females (*Smad4*$^{F/F}$:ZP3*Cre*; n = 8)	
	Female pups	Male pups	Female pups	Male pups
Deleted *Smad4* alleles	0% (n = 14)	0% (n = 17)	100% (n = 26)	100% (n = 37)

the transforming growth factor β (TGF-β) family. Two of the most well known are produced by the oocyte; bone morphogenetic protein 15 (BMP15) and growth differentiation factor 9 (GDF9) [3–5]. Granulosa cells are targeted by these oocyte-secreted factors that regulate granulosa cell proliferation and differentiation, and follicle development [4,6,7].

Smad proteins are intracellular mediators of TGF-β signaling which form transcriptional complexes once TGF-β membrane receptors are activated. Smads are divided into three groups: (1) the receptor-regulator or R-Smads (Smads 1, 2, 3, 5, and 8) that are directly activated by TGF-β receptors, (2) co-Smad (the only member is Smad4) that is a mediator for R-Smads transcriptional activity, and (3) inhibitory Smads (Smads 6 and 7) that either interfere with Smad-receptor or Smad–Smad interactions [8]. R-Smads 1, 5, and 8 are activated by BMPs and anti-Müllerian hormone, and R-Smads 2 and 3 by TGF-β, activin, and Nodal [9]. Once activated, R-Smads are transported into the nucleus where they have transcriptional regulatory activity on targeted genes. Smad4 protein is the central regulator of Smad activity and participates in R-Smads activation. Once TGF-β receptors are activated, Smad1/5/8 (for BMP signaling) or Smad2/3 (for TGF-β–like signaling) become phosphorylated and form a complex with Smad4. This complex then translocates into the nucleus and regulates gene expression [8–11].

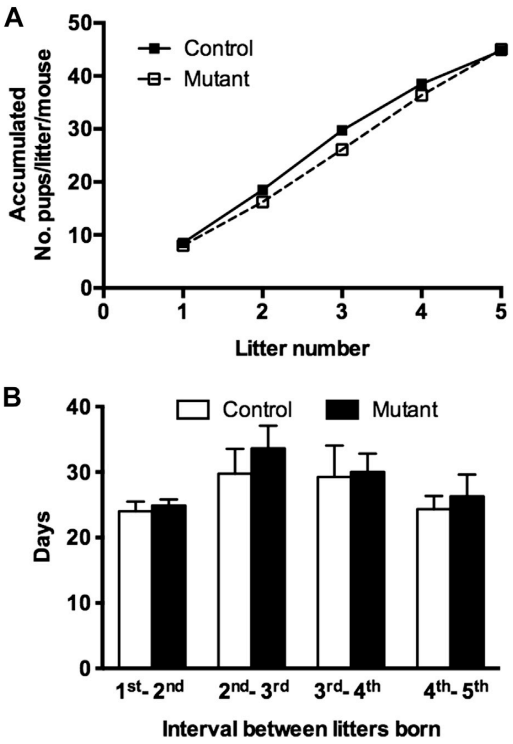


Fig. 1. Evaluation of fertility. (A) Accumulated number of pups per litter from *Smad4*$^{F/F}$:*ZP3Cre* (Mutant) and *Smad4*$^{F/F}$ (Control) females. (B) Interval between litters produced by Control and Mutant females. Results are expressed as mean ± standard error of the mean.

It has previously been reported that TGF-β signaling mediated by Smad proteins has a critical role in early embryo development. Mouse models mutant for Smads have revealed that downregulated Smad signaling results in impaired embryo development in several systems and organs, including cardiovascular development [12], primordial germ cell differentiation [13], and establishment of left–right asymmetry [14]. During murine embryo development, Smad4 is a crucial regulator of the Smad pathway, homozygous Smad4 mutant embryos with either complete deletion of *Smad4* [15], lacking exon 1 [17,18] or lacking exon 8 [16] exhibit retarded development by embryonic day 6.5 (E6.5) [15–17] exhibiting a variety of defects such as defects in gastrulation [15,16], patterning [17], and basement membrane deposition [18] and die by E8.5 [15,16]. However, although these results imply that Smad4 is not required for preimplantation embryo development, these studies used embryos generated from heterozygous mothers which contain maternal transcripts that are expressed during early stages of embryo development [19]. Therefore, the requirement for Smad4 during preimplantation embryo development remains unknown.

Within the ovary, TGF-β family members are a major signaling pathway and are involved in both follicle development [20,21] and oocyte meiotic maturation [22]. Smad proteins are thus also critical for ovarian function and female fertility. Since absence of Smads by direct gene knockout leads to embryo lethality, to investigate roles of these proteins in fertility, *Cre/loxP* technology has been used to delete Smad genes in specific cells and tissues. Thus, it has been reported that Smad5 is required for primordial germ cells development in mouse [13]. On the other hand, expression levels of Smads 2, 3, and 4 in human granulosa cells are correlated with oocyte quality and may contribute to fertilization rates [23].

Interestingly, granulosa cell–specific knockout mice for Smad proteins have detrimental effects on fertility including reduced numbers of antral follicles, diminished ovulation rates, cumulus cell defects, and increased luteinization [24–26]. Furthermore, specific deletion of *Smad4* in granulosa cells in mouse ovaries leads to a severe reduction of fertility demonstrated by a decreased litter size, premature ovarian failure, disrupted follicle

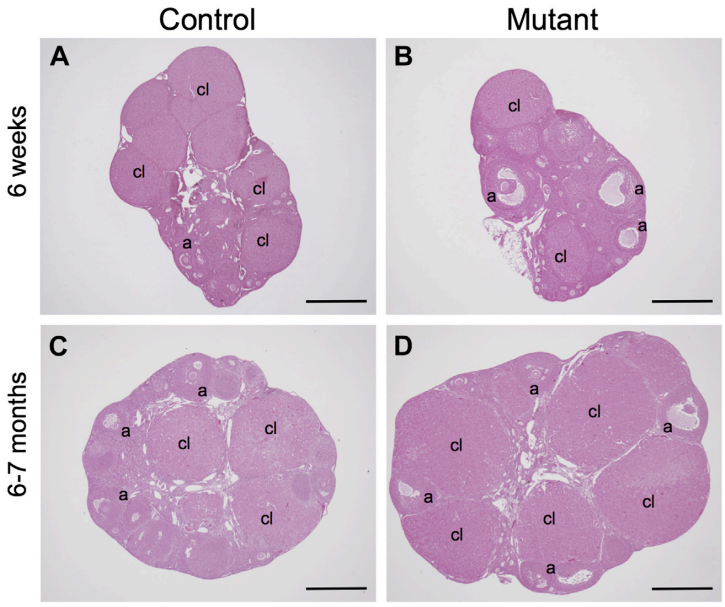


Fig. 2. Morphology of ovaries from Control and Mutant females. Representative images of ovarian sections from Control (A, C) and Mutant (B, D) females at 6 weeks (A, B) and 7 months of age (C, D). Corpora lutea (cl) and antral follicles (a) were present in all ovaries along with all stages of follicle development. Bar scale 500 μm. (For interpretation of the references to color in this figure, the reader is referred to the Web version of this article.)

development (from preantral stage onwards), and premature luteinization of follicles demonstrating that Smad4, and therefore TGF-β signaling, is a central regulator in granulosa cell development, follicle formation, and fertility [25].

Although these studies indicate that TGF-β signaling through Smad4 is key for normal ovarian physiology, recently Li et al. [27] reported only a minor effect in the fertility of mice with a conditional deletion of Smad4 in the oocyte at the primordial follicle stage using a *GDF9iCre* transgene. Decrease in fertility in this model was due to a reduction in pups per litter; however, ovarian morphology and function appeared unaffected. Despite this evidence, the role of Smad4 in the oocyte remains unclear, and more studies are needed to fulfill our understanding of TGF-β signaling within the oocyte.

The aim of this study was to investigate the role of Smad4 as a mediator for TGF-β signaling in the oocyte and determine whether Smad4 is required for preimplantation embryo development.

2. Materials and methods

2.1. Generation of female mice with oocyte-specific deletion of *Smad4*

Female mice carrying the floxed *Smad4* allele were generously provided by Professor Elizabeth Robertson. To generate female mice with targeted deletion of Smad4, *Cre-loxP* technology was used. Oocyte-specific deletion of *Smad4* was achieved using $Smad4^{F/F}$ females (homozygous floxed *Smad4* gene) carrying a *Cre* recombinase transgene under the control of the ZP3 promoter. Deletion of *Smad4* in the oocyte occurs when ZP3 is expressed during the early stages of oocyte development, from the primary stage onward [28]. The ZP3*Cre* recombinase transgene does not affect fertility [29], and *Smad4* floxed alleles are functionally wild type [17]. $Smad4^{F/F}$:ZP3*Cre* genotype results in an oocyte-specific deletion of *Smad4* (Mutant females); meanwhile, $Smad4^{F/F}$ females lacking the ZP3*Cre* transgene were used as Controls.

The protocols involving the use of animals were in compliance with the Animals (Scientific Procedures) Act 1986, UK. Animals were maintained in a 12 to 12 light/darkness conditions and provided with food and water *ad libitum*.

2.2. Genotyping

All genotypes were determined by polymerase chain reaction (PCR) of genomic DNA, obtained from ear biopsies or digests of E6.5 embryos. The following primers were used to detect the floxed or deleted *Smad4* alleles: *Smad4*-F2 5′-AAAATGGGAAAACCAACGAG-3′, *Smad4*-F1 5′-CTTTTATTTT-CAGATTCAGGGGTTC-3′, and *Smad4*-R1 5′-TACAAGTGC-TATGTCTTCAGCG-3′ [17]. The PCRs were performed with an initialization step of 2 minutes at 94 °C followed for 35 cycles of 30 seconds at 94 °C (denaturation), 30 seconds at 58 °C (annealing), and 1 minute at 72 °C (extension). F2 and R1 primers amplify a 625-bp and a 675-bp PCR product for the wild type ($Smad4^{+}$) and the floxed ($Smad4^{F}$) alleles, respectively. F1 and R1 primers amplify a 512-bp PCR

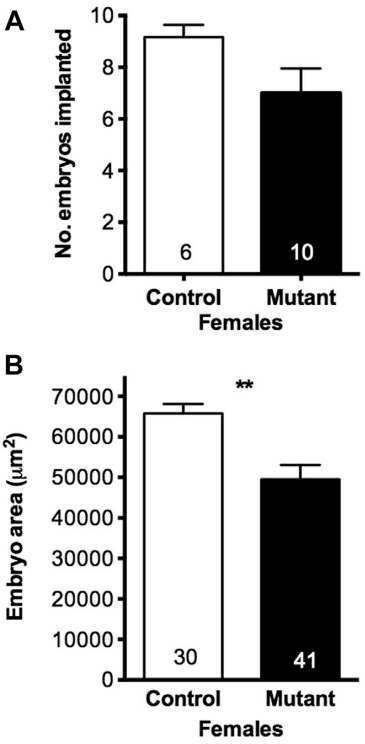


Fig. 3. Analysis of embryos at embryonic day 6.5 (E6.5) from Control and Mutant females. (A) Number of embryos implanted in Control and Mutant females. (B) Embryonic size (evaluated as total area) in embryos from Control and Mutant females. The number in each bar is the number of females (A) or embryos (B) analyzed. Results are expressed as mean ± standard error of the mean, $^{**}P < 0.01$.

product corresponding to the deleted (*Smad4*^{del}) allele. Detection of the *Cre* transgene was performed using primers previously described [29]. Polymerase chain reaction conditions were the same as described above for *Smad4* genotyping but with an annealing temperature of 56 °C.

2.3. Evaluation of fertility

Smad4$^{F/F}$:ZP3*Cre* (Mutant) and *Smad4*$^{F/F}$ (Control) female mice were mated with control males (*Smad4*$^{F/+}$, *Smad4*$^{F/F}$, *Smad4*$^{+/+}$, or *C1galt1*$^{F/F}$) for a 6-month period. Five consecutive litters were used to evaluate fertility, litter size, and interlitter period.

2.4. Superovulation

Mutant and Control females aged 6 weeks and 6 months were superovulated by intraperitoneal injection of 5 IU of pregnant mare serum gonadotropin (Intervet UK Ltd, Milton Keynes, UK) followed 46 to 48 hours later by 5 IU of hCG (Chorulon, Intervet UK Ltd). Oviducts were dissected from females 14 to 16 hours later into warmed M2 medium (Sigma–Aldrich, Gillingham, Dorset, UK). Oviducts were ripped to release the cumulus mass, and eggs were counted.

2.5. Histologic analysis of ovaries

Ovaries were collected from Mutant and Control female mice at either 6 weeks or between 6 and 7 months of age. Tissue was fixed in 10% buffered formalin (Sigma–Aldrich) for 8 hours, embedded in paraffin, and 5-μm serial sections were collected onto positively charged slides. Morphological evaluation of ovaries was carried out on slides stained with hematoxylin (Thermo Scientific, Cheshire, UK) and eosin (Sigma–Aldrich).

2.6. Embryo collection

Embryos were collected from Mutant and Control females mated with *Smad4*$^{del/+}$ or *Smad4*$^{del/F}$ males. To establish the timing of gestation, noon of the day, when the vaginal plug was observed, was designated E0.5. On E6.5, the uterus was collected in prewarmed M2 medium (Sigma–Aldrich) at 37 °C and the number of embryos implanted in each uterine horn recorded. Deciduae were removed from uterine horns using a dissection microscope (Leica microsystems, Germany), and embryos were extracted as previously described [30]. Briefly, individual embryos were separated by cutting uterine horns between implantation sites. The muscular layer was peeled out using watchmaker's forceps, and deciduae were exposed. Embryos were shelled out by tearing the decidua apart, and then, Reichert's membrane and ectoplacental cone were removed using microneedles.

Each embryo was evaluated, photographed, and then placed in digestion buffer (50 mM Tris HCl, 1 mM EDTA, and 0.5% Tween 20) to obtain DNA for PCR analysis. Embryo area was measured from digital images using ImageJ software (National Institutes of Health, USA).

3. Results

3.1. *Smad4*$^{F/F}$:*ZP3Cre females have normal fertility*

Efficiency of oocyte-specific *Smad4* deletion was evaluated by analysis of offspring from six consecutive litters from Control (*Smad4*$^{F/F}$) and Mutant (*Smad4*$^{F/F}$:ZP3*Cre*) females mated with control males (*Smad4*$^{F/+}$, *Smad4*$^{F/F}$, *Smad4*$^{+/+}$, or *C1galt1*$^{F/F}$). As expected, 100% of the offspring from Mutant females had a deleted *Smad4* allele (Table 1). Fertility was evaluated in Control and Mutant females, mated continuously with control males during a 6-month period. Oocyte-specific deletion of *Smad4* did not affect fertility assessed as litter size (Controls 9.42 ± 0.4, n = 4 females, 19 litters; Mutants 9.23 ± 0.4, n = 8 females, 39 litters) and the interval between litters (Fig. 1). The proportion between genders was also unaltered (data not shown).

Mutant females responded to exogenous gonadotropins to the same extent as Controls at both 6 weeks (Mutant: 21 ± 4.8, n = 5; Control: 16.7 ± 4.8, n = 3) and 6 months of age (Mutant: 23.7 ± 6.5, n = 3; Control: 35 and 20, n = 2).

3.2. *Smad4*$^{F/F}$:*ZP3Cre females have normal ovarian morphology*

Ovarian histology in oocyte-specific *Smad*4 Mutant and Control females was analyzed at 6 weeks and 6 to 7 months

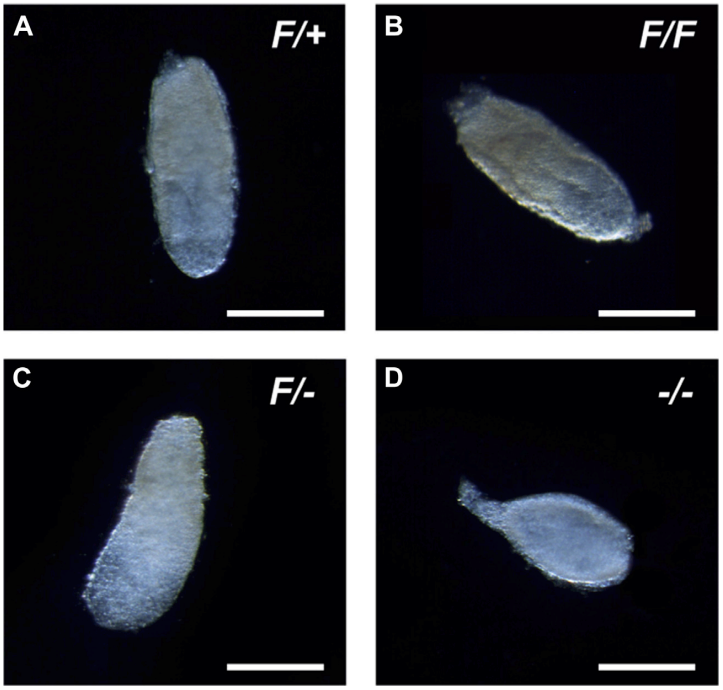


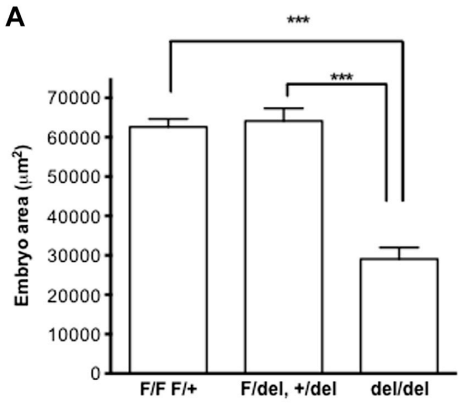
Fig. 4. Morphology of embryos at embryonic day 6.5 (E6.5) according to *Smad4* genotype. Normal development in embryos homozygous (A and B) or heterozygous (C) for functionally wild-type *Smad4* alleles. Disrupted development in *Smad4*$^{del/del}$ embryos (D). Bar scale 200 μm. (For interpretation of the references to color in this figure, the reader is referred to the Web version of this article.)

of age. Ovarian histology in Mutant mice was not different from Control females because follicles at all stages of development and corpora lutea were observed at both ages (Fig. 2).

3.3. Embryo development at E6.5 is compromised by deletion of Smad4

We evaluated embryo development at E6.5 from Mutant and Control females, mated with heterozygous males (*Smad4*$^{del/+}$ or *Smad4*$^{del/F}$). The number of embryos implanted was similar in Control and Mutant females (Control: 9.1 ± 0.4, n = 6; Mutant: 7.0 ± 0.9, n = 10; Fig. 3A). However, the embryo size, assessed as total embryo area, was significantly diminished in Mutant (49,497 ± 3578 μm^2, n = 41 embryos) compared with Control (65,756 ± 2346 μm^2, n = 30 embryos) females (Fig. 3B). To determine whether this decrease in the embryo size observed in Mutant females was related with the embryo genotype, embryos were grouped according to their genotype. We identified three groups of embryos: homozygous for functional *Smad4* alleles (*Smad4*$^{F/+,\ F/F}$), heterozygous for deleted *Smad4* alleles (*Smad4*$^{+/-,\ F/-}$), and knockout for *Smad4* allele (*Smad4*$^{del/del}$). Gross morphology was normal in homozygous and heterozygous embryos, whereas development was altered in knockout embryos (Fig. 4). Our results indicate that normal embryo development at E6.5 requires only one functional allele of *Smad4* (either maternal or paternal) because embryos homozygous and heterozygous for a functional *Smad4* allele have the same embryo size (62,598 ± 2047 and 64,146 ± 3209 μm^2, respectively), whereas *Smad4*$^{del/del}$ embryo size was significantly reduced (29,099 ± 2928 μm^2; Fig. 5A). As expected, no *Smad4*$^{del/del}$ embryos were retrieved from Control females (Fig. 5B). One embryo of the 38 assessed from Mutant females was homozygous *Smad4*$^{F/F}$ indicating that *Smad4* was not deleted in the oocyte. This unexpected finding led us to calculate deletion efficiency by assessing all pups (n = 63) and embryos (n = 38) from Mutant mothers. This analysis revealed that only one embryo of all 101 analyzed carried a floxed allele, and therefore, the efficiency of deletion was 99.01%.

Unexpectedly, only 26.3% of the embryos that originated from Mutant females were *Smad4*$^{del/del}$ as opposed to the expected 50% (Fig. 5B). Since 26.3% of the embryos were obtained taking into account all embryos from Mutant females, we determined the percentage of *Smad4*$^{del/del}$ embryos per Mutant female (n = 8; 0, 0, 20, 29, 33, 38, 50, 100) and compared that with an expected 50% for n = 8. The statistical analysis demonstrated that the percentage is decreased in the Mutant group ($P < 0.05$). Two possible explanations exist for these data. First, the lower than expected level of *Smad4*$^{del/del}$ embryos most likely indicates that the number of *Smad4*^{del} sperm fertilizing the oocytes is reduced indicating a potential novel role for Smad4 in



B

	Control (n=6)	Mutant (n=8)
Embryos homozygous for functional *Smad4* (F/F and F/+)	65.7% (23)	2.6% (1)
Embryos heterozygous for functional *Smad4* (F/del, +/del)	34.3% (12)	71.1% (27)
Embryos homozygous knock out for *Smad4* (del/del)	0	26.3% (10)

Fig. 5. Analysis of embryo development at embryonic day 6.5 (E6.5) by genotype. (A) Embryo size (assessed as total area) according to embryo genotype. (B) Proportion of embryo genotypes generated from Control and Mutant females when mated with a heterozygous male. Results are expressed as mean ± standard error of the mean, ***$P < 0.001$.

sperm. Second, the origin of the lower proportion of *Smad4*$^{del/del}$ embryos observed in Mutant females could be due to either selective rejection of *Smad4*$^{del/del}$ embryos by the endometrium during implantation or defects in *Smad4*$^{del/del}$ blastocysts implantation efficiency.

4. Discussion

Transforming growth factor β signaling has been implicated in critical events in mouse gonad development, including primordial germ cell formation, and ovary function. Bmp4 and Bmp8b knockout mice have a reduced or total absence of primordial germ cells [31]. On the other hand, Smad5 is required for mouse primordial germ cell development and migration [13]. Particularly in the ovary, numerous studies have been reported that TGF-β family proteins are key regulators in follicle development, granulosa cell differentiation, and steroidogenesis [32–34]. Molecular interaction between somatic cells and the oocyte are critical for oogenesis. Among these interactions, TGF-β/Smad signaling has been shown to be essential. Particularly, oocyte-secreted growth factors, BMP15 and GDF9 regulate follicle development, granulosa cell function, and fertility [4,6,7]. On the other hand, Smad protein expression in human granulosa cells has been correlated with oocyte quality [23]. Mice with a conditional knockout of *Smad4* in granulosa cells have cumulus cell defects and undergo premature ovarian failure, suggesting a role of TGF-β signaling in granulosa cell differentiation and function [25].

Despite the fact that TGF-β and therefore Smad4 signaling are very important for female fertility, our results indicate that oocyte-specific deletion of *Smad4* seems to have no effect on oocyte development, ovulation, and preimplantation embryo development because Mutant females have the same litter size and interlitter interval as Controls. Moreover, deletion of *Smad4* in the oocyte has no effect on ovarian morphology. These findings are in agreement with Li et al. [27] which reported just a minimal effect in the fertility of mice with oocyte-specific deletion of *Smad4* using *Gdf9iCre* recombinase which is expressed at the primordial stage of follicle development. The same study reveals that conditional deletion of *Smad4* with a ZP3*Cre* transgene (expressed from the primary stage of follicle development onward) had no effect on fertility or ovarian morphology. Therefore, according to these results, Smad4 should not have a critical role in oocyte development. Since our mouse model uses a ZP3*Cre* transgene, our results confirm that Smad4 in the oocyte is not critical for follicle development and ultimately is unnecessary in the regulation of fertility.

Transforming growth factor β signaling has been shown to play a variety of critical roles in early embryo development. Unsurprisingly, Smad4 as a central regulator for the TGF-β signaling pathway is key for embryo development. Homozygous *Smad4* knockout embryos are severely retarded in development by E6.5 displaying a severe disruption of gastrulation [15,16] and die by E8.5 [15]. Our results are consistent with these demonstrating that *Smad4*$^{del/del}$ embryos at E6.5 are smaller compared with embryos either homozygous or heterozygous carriers of a functional *Smad4* allele. Furthermore, we have determined that preimplantation embryo development does not require Smad4. This was previously a point of contention because these studies used heterozygous mothers to generate *Smad4*-null embryos [15], and thus, maternal Smad4 messenger RNAs stored in the oocyte before fertilization could support early embryo development; as has been observed for other molecules [19]. The disruption of development that we observed is at the same stage as these previous reports [15–18], therefore, we have firmly established that Smad4 is not required for preimplantation development.

In conclusion, we have shown that only one copy of *Smad4* is required to ensure embryos develop up to E6.5 consistent with previous studies. Moreover, our study demonstrates that oocyte-derived *Smad4*, and thus TGF-β signaling, is not required for oocyte or follicle development, ovulation, fertilization, or preimplantation development.

Acknowledgments

This research was funded by The John Fell OUP Fund, University of Oxford with a grant to Dr. Suzannah A. Williams (092/259). The authors thank Dr. Patricia Grasa

and Dr. Bradley Joyce for technical assistance and Dr. Juan Montiel for advice in morphologic analysis.

Heidy Kaune is funded by a scholarship from Becas Chile (Comisión Nacional de Investigación Científica y Tecnológica) and Diego Portales University, Chile.

References

[1] Buccione R, Vanderhyden BC, Caron PJ, Eppig JJ. FSH-induced expansion of the mouse cumulus oophorus in vitro is dependent upon a specific factor(s) secreted by the oocyte. Dev Biol 1990;138:16–25.
[2] Buccione R, Schroeder AC, Eppig JJ. Interactions between somatic cells and germ cells throughout mammalian oogenesis. Biol Reprod 1990;43:543–7.
[3] Elvin JA, Yan C, Matzuk MM. Oocyte-expressed TGF-beta superfamily members in female fertility. Mol Cell Endocrinol 2000;159:1–5.
[4] Yan C, Wang P, DeMayo J, DeMayo FJ, Elvin JA, Carino C, et al. Synergistic roles of bone morphogenetic protein 15 and growth differentiation factor 9 in ovarian function. Mol Endocrinol 2001;15:854–66.
[5] Findlay JK, Drummond AE, Dyson ML, Baillie AJ, Robertson DM, Ethier J-F. Recruitment and development of the follicle; the roles of the transforming growth factor-beta superfamily. Mol Cell Endocrinol 2002;191:35–43.
[6] Su Y-Q, Wu X, O'Brien MJ, Pendola FL, Denegre JN, Matzuk MM, et al. Synergistic roles of BMP15 and GDF9 in the development and function of the oocyte-cumulus cell complex in mice: genetic evidence for an oocyte-granulosa cell regulatory loop. Dev Biol 2004;276:64–73.
[7] Dong J, Albertini DF, Nishimori K, Kumar TR, Lu N, Matzuk MM. Growth differentiation factor-9 is required during early ovarian folliculogenesis. Nature 1996;383:531–5.
[8] Attisano L, Wrana JL. Signal transduction by the TGF-beta superfamily. Science 2002;296:1646–7.
[9] Massagué J, Seoane J, Wotton D. Smad transcription factors. Genes Dev 2005;19:2783–810.
[10] Massagué J. TGF-beta signal transduction. Annu Rev Biochem 1998;67:753–91.
[11] Massagué J, Hata A. TGF-beta signalling through the Smad pathway. Trends Cell Biol 1997;7:187–92.
[12] Chen Q, Chen H, Zheng D, Kuang C, Fang H, Zou B, et al. Smad7 is required for the development and function of the heart. J Biol Chem 2009;284:292–300.
[13] Chang H, Matzuk MM. Smad5 is required for mouse primordial germ cell development. Mech Dev 2001;104:61–7.
[14] Chang H, Zwijsen A, Vogel H, Huylebroeck D, Matzuk MM. Smad5 is essential for left–right asymmetry in mice. Dev Biol 2000;219:71–8.
[15] Sirard C, la Pompa de JL, Elia A, Itie A, Mirtsos C, Cheung A, et al. The tumor suppressor gene Smad4/Dpc4 is required for gastrulation and later for anterior development of the mouse embryo. Genes Dev 1998;12:107–19.
[16] Yang X, Li C, Xu X, Deng C. The tumor suppressor SMAD4/DPC4 is essential for epiblast proliferation and mesoderm induction in mice. Proc Natl Acad Sci U S A 1998;95:3667–72.
[17] Chu GC, Dunn NR, Anderson DC, Oxburgh L, Robertson EJ. Differential requirements for Smad4 in TGFbeta-dependent patterning of the early mouse embryo. Development 2004;131:3501–12.
[18] Costello I, Biondi CA, Taylor JM, Bikoff EK, Robertson EJ. Smad4-dependent pathways control basement membrane deposition and endodermal cell migration at early stages of mouse development. BMC Dev Biol 2009;9:54.
[19] Ioffe E, Liu Y, Stanley P. Complex N-glycans in Mgat1 null preimplantation embryos arise from maternal Mgat1 RNA. Glycobiology 1997;7:913–9.
[20] Tsafriri A, Vale W, Hsueh AJ. Effects of transforming growth factors and inhibin-related proteins on rat preovulatory graafian follicles in vitro. Endocrinology 1989;125:1857–62.
[21] Drummond AE. TGFbeta signalling in the development of ovarian function. Cell Tissue Res 2005;322:107–15.
[22] Brucker C, Alexander NJ, Hodgen GD, Sandow BA. Transforming growth factor-alpha augments meiotic maturation of cumulus cell-enclosed mouse oocytes. Mol Reprod Dev 1991;28:94–8.
[23] Kuo F-T, Fan K, Ambartsumyan G, Menon P, Ketefian A, Bentsi-Barnes IK, et al. Relative expression of genes encoding SMAD signal transduction factors in human granulosa cells is correlated with oocyte quality. J Assist Reprod Genet 2011;28:931–8.
[24] Pangas SA. Bone morphogenetic protein signaling transcription factor (SMAD) function in granulosa cells. Mol Cell Endocrinol 2012;356:40–7.
[25] Pangas SAS, Li XX, Robertson EJE, Matzuk MMM. Premature luteinization and cumulus cell defects in ovarian-specific Smad4 knockout mice. Mol Endocrinol 2006;20:1406–22.
[26] Li Q, Pangas SA, Jorgez CJ, Graff JM, Weinstein M, Matzuk MM. Redundant roles of SMAD2 and SMAD3 in ovarian granulosa cells in vivo. Mol Cell Biol 2008;28:7001–11.
[27] Li X, Tripurani SK, James R, Pangas SA. Minimal fertility defects in mice deficient in oocyte-expressed Smad4. Biol Reprod 2012;86:1–6.
[28] Philpott CC, Ringuette MJ, Dean J. Oocyte-specific expression and developmental regulation of ZP3, the sperm receptor of the mouse zona pellucida. Dev Biol 1987;121:568–75.
[29] Williams SA, Xia L, Cummings RD, McEver RP, Stanley P. Fertilization in mouse does not require terminal galactose or N-acetylglucosamine on the zona pellucida glycans. J Cell Sci 2007;120:1341–9.
[30] Shea K, Geijsen N. Dissection of 6.5 dpc mouse embryos. J Vis Exp 2007:160.
[31] Ying Y, Liu XM, Marble A, Lawson KA, Zhao GQ. Requirement of Bmp8b for the generation of primordial germ cells in the mouse. Mol Endocrinol 2000;14:1053–63.
[32] Erickson GF, Shimasaki S. The spatiotemporal expression pattern of the bone morphogenetic protein family in rat ovary cell types during the estrous cycle. Reprod Biol Endocrinol 2003;1:9.
[33] Tian X, Halfhill AN, Diaz FJ. Localization of phosphorylated SMAD proteins in granulosa cells, oocytes and oviduct of female mice. Gene Expr Patterns 2010;10:105–12.
[34] Pangas SA, Matzuk MM. Genetic models for transforming growth factor beta superfamily signaling in ovarian follicle development. Mol Cell Endocrinol 2004;225:83–91.

Appendix B: Differentially expressed genes in 9-week DM ovaries

Probe ID	Gene symbol	Gene name	Log_2FC	Average expression	t	P, Value	Adj,P,Val	B
lxRFKlAFReCEfpiAlI	Apoa1	apolipoprotein A-I	-1.8922	11.0958	-14.5771	4.11E-10	8.63E-06	12.9419
roRBKk,94i_6He56yE	Ctsk	cathepsin K	1.3272	9.4337	13.1799	1.63E-09	1.70788E-05	11.7949
rp,5Z99CDX8Wdp96II	Bcl2l10	Bcl2-like 10	-2.0058	11.2019	-12.6171	2.93E-09	2.05351E-05	11.2897
0XogiXiogrQdfziRXo	Apoa4	apolipoprotein A-IV	-1.8910	10.3574	-12.0941	5.18E-09	2.71872E-05	10.7960
344oV5w4FH9Q4oVZw4	Gm15698	transcription elongation factor B (SIII) polypeptide 2 pseudogene	-2.2373	11.5045	-11.5130	9.97E-09	4.19059E-05	10.2180
cFL9C2e3ddU3QJEk68	Bmp15	bone morphogenetic protein 15	-2.3229	11.5912	-11.1005	1.62E-08	5.04626E-05	9.7879
f_4VibVQBeo5AhLj3k	Nr5a2	nuclear receptor subfamily 5 group A member 2	-1.4089	12.3878	-10.9637	1.90E-08	5.04626E-05	9.6415
9HVfiIHiuHFe0e7UIU	E330034G19Rik	RIKEN cDNA E330034G19 gene	-2.2523	11.3725	-10.9548	1.92E-08	5.04626E-05	9.6320
9f,jihXnDgUf1DihVk	Gm15698	transcription elongation factor B (SIII) polypeptide 2 pseudogene	-2.0547	11.4206	-10.8172	2.27E-08	5.29477E-05	9.4825
lPQJPuoJe5SSOSdXuI	Kntc1	kinetochore associated 1	-0.7397	9.7905	-10.3109	4.24E-08	8.89938E-05	8.9156
iku1srsCpEdHrb5TAU	Gdf9	growth differentiation factor 9	-2.0476	13.1259	-10.0920	5.59E-08	9.05223E-05	8.6617
WVEy90fXI4J7yrxXpk	Slc38a5	solute carrier family 38 member 5	-3.2870	12.4059	-10.0603	5.82E-08	9.05223E-05	8.6244
Nr4Hj97U2kNxGoJuZM	Skp2	S-phase kinase-associated protein 2 (p45)	-0.6862	9.9377	-10.0510	5.89E-08	9.05223E-05	8.6135
EoJUh4EF9x9Nq7AKsU	E330017A01Rik	RIKEN cDNA E330017A01 gene	-1.5968	10.4502	-10.0258	6.09E-08	9.05223E-05	8.5838
rq3K7qDfp6O3_X3np4	Car14	carbonic anhydrase 14	-2.3981	11.1503	-9.9790	6.46E-08	9.05223E-05	8.5285
xm,gKR2AglCiOFK4yY	Gm813	predicted gene 813	-1.5028	10.3194	-9.7896	8.27E-08	0.0001	8.3019
oRRnKCdTnvoK3RurBs	Ncaph	non-SMC condensin I complex subunit H	-0.8272	10.3012	-9.7081	9.20E-08	0.0001	8.2031
Qf16FV6L_4_7FylXq0	Omt2b	oocyte maturation beta	-2.0041	10.9421	-9.5984	1.06E-07	0.0001	8.0688
xnOrQaXQudUAGpDWNQ	Cpsf4l	cleavage and polyadenylation specific factor 4-like	-1.7135	11.4638	-9.4072	1.37E-07	0.0001	7.8314
coR1vV4BT8A9lQCpVI	Ncam1	neural cell adhesion molecule 1	0.9955	9.6569	9.3887	1.41E-07	0.0001	7.8082
Wr7023REcY0b3j4nRU	Mcm6	minichromosome maintenance deficient 6 (MIS5 homolog S, pombe) (S, cerevisiae)	-0.8411	10.8894	-9.3540	1.48E-07	0.0001	7.7646
0fXSJ64Ojvk3kgLNCY	Gm13023	predicted gene 13023	-1.5578	10.4678	-9.3104	1.57E-07	0.0001	7.7095
ZykpG7XnKwV3cxFKhU	Aph1a	anterior pharynx defective 1a homolog (C, elegans)	-1.7965	10.3491	-9.1681	1.90E-07	0.0002	7.5282
HjQB92v9T91IOyOt64	Oosp1	oocyte secreted protein 1	-1.7417	11.0647	-9.1473	1.96E-07	0.0002	7.5015
69fpKOOuFduFbAjNVU	Dppa5a	developmental pluripotency associated 5A	-1.5978	11.1461	-9.1237	2.02E-07	0.0002	7.4711
lrmh4eejurV34_HIrk	Gm9961	predicted gene 9961	-1.6303	10.0517	-8.9612	2.53E-07	0.0002	7.2599
BHUnxF3S9fhi1KXzpQ	Gm4745	predicted gene 4745	-0.9698	9.6808	-8.9574	2.54E-07	0.0002	7.2549
llOodoyA5cJ3XRfy7o	Mcm10	minichromosome maintenance deficient 10 (S, cerevisiae)	-1.0980	10.4733	-8.9380	2.61E-07	0.0002	7.2295
05zVBWp1ieVeCmftEo	Igfbp2	insulin-like growth factor binding protein 2	1.2064	9.9142	8.9203	2.68E-07	0.0002	7.2063
Q5VQt0c0EjCrs9_zNc	Ccnb1	cyclin B1	-0.9470	10.5198	-8.9150	2.70E-07	0.0002	7.1992

Probe ID	Gene symbol	Gene name	Log_2FC	Average expression	t	P, Value	Adj,P,Val	B
Zlqe6gHuxeiutTll10	Dctd	dCMP deaminase	-0.9547	10.5020	-8.8830	2.82E-07	0.0002	7.1571
BtFOPzWQJSpYHXLlF4	Raet1b	retinoic acid early transcript beta	-0.9992	9.7700	-8.8795	2.84E-07	0.0002	7.1525
9XXRSpdFIrXq1NDAxI	H19	H19 imprinted maternally expressed transcript	-1.5062	10.8853	-8.8440	2.98E-07	0.0002	7.1056
cjO6kSlnVyP,hePe7s	Mphosph6	M phase phosphoprotein 6	-0.8320	11.4523	-8.8122	3.12E-07	0.0002	7.0633
ldOd_opUtFtfi9M1Il	Slco2a1	solute carrier organic anion transporter family member 2a1	0.5977	9.1441	8.7851	3.24E-07	0.0002	7.0272
Tu3ExUudMii_eIYp6A	Dpep2	dipeptidase 2	0.8481	8.9086	8.7525	3.40E-07	0.0002	6.9838
coilFB4Xl4wtyKJS1U	Kif4	kinesin family member 4	-0.6141	10.0192	-8.6376	4.00E-07	0.0002	6.8292
EoX_1BP_fvSoEVeWEg	Htra1	HtrA serine peptidase 1	-0.9228	12.9998	-8.6200	4.10E-07	0.0002	6.8054
Q01Pazr,VLV_xE16,g	Slc24a3	solute carrier family 24 (sodium/potassium/calcium exchanger) member 3	0.9528	10.0211	8.5854	4.31E-07	0.0002	6.7585
oXoleoN6Uu9NCuR794	Oas1d	2'-5' oligoadenylate synthetase 1D	-1.5950	11.7928	-8.5709	4.40E-07	0.0002	6.7388
fcoDfxb8Lst59VOLRQ	Sel1l3	sel-1 suppressor of lin-12-like 3 (C, elegans)	-1.3011	9.8145	-8.5130	4.79E-07	0.0002	6.6598
K4ntXrldJU0SSSEXtc	Apoa4	apolipoprotein A-IV	-2.2159	10.6952	-8.4750	5.06E-07	0.0003	6.6077
3l7SVOZXqH4gi9MBsk	Pbk	PDZ binding kinase	-0.9347	11.2560	-8.4445	5.29E-07	0.0003	6.5658
Ep8OSF,F7iVcpQp7JM	Mcm2	minichromosome maintenance deficient 2 mitotin (S, cerevisiae)	-0.8623	10.1163	-8.4408	5.31E-07	0.0003	6.5606
lN9qlC606bx6N7muWc	Psmb8	proteasome (prosome macropain) subunit beta type 8 (large multifunctional peptidase 7)	0.6477	10.5505	8.3207	6.33E-07	0.0003	6.3941
3X6s4Cec4S2eLHTBck	Rfpl4	ret finger protein-like 4	-1.5503	10.4903	-8.2222	7.33E-07	0.0003	6.2560
N05SLUuTddSSEqJSCg	Spin2c	spindlin family member 2C	-1.2829	10.8661	-8.1991	7.58E-07	0.0003	6.2235
rlU5VQ97pk1I_4A7EM	Vamp2	vesicle-associated membrane protein 2	0.5374	9.9592	8.1757	7.85E-07	0.0003	6.1903
BsoqIKXCgV6IrAp71U	Accsl	1-aminocyclopropane-1-carboxylate synthase (non-functional)-like	-1.0971	9.9280	-8.1503	8.15E-07	0.0003	6.1544
ipVHePXg3n8,d5MKBU	Fbxl22	F-box and leucine-rich repeat protein 22	0.8685	9.3101	8.1309	8.39E-07	0.0004	6.1269
9J2aCoglvlqgjL7u3s	Snrpa	small nuclear ribonucleoprotein polypeptide A	-0.5228	10.2732	-8.1190	8.54E-07	0.0004	6.1100
WqUqWc60CPj,VBHtQA	Plekha4	pleckstrin homology domain containing family A (phosphoinositide binding specific) member 4	0.6153	9.9930	8.0866	8.96E-07	0.0004	6.0637
Nc3nvTev1PwpTDXNeo	Nasp	nuclear autoantigenic sperm protein (histone-binding)	-0.5415	10.5060	-8.0793	9.06E-07	0.0004	6.0533
ct6oCNE6tir93HrSjk	Icam1	intercellular adhesion molecule 1	0.4511	9.1953	8.0600	9.33E-07	0.0004	6.0258
oqHXoHN_ooQuuBKcC0	Mycl	v-myc myelocytomatosis viral oncogene homolog lung carcinoma derived (avian)	-1.9937	11.0247	-8.0466	9.52E-07	0.0004	6.0065
re1dJUylHuMPt50k,U	Car12	carbonic anyhydrase 12	1.1867	9.4527	8.0338	9.70E-07	0.0004	5.9883
EkhUEulODOKlKAF7mA	Dpt	dermatopontin	0.8595	9.6316	8.0267	9.81E-07	0.0004	5.9780
BpfnmnlUs0h43,nRfQ	Rangrf	RAN guanine nucleotide release factor	-0.6543	10.4504	-8.0228	9.87E-07	0.0004	5.9724

Probe ID	Gene symbol	Gene name	Log_2FC	Average expression	t	P, Value	Adj,P,Val	B
uXtOX3QQji3okoEpXo	Mcm5	minichromosome maintenance deficient 5 cell division cycle 46 (S, cerevisiae)	-0.9853	11.7892	-7.9965	1.03E-06	0.0004	5.9346
Wtd3qmFr4_9LFFxwG4	Myo5c	myosin VC	-0.8200	9.3787	-7.9856	1.04349E-06	0.0004	5.9189
rV4E6_1kqkOCE_48W4	Htra1	HtrA serine peptidase 1	-0.8461	13.1838	-7.9656	1.08E-06	0.0004	5.8900
Zil8Sm,WBVoF4Q08Yc	Bex4	brain expressed gene 4	-1.3892	13.5217	-7.9567	1.09E-06	0.0004	5.8771
Ze5DUkolyFVMQjE1Pk	Slc37a2	solute carrier family 37 (glycerol-3-phosphate transporter) member 2	0.6430	9.3769	7.9253	1.14E-06	0.0004	5.8317
iXy38Cgj2O5_1_pl9w	Nipal2	NIPA-like domain containing 2	0.7992	9.3654	7.9110	1.17E-06	0.0004	5.8111
Zd76F9Mlobr0l7nUgk	Sfrp1	secreted frizzled-related protein 1	0.9386	11.0467	7.9023	1.18E-06	0.0004	5.7983
Tq9T7frrvElXvNT8AM	Bcl11a	B cell CLL/lymphoma 11A (zinc finger protein)	-0.6762	9.8013	-7.9013	1.19E-06	0.0004	5.7969
uXn6fEwcjz2t7eDutE	Esr2	estrogen receptor 2 (beta)	-1.2957	11.1588	-7.8998	1.19E-06	0.0004	5.7947
fbpAT,80lio0GKhTt8	Kpna7	karyopherin alpha 7 (importin alpha 8)	-0.9611	9.7237	-7.8973	1.19E-06	0.0004	5.7911
W16BROtHclK1QKFePc	Prkcb	protein kinase C beta	0.6463	9.2796	7.8927	1.20E-06	0.0004	5.7844
lXnH_11CyQLtI1CSn4	Arhgef19	Rho guanine nucleotide exchange factor (GEF) 19	0.5698	9.1014	7.8151	1.35E-06	0.0004	5.6711
NTKAd6hArrSl4CUuoU	Slit3	slit homolog 3 (Drosophila)	0.8583	9.6138	7.8012	1.38E-06	0.0004	5.6507
HuRyrsYJfKi7wClEkU	Spink8	serine peptidase inhibitor Kazal type 8	0.7095	8.7851	7.7771	1.43E-06	0.0004	5.6154
uve_nhfjt4U_OUeB7o	Slit2	slit homolog 2 (Drosophila)	0.6014	9.0582	7.7731	1.44E-06	0.0004	5.6094
QQou4qglQGs3uSWU_4	Wfdc10	WAP four-disulfide core domain 10	-1.4332	11.4998	-7.7057	1.60E-06	0.0005	5.5099
up2u3uy5xFw,OuVA4k	Ivns1abp	influenza virus NS1A binding protein	-0.8644	13.5779	-7.6592	1.72E-06	0.0005	5.4408
BkHSwu82nkASCGn1Gk	Fbxw18	F-box and WD-40 domain protein 18	-1.4569	10.6977	-7.6561	1.73E-06	0.0005	5.4362
BSJ7uOY1_CnFUlklJI	Psmc3ip	proteasome (prosome macropain) 26S subunit ATPase 3 interacting protein	-0.8256	10.5272	-7.6409	1.7692E-06	0.0005	5.4136
BpTo4voZ7UmoMUnB7g	Ndc80	NDC80 homolog kinetochore complex component (S, cerevisiae)	-0.5812	9.3671	-7.6390	1.77E-06	0.0005	5.4107
0ooImiSt4gkgn2aZF4	Bex4	brain expressed gene 4	-1.2033	12.1459	-7.6248	1.81E-06	0.0005	5.3896
3rrxFN0gHVLVMCLoCg	Bmpr1b	bone morphogenetic protein receptor type 1B	-0.8984	10.2432	-7.6119	1.85E-06	0.0005	5.3703
ZS6WrS6jt3eYkQKfNA	Antxr2	anthrax toxin receptor 2	0.8094	10.5960	7.5919	1.91E-06	0.0005	5.3404
fgdoF,6XE6qJuT,tMI	Ugt1a7c	UDP glucuronosyltransferase 1 family polypeptide A7C	0.5070	8.8643	7.5880	1.92098E-06	0.0005	5.3345
coF_,tX8tPJDohUbtU	Agtr1a	angiotensin II receptor type 1a	0.7276	9.0942	7.5778	1.95E-06	0.0005	5.3193
Th4TJLJ4J1LSnpM55U	Obox5	oocyte specific homeobox 5	-1.4727	10.2726	-7.5641	1.99E-06	0.0005	5.2988
uVYgCh7t53vrYPVS6c	Cmya5	cardiomyopathy associated 5	-0.9566	9.8869	-7.5591	2.01E-06	0.0005	5.2913
xro6pwtG7ecofCnn4U	Fads3	fatty acid desaturase 3	0.6818	9.1211	7.5526	2.03E-06	0.0005	5.2814
36UvNE2,skOzjoobUo	Raet1b	retinoic acid early transcript beta	-0.7158	9.3089	-7.5125	2.16184E-06	0.0005	5.2210
9bsknwFRN7tU0JeASU	Slc6a8	solute carrier family 6 (neurotransmitter transporter creatine) member 8	0.7309	10.0684	7.4945	2.22E-06	0.0005	5.1939

Probe ID	Gene symbol	Gene name	Log_2FC	Average expression	t	P, Value	Adj,P,Val	B
3kjfTVsok26nsg,dGo	Spin2c	spindlin family member 2C	-1.1528	10.6789	-7.4856	2.26E-06	0.0005	5.1805
3eUXiApRefnqSNT6PI	Fst	follistatin	-1.5123	11.7237	-7.4754	2.29E-06	0.0005	5.1650
TRk1Sf9SUqXXJKN8iA	Birc5	baculoviral IAP repeat-containing 5	-0.8925	11.1924	-7.4512	2.38E-06	0.0005	5.1283
lIJelk1lI7rnogpniA	Esr2	estrogen receptor 2 (beta)	-1.1150	10.5457	-7.4395	2.42513E-06	0.0005	5.1105
KlynhySf17P5egL3os	Klf17	Kruppel-like factor 17	-0.6972	9.2580	-7.4353	2.44126E-06	0.0005	5.1041
xX4lf_ETSOHp_U4gFU	Obox1	oocyte specific homeobox 1	-0.9922	9.7267	-7.4341	2.45E-06	0.0005	5.1022
EnRQnn11SDCIyoS56Q	Oosp2	oocyte secreted protein 2	-1.1952	10.2359	-7.4296	2.46E-06	0.0005	5.0954
cP7sCErKHqB6g5XkSU	Eif4e1b	eukaryotic translation initiation factor 4E family member 1B	-0.6596	9.2195	-7.3974	2.59E-06	0.0006	5.0463
6tpX3nsd4Dn_4L15r4	Cklf	chemokine-like factor	-0.6356	11.3965	-7.3939	2.61E-06	0.0006	5.0411
NuKvdUrkgCg_kbNV74	AU022751	expressed sequence AU022751	-1.4417	10.2416	-7.3765	2.67941E-06	0.0006	5.0145
QV,S4qKUiKKeCILeKI	Ranbp1	RAN binding protein 1	-0.8012	12.8616	-7.3742	2.69E-06	0.0006	5.0109
KbnkDSv8ztK18k,VbQ	2810417H13Rik	RIKEN cDNA 2810417H13 gene	-0.9556	9.8251	-7.3525	2.78E-06	0.0006	4.9778
HnSXSd3h9M5fgTed_A	Fbxw15	F-box and WD-40 domain protein 15	-1.3698	11.0939	-7.3406	2.84E-06	0.0006	4.9595
r7UgkeB5HSyqyvnRt0	Nlrp14	NLR family pyrin domain containing 14	-1.4179	13.0313	-7.3405	2.84E-06	0.0006	4.9593
Hpd5J7m5jiNuz7,PHo	Entpd5	ectonucleoside triphosphate diphosphohydrolase 5	0.5211	9.4108	7.3213	2.93E-06	0.0006	4.9298
Te4EYFTm5HxSSmYh34	Fam78a	family with sequence similarity 78 member A	-1.3771	11.5896	-7.3083	2.99E-06	0.0006	4.9098
i46gul,yI6sn_Bd3lI	Cdca7	cell division cycle associated 7	-1.1778	11.2068	-7.3058	3.00E-06	0.0006	4.9060
0RLhbrqTVVIh4ydoyA	Cdc45	cell division cycle 45	-0.6283	9.6449	-7.3033	3.01E-06	0.0006	4.9021
xjn0tTp4isUXmUkAKI	Dppa5a	developmental pluripotency associated 5A	-1.4348	11.0910	-7.2766	3.14E-06	0.0006	4.8610
xtIs2UiXER8X2dQjiU	Nop56	NOP56 ribonucleoprotein	-0.6075	11.0894	-7.2231	3.42E-06	0.0007	4.7782
WXSC_irh6ES8IdIiUk	Nod1	nucleotide-binding oligomerization domain containing 1	0.6401	10.0248	7.2169	3.46E-06	0.0007	4.7684
6stoBgjbUVyReVBSOs	Kif23	kinesin family member 23	-0.7534	10.2027	-7.2129	3.48E-06	0.0007	4.7623
ulV4fSAp_k40UXFl04	Cpne9	copine family member IX	-0.6566	9.2750	-7.1875	3.63E-06	0.0007	4.7229
EkYbStXp_rRFmf7Ftc	Mif	macrophage migration inhibitory factor	-0.5813	11.7750	-7.1870	3.63E-06	0.0007	4.7221
0X7d_XqnE7sEf_7p40	AA792892	expressed sequence AA792892	-1.3988	10.2941	-7.1795	3.67E-06	0.0007	4.7104
ZV7V9FRF0ORffR_i30	Pdlim1	PDZ and LIM domain 1 (elfin)	-1.1348	11.6485	-7.1631	3.77E-06	0.0007	4.6847
Z5IpdWKBWeZOX3lNic	Inha	inhibin alpha	-1.0158	14.0866	-7.1412	3.90677E-06	0.0007	4.6506
WfpZSUkSa1d_EcX3,A	Kif22	kinesin family member 22	-0.9735	11.0581	-7.1393	3.92E-06	0.0007	4.6477
fAoEvWkbu_nkmjmuVo	Smc2	structural maintenance of chromosomes 2	-0.6196	9.6491	-7.1343	3.95E-06	0.0007	4.6398
0VEj,dQEPqC5ci1KVY	Fbxo27	F-box protein 27	0.5002	9.0730	7.0958	4.21E-06	0.0007	4.5794
6XeXlFd6reMTnccbuE	Zp1	zona pellucida glycoprotein 1	-0.8359	9.7260	-7.0833	4.29214E-06	0.0008	4.5597
iPiRVRYl7kiJ6W8WP4	Psmb10	proteasome (prosome macropain) subunit beta type 10	0.5768	10.9864	7.0777	4.33E-06	0.0008	4.5510
u7sUUW3pJ,KA,7ukwI	Ska3	spindle and kinetochore associated complex subunit 3	-0.5503	9.1783	-7.0765	4.34E-06	0.0008	4.5491

Probe ID	Gene symbol	Gene name	Log_2FC	Average expression	t	P, Value	Adj,P,Val	B
KguCHxjV3rh1EfUH70	Nop58	NOP58 ribonucleoprotein	-0.9135	11.9932	-7.0504	4.53E-06	0.0008	4.5079
QKnnHuDOUKHh6lydoE	Mfsd2a	major facilitator superfamily domain containing 2A	-0.9832	10.2577	-7.0469	4.55E-06	0.0008	4.5024
lREMevn0quOVXtdl6A	Map7d1	MAP7 domain containing 1	0.8038	11.3000	7.0423	4.59E-06	0.0008	4.4952
Wr3HuE60VxZ1OkClTo	Fbxw22	F-box and WD-40 domain protein 22	-0.6673	9.1617	-7.0005	4.9127E-06	0.0008	4.4290
ELiaujnucbuA3t,lKU	Hoxb5	homeobox B5	0.3003	8.7707	6.9994	4.92E-06	0.0008	4.4273
rnfKgihUn17KWfS5Pk	Cdca2	cell division cycle associated 2	-0.7994	10.3464	-6.9934	4.97E-06	0.0008	4.4177
f2X7nXwd5bmK5Curlw	Car12	carbonic anyhydrase 12	0.5028	8.6992	6.9927	4.98E-06	0.0008	4.4166
xehIU_lV0lFeEJDADo	Stab1	stabilin 1	-0.9195	11.4461	-6.9812	5.07E-06	0.0008	4.3984
Bl_qv1FNfUjOs4lNzk	Fam129b	family with sequence similarity 129 member B	0.5519	10.4615	6.9800	5.0802E-06	0.0008	4.3966
9XuEDUpP9oPUvBVQwo	Rfpl4	ret finger protein-like 4	-1.2326	10.0328	-6.9760	5.11E-06	0.0008	4.3902
liKi9CUvOJBFx3eHiU	Slc46a1	solute carrier family 46 member 1	0.6259	9.4065	6.9672	5.19E-06	0.0008	4.3761
rzIUoXihMXoQJF1FqU	Cdk4	cyclin-dependent kinase 4	-0.6338	12.0273	-6.9634	5.22048E-06	0.0008	4.3702
WcWL36QFolLV4l75lg	Aatf	apoptosis antagonizing transcription factor	-0.5293	9.9051	-6.9569	5.28E-06	0.0008	4.3598
HClcpCXle_vstuLrfo	Fscn1	fascin homolog 1 actin bundling protein (Strongylocentrotus purpuratus)	-0.9870	10.5148	-6.9300	5.52E-06	0.0009	4.3169
ZXjOQuO6fuFMl_pDXE	Sall4	sal-like 4 (Drosophila)	-0.9436	9.6360	-6.9165	5.64E-06	0.0009	4.2953
r7azVIFkisQVI7VSUI	Vsig8	V-set and immunoglobulin domain containing 8	0.6005	8.6968	6.9105	5.70E-06	0.0009	4.2858
cocXnywupOfeNRxxSo	Sash3	SAM and SH3 domain containing 3	0.3259	8.6508	6.9064	5.73456E-06	0.0009	4.2792
KOSuBLt5SohJpJtzus	C1rl	complement component 1 r subcomponent-like	0.4349	9.0628	6.8850	5.94E-06	0.0009	4.2450
HukeOdRvl9S_eU657g	Zfp41	zinc finger protein 41	-1.0903	11.4488	-6.8774	6.02E-06	0.0009	4.2328
W78WBOkIEbQtWpD1Il	Fbxw24	F-box and WD-40 domain protein 24	-1.2727	10.3348	-6.8672	6.12E-06	0.0009	4.2164
NJIl5n2L10HFZX0Zkk	Fgf8	fibroblast growth factor 8	-0.5554	9.0467	-6.8295	6.51E-06	0.0010	4.1559
KhVHuUumiNCVbPEiSs	Gpx7	glutathione peroxidase 7	-0.5924	12.0858	-6.7749	7.13E-06	0.0010	4.0676
QrThF6,eOkzl_DN534	Fbxw27	F-box and WD-40 domain protein 27	-1.0307	10.0252	-6.7620	7.29E-06	0.0011	4.0468
rnkR23W9XJIR7FR8Eg	Aqp1	aquaporin 1	0.7214	9.6883	6.7616	7.29E-06	0.0011	4.0461
9Vf1r0XR6SfrPnq3fk	Fmo1	flavin containing monooxygenase 1	0.6735	9.9356	6.7503	7.43E-06	0.0011	4.0277
9MtTlgdbpeobru9_e4	LOC382202	uncharacterized LOC382202	0.8604	8.9766	6.7216	7.80E-06	0.0011	3.9811
oifeb7n_uZEbXkTWFc	Rasl10a	RAS-like family 10 member A	-1.1482	10.1607	-6.7121	7.92E-06	0.0011	3.9656
NdTJuz17nc7yLkw4mY	Cables1	CDK5 and Abl enzyme substrate 1	-1.6224	11.8761	-6.7030	8.04E-06	0.0011	3.9509
irgnNTKeel_PBo_yHE	Msh6	mutS homolog 6 (E, coli)	-0.5728	11.7933	-6.7029	8.04E-06	0.0011	3.9507
36ZUGqrV4h_TsActyM	Camta1	calmodulin binding transcription activator 1	-0.5896	9.2212	-6.6960	8.14E-06	0.0011	3.9395
QklJkJklkKInHa7G7E	Hist1h2be	histone cluster 1 H2be	0.9690	10.9430	6.6845	8.30E-06	0.0011	3.9207
6nIojF7QELQCrp1Ugk	Npm2	nucleophosmin/nucleoplasmin 2	-0.8712	9.7937	-6.6758	8.41977E-06	0.0012	3.9064
EiTkjwou4nlMhCjuo0	Ak1	adenylate kinase 1	0.5107	8.9862	6.6606	8.64E-06	0.0012	3.8817
EntCWbF7Rx63sd,o_k	Serpine2	serine (or cysteine) peptidase inhibitor clade E member 2	-1.2958	11.1567	-6.6557	8.70829E-06	0.0012	3.8737

Probe ID	Gene symbol	Gene name	Log_2FC	Average expression	t	P, Value	Adj,P,Val	B
0eTXFa3vip3hTp,NBQ	Hn1l	hematological and neurological expressed 1-like	-0.4909	9.8756	-6.6516	8.77E-06	0.0012	3.8668
xs1I0b5X,8_4f,Qed4	Kif23	kinesin family member 23	-0.7797	11.2388	-6.6428	8.90E-06	0.0012	3.8525
lTmrUpkad1z3vtP7lc	Cdca8	cell division cycle associated 8	-0.8484	10.9731	-6.6366	8.99E-06	0.0012	3.8423
0l719LiU5UV_77LiAc	Zmym3	zinc finger MYM-type 3	-0.9065	11.9396	-6.6077	9.44318E-06	0.0012	3.7949
in56LE6p55dvVhJw_0	Chchd4	coiled-coil-helix-coiled-coil-helix domain containing 4	-0.5575	10.5356	-6.6037	9.51E-06	0.0012	3.7884
oVzp4K,SEVjF5TrOvM	Cenpa	centromere protein A	-0.8728	12.7306	-6.5978	9.60E-06	0.0012	3.7786
faiXXl6dyojo0SEXkc	Inf2	inverted formin FH2 and WH2 domain containing	0.3753	9.0530	6.5972	9.61E-06	0.0012	3.7777
EChH7pLlmFXoYTT50E	Cirh1a	cirrhosis autosomal recessive 1A (human)	-0.5295	11.0796	-6.5954	9.64E-06	0.0012	3.7746
6eZOlN5QOcofXiBe50	Rrp15	ribosomal RNA processing 15 homolog (S, cerevisiae)	-0.4547	10.5277	-6.5669	1.01195E-05	0.0013	3.7276
cVAWIVJB4QA6UXYNS4	Fxyd5	FXYD domain-containing ion transport regulator 5	0.4473	9.1254	6.5493	1.04263E-05	0.0013	3.6986
0qru7rf1Ht_yQTfgHo	Rimkla	ribosomal modification protein rimK-like family member A	-0.7481	9.6743	-6.5458	1.04871E-05	0.0013	3.6929
K9eOi9JJaq5Su4pfKE	C4b	complement component 4B (Chido blood group)	0.5092	9.0249	6.5437	1.05253E-05	0.0013	3.6894
Z3ELkBrfFR4lN30aNk	Ahcy	S-adenosylhomocysteine hydrolase	-0.3431	9.0142	-6.5396	1.05983E-05	0.0013	3.6827
ZkojR1X6VVI6AwAJSE	Wnt6	wingless-type MMTV integration site family member 6	0.7670	10.5083	6.5382	1.06235E-05	0.0013	3.6803
TJ44h3Gvumef4joV5U	Cdc20	cell division cycle 20	-0.9833	11.0932	-6.5299	1.07757E-05	0.0013	3.6665
W9XiuxhCN5CmkKR4ko	Dhcr24	24-dehydrocholesterol reductase	0.6430	9.2973	6.5197	1.09634E-05	0.0013	3.6497
uIJEZZQKQibf34Ujgg	Bzw2	basic leucine zipper and W2 domains 2	-0.5702	12.1801	-6.5155	1.10422E-05	0.0013	3.6427
NfdcEvd5kyN_,tJN4U	Blm	Bloom syndrome RecQ helicase-like	-0.6016	10.1294	-6.5086	1.11726E-05	0.0014	3.6313
3FeaeaSkmIaW,vnPDw	Mta3	metastasis associated 3	-0.6913	11.0716	-6.5019	1.13022E-05	0.0014	3.6201
uUhd517f0fBIz8,_Z0	Wnt10a	wingless-type MMTV integration site family member 10A	1.2523	9.0304	6.4953	1.14298E-05	0.0014	3.6091
u_eSCEgl6eLR3Ubc14	Fam98a	family with sequence similarity 98 member A	-0.6971	12.2415	-6.4704	1.19263E-05	0.0014	3.5677
Hl5JFXADtR6P8CCRBI	Mtmr1	myotubularin related protein 1	0.3013	8.9442	6.4689	1.19567E-05	0.0014	3.5652
9SRXqV,cjFXXiF6Dos	Alpk3	alpha-kinase 3	-0.6592	9.1125	-6.4549	1.22466E-05	0.0014	3.5419
l15UCh2r7eE2eTjk3Q	Mmp2	matrix metallopeptidase 2	0.8643	12.7923	6.4372	1.2623E-05	0.0015	3.5124
WbUQ4p3UBU0cd9VAkc	Prc1	protein regulator of cytokinesis 1	-1.0225	12.5448	-6.4357	1.26558E-05	0.0015	3.5099
WpXsrFIl8iq_X116Cc	Cldn5	claudin 5	0.8143	10.9865	6.4175	1.30568E-05	0.0015	3.4795
Nsu97vzUWsmOVF9SWo	Mif	macrophage migration inhibitory factor	-0.4932	14.6938	-6.4048	1.33442E-05	0.0015	3.4583
Wr,PEodkUrHxlZld10	Myo1e	myosin IE	-0.9288	10.3292	-6.4008	1.34377E-05	0.0015	3.4515
oFV,4P5HC2Pkev6LVo	H19	H19 imprinted maternally expressed transcript	-0.6372	9.2534	-6.4006	1.34406E-05	0.0015	3.4513
EKK7d1fSCe0P0kkFXs	Foxo1	forkhead box O1	-1.2529	11.4232	-6.4002	1.34516E-05	0.0015	3.4505
6HoQkXmkgkVIjpeJTM	Zfp296	zinc finger protein 296	-0.6388	9.3243	-6.3900	1.36896E-05	0.0015	3.4334
WU90slFSieC,VR59R4	Tmem35	transmembrane protein 35	0.6055	10.1219	6.3836	1.384E-05	0.0015	3.4227

Probe ID	Gene symbol	Gene name	Log_2FC	Average expression	t	P, Value	Adj,P,Val	B
Bu7UzqN7e1NXu_ue7U	Slc30a3	solute carrier family 30 (zinc transporter) member 3	-1.1830	10.4009	-6.3833	1.38481E-05	0.0015	3.4222
Kjn1Io5KCooqBque8E	Ccdc141	coiled-coil domain containing 141	0.4358	8.8629	6.3728	1.41015E-05	0.0016	3.4045
6anecdzCpd5HW,d_0o	Masp1	mannan-binding lectin serine peptidase 1	-1.1643	11.4744	-6.3617	1.43738E-05	0.0016	3.3858
iMhk1lK6P8L9fTS5eQ	Aurkc	aurora kinase C	-0.5817	9.1875	-6.3485	1.47038E-05	0.0016	3.3637
unqdEsfXe4Hv7g,l9U	Prkcd	protein kinase C delta	-0.9811	11.3226	-6.3465	1.47542E-05	0.0016	3.3604
xxBUxcq0oKQlVeIEdI	H1foo	H1 histone family member O oocyte-specific	-1.4687	10.5392	-6.3313	1.51475E-05	0.0016	3.3347
BUSo_7HvchWLHvsV5s	Zfp385b	zinc finger protein 385B	-1.1360	10.8767	-6.3277	1.52415E-05	0.0016	3.3287
WnDX_w1SO_gsIK5T7s	Thsd7b	thrombospondin type I domain containing 7B	0.3000	8.5930	6.3264	1.52767E-05	0.0016	3.3264
3w1mcagUbrnnnADkp0	Amh	anti-Mullerian hormone	-1.1128	9.5852	-6.3186	1.54821E-05	0.0017	3.3134
coF9yKV5MF4BXh27GU	Rimkla	ribosomal modification protein rimK-like family member A	-0.7177	9.6116	-6.3099	1.57175E-05	0.0017	3.2987
rlXuDK9Bp1LgjlJSiE	Mcm6	minichromosome maintenance deficient 6 (MIS5 homolog S, pombe) (S, cerevisiae)	-0.7783	10.5493	-6.3086	1.57528E-05	0.0017	3.2965
c,aX5SJv6DFjGLsREY	Cdk1	cyclin-dependent kinase 1	-0.7366	11.2009	-6.3040	1.58801E-05	0.0017	3.2887
9XSC0oR1XtK6,6IgYo	Wipi1	WD repeat domain phosphoinositide interacting 1	0.4016	10.0630	6.2964	1.60901E-05	0.0017	3.2758
N57ohyoZMiS,rn6y4U	Cdo1	cysteine dioxygenase 1 cytosolic	-0.6552	9.5510	-6.2906	1.62525E-05	0.0017	3.2660
E7Xx7uiT7ufrMHpJbE	Mcm4	minichromosome maintenance deficient 4 homolog (S, cerevisiae)	-0.8757	12.2480	-6.2715	1.6801E-05	0.0017	3.2337
Bljrp5Ijq7uowce7gg	Cct6a	chaperonin containing Tcp1 subunit 6a (zeta)	-0.5255	12.7037	-6.2572	1.72231E-05	0.0018	3.2094
9alNIhed1CAEkKLfMA	Arhgef28	Rho guanine nucleotide exchange factor (GEF) 28	-0.4568	9.0087	-6.2307	1.80355E-05	0.0019	3.1645
uUnuJz,5QTtmsMTtks	Skp2	S-phase kinase-associated protein 2 (p45)	-0.9261	10.5754	-6.2236	1.82597E-05	0.0019	3.1524
WYOminp9NR5XFiBiXg	Birc5	baculoviral IAP repeat-containing 5	-0.7881	10.6081	-6.2191	1.8404E-05	0.0019	3.1447
oxX657tLvuRPochPec	Zfp41	zinc finger protein 41	-1.0558	11.0714	-6.2183	1.843E-05	0.0019	3.1433
x360EClKjYJ642uqSs	Ggt5	gamma-glutamyltransferase 5	0.3873	8.8693	6.2062	1.88244E-05	0.0019	3.1227
le,det23Z2oSIb0Ch4	Cxcl1	chemokine (C-X-C motif) ligand 1	-0.5006	9.2172	-6.2026	1.89437E-05	0.0019	3.1165
Nn1b9VM4iYl_gsXo9I	Mrps18b	mitochondrial ribosomal protein S18B	-0.4459	9.9391	-6.2024	1.89488E-05	0.0019	3.1162
KJ15bcOCh59cE5f51U	Rad54b	RAD54 homolog B (S, cerevisiae)	-0.8433	10.2567	-6.1965	1.9146E-05	0.0019	3.1061
0NR566AXZ5iuWe4ruU	Kif2c	kinesin family member 2C	-0.7666	10.3162	-6.1941	1.92245E-05	0.0019	3.1021
NsXQgcWTZRfQgelfXo	Birc5	baculoviral IAP repeat-containing 5	-0.9109	10.9169	-6.1912	1.93237E-05	0.0019	3.0971
K4rn3946hHq0rtEA9U	Pcgf6	polycomb group ring finger 6	-0.5884	10.3613	-6.1885	1.94151E-05	0.0019	3.0925
iU6_3TnU0sh3ARac4k	Esco2	establishment of cohesion 1 homolog 2 (S, cerevisiae)	-0.8197	9.8203	-6.1883	1.94228E-05	0.0019	3.0921
EulxAFU0OClaxExTVU	Mad2l1	MAD2 mitotic arrest deficient-like 1	-0.6960	11.0215	-6.1556	2.05673E-05	0.0020	3.0362
NEV4BeNoE9N4V5h0FU	Nmral1	NmrA-like family domain containing 1	-0.6801	10.1540	-6.1532	2.06537E-05	0.0020	3.0321

Probe ID	Gene symbol	Gene name	Log_2FC	Average expression	t	P, Value	Adj,P,Val	B
lUknoWD49Hi4krtffo	Egfl7	EGF-like domain 7	0.5927	9.6491	6.1479	2.08437E-05	0.0020	3.0232
Wl9KiX_8eku9,eCUWo	Slco2a1	solute carrier organic anion transporter family member 2a1	0.6974	9.5080	6.1469	2.08814E-05	0.0020	3.0214
3l6Pe37HrxFp0HagkM	Fam3c	family with sequence similarity 3 member C	-0.6851	11.6747	-6.1433	2.10134E-05	0.0020	3.0152
cjp77RXRdc7HUq3OqI	Banf1	barrier to autointegration factor 1	-0.5700	12.1084	-6.1428	2.10334E-05	0.0020	3.0143
EVnu_BDSh5vROIV_yw	Flrt3	fibronectin leucine rich transmembrane protein 3	-0.6191	9.4718	-6.1422	2.10564E-05	0.0020	3.0132
o4Iho95HYfqgTWJll0	Lsm8	LSM8 homolog U6 small nuclear RNA associated (S, cerevisiae)	-0.4782	11.5002	-6.1380	2.12116E-05	0.0020	3.0061
iwtZ1ZVggqdQgpbhQo	Hist1h2bf	histone cluster 1 H2bf	0.8928	10.9720	6.1373	2.12361E-05	0.0020	3.0049
NiHYT12s,Pt7VRcYXU	Dmpk	dystrophia myotonica-protein kinase	0.8276	9.9622	6.1292	2.15411E-05	0.0020	2.9910
BWTiq0SVf5QXwtOe7k	Inhba	inhibin beta-A	-2.4207	12.4678	-6.1285	2.15685E-05	0.0020	2.9898
9WfSAxiSU4RzE9M7JA	Sparcl1	SPARC-like 1	0.4916	9.1269	6.1122	2.21925E-05	0.0021	2.9619
loUvkzIIR1U_d8qF9U	Sphk1	sphingosine kinase 1	1.0294	10.5146	6.1099	2.22852E-05	0.0021	2.9578
ljdd37j_vkfyBP,uWw	Stc1	stanniocalcin 1	-1.7549	11.5652	-6.0978	2.27619E-05	0.0021	2.9372
B5WcShEBdXVG1N8QHI	Crabp2	cellular retinoic acid binding protein II	-0.6954	9.5850	-6.0948	2.28842E-05	0.0021	2.9319
irCOa674pfCPbebrRY	Timm9	translocase of inner mitochondrial membrane 9	-0.5095	12.5558	-6.0862	2.32336E-05	0.0021	2.9171
Hqyj2f9gNdSoRJU_Yg	Nnat	neuronatin	-0.6949	9.3883	-6.0833	2.33532E-05	0.0021	2.9121
KfS3UeesUAIieZQKgU	Top2a	topoisomerase (DNA) II alpha	-0.9856	10.9092	-6.0787	2.35432E-05	0.0021	2.9042
KRqUjeURSA1KI_eMK8	Gm5483	predicted gene 5483	0.5132	8.6475	6.0722	2.38162E-05	0.0021	2.8929
Z4LOQIq47nhVIkpWzU	Mrto4	MRT4 mRNA turnover 4 homolog (S, cerevisiae)	-0.5446	10.4417	-6.0714	2.38499E-05	0.0021	2.8915
0iRHyETSS19HKrR3Sw	Bub1b	budding uninhibited by benzimidazoles 1 homolog beta (S, cerevisiae)	-0.9333	10.8971	-6.0534	2.46182E-05	0.0022	2.8605
Hf6CV7pROztLCr7EAw	Rap1gap	Rap1 GTPase-activating protein	0.6248	9.6796	6.0504	2.47478E-05	0.0022	2.8554
Kfotdz7yc96XNXsp7U	Dhh	desert hedgehog	-0.9812	10.7344	-6.0448	2.49957E-05	0.0022	2.8457
olS5EOpIF3FKd40oq0	Sgol1	shugoshin-like 1 (S, pombe)	-0.4676	9.5451	-6.0432	2.50675E-05	0.0022	2.8428
fSe064T,9,9Pli8TW4	Prkcb	protein kinase C beta	0.2765	8.5915	6.0410	2.51653E-05	0.0022	2.8390
r313nVIhbnSuHj33Qo	H2-DMa	histocompatibility 2 class II locus DMa	0.5644	9.3420	6.0364	2.53712E-05	0.0022	2.8311
KBAdZK7e7e09cC5O0o	Pdlim3	PDZ and LIM domain 3	0.8025	10.1561	6.0301	2.56538E-05	0.0022	2.8202
uWnUB7QnHw37lMIbf8	Gstt3	glutathione S-transferase theta 3	0.4532	9.3380	6.0225	2.60004E-05	0.0022	2.8071
WHit9YpokbqdzuUB7g	Igfbp6	insulin-like growth factor binding protein 6	0.5617	10.8487	6.0194	2.61431E-05	0.0022	2.8018
cgh8lyOXIB5_y9auX4	Sag	S-antigen retina and pineal gland (arrestin)	0.4695	9.0376	6.0146	2.63666E-05	0.0022	2.7934
ZaR7SHUVTs1,_,d_58	Cdca4	cell division cycle associated 4	-0.6207	11.5639	-6.0136	2.64157E-05	0.0022	2.7916
fzjxcReJZeqxEXt5ak	Pafah1b3	platelet-activating factor acetylhydrolase isoform 1b subunit 3	-0.5446	11.3766	-6.0131	2.64378E-05	0.0022	2.7908
Ep6,5a39PunCpL1KMU	B430105G09Rik	RIKEN cDNA B430105G09 gene	-0.4244	9.7359	-6.0122	2.648E-05	0.0022	2.7892
EdOld3lPt,T9Ue5DyE	Efna5	ephrin A5	-0.9110	10.1340	-6.0071	2.67222E-05	0.0022	2.7803
oVlWCCp1CCltFClSCA	Hist1h2bk	histone cluster 1 H2bk	0.7987	9.9171	6.0046	2.68387E-05	0.0022	2.7761
B0RJPO0snSKY7oV71U	Snrpb	small nuclear ribonucleoprotein B	-0.4715	12.0062	-6.0035	2.68931E-05	0.0022	2.7741

Probe ID	Gene symbol	Gene name	Log_2FC	Average expression	t	P, Value	Adj,P,Val	B
EgEZSFdK6g4kKSOCKU	Peo1	progressive external ophthalmoplegia 1 (human)	-0.2724	9.3988	-6.0018	2.69746E-05	0.0022	2.7712
WRvZf4no7oNkgqR6nE	Cpsf4l	cleavage and polyadenylation specific factor 4-like	-0.8965	9.8141	-6.0013	2.69988E-05	0.0022	2.7703
HsBl4hIIouc_9W7oFo	Ralgps2	Ral GEF with PH domain and SH3 binding motif 2	-0.2944	9.0297	-5.9962	2.72435E-05	0.0023	2.7615
c5Evkjfi4QQhIElroQ	Trim61	tripartite motif-containing 61	-0.3992	8.9974	-5.9933	2.73809E-05	0.0023	2.7565
KR7lfBRPuBYiUT30rk	Aqp1	aquaporin 1	0.3780	9.0438	5.9888	2.76028E-05	0.0023	2.7486
xJSeToXndXZ2dafd58	Dhcr24	24-dehydrocholesterol reductase	0.6089	9.6363	5.9714	2.84705E-05	0.0023	2.7184
cVFO998ltF_qdTEOgs	Ank3	ankyrin 3 epithelial	-1.1192	10.0924	-5.9649	2.87996E-05	0.0023	2.7071
fl6WHiui1Z77gNGeS0	Ano4	anoctamin 4	-0.9883	9.9016	-5.9634	2.88782E-05	0.0023	2.7045
0tyLDeStdKre,elenI	Lmnb2	lamin B2	-0.5940	9.8127	-5.9574	2.91874E-05	0.0024	2.6940
QCqT1L51LR1dzJTR7c	Ei24	etoposide induced 2,4 mRNA	0.5154	11.2327	5.9549	2.93184E-05	0.0024	2.6897
ER3rOvlf6kkTr4XnLg	Carhsp1	calcium regulated heat stable protein 1	-0.9142	12.4571	-5.9451	2.98356E-05	0.0024	2.6725
okvheViUu3N7sHo4Mw	Scamp5	secretory carrier membrane protein 5	0.4617	10.0489	5.9406	3.00762E-05	0.0024	2.6647
0etl7fXyiHuBB3EEq0	Lypd3	Ly6/Plaur domain containing 3	-0.7489	9.5093	-5.9391	3.01549E-05	0.0024	2.6621
KofgjVf8Qa6d6Xf7eg	Accsl	1-aminocyclopropane-1-carboxylate synthase (non-functional)-like	-1.1452	9.8818	-5.9367	3.02813E-05	0.0024	2.6580
BRHqNSV1,l0nr_qctw	Gyltl1b	glycosyltransferase-like 1B	-1.0335	10.2520	-5.9315	3.05667E-05	0.0024	2.6489
fw_9ST1DnfuTJKoewU	Sybu	syntabulin (syntaxin-interacting)	0.4249	9.1477	5.9311	3.05876E-05	0.0024	2.6482
xhxGulAiiaEXl4rkKE	Htra3	HtrA serine peptidase 3	0.6557	10.5768	5.9284	3.07359E-05	0.0024	2.6435
iij55C,ClJe3EyorUo	Rragb	Ras-related GTP binding B	-0.4562	9.4610	-5.9231	3.10276E-05	0.0024	2.6342
rojR1X6VVl6AwgJSHc	Wnt6	wingless-type MMTV integration site family member 6	0.7246	10.4939	5.9210	3.11445E-05	0.0024	2.6305
x6Inv83UOnuHS5Cj1E	Araf	v-raf murine sarcoma 3611 viral oncogene homolog	0.3779	11.1184	5.8999	3.23381E-05	0.0025	2.5937
rSVlDj7iHOroVb07TQ	Fbxw24	F-box and WD-40 domain protein 24	-1.1572	10.0820	-5.8940	3.26811E-05	0.0025	2.5834
fejlIV7fsXH3XcQRTo	Loxl1	lysyl oxidase-like 1	0.8128	11.7704	5.8903	3.28992E-05	0.0025	2.5769
EoqegAhGJVfOVERVEM	Gm6484	predicted gene 6484	0.3118	8.6550	5.8774	3.36706E-05	0.0026	2.5542
3SpHbKTnw,ft7Uakac	Dnah11	dynein axonemal heavy chain 11	-0.6551	9.8157	-5.8721	3.3988E-05	0.0026	2.5450
BYlPvQGEmue,dd7pf0	Mapre1	microtubule-associated protein RP/EB family member 1	-0.5272	13.2714	-5.8679	3.42475E-05	0.0026	2.5376
ZpboShWLc8SjNUoseg	Fam151a	family with sequence simliarity 151 member A	-0.5596	9.1262	-5.8674	3.42791E-05	0.0026	2.5367
NW5aKKcq0owI_oW,6E	Tap2	transporter 2 ATP-binding cassette sub-family B (MDR/TAP)	0.8723	9.1625	5.8643	3.44688E-05	0.0026	2.5313
3B4p7KeepHr6d7znm4	Tmem208	transmembrane protein 208	0.3067	12.4615	5.8637	3.45087E-05	0.0026	2.5302
o_0Ln2qJKcoJLVlGLM	Aimp2	aminoacyl tRNA synthetase complex-interacting multifunctional protein 2	-0.4941	10.2703	-5.8563	3.49685E-05	0.0026	2.5172
TWK6F62F04AL_6KMQA	Cbr3	carbonyl reductase 3	0.4713	9.2228	5.8540	3.51107E-05	0.0026	2.5132
uuHe9l1kEl14ieUo94	Bicc1	bicaudal C homolog 1 (Drosophila)	0.5175	10.1291	5.8507	3.5322E-05	0.0026	2.5073
iFIXVgI3CoWjiIgsc	Ano4	anoctamin 4	-0.5081	9.0886	-5.8414	3.59132E-05	0.0027	2.4911

Probe ID	Gene symbol	Gene name	Log_2FC	Average expression	t	P, Value	Adj,P,Val	B
NjUniV4p4QlgbodFn0	Gtse1	G two S phase expressed protein 1	-0.2737	8.8433	-5.8411	3.5932E-05	0.0027	2.4906
9iBHU7nYg3Mdzp08o0	Cox20	COX20 Cox2 chaperone	0.7520	10.3421	5.8408	3.59528E-05	0.0027	2.4900
ZHu5UUinT4RQdAB30s	Hey2	hairy/enhancer-of-split related with YRPW motif 2	-0.6059	9.2105	-5.8305	3.66287E-05	0.0027	2.4718
cSSLj9TdHkpO5Le3qI	Orc6	origin recognition complex subunit 6	-0.4952	11.3226	-5.8281	3.67814E-05	0.0027	2.4677
iFKiuXx1pgXSxuSzks	Mos	Moloney sarcoma oncogene	-0.8641	9.7274	-5.8248	3.69996E-05	0.0027	2.4619
iQKQCHvEcqnUSNQ1RU	Mex3a	mex3 homolog A (C, elegans)	-0.5557	10.1144	-5.8043	3.83928E-05	0.0028	2.4257
KRnnOfl8ue0KoCeQVs	Them6	thioesterase superfamily member 6	1.0277	9.9795	5.7966	3.8928E-05	0.0028	2.4122
KXVeCr3JRRlRKPVPK8	Plvap	plasmalemma vesicle associated protein	0.4106	9.4267	5.7948	3.90534E-05	0.0028	2.4090
0TRyXil,LFGi1DxVKs	Irf5	interferon regulatory factor 5	0.2607	8.8261	5.7807	4.00648E-05	0.0029	2.3840
W4nXq0ntIlycQvyOtE	Cphx1	cytoplasmic polyadenylated homeobox 1	-0.7317	9.3035	-5.7705	4.08063E-05	0.0029	2.3660
3vcp4Ooi11EHV7uXTo	Tns4	tensin 4	-0.3544	8.9840	-5.7674	4.10357E-05	0.0029	2.3605
Qq6QoL5rKodIKWT_jc	Dync1i1	dynein cytoplasmic 1 intermediate chain 1	0.5313	9.4346	5.7614	4.14841E-05	0.0029	2.3499
6nviyqd5Sg_FJ8uKJQ	Cdk16	cyclin-dependent kinase 16	0.8631	10.1518	5.7606	4.1541E-05	0.0029	2.3485
Bj7Wu5Ox,iuL6gLkug	Ppp1r3c	protein phosphatase 1 regulatory (inhibitor) subunit 3C	0.8643	9.9508	5.7570	4.18104E-05	0.0029	2.3422
Nt7wFwUlP3SOaOU3ng	Sulf1	sulfatase 1	0.3011	9.4709	5.7566	4.18464E-05	0.0029	2.3414
6cV0Tr06c6If_e0MDI	Crip2	cysteine rich protein 2	0.7175	11.2966	5.7562	4.18749E-05	0.0029	2.3407
6LkVYRazddQpTqTTgc	Hist1h2bj	histone cluster 1 H2bj	0.9468	10.6874	5.7550	4.1967E-05	0.0029	2.3385
9euOrhPUknvDk9Sgkk	Nasp	nuclear autoantigenic sperm protein (histone-binding)	-0.7357	11.1644	-5.7538	4.20558E-05	0.0029	2.3365
ZiBEDl8KAu5Wc1eqd4	Rhpn2	rhophilin Rho GTPase binding protein 2	-0.7542	9.6251	-5.7515	4.223E-05	0.0029	2.3324
ruOG_shu4I8dQ0fdeo	Ccrn4l	CCR4 carbon catabolite repression 4-like (S, cerevisiae)	-0.5298	9.6582	-5.7448	4.27502E-05	0.0030	2.3204
WuliShDihLhhTnjii4	Kif4	kinesin family member 4	-0.3453	9.0871	-5.7370	4.33573E-05	0.0030	2.3066
BvVHsXu0_fuzh_ggqU	Laptm5	lysosomal-associated protein transmembrane 5	0.8690	11.0822	5.7368	4.33687E-05	0.0030	2.3064
uRT153qfRFIItcpfK0	Smg6	Smg-6 homolog nonsense mediated mRNA decay factor (C, elegans)	0.3426	8.9812	5.7365	4.33933E-05	0.0030	2.3058
T7REK0sH3nOKU43enU	Sla	src-like adaptor	0.3627	9.0369	5.7256	4.42609E-05	0.0030	2.2864
uVzOxQuxcvp5dWUd4c	Mmp14	matrix metallopeptidase 14 (membrane-inserted)	0.6569	12.1923	5.7234	4.44329E-05	0.0030	2.2826
o2lhTleeLGfQfIqcAU	Rnps1	ribonucleic acid binding protein S1	-0.4931	11.0811	-5.7230	4.44672E-05	0.0030	2.2818
W_frzSSd5_huXlKEqI	Rrm1	ribonucleotide reductase M1	-0.4680	10.6076	-5.7060	4.58641E-05	0.0031	2.2515
lX,VMte,SrRH_MRbA4	Gas2l3	growth arrest-specific 2 like 3	-0.6919	10.0490	-5.7027	4.61398E-05	0.0031	2.2457
c1wuo9cje7k7Sl5wgk	Lipt2	lipoyl(octanoyl) transferase 2 (putative)	-0.2907	8.9608	-5.6995	4.64023E-05	0.0031	2.2401
W0J2pTdd3RXN,iOaNU	Lgi3	leucine-rich repeat LGI family member 3	0.5593	8.9247	5.6974	4.65852E-05	0.0031	2.2363
6pfudyDrFDUs0OzhC4	Oasl2	2'-5' oligoadenylate synthetase-like 2	0.6517	9.7697	5.6886	4.73286E-05	0.0032	2.2207
9_H2wkKl725HeYIl5I	Serhl	serine hydrolase-like	0.3338	9.3479	5.6865	4.75123E-05	0.0032	2.2169

Probe ID	Gene symbol	Gene name	Log_2FC	Average expression	t	P, Value	Adj,P,Val	B
3t1UcwonjdK0af5UgU	Cdc20	cell division cycle 20	-0.8359	10.0223	-5.6863	4.75278E-05	0.0032	2.2166
TCOlxRnpeTlDvlulBM	Aifm2	apoptosis-inducing factor mitochondrion-associated 2	0.3904	9.2239	5.6784	4.82213E-05	0.0032	2.2024
cdSVG6vre1tzNMSfks	Evc2	Ellis van Creveld syndrome 2	-0.8837	11.1054	-5.6761	4.84242E-05	0.0032	2.1983
Hq,eyAtfKi727eHSmU	Edn1	endothelin 1	-0.3294	9.1723	-5.6742	4.85893E-05	0.0032	2.1950
HgT5,Qc4TlIodoRcXk	Ddx39b	DEAD (Asp-Glu-Ala-Asp) box polypeptide 39B	-0.6271	11.4682	-5.6728	4.87139E-05	0.0032	2.1925
cqexKAKVJQewouz5ac	Creld2	cysteine-rich with EGF-like domains 2	-0.8364	11.0276	-5.6693	4.90269E-05	0.0032	2.1862
6fRFMeRJFoSxSi5eSc	Nup107	nucleoporin 107	-0.4116	9.5059	-5.6659	4.93263E-05	0.0032	2.1802
T3oGKAkpJC1k56IX68	Skp2	S-phase kinase-associated protein 2 (p45)	-0.4327	9.3018	-5.6651	4.93972E-05	0.0032	2.1788
Bp5e4GiPe018Rk3,L4	Adam23	a disintegrin and metallopeptidase domain 23	0.5872	9.6474	5.6633	4.95589E-05	0.0032	2.1756
B1j7pXl,YJ6IccblyI	Bex2	brain expressed X-linked 2	-0.4459	9.6743	-5.6625	4.96346E-05	0.0032	2.1741
9S7YCeJuIL6OK_7W18	Clspn	claspin	-0.6730	9.7674	-5.6600	4.98642E-05	0.0032	2.1696
3IMK_OiO2Ch1fcrgCo	Mcm7	minichromosome maintenance deficient 7 (S, cerevisiae)	-0.6753	9.8598	-5.6442	5.13174E-05	0.0033	2.1414
HgJH1H4nXzouJ9XuVE	Erlin1	ER lipid raft associated 1	-0.3948	10.0391	-5.6369	5.1999E-05	0.0033	2.1285
fC1nXlWCCp1CCleFCk	Hist1h2bh	histone cluster 1 H2bh	0.8127	10.4334	5.6351	5.21702E-05	0.0033	2.1253
37v1fjd7T78TJLnhEo	Ppid	peptidylprolyl isomerase D (cyclophilin D)	-0.6302	12.5344	-5.6340	5.22778E-05	0.0033	2.1233
HURQnSU0nBNROeLkSo	Fam216a	family with sequence similarity 216 member A	-0.4220	11.0805	-5.6312	5.25455E-05	0.0033	2.1183
Ql07p_hIt_KMRKNZDU	Wdr74	WD repeat domain 74	-0.4882	10.5559	-5.6312	5.25507E-05	0.0033	2.1182
oeRD35SBA5TQeXSpHU	Ak4	adenylate kinase 4	-0.4717	9.2274	-5.6287	5.27854E-05	0.0033	2.1138
6HPxcHk658KVZhFQiU	Nfic	nuclear factor I/C	0.4420	9.7440	5.6262	5.30263E-05	0.0033	2.1093
EXkJIh_heI1USjuksg	Tmc6	transmembrane channel-like gene family 6	0.4600	9.4952	5.6239	5.32491E-05	0.0033	2.1052
xQkZrtoqRQp7RQsRSc	Hist1h2be	histone cluster 1 H2be	1.0263	10.5157	5.6226	5.3383E-05	0.0033	2.1028
ThLV65BEoDnoOX,mz4	Ccno	cyclin O	-1.2252	11.2222	-5.6205	5.35803E-05	0.0033	2.0991
fDskPewJO7NS75cv4U	Nap1l5	nucleosome assembly protein 1-like 5	-1.2334	10.2611	-5.6186	5.3771E-05	0.0033	2.0957
9ILpd0dA9e,k3UYlMQ	Gulo	gulonolactone (L-) oxidase	-0.6570	9.1915	-5.6168	5.39469E-05	0.0033	2.0925
HdS1,lBGRZBfn,5fq4	Tnfsf13b	tumor necrosis factor (ligand) superfamily member 13b	0.3843	9.0357	5.6117	5.44484E-05	0.0034	2.0834
9dIpV917QZDgdf78Lc	Nrcam	neuronal cell adhesion molecule	1.6310	9.5569	5.6081	5.48141E-05	0.0034	2.0768
oLlJN9OrQjCKnjNQrk	Hsd17b1	hydroxysteroid (17-beta) dehydrogenase 1	-1.0349	13.2850	-5.6065	5.49735E-05	0.0034	2.0740
Be0x6QPOJZqiXXggdA	Wdr86	WD repeat domain 86	0.4981	9.5861	5.6063	5.49947E-05	0.0034	2.0736
iuEVPSrfv1LbeCVuag	Aurka	aurora kinase A	-0.9174	10.3390	-5.5967	5.59664E-05	0.0034	2.0564
Ha4JzUynnpfjwaPshw	Msh6	mutS homolog 6 (E, coli)	-0.6035	11.7064	-5.5963	5.60024E-05	0.0034	2.0558
6lnjU90jinoVrXfwIU	Ext1	exostoses (multiple) 1	-0.8300	11.8878	-5.5904	5.66163E-05	0.0034	2.0451
xuhfFe8xCJetLoJB9Q	Hirip3	HIRA interacting protein 3	-0.8111	10.7194	-5.5788	5.78355E-05	0.0035	2.0242
KeTYvrqDkhflffv_8k	Rsc1a1	regulatory solute carrier protein family 1 member 1	-0.3185	9.2674	-5.5631	5.95213E-05	0.0036	1.9960
Kh0eXVLR0kUZ,N,Ksk	Lekr1	leucine glutamate and lysine rich 1	-0.3684	9.2122	-5.5619	5.96453E-05	0.0036	1.9940
lTs396eV3rpb3jHhJc	Gpr1	G protein-coupled receptor 1	-0.6570	9.4353	-5.5613	5.97166E-05	0.0036	1.9928
oU_BfVLnpcL3Sid3pU	Trim28	tripartite motif-containing 28	-0.6054	11.7385	-5.5447	6.1559E-05	0.0037	1.9630
0xEh8lxJE0pWolK3pU	Leprel2	leprecan-like 2	0.4509	9.6960	5.5407	6.20207E-05	0.0037	1.9557

Probe ID	Gene symbol	Gene name	Log_2FC	Average expression	t	P, Value	Adj,P,Val	B
ZXvxHuC6s3xogRFJfo	Sall4	sal-like 4 (Drosophila)	-1.0980	9.6734	-5.5395	6.2153E-05	0.0037	1.9536
uru7rnqjcHUK5798qk	Ung	uracil DNA glycosylase	-0.9302	10.4124	-5.5337	6.28209E-05	0.0037	1.9431
lnhXsHQKEByenAdPfo	Raly	hnRNP-associated with lethal yellow	0.3797	9.4958	5.5330	6.29014E-05	0.0037	1.9419
NVt4_n,itd94n_,Snc	Slamf9	SLAM family member 9	0.5858	9.1038	5.5306	6.31791E-05	0.0037	1.9375
ujhIXSkjbRIkbknHk4	Pparg	peroxisome proliferator activated receptor gamma	-0.6507	10.8348	-5.5202	6.4403E-05	0.0038	1.9187
iVR64Ld3mUJOk_DFKl	Fads2	fatty acid desaturase 2	0.4845	9.2251	5.5125	6.53204E-05	0.0038	1.9049
ZajXR4gkDj,b1i9TJE	Hsd17b11	hydroxysteroid (17-beta) dehydrogenase 11	0.2678	9.0031	5.5090	6.57392E-05	0.0038	1.8986
utxMVLnTIovniGKeg4	Dpep2	dipeptidase 2	0.7329	8.9852	5.5072	6.59519E-05	0.0038	1.8954
WKBuCiOVAF6VeOHfUI	Chaf1b	chromatin assembly factor 1 subunit B (p60)	-0.7052	10.1065	-5.5055	6.61698E-05	0.0039	1.8922
Ko7ghRKLGj7j1JE0ho	Pex7	peroxisomal biogenesis factor 7	0.2618	9.0049	5.5025	6.6532E-05	0.0039	1.8868
l389Hh3iLRH925E1lk	Srpk1	serine/arginine-rich protein specific kinase 1	-0.5060	10.9194	-5.4881	6.83225E-05	0.0040	1.8608
r4uzXulxO7fTX1cOW0	Ddrgk1	DDRGK domain containing 1	0.3817	12.5686	5.4842	6.88106E-05	0.0040	1.8538
3dVuTz6U7d3r1Elxb4	Igf1r	insulin-like growth factor I receptor	-0.4347	10.8008	-5.4829	6.89786E-05	0.0040	1.8514
ir6NpaJX9dS2lf8Few	Dab2ip	disabled 2 interacting protein	0.4747	10.4611	5.4810	6.92188E-05	0.0040	1.8480
cie0kVSRULh9dHewO0	Dpysl5	dihydropyrimidinase-like 5	-0.4696	9.1939	-5.4661	7.11519E-05	0.0041	1.8210
ES,PAOXhB5H1LRWpfk	Srsf2	serine/arginine-rich splicing factor 2	-0.5803	13.0009	-5.4624	7.16439E-05	0.0041	1.8142
TpX7u2_NV_T2DArbvU	Spon2	spondin 2 extracellular matrix protein	1.5061	11.1932	5.4603	7.19215E-05	0.0041	1.8104
67St3yXmHSritT1i6I	Entpd2	ectonucleoside triphosphate diphosphohydrolase 2	0.3518	8.9836	5.4522	7.30087E-05	0.0041	1.7957
rmU764Oalexz,v99ek	Angpt2	angiopoietin 2	-0.7555	11.1247	-5.4463	7.38021E-05	0.0042	1.7851
6IkK4KkEaCp5IKd6CE	Apoa4	apolipoprotein A-IV	-1.0364	9.5130	-5.4409	7.45406E-05	0.0042	1.7753
TXpfszXN4lO2gkbdb4	Gbx2	gastrulation brain homeobox 2	-1.2201	10.1207	-5.4373	7.50432E-05	0.0042	1.7687
6eLeXokA74mk2qnm58	H2-Ab1	histocompatibility 2 class II antigen A beta 1	0.8317	9.9560	5.4319	7.57996E-05	0.0042	1.7589
TUW6pZ623H6S5Ep400	Dnajc11	DnaJ (Hsp40) homolog subfamily C member 11	-0.4042	9.5167	-5.4311	7.59031E-05	0.0042	1.7576
Z,koCAG3QFdhFZRV3U	Grin2b	glutamate receptor ionotropic NMDA2B (epsilon 2)	0.4150	8.8795	5.4307	7.59722E-05	0.0042	1.7567
luRIL7le977iRTsxAI	Pcdhb3	protocadherin beta 3	0.3911	8.9945	5.4216	7.72627E-05	0.0043	1.7401
BwVS1ujd6JeD3uBLak	Snrpd1	small nuclear ribonucleoprotein D1	-0.5901	12.4859	-5.4211	7.7326E-05	0.0043	1.7393
QHuJpl3H23mL1X3lgU	Clec11a	C-type lectin domain family 11 member a	0.2913	8.7508	5.4175	7.78525E-05	0.0043	1.7327
Npe1zmhFAn,J9d6g0o	Sgpp2	sphingosine-1-phosphate phosphotase 2	-0.6080	9.1387	-5.4146	7.82672E-05	0.0043	1.7275
oUtAuQhxcVHlOAFPko	Scd1	stearoyl-Coenzyme A desaturase 1	1.5920	10.2355	5.4143	7.83086E-05	0.0043	1.7269
lt7gSQ7d5333e6Lh0U	Rasgrp1	RAS guanyl releasing protein 1	0.5541	9.1699	5.4115	7.8719E-05	0.0043	1.7218
6SgbtT20kRcF4TK3Bc	Cep78	centrosomal protein 78	-0.4981	10.3345	-5.4073	7.93397E-05	0.0044	1.7141
KnR19lvuWJWSKLZTiQ	Snrpg	small nuclear ribonucleoprotein polypeptide G	-0.4231	12.7096	-5.4021	8.00959E-05	0.0044	1.7048
NgiLeUhHN0rl8wLHUl	Snai2	snail family zinc finger 2	0.4628	10.3331	5.4010	8.0266E-05	0.0044	1.7027
0UJLbUES7l8cBIlU3s	Pqlc3	PQ loop repeat containing	0.7113	9.9565	5.4005	8.03412E-05	0.0044	1.7018
3gP4H55eeLUsvuSoul	Fen1	flap structure specific endonuclease 1	-0.7540	11.1567	-5.3967	8.09121E-05	0.0044	1.6948

Probe ID	Gene symbol	Gene name	Log_2FC	Average expression	t	P, Value	Adj,P,Val	B
rs9c0k9f0OXM_T9cu4	Ccnb1	cyclin B1	-0.6446	9.9688	-5.3964	8.09459E-05	0.0044	1.6944
ltV1316rVaFMz8_TmU	Hic1	hypermethylated in cancer 1	0.5083	9.5121	5.3885	8.21451E-05	0.0044	1.6800
xjl49EiYS4U0rue5LU	Sik3	SIK family kinase 3	-0.4650	9.7157	-5.3879	8.22409E-05	0.0044	1.6789
upa70Ut3LC9enSRIV4	Nup43	nucleoporin 43	-0.5250	10.7992	-5.3870	8.23843E-05	0.0044	1.6772
NUBf_7vh4lS9Ut366k	Mras	muscle and microspikes RAS	-0.8454	10.8894	-5.3863	8.24782E-05	0.0044	1.6760
irXFVDn0qE,DStA_o0	H2-T10	histocompatibility 2 T region locus 10	0.5097	9.1520	5.3798	8.34837E-05	0.0044	1.6641
93ScW6OSVEGXs10U0k	Vpreb3	pre-B lymphocyte gene 3	-0.5178	8.8713	-5.3792	8.35818E-05	0.0044	1.6630
KIQuGSXnWvV4CWPh6M	Hsd17b11	hydroxysteroid (17-beta) dehydrogenase 11	0.7997	9.7896	5.3785	8.36892E-05	0.0044	1.6617
3Xq797cPkX7e_e8qAo	Cdk20	cyclin-dependent kinase 20	-0.6905	9.9288	-5.3784	8.36983E-05	0.0044	1.6616
Ez_glhQR4nSCVV3hVU	Igfbp2	insulin-like growth factor binding protein 2	0.9263	9.8782	5.3721	8.46971E-05	0.0045	1.6500
ZeUiYr6fdUXa5QwIAY	Cd160	CD160 antigen	-0.4469	9.0668	-5.3685	8.52639E-05	0.0045	1.6434
6vU1pHvqWnf60biVb8	Ldhd	lactate dehydrogenase D	0.7478	9.1588	5.3629	8.61476E-05	0.0045	1.6333
3olIF10FxQoI14gFbk	Prkcdbp	protein kinase C delta binding protein	0.5978	11.9201	5.3553	8.73752E-05	0.0046	1.6194
KSUHokI4O6BDFe1d6l	LOC665290	PRAME family member 12-like	-0.5011	9.1960	-5.3511	8.80633E-05	0.0046	1.6117
cUiq_NCdVQBSUqE,Pw	Tmem169	transmembrane protein 169	-0.2618	8.8681	-5.3465	8.88216E-05	0.0046	1.6033
xEotJJcT5IIMdGXmSU	Mcm3	minichromosome maintenance deficient 3 (S, cerevisiae)	-0.5102	9.5033	-5.3396	8.99686E-05	0.0047	1.5907
0l37nO6o3Q7p04ID4U	Tmem55b	transmembrane protein 55b	-0.5225	11.7434	-5.3372	9.03729E-05	0.0047	1.5863
ceW5JX9_n3UZ5bROec	Txnl4a	thioredoxin-like 4A	-0.4067	11.6847	-5.3356	9.06396E-05	0.0047	1.5834
rIBFIifdV0QtKIlpRl	Efs	embryonal Fyn-associated substrate	0.5234	9.7541	5.3303	9.1554E-05	0.0047	1.5736
0p6SJcfXttdn1O5N8A	Lig3	ligase III DNA ATP-dependent	-0.4707	10.1166	-5.3274	9.20512E-05	0.0047	1.5683
WbnnlQghYiUUQpQqAM	Hist1h2ap	histone cluster 1 H2ap	-0.5805	14.9329	-5.3264	9.22244E-05	0.0047	1.5664
EXVcHkS66OkOruOreQ	Tle6	transducin-like enhancer of split 6 homolog of Drosophila E(spl)	-0.9197	12.3054	-5.3250	9.24649E-05	0.0047	1.5639
TnlLed6n7ksrdxOpS8	Tmem160	transmembrane protein 160	0.5483	11.3834	5.3223	9.29252E-05	0.0048	1.5590
uioaVJewjHsTkeeyMw	Bbc3	BCL2 binding component 3	0.3542	9.0205	5.3154	9.41287E-05	0.0048	1.5464
rllpS9fdx1SgN6Agp8	Rsl1d1	ribosomal L1 domain containing 1	-0.5322	11.5507	-5.3149	9.42217E-05	0.0048	1.5454
roEHsT_UOr,VRCHGv8	Vav2	vav 2 oncogene	0.4068	10.1654	5.3145	9.42913E-05	0.0048	1.5447
cSScjt6EqBO_v1y78Y	Nt5e	5' nucleotidase ecto	0.4796	9.3880	5.3031	9.63205E-05	0.0049	1.5238
Th0mufD54W1PX,XT0l	Serpinb6e	serine (or cysteine) peptidase inhibitor clade B member 6e	0.2344	8.5072	5.2927	9.8208E-05	0.0050	1.5047
Wno57BdCEuQOrjHJI8	Hist1h2bc	histone cluster 1 H2bc	1.2525	10.8896	5.2877	9.91337E-05	0.0050	1.4955
cpYS670coiOe9EclTl	Sap30	sin3 associated polypeptide	-0.8408	11.7790	-5.2842	9.97864E-05	0.0050	1.4891
W10ghXR6RvmSGCLntU	Esr2	estrogen receptor 2 (beta)	-0.5060	9.0782	-5.2837	9.9875E-05	0.0050	1.4882
9BwJcHUnUqjWkV33tU	Slc16a9	solute carrier family 16 (monocarboxylic acid transporters) member 9	0.7937	9.8405	5.2783	0.0001	0.0051	1.4782
KuRF,HXpH6ikikoo3c	Ifngr2	interferon gamma receptor 2	0.4970	10.0369	5.2749	0.0001	0.0051	1.4720
r3qwXZIIWKfeBnmn5A	Dok1	docking protein 1	0.3823	8.7563	5.2742	0.0001	0.0051	1.4708
Zq,Jz58Xn7D9StVd2E	Cdca3	cell division cycle associated 3	-0.5578	9.5550	-5.2638	0.0001	0.0052	1.4517
r6V9f4IigEtK3lWUig	Ddx27	DEAD (Asp-Glu-Ala-Asp) box polypeptide 27	-0.5013	10.4672	-5.2611	0.0001	0.0052	1.4467

Probe ID	Gene symbol	Gene name	Log_2FC	Average expression	t	P, Value	Adj,P,Val	B
fS78CzoJEFuxZ3sW14	Stxbp1	syntaxin binding protein 1	0.4547	10.0569	5.2561	0.0001	0.0052	1.4375
QgxD,_e,QUVDErQOf8	Col3a1	collagen type III alpha 1	0.7370	10.2364	5.2457	0.0001	0.0053	1.4183
WmGse2e8G4Ozd0fVV0	Me2	malic enzyme 2 NAD(+)-dependent mitochondrial	-0.5019	10.4888	-5.2451	0.0001	0.0053	1.4172
QrYinetF7Exl10gDx4	Uck2	uridine-cytidine kinase 2	-0.3925	10.6486	-5.2365	0.0001	0.0054	1.4014
QefWM5R_ay6Nu6LgKQ	Sh3gl2	SH3-domain GRB2-like 2	0.5159	9.7358	5.2253	0.0001	0.0055	1.3807
fXK4Sosui7KReC5Cvo	Chaf1a	chromatin assembly factor 1 subunit A (p150)	-0.6468	9.8489	-5.2211	0.0001	0.0055	1.3730
NroX_noASFBEKnluY4	Mak16	MAK16 homolog (S, cerevisiae)	-0.4196	11.8609	-5.2175	0.0001	0.0055	1.3663
QKBEi8HyKHlp5q5K1I	Ifi35	interferon-induced protein 35	0.3476	9.3637	5.2142	0.0001	0.0055	1.3602
lSoSPldeuCrmJUQy4c	Cdc25c	cell division cycle 25C	-0.3023	9.0128	-5.2131	0.0001	0.0055	1.3583
uqWi6_T,kJ7pihTFuA	Elp2	elongator acetyltransferase complex subunit 2	-0.4110	11.6455	-5.2120	0.0001	0.0055	1.3563
fnSKCHhJYhiceLO9E0	Arhgap15	Rho GTPase activating protein 15	0.3819	8.8203	5.2087	0.0001	0.0056	1.3500
3cYkjjomnnojkoaZcU	Spc24	SPC24 NDC80 kinetochore complex component homolog (S, cerevisiae)	-0.3980	9.1316	-5.2069	0.0001	0.0056	1.3468
T3U6U14KF,5JESUHok	Gm16367	predicted gene 16367	-0.5849	9.4055	-5.2047	0.0001	0.0056	1.3427
QVxXzF1zVlN3FVepP8	Igfbp4	insulin-like growth factor binding protein 4	0.7236	12.6288	5.1983	0.0001	0.0056	1.3309
0qV_XpP6oe756Bw_Cc	Fpgs	folylpolyglutamyl synthetase	-0.4691	10.9206	-5.1946	0.0001	0.0056	1.3239
okjooosTU0nu4oTTUk	Cct3	chaperonin containing Tcp1 subunit 3 (gamma)	-0.5769	11.9173	-5.1938	0.0001	0.0056	1.3225
oVJv3F,u1W3QAQOqio	Dync1i1	dynein cytoplasmic 1 intermediate chain 1	0.5256	9.3721	5.1937	0.0001	0.0056	1.3223
lgKEMKiWrAtfaIQj2I	Hoxb4	homeobox B4	0.3354	8.8817	5.1877	0.0001	0.0057	1.3112
cfShFUf37tMeXc9K1U	H2-DMb1	histocompatibility 2 class II locus Mb1	0.4718	9.0117	5.1860	0.0001	0.0057	1.3082
QGuOq3al1G8_ahgidg	Chp1	calcineurin-like EF hand protein 1	0.3473	9.0379	5.1828	0.0001	0.0057	1.3022
BX2M091_uQpROoRA1w	Rrbp1	ribosome binding protein 1	0.4590	9.3668	5.1816	0.0001	0.0057	1.3000
0vrhLKV63N5O9wBNdc	Mns1	meiosis-specific nuclear structural protein 1	-0.7213	10.7595	-5.1796	0.0001	0.0057	1.2964
6U4qElXbT6DelKVSNI	Tcl1	T cell lymphoma breakpoint 1	-0.7723	9.5613	-5.1793	0.0001	0.0057	1.2956
xiKElSfVA4dRN6a3oI	Mmp15	matrix metallopeptidase 15	0.3366	8.8773	5.1784	0.0001	0.0057	1.2941
fv3apeo_4fx76QeNEs	Ihh	Indian hedgehog	-0.7687	9.2579	-5.1776	0.0001	0.0057	1.2925
0KpCeVLB9TCll4H4vc	Oosp3	oocyte secreted protein 3	-0.6229	9.3446	-5.1705	0.0001	0.0058	1.2794
354HWfkxGOwUnuX1,k	Elk3	ELK3 member of ETS oncogene family	0.5618	11.2080	5.1695	0.0001	0.0058	1.2776
QhI5Je4EYiy5JADj,Q	Tor1aip2	torsin A interacting protein 2	0.4082	9.0144	5.1671	0.0001	0.0058	1.2731
fmTSbcfcLhEAu1X9Qk	Edrf1	erythroid differentiation regulatory factor 1	-0.3621	10.0479	-5.1556	0.0001	0.0059	1.2517
lJyLgJBKiwHFsFbnp8	Fignl1	fidgetin-like 1	-0.6020	10.0064	-5.1493	0.0001	0.0059	1.2402
Nhe_KkgQBzl1tRbrv0	Gemin4	gem (nuclear organelle) associated protein 4	-0.5526	10.5502	-5.1487	0.0001	0.0059	1.2390
34hI4Lp854MSS1eSdI	Mug2	murinoglobulin 2	-0.8077	9.2124	-5.1456	0.0001	0.0059	1.2333
un_E1Ced7h173eEOE0	Umodl1	uromodulin-like 1	-0.7625	9.5343	-5.1455	0.0001	0.0059	1.2330
HAIaFKRUo7xU4r55Yk	Gm9983	predicted gene 9983	0.5779	10.5930	5.1453	0.0001	0.0059	1.2327
u7ZSXeV_g02UGToIiQ	Lama1	laminin alpha 1	-0.7698	11.7443	-5.1449	0.0001	0.0059	1.2321
0RaduofhuD3urw5FKc	Snx18	sorting nexin 18	-0.6354	12.1774	-5.1432	0.0001	0.0060	1.2288

Probe ID	Gene symbol	Gene name	Log_2FC	Average expression	t	P, Value	Adj,P,Val	B
rqdOnmFdqkjvMtHjfg	Vcpkmt	valosin containing protein lysine (K) methyltransferase	0.4297	9.0881	5.1363	0.0001	0.0060	1.2160
BVSQE20yHfeTchESlo	Qsox1	quiescin Q6 sulfhydryl oxidase 1	0.4215	8.8248	5.1313	0.0001	0.0061	1.2068
Wslzu4SHndSjqsjvl0	Prmt3	protein arginine N-methyltransferase 3	-0.2995	11.9391	-5.1298	0.0001	0.0061	1.2040
rVV6F3htfq_vfLnH38	Pitpna	phosphatidylinositol transfer protein alpha	0.5397	10.6292	5.1285	0.0001	0.0061	1.2016
00e5PHiFe0Ql97VURI	Ube2e2	ubiquitin-conjugating enzyme E2E 2	0.5590	11.0130	5.1282	0.0001	0.0061	1.2009
rojiekh3lfgN9ASm0k	Tgfbi	transforming growth factor beta induced	0.4195	9.3651	5.1276	0.0001	0.0061	1.1998
KV6oUCBDdv0Ffo5dPk	Entpd5	ectonucleoside triphosphate diphosphohydrolase 5	0.4663	9.5304	5.1249	0.0001	0.0061	1.1949
lOWEG0KkrRV6f89X3Y	Cyp4f18	cytochrome P450 family 4 subfamily f polypeptide 18	0.6492	8.7123	5.1196	0.0001	0.0061	1.1851
Ql6ngHTonVyEotCl4E	B3galnt1	UDP-GalNAc:betaGlcNAc beta 13-galactosaminyltransferase polypeptide 1	-0.5823	10.7543	-5.1166	0.0001	0.0061	1.1794
QKYp9WXpk8QQmdhTRs	Hist1h2bm	histone cluster 1 H2bm	0.7316	9.6782	5.1161	0.0001	0.0061	1.1784
TIR7kUnuc7_CXiulEg	Siva1	SIVA1 apoptosis-inducing factor	-0.5898	12.8519	-5.1147	0.0001	0.0061	1.1760
xS4Y5_rCQ6hcXoHigl	Osbpl3	oxysterol binding protein-like 3	0.4622	9.3660	5.1133	0.0001	0.0061	1.1733
oid6dTSh5I833iRHuA	Fam20a	family with sequence similarity 20 member A	0.5261	9.2610	5.1127	0.0001	0.0061	1.1723
Tqencde,zxTF5QIfU4	Aoc1	amine oxidase copper-containing 1	0.5725	8.7061	5.1100	0.0001	0.0061	1.1671
QiI,_JX0LXlEW1WkmM	Mcm7	minichromosome maintenance deficient 7 (S, cerevisiae)	-0.7884	9.9177	-5.1092	0.0001	0.0061	1.1658
cnk9LgjfcJChUKm6as	Lgals7	lectin galactose binding soluble 7	0.5635	10.3115	5.1092	0.0001	0.0061	1.1656
uVdN7JS7RKEpw6v7Es	Ppp1r8	protein phosphatase 1 regulatory (inhibitor) subunit 8	-0.3688	10.3160	-5.1063	0.0001	0.0062	1.1603
9XSfVgmfn8xu7ttHgg	Hist1h1c	histone cluster 1 H1c	1.0037	11.5198	5.1033	0.0001	0.0062	1.1548
cH9aSteiZuG_BZL1L0	Gnl3	guanine nucleotide binding protein-like 3 (nucleolar)	-0.4799	9.6367	-5.1018	0.0001	0.0062	1.1520
on9ez_XoC96LwFFSek	Klf17	Kruppel-like factor 17	-0.7075	9.2918	-5.0986	0.0001	0.0062	1.1459
fSSKUCn8z1F5eIwknU	Shmt1	serine hydroxymethyltransferase 1 (soluble)	-0.6422	9.9650	-5.0982	0.0001	0.0062	1.1452
um3u0PSshOHhigaWjk	Gsta3	glutathione S-transferase alpha 3	0.6230	10.3396	5.0969	0.0001	0.0062	1.1428
3kodngov7kv7ud4ado	Nfix	nuclear factor I/X	0.6650	11.1116	5.0937	0.0001	0.0062	1.1369
E5UV,6uaKQN4EE_uEU	Agt	angiotensinogen (serpin peptidase inhibitor clade A member 8)	-0.4550	9.7718	-5.0935	0.0001	0.0062	1.1365
fOCOsll7ShbigTqvfY	Xrcc6bp1	XRCC6 binding protein 1	-0.5148	10.4534	-5.0915	0.0001	0.0062	1.1329
9SXtTjhnEUJSFFufus	Nxt1	NTF2-related export protein 1	-0.4836	10.7453	-5.0908	0.0001	0.0062	1.1314
QVdUWSqXoSAQwwlhCQ	Des	desmin	1.1254	10.0267	5.0888	0.0001	0.0062	1.1278
TNiNWdCtiNCNStz9GE	Srsf7	serine/arginine-rich splicing factor 7	-0.5076	11.4882	-5.0850	0.0001	0.0063	1.1206
BYoDdB7d3PwkQ1RT,8	Pqlc3	PQ loop repeat containing	0.3673	8.6932	5.0827	0.0001	0.0063	1.1165
KfpKJIme5Ufnj7946I	Atp2a3	ATPase Ca++ transporting ubiquitous	0.5120	9.7144	5.0787	0.0001	0.0063	1.1090

Probe ID	Gene symbol	Gene name	Log_2FC	Average expression	t	P, Value	Adj,P,Val	B
WrX_eUHnT34fJ3JT_4	Pik3r3	phosphatidylinositol 3 kinase regulatory subunit polypeptide 3 (p55)	0.6381	9.4860	5.0745	0.0001	0.0063	1.1011
Z9bVC5hiBrBz_UdS5Q	Cd74	CD74 antigen (invariant polypeptide of major histocompatibility complex class II antigen-associated)	0.3834	8.9921	5.0735	0.0001	0.0063	1.0993
6UvTqYucfRQahkmTGM	H2-Ab1	histocompatibility 2 class II antigen A beta 1	1.1081	10.2780	5.0718	0.0001	0.0064	1.0961
clglAlujvcHlSCXglQ	Defb36	defensin beta 36	0.2441	8.6395	5.0569	0.0002	0.0065	1.0682
HTt,iCJJHqNhRkiiOg	Mrs2	MRS2 magnesium homeostasis factor homolog (S, cerevisiae)	0.2929	8.8814	5.0505	0.0002	0.0066	1.0563
iFLL3QXurVB1firRNI	Dtl	denticleless homolog (Drosophila)	-0.2761	8.8631	-5.0501	0.0002	0.0066	1.0556
oiq0tCCOJ4ruFOdcFc	Rogdi	rogdi homolog (Drosophila)	0.3118	9.4255	5.0458	0.0002	0.0066	1.0476
xHGofx5h6PvVKnEeCI	Pbdc1	polysaccharide biosynthesis domain containing 1	-0.3693	11.6244	-5.0403	0.0002	0.0067	1.0373
9UqhWmROSkAZQZzIMA	Commd6	COMM domain containing 6	0.4841	11.1774	5.0400	0.0002	0.0067	1.0367
oXJFcncne0jG8OTE10	Nap1l1	nucleosome assembly protein 1-like 1	-0.3192	11.9347	-5.0386	0.0002	0.0067	1.0340
NrRJV,MuizeId2ORMo	Olfml1	olfactomedin-like 1	0.5841	10.9854	5.0346	0.0002	0.0067	1.0267
udUXsTE_zKUXsTNUiA	Vldlr	very low density lipoprotein receptor	0.4735	11.3174	5.0343	0.0002	0.0067	1.0260
KHnnjjYFuIN6ClRB_Q	Kif21a	kinesin family member 21A	-0.4191	9.4354	-5.0325	0.0002	0.0067	1.0227
Tp3n9dOKF5yKugdC0U	Sgol2	shugoshin-like 2 (S, pombe)	-0.6252	9.8431	-5.0296	0.0002	0.0067	1.0173
BRu,WWpGTEZG1eFNe8	Prrg2	proline-rich Gla (G-carboxyglutamic acid) polypeptide 2	0.6396	10.1484	5.0229	0.0002	0.0068	1.0048
Np07eoFBPw3dHfRcJU	Pigh	phosphatidylinositol glycan anchor biosynthesis class H	-0.9356	10.0813	-5.0047	0.0002	0.0070	0.9707
KgnpfeB9uoBSH558tE	Polr2h	polymerase (RNA) II (DNA directed) polypeptide H	-0.3980	11.7748	-5.0027	0.0002	0.0071	0.9669
HiCeeSkS7Rev917iEQ	Zfp277	zinc finger protein 277	-0.7647	12.6568	-4.9950	0.0002	0.0071	0.9525
KRqkygKfkfq6RJuHy4	Apitd1	apoptosis-inducing TAF9-like domain 1	-0.5753	9.7044	-4.9942	0.0002	0.0071	0.9511
TurRSxLdz6F,9IQmKI	Dbf4	DBF4 homolog (S, cerevisiae)	-0.5287	10.1221	-4.9835	0.0002	0.0073	0.9310
ZO0oIpCSrpCnZlClCE	Hist1h2ak	histone cluster 1 H2ak	-0.8646	13.8861	-4.9822	0.0002	0.0073	0.9286
leeLpXvzuTizvpKeHo	Nol10	nucleolar protein 10	-0.3513	10.6729	-4.9764	0.0002	0.0073	0.9177
05,oROniFEUKHzqp5U	Cd248	CD248 antigen endosialin	0.7354	9.7181	4.9752	0.0002	0.0073	0.9154
3ObqEV_6J,kytLngl4	Spdl1	spindle apparatus coiled-coil protein 1	-0.4756	9.4813	-4.9663	0.0002	0.0075	0.8987
rwdVChL_S8OyE6Tf8o	Ptger2	prostaglandin E receptor 2 (subtype EP2)	0.2971	8.7647	4.9629	0.0002	0.0075	0.8923
6q45A1SCTqXNlHwKJY	Cfl1	cofilin 1 non-muscle	0.3758	9.1933	4.9620	0.0002	0.0075	0.8907
xQj0onuJkeF6pf3lxE	Pqlc3	PQ loop repeat containing	0.3464	8.9733	4.9604	0.0002	0.0075	0.8877
K3kHUU9ed6n0RSCLXI	Smg6	Smg-6 homolog nonsense mediated mRNA decay factor (C, elegans)	0.3096	8.8711	4.9550	0.0002	0.0076	0.8775
Q1EQsEoVlJdl7jlyKg	Alyref	Aly/REF export factor	-0.4269	12.2364	-4.9545	0.0002	0.0076	0.8766
fnbpWYlB1,J7PfX0,8	Syt1	synaptotagmin I	0.5198	9.3907	4.9513	0.0002	0.0076	0.8705

Probe ID	Gene symbol	Gene name	Log_2FC	Average expression	t	P, Value	Adj,P,Val	B
usiHkvefeaPjhPt3pQ	Cct3	chaperonin containing Tcp1 subunit 3 (gamma)	-0.4495	12.9216	-4.9506	0.0002	0.0076	0.8692
9tJ9euUQHy17WKLrSY	E2f2	E2F transcription factor 2	-0.4620	9.5717	-4.9496	0.0002	0.0076	0.8674
HkBUqmy7gKfL67ohyU	Lgals8	lectin galactose binding soluble 8	0.4950	10.0359	4.9477	0.0002	0.0076	0.8638
TrHlPM5f_PdCHrgefk	Gdap1	ganglioside-induced differentiation-associated-protein 1	-0.5430	9.4154	-4.9446	0.0002	0.0076	0.8579
xdB6fJfXQyefg1TX8Y	Gpr1	G protein-coupled receptor 1	-0.6178	9.2896	-4.9443	0.0002	0.0076	0.8574
QQunr0,r4R41l,BRjo	Rhobtb1	Rho-related BTB domain containing 1	-0.6741	12.1724	-4.9419	0.0002	0.0076	0.8529
felCRlu2ipFCntFCzE	Hist1h2bk	histone cluster 1 H2bk	0.7736	9.9423	4.9405	0.0002	0.0076	0.8503
EGawkqaQp2ZQpQhWdc	Hist1h2ah	histone cluster 1 H2ah	-1.0026	13.7408	-4.9370	0.0002	0.0077	0.8436
WiZ5FZAl1KuC_BI_c4	Smc4	structural maintenance of chromosomes 4	-0.2783	9.0235	-4.9337	0.0002	0.0077	0.8374
uvE44l0x7bpNwQ6lpM	Pcca	propionyl-Coenzyme A carboxylase alpha polypeptide	0.3619	10.3510	4.9176	0.0002	0.0079	0.8072
oN11UiVQJ6E,6KwOh0	Ihh	Indian hedgehog	-0.3871	8.9957	-4.9156	0.0002	0.0079	0.8035
NfrTekLi_CgW5eL6U0	Crym	crystallin mu	0.5640	8.7774	4.9156	0.0002	0.0079	0.8033
im2d0au22jcNbd,2Dk	Rps27a	ribosomal protein S27A	-0.4641	12.3778	-4.9148	0.0002	0.0079	0.8019
Hsfwg3U9BM0gztSUTc	Spon1	spondin 1 (f-spondin) extracellular matrix protein	0.2884	8.6686	4.9122	0.0002	0.0079	0.7971
rLRJQphbne5N8xXvwo	Rpa3	replication protein A3	-0.5696	11.1469	-4.9120	0.0002	0.0079	0.7966
xbqICyqKLUBSlFIjr4	Vdr	vitamin D receptor	0.2661	8.8190	4.9108	0.0002	0.0079	0.7943
WtYBS6yzF3uS7PlAng	Dyrk3	dual-specificity tyrosine-(Y)-phosphorylation regulated kinase 3	-0.3989	9.3356	-4.9050	0.0002	0.0080	0.7834
Nl7RiiIAllQueelAxQ	Cdc25a	cell division cycle 25A	-0.5294	9.9544	-4.9019	0.0002	0.0080	0.7775
x1LtxS3QP1POUKLfeg	Fbxw16	F-box and WD-40 domain protein 16	-0.5836	9.2554	-4.9016	0.0002	0.0080	0.7771
lxCl5IP1SJTdVPh5N8	Uxt	ubiquitously expressed transcript	-0.4173	11.0317	-4.8961	0.0002	0.0081	0.7666
Qv50TwY14KC14QtFP4	Upk1b	uroplakin 1B	0.8681	10.2505	4.8948	0.0002	0.0081	0.7642
lt9XAkAOKcCUIDlVLI	Btg4	B cell translocation gene 4	-0.3223	9.0987	-4.8931	0.0002	0.0081	0.7609
NSQJPrTu7P,Uy1Rfok	Meis1	Meis homeobox 1	0.5843	10.3918	4.8928	0.0002	0.0081	0.7605
HVSpdDhC6,r0kvUkRI	Alg8	asparagine-linked glycosylation 8 (alpha-13-glucosyltransferase)	-0.1900	8.8734	-4.8928	0.0002	0.0081	0.7604
BQq,5,zSf0WWoo55G4	Eif3g	eukaryotic translation initiation factor 3 subunit G	-0.3815	13.2391	-4.8912	0.0002	0.0081	0.7574
N7VtyooTtErveJjSlI	Psip1	PC4 and SFRS1 interacting protein 1	-0.7589	11.1043	-4.8894	0.0002	0.0081	0.7540
6_nhFSsdJ6VDcSUh1I	Slc39a13	solute carrier family 39 (metal ion transporter) member 13	0.3972	9.7999	4.8876	0.0002	0.0081	0.7505
Kni7d52fte61,96oIo	Dock4	dedicator of cytokinesis 4	-0.4369	9.5070	-4.8764	0.0002	0.0083	0.7295
9X2wuQPnl4iwiieniA	Vwa5a	von Willebrand factor A domain containing 5A	0.6672	10.3403	4.8762	0.0002	0.0083	0.7292
HQnfRL1l1OhVlLrUJw	Zp3	zona pellucida glycoprotein 3	-1.0150	11.4580	-4.8727	0.0002	0.0083	0.7225
Wu176AVcA_3nU0qB8U	Hs2st1	heparan sulfate 2-O-sulfotransferase 1	-0.3207	9.8188	-4.8709	0.0002	0.0083	0.7190
9yhAN5Tn11WLXnot_c	Rpp25	ribonuclease P/MRP 25 subunit	0.7724	10.9733	4.8675	0.0002	0.0084	0.7127
x65cVn9dTuel4RTP4Q	Mcm10	minichromosome maintenance deficient 10 (S, cerevisiae)	-0.4493	9.0714	-4.8668	0.0002	0.0084	0.7114

Probe ID	Gene symbol	Gene name	Log_2FC	Average expression	t	P, Value	Adj,P,Val	B
QV,m4SzySukvtu4oml	Mras	muscle and microspikes RAS	-0.7510	12.7073	-4.8642	0.0002	0.0084	0.7065
HwLhyx_j1KCnR6p0og	Taf1a	TATA box binding protein (Tbp)-associated factor RNA polymerase I A	-0.5091	10.0834	-4.8634	0.0002	0.0084	0.7050
3d7XX8d3upExInk0Zc	Pkp2	plakophilin 2	-0.5073	10.5981	-4.8602	0.0002	0.0084	0.6989
Ennll87T,F1PguvCAk	Ccne2	cyclin E2	-0.5077	9.2360	-4.8575	0.0002	0.0085	0.6938
uqOv,UCejfdFAtUiYk	Cenpp	centromere protein P	-0.8132	9.9983	-4.8525	0.0002	0.0085	0.6843
rKNAilaB0t5NNUdZKc	Rrp9	RRP9 small subunit (SSU) processome component homolog (yeast)	-0.3582	9.4887	-4.8455	0.0002	0.0086	0.6712
EEq2Ei7uMTkBINfou4	Irf8	interferon regulatory factor 8	0.4366	8.7412	4.8447	0.0002	0.0086	0.6695
9oBrYui8QeodXu67Y4	Enpp1	ectonucleotide pyrophosphatase/phosphodiesterase 1	0.4337	9.4816	4.8422	0.0002	0.0087	0.6648
Z4eg5f4U96nojnewpc	Nlrp9a	NLR family pyrin domain containing 9A	-0.7405	9.4122	-4.8408	0.0002	0.0087	0.6623
W6_,el3l6hLAo6KNKU	Ccbl1	cysteine conjugate-beta lyase 1	0.4299	9.6361	4.8399	0.0002	0.0087	0.6604
xBeBuUp7iupN3kHlB0	Slc38a8	solute carrier family 38 member 8	-0.2777	8.8649	-4.8392	0.0002	0.0087	0.6593
0rgjR6dd_aKF5PU9ck	Tmem128	transmembrane protein 128	0.2664	9.6545	4.8337	0.0002	0.0087	0.6489
imUU,pN,7u9QjFdRUg	Spsb4	splA/ryanodine receptor domain and SOCS box containing 4	-0.7861	10.3148	-4.8336	0.0002	0.0087	0.6486
3CNet4eVORFeKdSSvg	Slco2a1	solute carrier organic anion transporter family member 2a1	0.3443	8.9385	4.8323	0.0002	0.0087	0.6461
iUoOLiWqB9JqDB9OUk	Rpa2	replication protein A2	-0.5184	10.0393	-4.8305	0.0002	0.0088	0.6426
ZYgeipI5_1NCeLAr64	Pold3	polymerase (DNA-directed) delta 3 accessory subunit	-0.5183	10.3935	-4.8260	0.0002	0.0088	0.6341
cWBntPkL9HrnnO0Dkl	Wnt5a	wingless-type MMTV integration site family member 5A	0.5128	9.3361	4.8220	0.0002	0.0089	0.6267
oVlunTkUyd1yoaVEBM	Gabrb3	gamma-aminobutyric acid (GABA) A receptor subunit beta 3	0.1926	8.5982	4.8204	0.0002	0.0089	0.6237
fZ5eObPCEzW6n55MHQ	Timp2	tissue inhibitor of metalloproteinase 2	0.7798	11.6727	4.8182	0.0002	0.0089	0.6194
xe,i5AHsclDGeC7ulQ	Ctnna2	catenin (cadherin associated protein) alpha 2	0.4462	9.2906	4.8138	0.0002	0.0090	0.6112
HQupJ7brl36goks8RM	H2-T23	histocompatibility 2 T region locus 23	0.7319	10.9986	4.8125	0.0002	0.0090	0.6086
fieuv5dBBMB9cONJnl	Hoxd8	homeobox D8	0.4806	10.2695	4.8083	0.0002	0.0090	0.6007
loCX6Tr3sCd_xZ6lBo	Tgfbi	transforming growth factor beta induced	0.5944	11.3592	4.8030	0.0002	0.0091	0.5905
6o9cILo0oo8oZ0l_lQ	Sp100	nuclear antigen Sp100	0.3216	8.8738	4.7987	0.0003	0.0092	0.5826
WXVQtUWVwdMHe_JUg0	Nfix	nuclear factor I/X	0.2258	8.6990	4.7957	0.0003	0.0092	0.5769
iknu7lv0iQvXSS7I4M	Snx10	sorting nexin 10	0.7046	10.2094	4.7929	0.0003	0.0092	0.5714
Ql1P3N_BlyXnerz3rk	Tmem97	transmembrane protein 97	-0.4333	11.0395	-4.7857	0.0003	0.0093	0.5579
ird_3ilP7rp_DKDpVU	Ptges	prostaglandin E synthase	-0.6099	10.1035	-4.7813	0.0003	0.0094	0.5495
ipy1JvxfcEqY6jH3lQ	Itga2	integrin alpha 2	-0.6086	9.1606	-4.7803	0.0003	0.0094	0.5476
3Suwavie1ZW7fhRVqM	Kctd17	potassium channel tetramerisation domain containing 17	0.5126	11.1157	4.7798	0.0003	0.0094	0.5465
67MAQA5O7a05kbkRsg	Rnf144a	ring finger protein 144A	0.4102	10.2942	4.7777	0.0003	0.0094	0.5426
ukmPXth1fESz433h7o	Cdr2	cerebellar degeneration-related 2	-0.5992	10.0852	-4.7736	0.0003	0.0095	0.5349

Probe ID	Gene symbol	Gene name	Log_2FC	Average expression	t	P, Value	Adj,P,Val	B
QIq4AS7pB4uEnVeyFM	Zwilch	zwilch kinetochore protein	-0.2887	8.8064	-4.7698	0.0003	0.0095	0.5277
3e3k5NXwyU,oyWgsi0	Fry	furry homolog (Drosophila)	0.2599	9.2145	4.7695	0.0003	0.0095	0.5271
Qsb,T3VIVOROSRweBI	Aldh1l2	aldehyde dehydrogenase 1 family member L2	0.3063	8.8629	4.7692	0.0003	0.0095	0.5265
Neo1Lkta,X,MCgeVL0	Ppan	peter pan homolog (Drosophila)	-1.0580	10.7237	-4.7658	0.0003	0.0096	0.5201
lVfeR1N_,s8mCQ7DL4	Prickle3	prickle homolog 3 (Drosophila)	0.3159	9.6121	4.7633	0.0003	0.0096	0.5152
xpGFloiDUCwIhe5qh8	Atp5sl	ATP5S-like	-0.3038	9.7321	-4.7549	0.0003	0.0097	0.4993
rgg3ruhS6T95XI6YPU	Eif3l	eukaryotic translation initiation factor 3 subunit L	-0.3894	13.0136	-4.7543	0.0003	0.0097	0.4982
Q8qiryco,gd0GeTnl0	Blmh	bleomycin hydrolase	0.5674	10.0343	4.7536	0.0003	0.0097	0.4968
uUq3hec18tD1SfpFIk	Dnd1	dead end homolog 1 (zebrafish)	-0.4657	10.1423	-4.7507	0.0003	0.0098	0.4912
HUBxN0LxRSJ35d7pco	Oaz2	ornithine decarboxylase antizyme 2	0.3198	10.7964	4.7506	0.0003	0.0098	0.4911
WUkQtNW8CFeDktl2uU	Ezh2	enhancer of zeste homolog 2 (Drosophila)	-0.8823	11.2898	-4.7442	0.0003	0.0098	0.4790
ok,klPiLpRC_aSkhiQ	Pprc1	peroxisome proliferative activated receptor gamma coactivator-related 1	-0.5747	9.8284	-4.7438	0.0003	0.0098	0.4782
NR5461E471,ZSxE4Io	Tipin	timeless interacting protein	-0.4928	11.3198	-4.7423	0.0003	0.0099	0.4753
fuUe4RRWIXQ2j6FCjc	Srm	spermidine synthase	-0.5166	10.7502	-4.7386	0.0003	0.0099	0.4683
cV41eX9NKeARJ3cgP8	Gtse1	G two S phase expressed protein 1	-0.6112	9.6455	-4.7381	0.0003	0.0099	0.4674
cR0N1ViJ7w6LfV5P78	Nup210	nucleoporin 210	-0.8455	10.0351	-4.7364	0.0003	0.0099	0.4641
9EgooZ6Kl_enFnNwKg	Cd74	CD74 antigen (invariant polypeptide of major histocompatibility complex class II antigen-associated)	0.7048	10.7644	4.7346	0.0003	0.0099	0.4607
3noFzpJEaP1EjhUgUg	Rnps1	ribonucleic acid binding protein S1	-0.5124	10.8167	-4.7328	0.0003	0.0100	0.4573
cUnp5dFEaeAIl0f,yA	Pfkl	phosphofructokinase liver B-type	-0.4056	11.3375	-4.7280	0.0003	0.0100	0.4482
6tXSTX7dSV4oBFwIgk	Tmem201	transmembrane protein 201	-0.4450	10.2694	-4.7260	0.0003	0.0101	0.4443
utEFyf7HvgNs_,V,is	Zfp346	zinc finger protein 346	0.3174	9.3751	4.7153	0.0003	0.0102	0.4240
uUXZeq_kJIE3U8KRGI	Rph3al	rabphilin 3A-like (without C2 domains)	-0.6442	9.2710	-4.7145	0.0003	0.0102	0.4225
67vaiJ4salqFqeeYns	Cdc20	cell division cycle 20	-0.3245	9.1079	-4.7141	0.0003	0.0102	0.4217
N607fKpApu6OuUOAV8	Jmjd6	jumonji domain containing 6	-0.4124	11.8797	-4.7130	0.0003	0.0102	0.4196
BfUpR7LUecLXQ3XsVM	Mrgprf	MAS-related GPR member F	0.3580	9.0640	4.7129	0.0003	0.0102	0.4194
0Q0qNpJ_defnarP,sI	Zcchc8	zinc finger CCHC domain containing 8	-0.4046	11.6703	-4.7084	0.0003	0.0103	0.4108
9p,oU4tPV2yAQY13Po	Saraf	store-operated calcium entry-associated regulatory factor	0.6345	12.2173	4.7041	0.0003	0.0104	0.4025
x1xqhtxF5uvSRJqF3g	H2-DMb2	histocompatibility 2 class II locus Mb2	0.4109	9.0051	4.7032	0.0003	0.0104	0.4009
Z5kv6v,O1Lm9bH44n0	Gtpbp4	GTP binding protein 4	-0.4658	11.6291	-4.6997	0.0003	0.0104	0.3941
HtI4n16FfnSAbh_N,o	Unc13b	unc-13 homolog B (C, elegans)	-0.5310	11.1108	-4.6994	0.0003	0.0104	0.3936
WqogxfiukvfKUlec_U	Col9a2	collagen type IX alpha 2	-0.8845	9.5930	-4.6993	0.0003	0.0104	0.3935
QrSS8S7uj2p55,02kI	Asz1	ankyrin repeat SAM and basic leucine zipper domain containing 1	-0.4110	9.1751	-4.6955	0.0003	0.0105	0.3863

Probe ID	Gene symbol	Gene name	Log_2FC	Average expression	t	P, Value	Adj,P,Val	B
BZ1b5yyie,yii,qt1E	Ank1	ankyrin 1 erythroid	-0.3443	8.9036	-4.6943	0.0003	0.0105	0.3840
Epfl51zUdB1RJc4I6o	Dnajb13	DnaJ (Hsp40) related subfamily B member 13	-1.0320	9.9820	-4.6928	0.0003	0.0105	0.3811
okRuUU5X344MV4KC0U	Epn2	epsin 2	-0.7385	10.5186	-4.6857	0.0003	0.0106	0.3674
ERlsEojcuN,6NCr1fU	Pank1	pantothenate kinase 1	0.6703	12.6532	4.6849	0.0003	0.0106	0.3660
EVOVl3sv6CIf_jurN0	Rars2	arginyl-tRNA synthetase 2 mitochondrial	-0.4511	10.3474	-4.6830	0.0003	0.0106	0.3624
BZRGLortLteSA3X4yI	Cpne8	copine VIII	0.4549	9.2433	4.6773	0.0003	0.0107	0.3514
lV0AsdasARQl5JL30M	2700060E02Rik	RIKEN cDNA 2700060E02 gene	0.5276	9.7286	4.6767	0.0003	0.0107	0.3504
ErO3sknr__,uytXO4U	Rbm8a	RNA binding motif protein 8a	-0.2779	9.8413	-4.6749	0.0003	0.0108	0.3468
B_xJOaIJ5GrX6kpL74	Timm21	tranlocase of inner mitochondrial membrane 21	-0.5864	11.1331	-4.6683	0.0003	0.0109	0.3343
WS4lebX0iOBHuVW0RM	5430435G22Rik	RIKEN cDNA 5430435G22 gene	0.4144	9.6577	4.6590	0.0003	0.0111	0.3165
6Fw6pAIKvoJ9vFOiNU	C1s1	complement component 1 s subcomponent 1	0.3062	8.8871	4.6476	0.0003	0.0113	0.2946
WVekdcfIECyX9,y9Uk	Serpina3n	serine (or cysteine) peptidase inhibitor clade A member 3N	1.2012	9.7928	4.6473	0.0003	0.0113	0.2941
0XFo7oiXmlcc0Knj4Q	Miox	myo-inositol oxygenase	-0.4552	9.3931	-4.6471	0.0003	0.0113	0.2937
ER1_juPp9delPu_Eug	Ugt1a10	UDP glycosyltransferase 1 family polypeptide A10	0.8320	9.7998	4.6466	0.0003	0.0113	0.2927
cLgeLJ957BBdGyBKEk	Lhfp	lipoma HMGIC fusion partner	0.8749	10.4482	4.6444	0.0003	0.0113	0.2885
KOVgUVJFE51O0Luxug	Cdca4	cell division cycle associated 4	-0.3848	9.8065	-4.6393	0.0003	0.0114	0.2788
WSnmKiGVJULP8,R4kQ	Asb2	ankyrin repeat and SOCS box-containing 2	0.4014	9.3777	4.6364	0.0003	0.0114	0.2733
inrHdRXuVDvf7x4ij8	Acap3	ArfGAP with coiled-coil ankyrin repeat and PH domains 3	0.3799	9.4637	4.6363	0.0003	0.0114	0.2731
ueJTR6QgvYeuerIpR0	Tcl1b3	T cell leukemia/lymphoma 1B 3	-0.5084	9.0620	-4.6361	0.0003	0.0114	0.2726
978wGWIuhJ53024pEo	Cmya5	cardiomyopathy associated 5	-0.6092	9.2214	-4.6345	0.0003	0.0114	0.2696
oh,iXl6J_36XS7RJd4	Tspan17	tetraspanin 17	0.6543	10.8386	4.6321	0.0003	0.0114	0.2651
o,fbeGg6YqWbudx9rg	Nt5dc2	5'-nucleotidase domain containing 2	-0.6861	10.4279	-4.6321	0.0003	0.0114	0.2650
KuTtE5RBTrRF0e03II	Pde4d	phosphodiesterase 4D cAMP specific	0.1911	8.5890	4.6314	0.0003	0.0114	0.2637
cSR2RAjneinMsu7frQ	Eif1a	eukaryotic translation initiation factor 1A	-0.4713	11.2971	-4.6308	0.0003	0.0114	0.2625
foohEyuwCjnOdO9ykk	H2-T23	histocompatibility 2 T region locus 23	0.8805	9.9485	4.6307	0.0003	0.0114	0.2624
xl7eoxRINd15f_xIvk	Heatr1	HEAT repeat containing 1	-0.5704	11.4285	-4.6283	0.0003	0.0114	0.2578
6ptPlEnBEvFVEzUoIk	Mvk	mevalonate kinase	0.2312	8.7107	4.6232	0.0004	0.0115	0.2480
cVWnp1GJH9x_5Op_vw	Camta2	calmodulin binding transcription activator 2	0.5906	10.6879	4.6199	0.0004	0.0116	0.2417
91OfmTXCS3sJIJlgQo	Nlrp4a	NLR family pyrin domain containing 4A	-0.3898	9.0399	-4.6181	0.0004	0.0116	0.2383
3qUi1wlVTnsDLettIs	Rusc2	RUN and SH3 domain containing 2	0.3537	10.0611	4.6157	0.0004	0.0116	0.2337
TIR0ooFLqAYRQpbnSI	Gnl2	guanine nucleotide binding protein-like 2 (nucleolar)	-0.3711	10.2394	-4.6151	0.0004	0.0116	0.2325
ocwpEYNHnXXSDp4pek	Lrrc14b	leucine rich repeat containing 14B	0.2750	8.7271	4.6117	0.0004	0.0117	0.2260
cgCeiIujoUAS7fdOZw	Rragb	Ras-related GTP binding B	-0.2551	8.7879	-4.6068	0.0004	0.0118	0.2167

Probe ID	Gene symbol	Gene name	Log_2FC	Average expression	t	P, Value	Adj,P,Val	B
0StV3S50ZLa0lEEZC4	Snrpd2	small nuclear ribonucleoprotein D2	-0.3330	13.6451	-4.5989	0.0004	0.0120	0.2015
6znfbWqI6bb3LZV1Pg	Lsm3	LSM3 homolog U6 small nuclear RNA associated (S, cerevisiae)	-0.5034	11.7073	-4.5988	0.0004	0.0120	0.2013
fWH1l,fHfnQqV00bnE	Ugt1a6a	UDP glucuronosyltransferase 1 family polypeptide A6A	0.6311	9.3650	4.5973	0.0004	0.0120	0.1983
0UonrAc,ruqeA9dp0c	Gbp3	guanylate binding protein 3	0.4893	10.1375	4.5903	0.0004	0.0121	0.1850
H7UgDVCSe7vjWLyKlI	Glrx	glutaredoxin	0.3686	12.4247	4.5861	0.0004	0.0122	0.1769
WpTH17VLrvTT22eQXQ	Slc6a15	solute carrier family 6 (neurotransmitter transporter) member 15	-0.5929	9.2154	-4.5852	0.0004	0.0122	0.1752
NrLUh60DO7pK0agKi0	Tfcp2l1	transcription factor CP2-like 1	0.5816	9.3095	4.5800	0.0004	0.0123	0.1651
9hUUmfWU,k7rqRTf4Q	Tmem53	transmembrane protein 53	0.2875	8.8776	4.5705	0.0004	0.0125	0.1470
u_EF7nU1erX06aiilg	Gm1070	predicted gene 1070	-0.5316	9.3669	-4.5701	0.0004	0.0125	0.1462
lAYerh6Wijunnfr3pw	Cryba4	crystallin beta A4	0.7644	9.2750	4.5696	0.0004	0.0125	0.1451
Eq1QEqclaHgCMJtAzk	Kcnb1	potassium voltage gated channel Shab-related subfamily member 1	0.3056	8.7642	4.5687	0.0004	0.0125	
6UgpkiUKuCgBpLSKOI	Whsc1	Wolf-Hirschhorn syndrome candidate 1 (human)	-0.2251	8.9573	-4.5687	0.0004	0.0125	0.1434
Z,slKo46R,up5N74hI	Thsd7b	thrombospondin type I domain containing 7B	0.3838	8.9622	4.5544	0.0004	0.0128	0.1160
cssNee6X9KwTr0R3k4	Fam49b	family with sequence similarity 49 member B	-0.4866	9.2547	-4.5539	0.0004	0.0128	0.1151
9jDdC1ERRbzTcfq1EE	Myl1	myosin light polypeptide 1	0.4817	9.0118	4.5529	0.0004	0.0128	0.1131
oSOwMgjCp8967hefXs	Fam198b	family with sequence similarity 198 member B	0.2846	8.9122	4.5516	0.0004	0.0128	0.1107
xmhE8Vo5,72II3ZG2o	Prrx1	paired related homeobox 1	0.4352	9.1909	4.5514	0.0004	0.0128	0.1102
0eVc4667c7eSpRQfko	Mybpc3	myosin binding protein C cardiac	-0.4191	9.1561	-4.5508	0.0004	0.0128	0.1091
rf1PfY4M8I6KV_UYvc	Akr1c18	aldo-keto reductase family 1 member C18	2.6444	10.2891	4.5506	0.0004	0.0128	0.1086
liHed814oceD3,BVxU	Pvrl2	poliovirus receptor-related 2	0.5949	11.1511	4.5462	0.0004	0.0129	0.1002
WJ9eQpiYr6ciKj396o	Sox5	SRY (sex determining region Y)-box 5	0.2109	9.0846	4.5455	0.0004	0.0129	0.0989
ihawfn4vVODI,iHg6Q	Col8a1	collagen type VIII alpha 1	0.2952	8.7164	4.5443	0.0004	0.0129	0.0965
NUVSAO,VdZ9eg_k3Co	Rtkn2	rhotekin 2	-0.2879	8.9883	-4.5440	0.0004	0.0129	0.0961
W9cnkFBwIRHrNeUqJU	Lmcd1	LIM and cysteine-rich domains 1	0.6185	10.5625	4.5405	0.0004	0.0130	0.0893
WeqPjlB6vAyb,Soi5U	Srsf10	serine/arginine-rich splicing factor 10	-0.3383	10.0618	-4.5396	0.0004	0.0130	0.0875
Eu2SA6QrpXyAEC53oo	Kcnab3	potassium voltage-gated channel shaker-related subfamily beta member 3	0.5843	9.0603	4.5390	0.0004	0.0130	0.0864
0d7Mbe30EDsKHAxV1Y	Gpr65	G-protein coupled receptor 65	0.2522	8.6469	4.5309	0.0004	0.0131	0.0708
ZS7Dwn1KNHFOAGWT3k	Bace1	beta-site APP cleaving enzyme 1	0.5813	10.2619	4.5277	0.0004	0.0132	0.0646
Tku1PkIu7,4J4fcX,I	Tnfaip8	tumor necrosis factor alpha-induced protein 8	0.3246	9.6998	4.5274	0.0004	0.0132	0.0641
Hp9LtgJ4m4gvo4r7tY	Clspn	claspin	-0.4342	9.5027	-4.5261	0.0004	0.0132	0.0616
uXFUkjXd6zgmC58ujg	Raet1c	retinoic acid early transcript gamma	-0.5673	9.2370	-4.5249	0.0004	0.0132	0.0593

Probe ID	Gene symbol	Gene name	Log_2FC	Average expression	t	P, Value	Adj,P,Val	B
fjv1R14npdIv91xXeU	Cln3	ceroid lipofuscinosis neuronal 3 juvenile (Batten Spielmeyer-Vogt disease)	-0.5988	10.2139	-4.5223	0.0004	0.0133	0.0542
EO6I4uKGXES54Vk_p0	Ruvbl2	RuvB-like protein 2	-0.6014	10.3740	-4.5222	0.0004	0.0133	0.0540
Wh_g6_kh_dSOQwIT5I	Pik3r3	phosphatidylinositol 3 kinase regulatory subunit polypeptide 3 (p55)	0.2916	8.9287	4.5199	0.0004	0.0133	0.0496
NtOtlXH,xONx,c4l6U	Tcl1b2	T cell leukemia/lymphoma 1B 2	-0.4721	9.0144	-4.5178	0.0004	0.0133	0.0457
HeV7LNUOjNHVLdA_p4	Slc44a1	solute carrier family 44 member 1	0.3473	9.4235	4.5175	0.0004	0.0133	0.0450
WkI70w6rQUFSQopQUk	Sbsn	suprabasin	0.4088	8.8328	4.5102	0.0004	0.0135	0.0309
WnXWoSDLfKSpMdcVXQ	Tmem39a	transmembrane protein 39a	-0.4712	11.4517	-4.5066	0.0004	0.0136	0.0240
BUvl,VVqvlRFoQ7QAQ	Ecm1	extracellular matrix protein 1	0.3676	8.7405	4.5064	0.0004	0.0136	0.0236
T67kt17q8RaLuOvumA	Cmtr2	cap methyltransferase 2	-0.3999	10.4120	-4.5055	0.0004	0.0136	0.0218
0KoXfILxI6Q7ghUl5I	Naa25	N(alpha)-acetyltransferase 25 NatB auxiliary subunit	-0.3412	10.3609	-4.5027	0.0004	0.0136	0.0166
lRG5RTlffjgxXgoLRU	Epn2	epsin 2	-0.8208	10.8814	-4.5027	0.0004	0.0136	0.0164
NVSyT7WooXh3gF6QD4	Mia	melanoma inhibitory activity	0.3926	9.3792	4.5010	0.0004	0.0136	0.0133
QniHZp,7Rfnu_37pJI	Adcy2	adenylate cyclase 2	0.3691	9.1545	4.5007	0.0004	0.0136	0.0127
Ee9iOe6CKWvEU_JL_I	Nnmt	nicotinamide N-methyltransferase	0.6022	9.8524	4.5003	0.0004	0.0136	0.0118
BoSlWK0iv5yeEF49q0	Dpep1	dipeptidase 1 (renal)	0.3220	9.2995	4.4980	0.0005	0.0136	0.0074
uRSOVFZRFXhca7pA1I	Pold4	polymerase (DNA-directed) delta 4	0.3790	9.6138	4.4965	0.0005	0.0137	0.0047
9F9t9RSb3TiiSZrfR4	Rad54l	RAD54 like (S, cerevisiae)	-0.4967	9.5801	-4.4888	0.0005	0.0138	-0.0102
o,l__iJyp7notNVCpE	Cdca3	cell division cycle associated 3	-0.7613	11.4348	-4.4851	0.0005	0.0139	-0.0174
fBQ0s37QzLSWNjYXRk	Rab5c	RAB5C member RAS oncogene family	0.2971	11.5663	4.4830	0.0005	0.0140	-0.0214
HpAirhC9CeBCEidCic	S100a4	S100 calcium binding protein A4	0.4974	8.7813	4.4777	0.0005	0.0141	-0.0317
EjjhOoiusqSSnbdTS4	Cxcl16	chemokine (C-X-C motif) ligand 16	0.3391	9.9208	4.4776	0.0005	0.0141	-0.0318
rOEVGjj0jV66kn9Jok	Acy1	aminoacylase 1	-0.1933	8.9823	-4.4765	0.0005	0.0141	-0.0340
cJh_0h4_gehbkJPuns	Tex14	testis expressed gene 14	-0.9735	10.1021	-4.4757	0.0005	0.0141	-0.0356
61a5dXjq13ClsSgQTg	Ugt1a6a	UDP glucuronosyltransferase 1 family polypeptide A6A	0.3995	8.9301	4.4736	0.0005	0.0141	-0.0396
cNl3E6SCPh_3dYJYIE	Cyb5a	cytochrome b5 type A (microsomal)	-0.6799	13.9718	-4.4721	0.0005	0.0141	-0.0426
lQp9KAVR6Tlf_lw8DQ	Nr1h4	nuclear receptor subfamily 1 group H member 4	0.6416	9.8021	4.4707	0.0005	0.0142	-0.0451
KRJztZCWFKgFcif4l4	Nacc2	nucleus accumbens associated 2 BEN and BTB (POZ) domain containing	0.6087	11.1855	4.4693	0.0005	0.0142	-0.0479
KeR,j_,XBL3vV15,j8	E2f1	E2F transcription factor 1	-0.6504	10.1299	-4.4669	0.0005	0.0142	-0.0524
QsudAtxXBOEth17n7I	Bmp3	bone morphogenetic protein 3	-0.7878	10.1822	-4.4656	0.0005	0.0142	-0.0549
l0CREHkR0SldJ9ViUQ	Sec14l1	SEC14-like 1 (S, cerevisiae)	0.3654	9.2819	4.4653	0.0005	0.0142	-0.0555
K15jxJ_Pp7qjUWIieU	Arl2bp	ADP-ribosylation factor-like 2 binding protein	0.5662	9.9563	4.4629	0.0005	0.0143	-0.0602
Nee3tKvXnqUgiA,r4s	G3bp1	GTPase activating protein (SH3 domain) binding protein 1	-0.6713	12.6465	-4.4602	0.0005	0.0143	-0.0653

Probe ID	Gene symbol	Gene name	Log_2FC	Average expression	t	P, Value	Adj,P,Val	B
W94o6kjXplJI6HiRAU	Nagk	N-acetylglucosamine kinase	0.4510	10.7325	4.4595	0.0005	0.0143	-0.0669
9ULN7BX4lXlSz5Td6U	Vldlr	very low density lipoprotein receptor	0.4428	10.8930	4.4566	0.0005	0.0144	-0.0723
xi3iC26XgnhCx5aeiA	Mgl2	macrophage galactose N-acetyl-galactosamine specific lectin 2	0.5216	9.5989	4.4512	0.0005	0.0145	-0.0829
lr9CWt5,0VHeSUrRB4	Zbtb8b	zinc finger and BTB domain containing 8b	-1.0518	10.5987	-4.4503	0.0005	0.0145	-0.0845
xy1uEC_5Afrgbed6p8	Cbr3	carbonyl reductase 3	0.4994	10.5907	4.4485	0.0005	0.0146	-0.0881
BxK2rpdHtR,Ztq_gf4	Smc2	structural maintenance of chromosomes 2	-0.7000	10.1680	-4.4457	0.0005	0.0146	-0.0934
KQEU0VJ4F0mnFgIF1l	Skp2	S-phase kinase-associated protein 2 (p45)	-0.4534	9.1954	-4.4443	0.0005	0.0146	-0.0961
lVLR1UbMdcuqBezafl	Mgll	monoglyceride lipase	0.6413	9.3878	4.4440	0.0005	0.0146	-0.0967
Tug56OXqOey4KOJKWs	Serpine2	serine (or cysteine) peptidase inhibitor clade E member 2	-0.9269	14.1162	-4.4345	0.0005	0.0149	-0.1151
rTJ6VH4a1eun3oqCew	Necap2	NECAP endocytosis associated 2	0.3539	10.1566	4.4331	0.0005	0.0149	-0.1178
6c7e0xXAOE_v,o,rOQ	Fzd1	frizzled homolog 1 (Drosophila)	0.3538	8.6741	4.4313	0.0005	0.0149	-0.1212
loAp5O0NfUFUyg7Iio	Nudt18	nudix (nucleoside diphosphate linked moiety X)-type motif 18	0.6438	10.1457	4.4312	0.0005	0.0149	-0.1214
ZmG1BX,gFJQXDxWx7o	Bcl11a	B cell CLL/lymphoma 11A (zinc finger protein)	-0.6015	9.4160	-4.4239	0.0005	0.0151	-0.1355
TGmk7eM3X6S3s7_7Yo	Cx3cr1	chemokine (C-X3-C motif) receptor 1	0.5882	9.1814	4.4187	0.0005	0.0153	-0.1456
ZueeVCCFiJRRClCqAw	Hist1h2ad	histone cluster 1 H2ad	-0.7031	14.6911	-4.4158	0.0005	0.0153	-0.1512
cUQupJ7brl36goks8Q	H2-T23	histocompatibility 2 T region locus 23	0.5951	10.8843	4.4130	0.0005	0.0154	-0.1567
icq3eu4Kt6guiKpIC4	Cd44	CD44 antigen	0.2545	8.9762	4.4114	0.0005	0.0154	-0.1598
Eer1UoRHEV3x,x9el0	Rras	Harvey rat sarcoma oncogene subgroup R	0.6201	10.9037	4.4102	0.0005	0.0154	-0.1620
cXoP12SERUDu33rSUI	Mybl2	myeloblastosis oncogene-like 2	-0.4721	9.5818	-4.4090	0.0005	0.0155	-0.1644
cEqlVEvR3R7yP_X,Uo	Dclk2	doublecortin-like kinase 2	-0.5284	9.2418	-4.4072	0.0005	0.0155	-0.1679
ZteIg,lKU0fNffMaBc	Fam198b	family with sequence similarity 198 member B	0.9114	11.1706	4.4055	0.0005	0.0155	-0.1712
W1UQh57RSUSNPAF9CU	Actg2	actin gamma 2 smooth muscle enteric	0.8758	12.4101	4.3998	0.0005	0.0156	-0.1823
WClvygKhAke4rqgRe4	Tnfrsf9	tumor necrosis factor receptor superfamily member 9	0.6938	8.7386	4.3993	0.0005	0.0156	-0.1832
iVG_193qRdclFCB9KE	Pold4	polymerase (DNA-directed) delta 4	0.3876	9.7666	4.3984	0.0005	0.0156	-0.1850
l_OXyLUi6bU1Jq7yWE	Pfdn4	prefoldin 4	-0.5895	12.5377	-4.3979	0.0005	0.0156	-0.1859
EtUFNLRR998SPV80T0	Fam122b	family with sequence similarity 122 member B	-0.5580	9.7074	-4.3976	0.0005	0.0156	-0.1865
upEt0c6J0p6f6HRzkk	Kif11	kinesin family member 11	-0.3184	9.2423	-4.3969	0.0006	0.0156	-0.1878
om6iAsqii1AUpRSI68	Vdr	vitamin D receptor	0.1915	8.6953	4.3966	0.0006	0.0156	-0.1885
rnijknXdKt4LdQN4Ds	Ppard	peroxisome proliferator activator receptor delta	0.3950	10.1010	4.3960	0.0006	0.0156	-0.1896
cnUqndPrf9384xDu5k	Trmt10a	tRNA methyltransferase 10A	-0.2785	9.6296	-4.3946	0.0006	0.0157	-0.1922
3npwed7LKU6e5ThAiE	Wdr75	WD repeat domain 75	-0.4293	11.4437	-4.3935	0.0006	0.0157	-0.1944
oVaBiCheblXSG7L3g8	Mrpl38	mitochondrial ribosomal protein L38	-0.2145	8.8543	-4.3932	0.0006	0.0157	-0.1950

Probe ID	Gene symbol	Gene name	Log_2FC	Average expression	t	P, Value	Adj,P,Val	B
6t51T_JawDwrhIi5uQ	Cyp2j9	cytochrome P450 family 2 subfamily j polypeptide 9	0.4235	9.4377	4.3919	0.0006	0.0157	-0.1975
9VfKy,yeDjn9,XOnnQ	Socs2	suppressor of cytokine signaling 2	-0.5406	13.8120	-4.3903	0.0006	0.0157	-0.2005
6BWfaKy8662P4idcWg	Zfp326	zinc finger protein 326	-0.5778	10.2048	-4.3892	0.0006	0.0157	-0.2027
0URUCCIJL96J6wnl4Y	Gemin4	gem (nuclear organelle) associated protein 4	-0.1632	8.6593	-4.3878	0.0006	0.0157	-0.2055
Wn5f5wsFeh40MGXUuk	Foxp2	forkhead box P2	-0.3632	8.8392	-4.3855	0.0006	0.0157	-0.2099
HVJOxe8UIQSxtNQwgQ	Cd55	CD55 antigen	0.6659	9.7839	4.3855	0.0006	0.0157	-0.2099
EgPgdzoMJZoKY1SUtl	Tnc	tenascin C	0.5359	9.0410	4.3854	0.0006	0.0157	-0.2101
3iE_UE3KLoDuG2cXeI	Rrp12	ribosomal RNA processing 12 homolog (S, cerevisiae)	-0.5146	10.0307	-4.3844	0.0006	0.0157	-0.2120
ulQHlLrjdEu6oDsNyE	Ppih	peptidyl prolyl isomerase H	-0.5398	11.3649	-4.3840	0.0006	0.0157	-0.2127
rf7_txI4_lc_R7q6mk	Pramef12	PRAME family member 12	-0.6278	9.7457	-4.3839	0.0006	0.0157	-0.2130
fYVI45lokiirQpf5lA	Ldhd	lactate dehydrogenase D	0.4150	8.7353	4.3820	0.0006	0.0158	-0.2167
csMPlKLEud__N_7S0o	Nme7	NME/NM23 family member 7	0.4721	11.7683	4.3761	0.0006	0.0159	-0.2282
KlnAqSJQhlLRHgkiCg	Tmpo	thymopoietin	-0.3216	9.8490	-4.3756	0.0006	0.0159	-0.2290
NVcK5r_SX48e36R6eI	Heatr1	HEAT repeat containing 1	-0.3231	9.5725	-4.3738	0.0006	0.0160	-0.2326
on9SBbiq,60XoEqdQ0	Rspo3	R-spondin 3 homolog (Xenopus laevis)	0.3661	8.9385	4.3707	0.0006	0.0161	-0.2386
xV3e4KMsA7cV3XsIEI	Il18	interleukin 18	0.6433	9.5150	4.3699	0.0006	0.0161	-0.2400
ieUyPc8l5HqMXFclHk	Zg16	zymogen granule protein 16	-0.6449	9.9696	-4.3676	0.0006	0.0161	-0.2446
6qjedfBv,iQ,e9Sf4U	Sin3b	transcriptional regulator SIN3B (yeast)	-0.2899	10.5226	-4.3670	0.0006	0.0161	-0.2457
ukWzjCiuRJR7yUiKR8	Gdap1	ganglioside-induced differentiation-associated-protein 1	-0.3952	9.1360	-4.3604	0.0006	0.0163	-0.2586
rmQuKNExO5ep9Tesg4	Fcrls	Fc receptor-like S scavenger receptor	0.6005	10.0923	4.3577	0.0006	0.0164	-0.2638
xefVO3Uii,jiO1aMuo	Stat1	signal transducer and activator of transcription 1	0.3856	9.7483	4.3530	0.0006	0.0165	-0.2728
BJLdJWQDZ0KBUtKKd4	Kctd14	potassium channel tetramerisation domain containing 14	-0.6446	10.5197	-4.3530	0.0006	0.0165	-0.2730
3Ik,Vfoz_nIRfWrSrs	Tgfb3	transforming growth factor beta 3	0.4029	9.9384	4.3427	0.0006	0.0168	-0.2929
QGLdHoikTS1_0UEoB4	St6galnac2	ST6 (alpha-N-acetyl-neuraminyl-23-beta-galactosyl-13)-N-acetylgalactosaminide alpha-26-sialyltransferase 2	0.4211	10.2339	4.3404	0.0006	0.0168	-0.2973
KprOxXp4LDPBTJ3qKM	Acer2	alkaline ceramidase 2	0.2922	9.0952	4.3388	0.0006	0.0169	-0.3005
BZ13SohcePpTj9Jzrg	Cep89	centrosomal protein 89	-0.2890	9.6385	-4.3381	0.0006	0.0169	-0.3017
iMln97l8QFJuXTpbEU	Ptbp1	polypyrimidine tract binding protein 1	-0.4545	10.2652	-4.3341	0.0006	0.0170	-0.3096
HluqE6C0,uTo7ku6EU	Ppa1	pyrophosphatase (inorganic) 1	-0.4666	12.7952	-4.3320	0.0006	0.0170	-0.3136
HM0uKICgZNWph5R3u4	Parm1	prostate androgen-regulated mucin-like protein 1	-0.7093	9.7786	-4.3270	0.0006	0.0172	-0.3233
oNy4hoI,5xP1PR16c4	Csgalnact1	chondroitin sulfate N-acetylgalactosaminyltransferase 1	0.5423	8.8133	4.3218	0.0006	0.0173	-0.3335
QnN_Un8UitKIzq3q7k	Tyms-ps	thymidylate synthase pseudogene	-0.4922	10.8816	-4.3210	0.0006	0.0173	-0.3350

Probe ID	Gene symbol	Gene name	Log_2FC	Average expression	t	P, Value	Adj,P,Val	B
Kg13OViyfEqX9d67RI	Cbs	cystathionine beta-synthase	-0.3386	8.8082	-4.3209	0.0006	0.0173	-0.3351
ouOO4kw_i04QMteVXk	Fbxw26	F-box and WD-40 domain protein 26	-0.5771	9.1828	-4.3197	0.0006	0.0173	-0.3375
rc1Xmf4G5SSV_,P5Uk	Orc5	origin recognition complex subunit 5	-0.6002	11.0474	-4.3140	0.0006	0.0175	-0.3486
irTC8RonhEih0ihSnk	Mybbp1a	MYB binding protein (P160) 1a	-0.2924	8.9926	-4.3128	0.0007	0.0175	-0.3508
3DA1K39RlLS7t1RTHk	Klhl6	kelch-like 6	0.3577	9.9080	4.3113	0.0007	0.0176	-0.3538
B6o0UUSVJ0L39368tQ	4833439L19Rik	RIKEN cDNA 4833439L19 gene	0.2748	9.1628	4.3109	0.0007	0.0176	-0.3545
r3SHslXg7d51g9eHll	H2-Ab1	histocompatibility 2 class II antigen A beta 1	0.8964	10.8137	4.3100	0.0007	0.0176	-0.3563
9UNTaLIB1dDgs6rSK0	Trim56	tripartite motif-containing 56	0.3637	9.0629	4.3068	0.0007	0.0177	-0.3625
6tUS_UU3W6f4DhRRTw	Eno2	enolase 2 gamma neuronal	0.2773	8.8794	4.3033	0.0007	0.0177	-0.3693
TV_c3RBcXlU7ESr,0A	Maob	monoamine oxidase B	0.4760	9.4764	4.3028	0.0007	0.0177	-0.3703
Bi8rNJ5cDtD7vEIdeg	Pf4	platelet factor 4	0.3467	9.0130	4.3021	0.0007	0.0177	-0.3717
ioUpHY17d7iDsx,Od0	Igf2bp3	insulin-like growth factor 2 mRNA binding protein 3	-0.4129	9.1974	-4.3021	0.0007	0.0177	-0.3717
HpbfUvcUmBAOKH0ElY	Dusp23	dual specificity phosphatase 23	0.3885	9.5147	4.2987	0.0007	0.0178	-0.3783
xuf3khccygl,SuW9E4	Bves	blood vessel epicardial substance	0.4917	9.1645	4.2978	0.0007	0.0178	-0.3801
Np5KiF7ns0f4UgoICU	Ints6	integrator complex subunit 6	0.3414	8.7884	4.2963	0.0007	0.0179	-0.3829
01F71J7uJ9OPu4Qd3U	Dram1	DNA-damage regulated autophagy modulator 1	0.4661	9.2530	4.2961	0.0007	0.0179	-0.3833
cUUhKEd7ofRRaSAndQ	Clspn	claspin	-0.6593	9.5353	-4.2911	0.0007	0.0180	-0.3931
u6lp3_tG4lW,knk1,U	Ldhd	lactate dehydrogenase D	0.6514	9.1166	4.2906	0.0007	0.0180	-0.3940
EoWlP7D1I7EkTd6It0	Lbp	lipopolysaccharide binding protein	0.2947	9.1286	4.2885	0.0007	0.0180	-0.3980
Zp56N9CncBJOlVz1PM	Rin1	Ras and Rab interactor 1	0.3251	8.7907	4.2884	0.0007	0.0180	-0.3982
0XKR6jBJRf5CVDV9VI	Lamc3	laminin gamma 3	-0.4251	9.1913	-4.2878	0.0007	0.0180	-0.3995
HmlxopdBiC3,shp_D8	Tob1	transducer of ErbB-2,1	0.4278	10.2614	4.2871	0.0007	0.0180	-0.4009
rEpVB6Ko3FYBV69EeA	Rab43	RAB43 member RAS oncogene family	0.2805	9.0235	4.2866	0.0007	0.0180	-0.4019
fSV9aopCCVZlF2Jgn8	Dcp1a	DCP1 decapping enzyme homolog A (S, cerevisiae)	-0.3690	10.1499	-4.2844	0.0007	0.0181	-0.4060
ZE3cEX0WO0U1J7eUOg	Sectm1a	secreted and transmembrane 1A	0.1895	8.6738	4.2840	0.0007	0.0181	-0.4069
9d7_O16RNVlHP0LESU	Scube2	signal peptide CUB domain EGF-like 2	0.3626	8.8856	4.2833	0.0007	0.0181	-0.4083
97UYuHv0W7X_76UTpg	Nr1h3	nuclear receptor subfamily 1 group H member 3	0.4447	9.2566	4.2807	0.0007	0.0182	-0.4132
Z4CDXgKCKUeiotKfCk	Fxyd5	FXYD domain-containing ion transport regulator 5	0.6028	9.2053	4.2793	0.0007	0.0182	-0.4160
uS80Tb_yQ7OOihtStQ	Raet1b	retinoic acid early transcript beta	-0.4464	9.1005	-4.2788	0.0007	0.0182	-0.4171
BJ54OrdNCtCmrGilJE	Sbsn	suprabasin	0.7463	9.5516	4.2787	0.0007	0.0182	-0.4173
WddRxJUgXXfOoXauEM	Wnt10b	wingless-type MMTV integration site family member 10B	0.7081	9.0916	4.2769	0.0007	0.0182	-0.4207
6VXhfQCO94rrfsCtlA	Col5a1	collagen type V alpha 1	0.7433	11.4607	4.2766	0.0007	0.0182	-0.4212
EFS7kgkbev7ssUnJGk	Ska2	spindle and kinetochore associated complex subunit 2	-0.2928	9.6816	-4.2755	0.0007	0.0182	-0.4234
B7VSVVKMTtI0Ioojuc	Zc3h14	zinc finger CCCH type containing 14	-0.3003	9.6289	-4.2709	0.0007	0.0184	-0.4323
lBNSlueeVCCFiJRCnA	Hist2h2ac	histone cluster 2 H2ac	-0.7824	14.8034	-4.2682	0.0007	0.0184	-0.4375

Probe ID	Gene symbol	Gene name	Log_2FC	Average expression	t	P, Value	Adj,P,Val	B
ZeJrerhjNe4_1olSLo	Wbp1l	WW domain binding protein 1 like	0.4914	12.3220	4.2643	0.0007	0.0185	-0.4451
Zk3lyiHUi0qk7XXfew	Oas1d	2'-5' oligoadenylate synthetase 1D	-0.6611	9.8855	-4.2639	0.0007	0.0185	-0.4460
Hmm,V4tuSL36j6aXeg	Gemin6	gem (nuclear organelle) associated protein 6	-0.3811	10.3328	-4.2633	0.0007	0.0185	-0.4472
NOs5aP6llN_kSYkolE	Map3k6	mitogen-activated protein kinase kinase kinase 6	-0.4200	9.7234	-4.2590	0.0007	0.0187	-0.4555
T6UNFf_h6gmc,1zKd0	Pip5k1b	phosphatidylinositol-4-phosphate 5-kinase type 1 beta	0.3981	9.7910	4.2560	0.0007	0.0188	-0.4612
idcnpHiD3Gq0Ugu5ek	Ippk	inositol 13456-pentakisphosphate 2-kinase	-0.5446	10.3895	-4.2553	0.0007	0.0188	-0.4627
9e_7Z5Lu3qhAlMIJc0	Pcyt1b	phosphate cytidylyltransferase 1 choline beta isoform	-0.3427	9.0134	-4.2540	0.0007	0.0188	-0.4652
c4JC7nL53gl_oXfo1U	Uap1l1	UDP-N-acteylglucosamine pyrophosphorylase 1-like 1	0.4718	9.7567	4.2500	0.0007	0.0189	-0.4729
iEUJ7HUpW4CviHq8kc	Paip2b	poly(A) binding protein interacting protein 2B	-0.5114	12.0745	-4.2497	0.0007	0.0189	-0.4736
o9dFILjr0vuKSV1JCE	2700094K13Rik	RIKEN cDNA 2700094K13 gene	-0.4097	13.6401	-4.2489	0.0007	0.0189	-0.4751
Eb5PA7bp9_tzjeiFQY	C87499	expressed sequence C87499	-0.7240	9.5563	-4.2489	0.0007	0.0189	-0.4752
3tHbTXUJMkLF8dKT5c	Gldn	gliomedin	-0.6257	9.3009	-4.2473	0.0007	0.0189	-0.4782
uZ9W,VTOImJfoLF6PQ	Mrps18b	mitochondrial ribosomal protein S18B	-0.2864	9.7355	-4.2459	0.0007	0.0189	-0.4810
K7a5BOSHR6IE2OIuS4	Stard10	START domain containing 10	0.2741	9.5804	4.2454	0.0007	0.0189	-0.4821
KStJ7yW3T6Uukk6kuU	Plxnd1	plexin D1	0.3533	9.8069	4.2442	0.0007	0.0189	-0.4843
Wd4pWArfcT4Wg5dQtw	Knop1	lysine rich nucleolar protein 1	-0.2659	10.3258	-4.2442	0.0007	0.0189	-0.4844
QW697g47iImfO7Croo	Tmem38b	transmembrane protein 38B	0.3835	9.7067	4.2440	0.0007	0.0189	-0.4848
WINVUrkeoFBt3jVRC4	Gsdmd	gasdermin D	0.3998	9.6518	4.2432	0.0007	0.0189	-0.4862
xVSXoFd40H56hcwbfl	Trp53inp2	transformation related protein 53 inducible nuclear protein 2	0.5876	10.2587	4.2414	0.0007	0.0190	-0.4898
fqqS500rn81sMQe07g	Dpp6	dipeptidylpeptidase 6	0.3092	8.9039	4.2376	0.0008	0.0191	-0.4972
i17B,lRP59aCSZEnt4	Osbpl3	oxysterol binding protein-like 3	0.4540	9.8246	4.2362	0.0008	0.0191	-0.4998
6MhLOh1L_SjcXxUo6s	Acot12	acyl-CoA thioesterase 12	0.1928	8.5016	4.2350	0.0008	0.0192	-0.5022
3uOEHT1NVJ,eOkzN_E	Fbxw13	F-box and WD-40 domain protein 13	-0.6394	9.3874	-4.2330	0.0008	0.0192	-0.5062
HSf0lPEu,Oe,qp1_lY	Mpdu1	mannose-P-dolichol utilization defect 1	0.2875	8.9672	4.2318	0.0008	0.0192	-0.5084
cWf7EgXpHe6uflghKE	Gar1	GAR1 ribonucleoprotein homolog (yeast)	-0.5616	11.8510	-4.2318	0.0008	0.0192	-0.5084
TJUqH514W0I6N,NlGk	Fbln1	fibulin 1	-0.5650	10.9754	-4.2270	0.0008	0.0194	-0.5179
BiyDse9ESbvuAqtdEU	Twsg1	twisted gastrulation homolog 1 (Drosophila)	0.3379	12.7127	4.2246	0.0008	0.0194	-0.5225
izD3S,jzUX5,eh_veA	Sdcbp	syndecan binding protein	0.3419	10.3289	4.2229	0.0008	0.0195	-0.5257
flSwBVEk6nO,cSj_xE	1810011O10Rik	RIKEN cDNA 1810011O10 gene	0.4394	8.9981	4.2226	0.0008	0.0195	-0.5263
fV7_qlB,99VHB974yU	Kbtbd7	kelch repeat and BTB (POZ) domain containing 7	-0.3841	9.7107	-4.2221	0.0008	0.0195	-0.5273

Probe ID	Gene symbol	Gene name	Log_2FC	Average expression	t	P, Value	Adj,P,Val	B
HhKuXzH_9y5PUK79Kk	Mmd2	monocyte to macrophage differentiation-associated 2	-0.4470	11.7666	-4.2220	0.0008	0.0195	-0.5276
NKrRUofaRpV3d74rfg	Tnc	tenascin C	0.2186	8.8190	4.2205	0.0008	0.0195	-0.5306
0rgkHAkWzCUkKZEiec	Fam210b	family with sequence similarity 210 member B	0.5135	9.1134	4.2194	0.0008	0.0195	-0.5325
BdXLqmAlKSN4OE17jU	Nnmt	nicotinamide N-methyltransferase	0.5105	9.7683	4.2194	0.0008	0.0195	-0.5327
fX_m3pQkSuve166hPg	Prmt7	protein arginine N-methyltransferase 7	-0.3697	9.5153	-4.2164	0.0008	0.0196	-0.5384
ot3rjXRQzrjHuF9KFU	5830428H23Rik	RIKEN cDNA 5830428H23 gene	-0.7229	10.3744	-4.2157	0.0008	0.0196	-0.5398
rixWAcxUlpNH6p3UgU	Pkp2	plakophilin 2	-0.3005	9.2784	-4.2154	0.0008	0.0196	-0.5405
cngMcwdoTkW5ZfbHlY	Srm	spermidine synthase	-0.5139	10.2130	-4.2139	0.0008	0.0196	-0.5433
3gKv9zh4nJ,3xqQip0	Ndst1	N-deacetylase/N-sulfotransferase (heparan glucosaminyl) 1	0.6047	9.7279	4.2126	0.0008	0.0196	-0.5460
HtO80ql53QGT3jd4nk	Cyp2s1	cytochrome P450 family 2 subfamily s polypeptide 1	-0.8413	10.3496	-4.2119	0.0008	0.0196	-0.5472
6nThXopESUkS4IpIPU	Ly6a	lymphocyte antigen 6 complex locus A	0.5710	10.5753	4.2112	0.0008	0.0196	-0.5486
HgUoX7N7ed7s79,kPg	Aqp1	aquaporin 1	0.6164	10.5178	4.2110	0.0008	0.0196	-0.5491
0X4IUgekl4Jid5EOeE	Ptn	pleiotrophin	0.4844	10.2393	4.2098	0.0008	0.0197	-0.5514
0rog4LIHSfV3SJe5WA	AI464131	expressed sequence AI464131	0.3938	8.9504	4.2024	0.0008	0.0199	-0.5658
KU3oZ53rfNJ3ddt8H8	Irx3	Iroquois related homeobox 3	-0.5578	11.2689	-4.1994	0.0008	0.0200	-0.5716
9,m_KEkWG0u50_KFFk	Ptges3l	prostaglandin E synthase 3 (cytosolic)-like	0.2833	8.8817	4.1986	0.0008	0.0200	-0.5731
HlSs6d3rpQHvosXhCg	Pola2	polymerase (DNA directed) alpha 2	-0.4144	9.6173	-4.1963	0.0008	0.0201	-0.5776
iUp,In4fXeIHoO6FfU	Eya3	eyes absent 3 homolog (Drosophila)	-0.2989	8.9905	-4.1950	0.0008	0.0201	-0.5802
KLF5Dar10EHXpV5ZJc	Foxl2	forkhead box L2	-0.2098	8.7262	-4.1901	0.0008	0.0203	-0.5898
EeQddH1EeIMMP4OwX4	H2-K1	histocompatibility 2 K1 K region	0.6959	9.7944	4.1896	0.0008	0.0203	-0.5906
QlLA3uKCi1CigFXgtE	Map1b	microtubule-associated protein 1B	-0.5432	10.7437	-4.1876	0.0008	0.0203	-0.5947
TSM6oa6dx,UixBaEe4	Hnrnph1	heterogeneous nuclear ribonucleoprotein H1	-0.4688	11.5821	-4.1875	0.0008	0.0203	-0.5949
Nis9rknnhVJQXnpAjQ	Ruvbl1	RuvB-like protein 1	-0.4476	11.2534	-4.1841	0.0008	0.0204	-0.6015
EXdXSH4l,EdKKv51CQ	Kdm2b	lysine (K)-specific demethylase 2B	-0.4654	10.1685	-4.1828	0.0008	0.0205	-0.6039
EcJJKGJ7i6n3kJaIKQ	Tceal3	transcription elongation factor A (SII)-like 3	0.1496	8.6360	4.1809	0.0008	0.0205	-0.6077
HVQV4,57gljyFEJSXl	Ermp1	endoplasmic reticulum metallopeptidase 1	0.4353	12.0501	4.1807	0.0008	0.0205	-0.6082
Ku37_,V3UD319,uRXk	Sox9	SRY (sex determining region Y)-box 9	0.4187	9.4573	4.1804	0.0008	0.0205	-0.6088
WfteXO_Ti0lqpEpwTo	Cldn1	claudin 1	-0.3850	9.1542	-4.1798	0.0008	0.0205	-0.6098
lWu3ofTm_u3kfid,u0	Sh3pxd2b	SH3 and PX domains 2B	0.4681	9.3894	4.1787	0.0008	0.0205	-0.6121
cp3tl0kg6OQtuX7o_U	Arhgap17	Rho GTPase activating protein 17	0.3577	11.9945	4.1780	0.0009	0.0205	-0.6133
fnUKPR6lKnq37X5T20	Nudc	nuclear distribution gene C homolog (Aspergillus)	-0.4202	13.6649	-4.1764	0.0009	0.0206	-0.6166
ExCywligJ5Cq4X3jf4	Nusap1	nucleolar and spindle associated protein 1	-0.6413	10.6902	-4.1763	0.0009	0.0206	-0.6168
EMIBm6gq5_VujIlo4k	Slc25a12	solute carrier family 25 (mitochondrial carrier Aralar) member 12	0.3042	9.3292	4.1755	0.0009	0.0206	-0.6183
orhAV_7h3wPujv1CVc	Rpl4	ribosomal protein L4	-0.3212	11.9632	-4.1722	0.0009	0.0207	-0.6246
oSLQ6OOfUoQNp9d1UU	Cpne2	copine II	0.1617	8.7780	4.1706	0.0009	0.0207	-0.6277

Probe ID	Gene symbol	Gene name	Log_2FC	Average expression	t	P, Value	Adj,P,Val	B
lVytJkFAo6AEHo0R5M	Kras	v-Ki-ras2 Kirsten rat sarcoma viral oncogene homolog	0.2774	8.9919	4.1701	0.0009	0.0207	-0.6287
KEk1JFfhV7jW1LQAUk	Rrp1b	ribosomal RNA processing 1 homolog B (S, cerevisiae)	-0.7097	10.8237	-4.1679	0.0009	0.0208	-0.6331
cbfsSBKpfT8rOAh4XU	Rftn2	raftlin family member 2	0.4428	9.6231	4.1678	0.0009	0.0208	-0.6334
NEZLYjf345_o3Qh7eU	Gtf2e2	general transcription factor II E polypeptide 2 (beta subunit)	-0.3536	11.1818	-4.1664	0.0009	0.0208	-0.6360
c56onte5ervs,6n6,k	Sohlh1	spermatogenesis and oogenesis specific basic helix-loop-helix 1	0.7334	9.6068	4.1663	0.0009	0.0208	-0.6361
EFEaNHikeOylXeQYfU	Tnc	tenascin C	0.9230	10.9988	4.1641	0.0009	0.0208	-0.6405
ErqodcTPY3q5T5Lkl4	3110082I17Rik	RIKEN cDNA 3110082I17 gene	-0.2842	9.2192	-4.1620	0.0009	0.0209	-0.6445
0JVL18iMqgSXV1FO4k	Mgll	monoglyceride lipase	0.2881	9.0539	4.1604	0.0009	0.0209	-0.6477
ieOLiSiC1RHe_4X_ro	Bves	blood vessel epicardial substance	0.4861	9.2217	4.1598	0.0009	0.0209	-0.6490
QV,Y6f_abR_xdLi15g	Plekhb2	pleckstrin homology domain containing family B (evectins) member 2	0.5365	9.5660	4.1597	0.0009	0.0209	-0.6491
9r54QOWnyd165wESTE	Kif18b	kinesin family member 18B	-0.4614	9.3771	-4.1580	0.0009	0.0210	-0.6524
Q3t9l0l5lHdqeuI6dl	Mpv17l	Mpv17 transgene kidney disease mutant-like	0.2784	9.0935	4.1575	0.0009	0.0210	-0.6533
rI8pXoRCYf4VIufVSI	Dtx4	deltex 4 homolog (Drosophila)	-0.2718	9.0558	-4.1552	0.0009	0.0210	-0.6578
uXivXjFCeh6ShuClOQ	Mrps5	mitochondrial ribosomal protein S5	-0.2479	9.5696	-4.1549	0.0009	0.0210	-0.6585
9SXh1LX1_Ls17pcTu0	Ddrgk1	DDRGK domain containing 1	0.3016	12.2502	4.1536	0.0009	0.0211	-0.6609
xVp6eUgjVh6KCVC7R8	Tgif1	TGFB-induced factor homeobox 1	-0.6283	9.5966	-4.1523	0.0009	0.0211	-0.6636
ob8WBuklEdQhWpA1Gl	Fbxw27	F-box and WD-40 domain protein 27	-0.6794	9.5749	-4.1518	0.0009	0.0211	-0.6645
fte1Dnj1f2DAj3K6R4	Tex261	testis expressed gene 261	0.2304	11.7754	4.1518	0.0009	0.0211	-0.6645
HRLB9Sut14u3p_MOV0	Myh10	myosin heavy polypeptide 10 non-muscle	-0.4722	10.8233	-4.1496	0.0009	0.0211	-0.6687
cvUSYLidXfqIueeQQE	Slc7a11	solute carrier family 7 (cationic amino acid transporter y+ system) member 11	-0.4213	8.9128	-4.1487	0.0009	0.0212	-0.6706
lU,HEpIehJEvcKvu,4	Uhrf1	ubiquitin-like containing PHD and RING finger domains 1	-0.8762	11.2216	-4.1481	0.0009	0.0212	-0.6717
Z6UT_Sblfe2IN71htI	S100a1	S100 calcium binding protein A1	0.4396	11.3926	4.1441	0.0009	0.0213	-0.6795
lnns3wXote2_XVWK3g	Fbxl6	F-box and leucine-rich repeat protein 6	-0.3038	10.7335	-4.1424	0.0009	0.0214	-0.6830
oUbHrE,8X3kmX1Se0c	Tmem107	transmembrane protein 107	-0.4034	10.2267	-4.1408	0.0009	0.0214	-0.6861
6TeGrbeX6MiYtCKOAU	Gnl3	guanine nucleotide binding protein-like 3 (nucleolar)	-0.5240	12.6403	-4.1401	0.0009	0.0214	-0.6873
TxQs3sFfiVchLPlN3o	Vldlr	very low density lipoprotein receptor	0.5318	11.0291	4.1400	0.0009	0.0214	-0.6876
lSglBRA9p67d7ekL_c	Klhl6	kelch-like 6	0.2770	9.6574	4.1383	0.0009	0.0214	-0.6908
9ptfTXjvNFA,ieFOV4	Farsb	phenylalanyl-tRNA synthetase beta subunit	-0.3978	12.3461	-4.1383	0.0009	0.0214	-0.6910
lJr0oU0fUnHNmqdOk0	Rab1b	RAB1B member RAS oncogene family	0.4559	10.4948	4.1377	0.0009	0.0214	-0.6921
Be6WJKEOKEuGFOeOKl	Kif4	kinesin family member 4	-0.3365	9.0146	-4.1374	0.0009	0.0214	-0.6927

Probe ID	Gene symbol	Gene name	Log_2FC	Average expression	t	P, Value	Adj,P,Val	B
Bgrd8WSiDaJLuy95ek	Tenm4	teneurin transmembrane protein 4	-0.7771	13.0202	-4.1366	0.0009	0.0214	-0.6942
c7d1iPsCbghJ5eh7Hg	H2-D1	histocompatibility 2 D region locus 1	0.4531	10.5830	4.1355	0.0009	0.0214	-0.6965
37zR09f60njWW5e6FU	Aprt	adenine phosphoribosyl transferase	-0.3724	12.5484	-4.1340	0.0009	0.0214	-0.6993
0ClAZ,epZNunZBJZCM	Rrad	Ras-related associated with diabetes	0.4843	9.2451	4.1335	0.0009	0.0214	-0.7003
Hleeu5Q0qNcE0qIofU	Ly6c1	lymphocyte antigen 6 complex locus C1	0.4751	10.6696	4.1334	0.0009	0.0214	-0.7004
0d_0XVIoLRv9RIHufU	Itpripl2	inositol 145-triphosphate receptor interacting protein-like 2	0.2022	9.1452	4.1329	0.0009	0.0214	-0.7015
KQhVJdlf_dN5IkK04I	Taf1d	TATA box binding protein (Tbp)-associated factor RNA polymerase I D	-0.4459	9.6715	-4.1321	0.0009	0.0214	-0.7030
oGXeXX191JdpXV9fXc	Bcam	basal cell adhesion molecule	0.1957	8.8928	4.1310	0.0009	0.0214	-0.7052
0V50TH97qeR7EFuoPI	Thsd1	thrombospondin type I domain 1	0.2533	8.8829	4.1309	0.0009	0.0214	-0.7053
coimR,Xiric6W606RU	Palm	paralemmin	0.4053	9.8373	4.1309	0.0009	0.0214	-0.7053
i5633PgVSNF8RfXqXg	Krt12	keratin 12	-0.3533	8.9921	-4.1300	0.0009	0.0215	-0.7071
KEu1_OHudOVC,VSdRo	Gm12538	predicted gene 12538	0.3099	8.6892	4.1296	0.0009	0.0215	-0.7079
xXYd,Zw6Qn_qZIe4q4	Ahnak2	AHNAK nucleoprotein 2	0.4702	9.1764	4.1283	0.0009	0.0215	-0.7105
6SSvkU7I6_n4leTSkE	Slc25a42	solute carrier family 25 member 42	-0.4724	9.3739	-4.1283	0.0009	0.0215	-0.7105
oXqP1VLfjn4KzqQul0	Rarb	retinoic acid receptor beta	0.1642	8.6018	4.1256	0.0009	0.0216	-0.7157
lq_HSp1ed1QKM5nkgA	Nrm	nurim (nuclear envelope membrane protein)	-0.5406	10.9592	-4.1224	0.0009	0.0217	-0.7219
x,9Guc1euceq7aop9c	Suv420h2	suppressor of variegation 4-20 homolog 2 (Drosophila)	0.5300	10.1409	4.1209	0.0010	0.0217	-0.7249
oZiHRS7XHtM7TFYqRU	Trmt61a	tRNA methyltransferase 61A	-0.4737	10.2011	-4.1198	0.0010	0.0217	-0.7270
0V9fSEw_EuvlPX6rEU	Rassf2	Ras association (RalGDS/AF-6) domain family member 2	0.4912	9.4858	4.1192	0.0010	0.0217	-0.7282
irYX146ii31zeTbnXo	Naa15	N(alpha)-acetyltransferase 15 NatA auxiliary subunit	-0.2707	9.2689	-4.1184	0.0010	0.0217	-0.7298
3SQ1wCvo6Mq57lir_U	Nqo2	NAD(P)H dehydrogenase quinone 2	0.4429	10.1807	4.1182	0.0010	0.0217	-0.7302
fijeAIQqedy52vV4gk	Sf3a3	splicing factor 3a subunit 3	-0.3165	12.2579	-4.1169	0.0010	0.0218	-0.7326
3ee,qf3gDjpCnlu1EA	Rpp30	ribonuclease P/MRP 30 subunit	-0.3724	10.8222	-4.1165	0.0010	0.0218	-0.7335
QVKuOOu5,Li937dx6I	Usp37	ubiquitin specific peptidase 37	-0.5210	10.6435	-4.1144	0.0010	0.0218	-0.7376
HriYUSlBSCaNFHXxOE	Polr2f	polymerase (RNA) II (DNA directed) polypeptide F	-0.3396	11.9237	-4.1108	0.0010	0.0220	-0.7446
BguHXKk9r6EoNDpTvA	Pon2	paraoxonase 2	0.6021	11.9763	4.1034	0.0010	0.0223	-0.7591
xVDuWrNxFIv8D9BF6M	Klk1	kallikrein 1	0.1996	8.7544	4.1026	0.0010	0.0223	-0.7606
xXrtfhZOOCCehdB7ho	S100a11	S100 calcium binding protein A11 (calgizzarin)	0.4277	13.8900	4.1024	0.0010	0.0223	-0.7610
Tfu5107lXUR5UUU,5E	Evi5l	ecotropic viral integration site 5 like	0.3048	9.2463	4.1017	0.0010	0.0223	-0.7624
W8Di_l6Zebu_RUnufo	Eif3d	eukaryotic translation initiation factor 3 subunit D	-0.3965	13.2536	-4.1011	0.0010	0.0223	-0.7635
ZbUxEgnTTVhfglitQU	Hsd17b2	hydroxysteroid (17-beta) dehydrogenase 2	0.3022	8.9192	4.1007	0.0010	0.0223	-0.7643

Probe ID	Gene symbol	Gene name	Log_2FC	Average expression	t	P, Value	Adj,P,Val	B
9inl_SOaCSE9eg1HSw	Cdk20	cyclin-dependent kinase 20	-0.6149	9.8902	-4.0971	0.0010	0.0224	-0.7714
rd79buePedenUZyQ94	Rab3d	RAB3D member RAS oncogene family	0.5698	10.6020	4.0970	0.0010	0.0224	-0.7716
ck8eV1Eb_eUvUAklHs	Cenpm	centromere protein M	-0.4753	9.4403	-4.0958	0.0010	0.0224	-0.7740
QspL7dD,l4NlEri5qU	Fxyd5	FXYD domain-containing ion transport regulator 5	0.6635	9.8652	4.0956	0.0010	0.0224	-0.7743
EV4gCCl415KeI6llfk	Srpx	sushi-repeat-containing protein	0.3303	9.4218	4.0951	0.0010	0.0224	-0.7754
fi5I25Av695,fqr73o	Gm5065	predicted gene 5065	-0.3784	8.9974	-4.0927	0.0010	0.0225	-0.7801
QNd3SN54B7_8m290ik	Mtmr11	myotubularin related protein 11	0.5050	9.2338	4.0906	0.0010	0.0225	-0.7842
BainOBWKh6IMJe6WAs	Emilin1	elastin microfibril interfacer 1	0.5132	9.6486	4.0902	0.0010	0.0225	-0.7849
Qq8PfPH64Ul637z_Tg	Ripply3	ripply3 homolog (zebrafish)	0.1875	8.6260	4.0902	0.0010	0.0225	-0.7850
rlaTqUWDFC5qyH,e8M	1700067K01Rik	RIKEN cDNA 1700067K01 gene	-0.3315	9.0493	-4.0900	0.0010	0.0225	-0.7853
9l1Lxs,x6ajx,ihSVc	Thg1l	tRNA-histidine guanylyltransferase 1-like (S, cerevisiae)	-0.3554	10.0033	-4.0841	0.0010	0.0228	-0.7969
KyXPyRBlvlLmUlxSQc	Tmem184a	transmembrane protein 184a	-0.6850	10.4512	-4.0830	0.0010	0.0228	-0.7991
ikqEj5XXrgq5iVEMuE	Cdc25c	cell division cycle 25C	-0.3272	9.0193	-4.0812	0.0010	0.0228	-0.8025
ohnL5SeXnXDsRS0ISA	Ddah1	dimethylarginine dimethylaminohydrolase 1	-0.5581	10.7496	-4.0800	0.0010	0.0229	-0.8049
Q6hFevkCU,sX_Kio5I	Acaa1a	acetyl-Coenzyme A acyltransferase 1A	0.4184	12.6736	4.0798	0.0010	0.0229	-0.8053
BYgS5wS7mdi041qfxg	Pip4k2a	phosphatidylinositol-5-phosphate 4-kinase type II alpha	0.5320	11.6751	4.0792	0.0010	0.0229	-0.8065
Enii9efs00SHKie3dI	Cdc7	cell division cycle 7 (S, cerevisiae)	-0.4969	10.3880	-4.0761	0.0010	0.0230	-0.8125
o0gdvVjUjUhEpMocgk	Rsrc2	arginine/serine-rich coiled-coil 2	-0.5674	11.7819	-4.0754	0.0010	0.0230	-0.8139
ZpOsnglR17kJTHoH0w	Rhobtb3	Rho-related BTB domain containing 3	-0.5894	11.5319	-4.0732	0.0010	0.0231	-0.8181
uR5Lo5dewnu116vk6I	Gm2589	predicted gene 2589	0.2816	8.9390	4.0726	0.0010	0.0231	-0.8194
Beuo70iezX_JSSUl3E	Gm1965	predicted gene 1965	-0.4012	8.9350	-4.0719	0.0011	0.0231	-0.8208
ZXHu5UUinT4RQdAB30	Hey2	hairy/enhancer-of-split related with YRPW motif 2	-0.5762	9.4067	-4.0698	0.0011	0.0231	-0.8249
6n36AK1_BTejrqS3pE	Shcbp1	Shc SH2-domain binding protein 1	-0.4873	9.4091	-4.0690	0.0011	0.0232	-0.8264
oRI6dtVTQXfQRJfafk	Mvp	major vault protein	0.4373	10.9338	4.0680	0.0011	0.0232	-0.8284
NRKDi4XWSgqOug7l4c	Khdc1c	KH domain containing 1C	-0.6907	9.7622	-4.0651	0.0011	0.0233	-0.8341
uogK26OS6lcxJtEtDk	Robo4	roundabout homolog 4 (Drosophila)	0.5843	10.5954	4.0623	0.0011	0.0234	-0.8396
xaEE2XOmyX3RLX_6G0	Wnt4	wingless-type MMTV integration site family member 4	0.7044	9.7160	4.0591	0.0011	0.0235	-0.8459
T7iSeeJpbmxNtFCrSc	Lmcd1	LIM and cysteine-rich domains 1	0.6386	10.2487	4.0534	0.0011	0.0238	-0.8570
Kt91YicTK,UIN0Cku4	Rbbp4	retinoblastoma binding protein 4	0.2143	9.3193	4.0516	0.0011	0.0238	-0.8605
E0o3U38VSkvrfX3ilE	Rad51ap1	RAD51 associated protein 1	-0.3250	9.0343	-4.0453	0.0011	0.0241	-0.8729
TtQgn4oTyhWc5feBW0	Sf3b3	splicing factor 3b subunit 3	-0.5796	11.3777	-4.0430	0.0011	0.0242	-0.8774
r5Azme6rUh1FdePbVI	Ethe1	ethylmalonic encephalopathy 1	0.4408	9.8597	4.0385	0.0011	0.0244	-0.8862

Probe ID	Gene symbol	Gene name	Log_2FC	Average expression	t	P, Value	Adj,P,Val	B
3efUx7ovv598vreFXU	Nucks1	nuclear casein kinase and cyclin-dependent kinase substrate 1	-0.2583	9.9184	-4.0379	0.0011	0.0244	-0.8873
6ovVXkELY6Xn4VAWcc	Eif2b5	eukaryotic translation initiation factor 2B subunit 5 epsilon	0.2740	9.9723	4.0371	0.0011	0.0244	-0.8889
ZpvqNGs9_XxbuznZ3c	Fam221a	family with sequence similarity 221 member A	-0.2796	9.1750	-4.0354	0.0011	0.0244	-0.8923
uu4EZE4hcSGtGdXR1c	Dapk1	death associated protein kinase 1	0.2405	8.7957	4.0353	0.0011	0.0244	-0.8925
9REfTDump7US6rl,5M	B4galt6	UDP-Gal:betaGlcNAc beta 14-galactosyltransferase polypeptide 6	-0.2497	8.9529	-4.0341	0.0011	0.0245	-0.8948
TqnneUzYgTwfXhIHu8	Mre11a	meiotic recombination 11 homolog A (S, cerevisiae)	-0.4256	9.8401	-4.0332	0.0011	0.0245	-0.8965
fae83t0tsT1L9L6xH4	Gch1	GTP cyclohydrolase 1	-0.6491	11.5881	-4.0279	0.0011	0.0247	-0.9070
oGFUqK06vn8N7nT4KY	Phf3	PHD finger protein 3	-0.4715	11.1092	-4.0257	0.0012	0.0248	-0.9113
ctFQIMcCx5LXs9Eeok	Mtmr2	myotubularin related protein 2	0.2993	9.1300	4.0254	0.0012	0.0248	-0.9119
fKKvx7rQ04e1d5KiHk	Dennd2c	DENN/MADD domain containing 2C	-0.2183	9.0978	-4.0237	0.0012	0.0249	-0.9151
WgnoUR5fVM2,eOeh9U	Pla2g15	phospholipase A2 group XV	0.5347	11.5634	4.0224	0.0012	0.0249	-0.9177
93E0HzlyiSSslR7QKk	Camkk1	calcium/calmodulin-dependent protein kinase kinase 1 alpha	0.2381	8.5855	4.0189	0.0012	0.0251	-0.9247
fQjR_n54iREZ3djVJY	Eprs	glutamyl-prolyl-tRNA synthetase	-0.4437	10.0500	-4.0177	0.0012	0.0251	-0.9269
EXpeLd1wFffJQrpIe4	B3gnt8	UDP-GlcNAc:betaGal beta-13-N-acetylglucosaminyltransferase 8	0.3827	9.2189	4.0156	0.0012	0.0252	-0.9311
HgeUi37Ruve7rtuoqI	Aldh4a1	aldehyde dehydrogenase 4 family member A1	0.4408	9.1797	4.0150	0.0012	0.0252	-0.9323
uV,eR8DF4SXvY2e5dY	Grb10	growth factor receptor bound protein 10	0.3340	11.6542	4.0129	0.0012	0.0252	-0.9364
6VnCKOzhN0dHufnqtc	Cyp2d22	cytochrome P450 family 2 subfamily d polypeptide 22	0.5058	10.5077	4.0127	0.0012	0.0252	-0.9368
9rfP1K0ojpw1EckJco	Tbx3	T-box 3	0.5619	9.4419	4.0073	0.0012	0.0255	-0.9473
xE3aZ4SN6mt_FW7p78	Tspan17	tetraspanin 17	0.4482	8.9514	4.0064	0.0012	0.0255	-0.9491
6cq6n_knurMph3ffFw	Ahnak	AHNAK nucleoprotein (desmoyokin)	0.7053	9.8398	4.0052	0.0012	0.0255	-0.9515
x5bk6AXoqJ6zbnQsTQ	Espl1	extra spindle pole bodies 1 (S, cerevisiae)	-0.3604	9.0243	-4.0049	0.0012	0.0255	-0.9521
Tl_TR3qeuOd7ineBRA	Nlrp9c	NLR family pyrin domain containing 9C	-0.5120	9.0706	-4.0046	0.0012	0.0255	-0.9527
0R,0hPjHBu5V0nniQk	Odc1	ornithine decarboxylase structural 1	-0.5823	12.7417	-4.0032	0.0012	0.0256	-0.9553
lNNUBTl3_KwT_4ngBI	Spc25	SPC25 NDC80 kinetochore complex component homolog (S, cerevisiae)	-0.4392	9.5038	-3.9974	0.0012	0.0258	-0.9667
Wie7kCiCeq1H1N_300	Islr	immunoglobulin superfamily containing leucine-rich repeat	0.6252	9.8391	3.9949	0.0012	0.0259	-0.9716
3t48AFcPN5dV31U0t0	Parva	parvin alpha	0.4640	11.1499	3.9944	0.0012	0.0259	-0.9726
9UHF4oG6fy6eiEeoOU	Ecm1	extracellular matrix protein 1	1.4632	11.1809	3.9936	0.0012	0.0260	-0.9742
TLdyhXp6LKj6_1_k0M	Sct	secretin	-0.5756	9.5250	-3.9898	0.0012	0.0261	-0.9816
BUk2ECAn2mQSitT344	Heph	hephaestin	-0.5954	10.6756	-3.9898	0.0012	0.0261	-0.9816
ZlEeVe5yE2XrtREOEM	Coro1a	coronin actin binding protein 1A	0.2019	8.7926	3.9869	0.0012	0.0262	-0.9873

Probe ID	Gene symbol	Gene name	Log_2FC	Average expression	t	P, Value	Adj,P,Val	B
xjhH3NJ0HQJexIcZKI	Ifi27l2a	interferon alpha-inducible protein 27 like 2A	1.1875	11.0497	3.9796	0.0013	0.0266	-1.0016
cRYCK0l6Pdi8iK40Eo	Rgs17	regulator of G-protein signaling 17	-0.3155	9.0590	-3.9776	0.0013	0.0267	-1.0056
lqHtEEmCdyQcJk63fU	Fbxw26	F-box and WD-40 domain protein 26	-0.5519	9.1836	-3.9743	0.0013	0.0268	-1.0120
KTSURSpFUlDASAu8SU	Bmp1	bone morphogenetic protein 1	0.4875	11.5859	3.9734	0.0013	0.0268	-1.0139
EiJN,CJ0CREHkR0Slc	Sec14l1	SEC14-like 1 (S, cerevisiae)	0.2396	8.9228	3.9727	0.0013	0.0268	-1.0152
xK,V_6kBJJxGff17nE	Elavl2	ELAV (embryonic lethal abnormal vision Drosophila)-like 2 (Hu antigen B)	-0.5524	9.9731	-3.9718	0.0013	0.0268	-1.0169
6rjkwQJIc9cS6hFeFU	Unc119	unc-119 homolog (C, elegans)	0.3131	9.3822	3.9718	0.0013	0.0268	-1.0170
QRV1F0300iSryvqOjY	Ccnd3	cyclin D3	0.5427	11.3333	3.9715	0.0013	0.0268	-1.0176
iR3G4GJuRAsjn6ekAo	Rerg	RAS-like estrogen-regulated growth-inhibitor	0.4961	11.3929	3.9706	0.0013	0.0269	-1.0194
xW7Qp6KKG4oN4GUy5A	Coro1a	coronin actin binding protein 1A	0.3827	9.5455	3.9685	0.0013	0.0270	-1.0235
KnqkrVeRPTTgcxCOKc	B3gnt9	UDP-GlcNAc:betaGal beta-13-N-acetylglucosaminyltransferase 9	0.4703	9.7897	3.9663	0.0013	0.0270	-1.0278
ow5,M3ep3wu1FQB0pU	Irak1	interleukin-1 receptor-associated kinase 1	0.2807	10.1407	3.9650	0.0013	0.0270	-1.0303
ZlLThuQu4EN971U5uo	Nek5	NIMA (never in mitosis gene a)-related expressed kinase 5	0.2514	8.7024	3.9643	0.0013	0.0270	-1.0317
EphJLiA8nvi3yXVr_w	Brca2	breast cancer 2	-0.4330	9.2702	-3.9638	0.0013	0.0270	-1.0326
TdUm6ThJWImfUgXoQg	Arpc1b	actin related protein 2/3 complex subunit 1B	0.8233	10.3135	3.9637	0.0013	0.0270	-1.0328
KXWvvg3rc4bh1F4nbo	Eif2b4	eukaryotic translation initiation factor 2B subunit 4 delta	-0.3771	11.3131	-3.9636	0.0013	0.0270	-1.0330
0aefqhSbteSL8dZeig	Ccnd3	cyclin D3	0.2136	8.9904	3.9634	0.0013	0.0270	-1.0334
ESXxLiih50hyEe97VU	8030451A03Rik	RIKEN cDNA 8030451A03 gene	-0.2600	8.9515	-3.9594	0.0013	0.0272	-1.0412
rSC6knuuuXfqCiSDxE	H2-K2	histocompatibility 2 K region locus 2	0.5361	11.9331	3.9578	0.0013	0.0273	-1.0444
cfUj98d_dCpXTRucXI	Ugt1a6b	UDP glucuronosyltransferase 1 family polypeptide A6B	0.6137	9.4502	3.9574	0.0013	0.0273	-1.0452
BhQU9eqvnqBALo7NOk	Cdca5	cell division cycle associated 5	-0.5927	9.5201	-3.9553	0.0013	0.0274	-1.0493
cgiO3pdXnnaCTdBC_Y	Far1	fatty acyl CoA reductase 1	-0.3961	9.7683	-3.9530	0.0013	0.0274	-1.0538
fYaKrUmCkiM4JFL0R4	Wfdc10	WAP four-disulfide core domain 10	-1.1149	10.6277	-3.9528	0.0013	0.0274	-1.0542
6noKJMju0FFwO3iER4	Gm13084	predicted gene 13084	-0.7261	9.7064	-3.9514	0.0013	0.0274	-1.0570
TRetyCuKsfdKDIdCdU	Nudt5	nudix (nucleoside diphosphate linked moiety X)-type motif 5	-0.3861	11.1983	-3.9512	0.0013	0.0274	-1.0573
ucju,wKpO,L1ixuboQ	Slc39a6	solute carrier family 39 (metal ion transporter) member 6	-0.3519	10.5846	-3.9511	0.0013	0.0274	-1.0576
WnVPR3Unt99eX0,gh0	Irf6	interferon regulatory factor 6	-0.2659	9.2958	-3.9505	0.0013	0.0274	-1.0588
HfAlIdeGE5SV,UESLs	Tdrd12	tudor domain containing 12	-0.5747	9.4243	-3.9505	0.0013	0.0274	-1.0588
3zJXp7Gg9ELi,iVLro	Rrm2	ribonucleotide reductase M2	-0.3447	8.9898	-3.9502	0.0013	0.0274	-1.0593

Probe ID	Gene symbol	Gene name	Log_2FC	Average expression	t	P, Value	Adj,P,Val	B
9VUpRfu,N6f4Rt79Ko	Lrg1	leucine-rich alpha-2-glycoprotein 1	0.4600	8.9516	3.9428	0.0014	0.0278	-1.0740
Kcs_FcINeIlTM7,U4k	Spc25	SPC25 NDC80 kinetochore complex component homolog (S, cerevisiae)	-0.4329	9.5770	-3.9422	0.0014	0.0278	-1.0751
ru5lFGlLq1,33yPZf4	Kif15	kinesin family member 15	-0.5139	9.6981	-3.9416	0.0014	0.0278	-1.0763
c1a1feeX,8X7Jyp0lU	Trp53	transformation related protein 53	-0.4272	10.2199	-3.9408	0.0014	0.0279	-1.0778
ZTojlR7jHKlJAufEso	Polr1a	polymerase (RNA) I polypeptide A	-0.2792	9.4092	-3.9359	0.0014	0.0281	-1.0874
xT4RP2tS7J7Ezqu6GE	Fat1	FAT tumor suppressor homolog 1 (Drosophila)	-0.5581	11.6347	-3.9341	0.0014	0.0282	-1.0910
KngvLS6FKc7gdFNX_k	Gstcd	glutathione S-transferase C-terminal domain containing	-0.2010	8.7114	-3.9316	0.0014	0.0283	-1.0960
Z,_FUi3Q_VfVJlAhkc	Prpf3	PRP3 pre-mRNA processing factor 3 homolog (yeast)	-0.2657	8.9637	-3.9289	0.0014	0.0284	-1.1012
Kvd7lfRoDgnmFSAfUo	Tnxb	tenascin XB	0.4329	8.9887	3.9289	0.0014	0.0284	-1.1012
NqeFkuufnsCXRP76F0	Gmip	Gem-interacting protein	0.2744	9.2720	3.9282	0.0014	0.0284	-1.1026
fefX3l4uH,qxChIh6E	Shbg	sex hormone binding globulin	-0.5756	9.2095	-3.9280	0.0014	0.0284	-1.1030
cvQL9KFe9,nz_ROtF8	Srxn1	sulfiredoxin 1 homolog (S, cerevisiae)	0.4568	9.1804	3.9240	0.0014	0.0286	-1.1107
u70PneUV_HpZK42LXk	Las1l	LAS1-like (S, cerevisiae)	-0.3060	9.3857	-3.9229	0.0014	0.0286	-1.1129
ZFokbkH3eTQezrpbqc	Dhx58	DEXH (Asp-Glu-X-His) box polypeptide 58	0.2222	8.6515	3.9223	0.0014	0.0286	-1.1141
oKJsk,kySo_5ezce7U	Gcnt2	glucosaminyl (N-acetyl) transferase 2 I-branching enzyme	0.2914	9.3381	3.9191	0.0014	0.0287	-1.1204
EodTTnUURVYpfH8q68	Polr1e	polymerase (RNA) I polypeptide E	-0.3924	9.9381	-3.9190	0.0014	0.0287	-1.1206
ZEaR5a0RU558glwl3k	Eng	endoglin	0.4569	9.6236	3.9190	0.0014	0.0287	-1.1207
fVrp9hF_AFDiAoGZkk	Rasip1	Ras interacting protein 1	0.4008	8.8836	3.9176	0.0014	0.0288	-1.1234
EqEqVN,rSrPa01hDl8	Igfbp4	insulin-like growth factor binding protein 4	0.7611	11.7341	3.9141	0.0014	0.0290	-1.1303
0LSjdTfxVKS_t9feKU	Rad51ap1	RAD51 associated protein 1	-0.2627	8.8953	-3.9104	0.0015	0.0292	-1.1375
Hv_nbauJfjqCuSzfug	Mtf2	metal response element binding transcription factor 2	-0.4970	11.7750	-3.9091	0.0015	0.0292	-1.1400
QtNXl1fslIvSme3rrk	Egfl7	EGF-like domain 7	0.6529	11.5309	3.9073	0.0015	0.0293	-1.1435
ZCs,xG7Xj,lGF6M_Cc	Hnrnpab	heterogeneous nuclear ribonucleoprotein A/B	-0.2810	14.0830	-3.9027	0.0015	0.0295	-1.1527
xmOaxQRZGC7sSPVLyE	Lynx1	Ly6/neurotoxin 1	0.1810	8.5943	3.9021	0.0015	0.0295	-1.1539
K6yE6ylV_ezPj7HnVk	Irak4	interleukin-1 receptor-associated kinase 4	0.2452	8.8077	3.9018	0.0015	0.0295	-1.1544
N6ojm1KAh8tXeJXoEc	Tmem63a	transmembrane protein 63a	0.3956	9.5091	3.9017	0.0015	0.0295	-1.1547
le4_xuDfLT4Jlrir54	Skap2	src family associated phosphoprotein 2	0.3410	11.0223	3.9013	0.0015	0.0295	-1.1555
ERTqXJxIgo76x3tOtE	Sgcb	sarcoglycan beta (dystrophin-associated glycoprotein)	0.4362	10.3739	3.8961	0.0015	0.0298	-1.1656
fVNu6iEiklg_U4qIoA	Timeless	timeless circadian clock 1	-0.5001	9.6916	-3.8957	0.0015	0.0298	-1.1664
0TMn1SO11_56AVI3qU	S1pr2	sphingosine-1-phosphate receptor 2	0.4007	11.3855	3.8955	0.0015	0.0298	-1.1668
uVd_3HR1ypv3_WP,g4	Adrbk1	adrenergic receptor kinase beta 1	0.3695	11.1102	3.8953	0.0015	0.0298	-1.1672
Er1fqXqpL,H6UgJLv4	Mdn1	midasin homolog (yeast)	-0.5207	9.8092	-3.8936	0.0015	0.0298	-1.1704
cpGiLm_77NeCLQBfmo	Wnk4	WNK lysine deficient protein kinase 4	0.2978	9.1735	3.8932	0.0015	0.0298	-1.1713

Probe ID	Gene symbol	Gene name	Log_2FC	Average expression	t	P, Value	Adj,P,Val	B
0GoK6ugvv6fWz9Tm5Y	Nras	neuroblastoma ras oncogene	-0.3363	12.4724	-3.8931	0.0015	0.0298	-1.1714
EU1e5KPunn,O797huI	Entpd6	ectonucleoside triphosphate diphosphohydrolase 6	-0.2870	9.1189	-3.8930	0.0015	0.0298	-1.1716
KrVfkBIec,PoXyhIlo	Klf2	Kruppel-like factor 2 (lung)	0.4102	9.7685	3.8916	0.0015	0.0298	-1.1744
NXunk,ThS_jeA5eqnU	Tmem9b	TMEM9 domain family member B	0.3142	10.7128	3.8894	0.0015	0.0299	-1.1787
lj3ksnfwCRJr6MkJ4c	Actr3	ARP3 actin-related protein 3	0.4474	11.3395	3.8889	0.0015	0.0299	-1.1798
0KSXU2dJ3RUCSyWRR4	Chmp4b	charged multivesicular body protein 4B	0.6976	10.4567	3.8863	0.0015	0.0301	-1.1849
0S5edLLh,3T4EqdxHI	Ppl	periplakin	0.4266	9.0779	3.8856	0.0015	0.0301	-1.1862
9RJeqCpL2nkuCAiIoI	Cnnm1	cyclin M1	-0.2271	8.7528	-3.8851	0.0015	0.0301	-1.1872
rewxdeFOLTQcRaEE,U	Usp3	ubiquitin specific peptidase 3	0.4437	11.0695	3.8813	0.0015	0.0303	-1.1946
rtXtP,S73_zt7s7veI	Aurkb	aurora kinase B	-0.3484	9.5170	-3.8813	0.0015	0.0303	-1.1947
0dE3qlTyRXf16_ugLk	Cercam	cerebral endothelial cell adhesion molecule	0.3957	10.4959	3.8809	0.0015	0.0303	-1.1955
Be,7F59,HLeVy5TUUk	Sin3a	transcriptional regulator SIN3A (yeast)	-0.5910	11.3684	-3.8803	0.0015	0.0303	-1.1967
WaQi7JHKP_r4JyspLo	Hist2h2aa1	histone cluster 2 H2aa1	0.2405	8.7106	3.8787	0.0015	0.0303	-1.1999
0l30xLfTEgfOhXSDXs	BC028528	cDNA sequence BC028528	0.3547	9.4291	3.8762	0.0016	0.0305	-1.2048
9lJJKaGC4aA050EP2E	Vamp5	vesicle-associated membrane protein 5	0.3414	9.0884	3.8755	0.0016	0.0305	-1.2061
ENOOSoo5HRHZNZRFRI	Ppp3cc	protein phosphatase 3 catalytic subunit gamma isoform	-0.3501	10.0788	-3.8733	0.0016	0.0306	-1.2103
WdHtIop6rutO4_,QCU	Riok1	RIO kinase 1 (yeast)	-0.3969	10.1908	-3.8723	0.0016	0.0306	-1.2123
fegNclOadFldOebves	Adck5	aarF domain containing kinase 5	-0.4590	10.9422	-3.8705	0.0016	0.0307	-1.2160
Hl4hHDijkJ_tCzpRSU	Gypc	glycophorin C	0.2033	9.3244	3.8693	0.0016	0.0307	-1.2183
HVRdIEk1PfvfR14Sik	Nol8	nucleolar protein 8	-0.6470	10.7024	-3.8688	0.0016	0.0307	-1.2193
idXuOrhf7se7fq1PM4	Rab15	RAB15 member RAS oncogene family	0.2773	9.1642	3.8685	0.0016	0.0307	-1.2197
QqS7LfJB67M,8zrv7M	Enpp2	ectonucleotide pyrophosphatase/phosphodiesterase 2	0.4598	8.7329	3.8673	0.0016	0.0307	-1.2223
iqF_,wlY_S6lMJ6g_U	Lpcat2	lysophosphatidylcholine acyltransferase 2	0.2248	8.6017	3.8671	0.0016	0.0307	-1.2226
NlxizMaH7voi7uzs8U	Cdc6	cell division cycle 6	-0.3665	9.2614	-3.8668	0.0016	0.0307	-1.2232
9Wlbp72Gll8ifsHLJQ	Nbl1	neuroblastoma suppression of tumorigenicity 1	0.5318	10.9397	3.8667	0.0016	0.0307	-1.2233
9gB4f1G7OZOWFsWW68	Hgsnat	heparan-alpha-glucosaminide N-acetyltransferase	0.5090	11.5513	3.8656	0.0016	0.0308	-1.2256
HX8soGOJEOXodXGKV4	Mthfd1	methylenetetrahydrofolate dehydrogenase (NADP+ dependent) methenyltetrahydrofolate cyclohydrolase formyltetrahydrofolate synthase	-0.2786	10.2688	-3.8646	0.0016	0.0308	-1.2274
0ok15OljVBJ,e8CSEU	Tspan11	tetraspanin 11	0.4335	8.8380	3.8642	0.0016	0.0308	-1.2283
9iR7ej4t1LV9EVCnpQ	Nuak2	NUAK family SNF1-like kinase 2	0.2961	8.7699	3.8617	0.0016	0.0309	-1.2332
rIimeoAl6SGV4EtyIs	Cwc22	CWC22 spliceosome-associated protein homolog (S, cerevisiae)	-0.2934	10.1639	-3.8602	0.0016	0.0310	-1.2362
fVeEsAnvXSgB6OqXU4	Phf11d	PHD finger protein 11D	0.1998	9.1154	3.8598	0.0016	0.0310	-1.2369

Probe ID	Gene symbol	Gene name	Log_2FC	Average expression	t	P, Value	Adj,P,Val	B
rF6Ng01e556BOl6Bt0	Lig1	ligase I DNA ATP-dependent	-0.3395	9.0196	-3.8593	0.0016	0.0310	-1.2378
BeY8Sfj6e6o1FiInlc	Arl2bp	ADP-ribosylation factor-like 2 binding protein	0.4226	10.0203	3.8585	0.0016	0.0310	-1.2395
x6pHr1d3bfKDD_fk6k	Rcl1	RNA terminal phosphate cyclase-like 1	-0.3526	10.7098	-3.8553	0.0016	0.0312	-1.2459
QEkgpe75RQBV1V6zT4	Ly6e	lymphocyte antigen 6 complex locus E	0.3807	10.4147	3.8537	0.0016	0.0313	-1.2489
0XI6Ef791TpUc7l6zQ	3110057O12Rik	RIKEN cDNA 3110057O12 gene	0.3036	8.9141	3.8511	0.0016	0.0314	-1.2540
ro9wbe6PonsjtHhSb4	Col8a2	collagen type VIII alpha 2	0.2852	9.0798	3.8499	0.0016	0.0314	-1.2564
lZ,1pT0wVS1ujd6JeA	Snrpd1	small nuclear ribonucleoprotein D1	-0.4825	12.2555	-3.8478	0.0016	0.0316	-1.2606
WIEkRLPF20iV1HSV54	Cpne8	copine VIII	0.2438	8.6841	3.8471	0.0017	0.0316	-1.2620
3hRxBUQhXiKeW56zjM	Shmt1	serine hydroxymethyltransferase 1 (soluble)	-0.3616	9.0530	-3.8452	0.0017	0.0317	-1.2656
Tl,XXfCH4kilOvyavo	Slc23a3	solute carrier family 23 (nucleobase transporters) member 3	0.4293	10.0496	3.8390	0.0017	0.0320	-1.2779
6Ye7BA2_73e,1wXRbs	Slc8a1	solute carrier family 8 (sodium/calcium exchanger) member 1	-0.3171	9.1945	-3.8383	0.0017	0.0320	-1.2791
KgkDQvX71RLBQpN9dc	Ralgapb	Ral GTPase activating protein beta subunit (non-catalytic)	0.2102	10.6326	3.8379	0.0017	0.0320	-1.2801
lo75HFUeXtVd64AwI0	Flot2	flotillin 2	0.3598	10.7950	3.8374	0.0017	0.0320	-1.2810
0p6fV,7ec_7Agxwb9U	Magee1	melanoma antigen family E 1	0.3512	10.0258	3.8371	0.0017	0.0320	-1.2817
ik9pJGOBMKFM3CrGSQ	5430435G22Rik	RIKEN cDNA 5430435G22 gene	0.5282	9.3571	3.8369	0.0017	0.0320	-1.2819
lCTVIjeoVZdBUsXhxg	Ocel1	occludin/ELL domain containing 1	0.2711	9.0235	3.8361	0.0017	0.0320	-1.2835
EICi1OaCCvpcMuTOq0	Cbr1	carbonyl reductase 1	0.3796	10.2295	3.8358	0.0017	0.0320	-1.2842
iUcxJceWC1rxKYOkR8	Usp2	ubiquitin specific peptidase 2	-0.3856	9.2559	-3.8339	0.0017	0.0321	-1.2879
oWJXZSQ0_ztLTv_77A	Atp12a	ATPase H+/K+ transporting nongastric alpha polypeptide	1.7945	9.1769	3.8323	0.0017	0.0322	-1.2910
3pegISgJS3XECqDoI0	Nr5a2	nuclear receptor subfamily 5 group A member 2	-0.7701	10.0683	-3.8304	0.0017	0.0323	-1.2947
W7nugpB3uTue6KI6l0	Sfrp1	secreted frizzled-related protein 1	0.6559	10.8017	3.8302	0.0017	0.0323	-1.2951
lVaJLNv,nOO6byLF6I	Ptprk	protein tyrosine phosphatase receptor type K	0.3442	10.0198	3.8294	0.0017	0.0323	-1.2968
9V7oJ6oIQ0laCf50dI	Bub1b	budding uninhibited by benzimidazoles 1 homolog beta (S, cerevisiae)	-0.6639	9.9067	-3.8289	0.0017	0.0323	-1.2977
xxEK7xCRJ5I16lNAlQ	Bmpr2	bone morphogenetic protein receptor type II (serine/threonine kinase)	-0.3852	8.9019	-3.8270	0.0017	0.0324	-1.3013
fX_l2u5ykU06k_3310	H2-DMa	histocompatibility 2 class II locus DMa	0.3281	8.9943	3.8250	0.0017	0.0325	-1.3054
oX63T5,3ea4d9953jI	Ncam1	neural cell adhesion molecule 1	0.1498	8.5221	3.8246	0.0017	0.0325	-1.3061
HuTHuwhde,wi,hcA7E	Sfrp4	secreted frizzled-related protein 4	1.6505	9.4111	3.8232	0.0017	0.0325	-1.3089
ffcYomnh_k9_14I4JE	Cbx3	chromobox 3	-0.4417	11.9937	-3.8230	0.0017	0.0325	-1.3094
EtQQ5TnShJeqHit_58	Bpifb4	BPI fold containing family B member 4	-0.8684	10.4616	-3.8197	0.0017	0.0327	-1.3159

Probe ID	Gene symbol	Gene name	Log_2FC	Average expression	t	P, Value	Adj,P,Val	B
6Bf,A4l4xe79JP6Ub4	Ptpre	protein tyrosine phosphatase receptor type E	-0.4224	10.3014	-3.8154	0.0018	0.0330	-1.3242
6V9AJEEQ1So5etHtVI	Hdac7	histone deacetylase 7	0.3070	9.3201	3.8141	0.0018	0.0330	-1.3267
ZiFVP_e7nH058CLeik	Mis18a	MIS18 kinetochore protein homolog A (S, pombe)	-0.5685	11.4412	-3.8120	0.0018	0.0332	-1.3309
f0KwsSj73bKDKa_e14	Gabrb3	gamma-aminobutyric acid (GABA) A receptor subunit beta 3	0.2430	8.7236	3.8091	0.0018	0.0333	-1.3366
x7dIvLxSfX4,TcxEOM	Arfgef2	ADP-ribosylation factor guanine nucleotide-exchange factor 2 (brefeldin A-inhibited)	0.2811	8.6846	3.8091	0.0018	0.0333	-1.3366
ZgKlCl6H35QlScd97o	Tenm4	teneurin transmembrane protein 4	-0.8696	13.1702	-3.8089	0.0018	0.0333	-1.3370
Zr3yjPtSdA7SFdLyk4	Mtch2	mitochondrial carrier homolog 2 (C, elegans)	0.2584	10.0106	3.8060	0.0018	0.0334	-1.3426
HlGRK7mLqE1TnUNAqM	Dennd5a	DENN/MADD domain containing 5A	0.2804	11.2011	3.8034	0.0018	0.0336	-1.3479
clC4N1Y5Oh3p7XYRoc	Doc2b	double C2 beta	0.3428	9.3243	3.8017	0.0018	0.0337	-1.3512
unsbni63z3cefabqnU	Dcp1a	DCP1 decapping enzyme homolog A (S, cerevisiae)	-0.4491	9.9813	-3.8014	0.0018	0.0337	-1.3518
0XBKf8ESu1N1He1Wt0	Tmbim6	transmembrane BAX inhibitor motif containing 6	0.3774	13.3063	3.8009	0.0018	0.0337	-1.3527
HiS0l9SFE764J5RJRQ	Cast	calpastatin	0.2146	8.7656	3.7999	0.0018	0.0337	-1.3548
BiecHE3Id3ee3g0SSo	Kank3	KN motif and ankyrin repeat domains 3	0.4862	10.5716	3.7983	0.0018	0.0338	-1.3579
leJjSlJ76,80pKMvTU	Psip1	PC4 and SFRS1 interacting protein 1	-0.6697	11.6272	-3.7979	0.0018	0.0338	-1.3586
Njt5DIdJfe4cHXBwUk	Mocs2	molybdenum cofactor synthesis 2	0.4124	11.1196	3.7959	0.0018	0.0339	-1.3626
QA9eaT,kpJP1vJpppo	Snrpb	small nuclear ribonucleoprotein B	-0.2511	9.8064	-3.7954	0.0018	0.0339	-1.3636
K4J8IBVQglViiehLro	Dusp22	dual specificity phosphatase 22	0.1964	8.8568	3.7947	0.0018	0.0339	-1.3650
cdF5IJS,v6U7hD7Xu8	Tek	endothelial-specific receptor tyrosine kinase	0.4527	9.9203	3.7945	0.0018	0.0339	-1.3652
TiaIZuv,kvn7pLJI7k	Sdk1	sidekick homolog 1 (chicken)	0.2681	8.8482	3.7932	0.0018	0.0340	-1.3679
BcIQUm3iiU4lAkqP5I	Aif1	allograft inflammatory factor 1	0.2886	9.2403	3.7915	0.0018	0.0340	-1.3713
cw4p70AP2j,S03YReU	Sox17	SRY (sex determining region Y)-box 17	0.1760	8.6812	3.7909	0.0018	0.0341	-1.3724
rqnH3JbjBFYEktHrSQ	Tbc1d2b	TBC1 domain family member 2B	0.3910	9.8051	3.7902	0.0019	0.0341	-1.3737
ZkREKFUVuqcHF5aIuI	Rab31	RAB31 member RAS oncogene family	0.2505	8.8608	3.7891	0.0019	0.0341	-1.3759
6oTRN3dC49JAk_lxeI	Rbpms	RNA binding protein gene with multiple splicing	0.3043	9.4702	3.7887	0.0019	0.0341	-1.3768
KoxXPLq6nuO6dbj5cU	Zkscan1	zinc finger with KRAB and SCAN domains 1	-0.2837	9.8069	-3.7862	0.0019	0.0343	-1.3816
QP0ijsae4XqtoamXXU	Gm8909	predicted gene 8909	0.2860	8.8919	3.7856	0.0019	0.0343	-1.3828
3n_VBgOygFBMh1S,tU	Aicda	activation-induced cytidine deaminase	-0.2078	8.6971	-3.7830	0.0019	0.0343	-1.3880
EnUkhQeVQgoegAlouQ	Rarres2	retinoic acid receptor responder (tazarotene induced) 2	0.3884	13.0262	3.7826	0.0019	0.0343	-1.3887
QpM4vJ1LkYEnHS75W4	Strap	serine/threonine kinase receptor associated protein	-0.3368	12.2246	-3.7825	0.0019	0.0343	-1.3890

Probe ID	Gene symbol	Gene name	Log_2FC	Average expression	t	P, Value	Adj,P,Val	B
uepWKt31zdsKAqCD5E	Pik3ip1	phosphoinositide-3-kinase interacting protein 1	-0.5191	9.8910	-3.7825	0.0019	0.0343	-1.3890
ZpRU14QXiCqTMQqh30	Sh3tc1	SH3 domain and tetratricopeptide repeats 1	0.3782	9.1081	3.7823	0.0019	0.0343	-1.3894
uA6_E0yIW7FumVkClo	Txnl4a	thioredoxin-like 4A	-0.4585	11.4558	-3.7819	0.0019	0.0343	-1.3901
QriYVx17hS71zl5nSl	Zfp296	zinc finger protein 296	-0.4563	8.9678	-3.7819	0.0019	0.0343	-1.3902
lWsfXulH0k6xHkfe6M	Nqo2	NAD(P)H dehydrogenase quinone 2	0.4400	10.6431	3.7806	0.0019	0.0344	-1.3926
xvnq,ligHseZURS4Q4	Tfdp1	transcription factor Dp 1	-0.4103	10.7938	-3.7802	0.0019	0.0344	-1.3934
9tx0E81M498XjU5Pz8	Cript	cysteine-rich PDZ-binding protein	0.3645	8.8104	3.7795	0.0019	0.0344	-1.3948
cpSx,nAUaBUK6c6a9Q	Gm10052	heterogeneous nuclear ribonucleoprotein A1 pseudogene	-0.4352	11.8646	-3.7767	0.0019	0.0346	-1.4003
NLkLtGq7anXmKwIbno	Wnt4	wingless-type MMTV integration site family member 4	0.8095	10.4972	3.7754	0.0019	0.0346	-1.4028
xvngnfeirdLVRQaUu8	Cdk5rap2	CDK5 regulatory subunit associated protein 2	-0.8768	10.7236	-3.7750	0.0019	0.0346	-1.4037
0U99HWV3X_MTH9gOsA	2310022B05Rik	RIKEN cDNA 2310022B05 gene	0.3502	11.3294	3.7749	0.0019	0.0346	-1.4038
cXkf8DXtC4j7slFSlc	Ttc30b	tetratricopeptide repeat domain 30B	0.3479	9.4638	3.7746	0.0019	0.0346	-1.4045
EiPoHkTo_kdf0VShdY	Car14	carbonic anhydrase 14	-0.3657	8.9723	-3.7737	0.0019	0.0346	-1.4063
Klx7_UhH8UCnlCtfnc	Faah	fatty acid amide hydrolase	0.3140	9.0313	3.7730	0.0019	0.0346	-1.4076
ohLmhdAKrJ0pKOL9t4	Slc52a3	solute carrier protein family 52 member 3	0.2257	8.9763	3.7691	0.0019	0.0349	-1.4153
TjVnaXTufdKQTTSUsg	Blm	Bloom syndrome RecQ helicase-like	-0.5629	9.9403	-3.7678	0.0019	0.0349	-1.4180
ZWghyWyc9oD3hXQhMU	Enpp2	ectonucleotide pyrophosphatase/phosphodiesterase 2	0.8622	9.9729	3.7660	0.0019	0.0350	-1.4214
xeIu1wUeu30,MVT,0c	Ifi205	interferon activated gene 205	0.2619	8.6802	3.7635	0.0020	0.0352	-1.4264
9hrSgEeg5gu6tOJNSo	Mlf1	myeloid leukemia factor 1	-0.7057	11.2073	-3.7605	0.0020	0.0354	-1.4323
l4PWRc,3QldAhA4vXo	Nipsnap3b	nipsnap homolog 3B (C, elegans)	0.3246	9.7314	3.7595	0.0020	0.0354	-1.4343
Thbro57lufvt4u_,7o	Cyld	cylindromatosis (turban tumor syndrome)	0.3510	10.9966	3.7590	0.0020	0.0354	-1.4352
oeJCSR106TSdeXcr14	Zfp2	zinc finger protein 2	-0.3467	9.3962	-3.7589	0.0020	0.0354	-1.4353
cu6ofefX9E_uf9TzlI	Brwd3	bromodomain and WD repeat domain containing 3	-0.2037	9.0163	-3.7586	0.0020	0.0354	-1.4360
lk1FT9SqhPcEeeBLSc	Neu3	neuraminidase 3	-0.3726	8.9491	-3.7581	0.0020	0.0354	-1.4370
uHeKz2uSeeFUlBeekA	Ruvbl1	RuvB-like protein 1	-0.5076	11.2079	-3.7575	0.0020	0.0354	-1.4381
KWBUjfXcu1D0v5Iw4o	Rhbdl3	rhomboid veinlet-like 3 (Drosophila)	0.1886	8.6977	3.7567	0.0020	0.0354	-1.4397
EeIKEAp_nRUU5Kfugk	Ip6k2	inositol hexaphosphate kinase 2	-0.2173	9.5390	-3.7552	0.0020	0.0355	-1.4426
uNyXgi1OKSldLT,okQ	Incenp	inner centromere protein	-0.3777	9.7320	-3.7548	0.0020	0.0355	-1.4435
ZhdXp75JftSF3iWLF4	Tmem223	transmembrane protein 223	0.2469	10.9538	3.7541	0.0020	0.0355	-1.4449
oniuu4yK3usBJIHyrk	Serpina5	serine (or cysteine) peptidase inhibitor clade A member 5	-1.2871	11.0827	-3.7526	0.0020	0.0356	-1.4477
c6Ot449EuiFe8HHO2E	Rps3	ribosomal protein S3	-0.4334	14.3049	-3.7501	0.0020	0.0358	-1.4528
EsXrZ6UYobCBKQPD7g	Ntn4	netrin 4	-0.4298	8.7947	-3.7485	0.0020	0.0358	-1.4559

Probe ID	Gene symbol	Gene name	Log_2FC	Average expression	t	P, Value	Adj,P,Val	B
6I4nRQnaIoIYEq_uWY	Pacsin1	protein kinase C and casein kinase substrate in neurons 1	-0.1961	8.6166	-3.7479	0.0020	0.0358	-1.4570
BgHk4wginiJb0h6SN8	Myo1b	myosin IB	-0.3622	9.7259	-3.7479	0.0020	0.0358	-1.4571
NCVOC014K4KHtVeeF0	Gstt1	glutathione S-transferase theta 1	0.3447	10.4567	3.7470	0.0020	0.0358	-1.4587
3akQXpeeC6eC,6yBPU	Dmkn	dermokine	0.3490	9.6105	3.7464	0.0020	0.0358	-1.4600
TAK9x3qe,l,Q,EiruU	Nanos1	nanos homolog 1 (Drosophila)	-0.4104	9.1896	-3.7463	0.0020	0.0358	-1.4601
KXdouAWF6Hk,_gAooE	Pinx1	PIN2/TERF1 interacting telomerase inhibitor 1	-0.2894	9.3532	-3.7447	0.0020	0.0359	-1.4633
0dFtlOnWxZ30ed5mec	Gsn	gelsolin	0.4253	9.0176	3.7425	0.0020	0.0360	-1.4677
HF_d14vrPXjBld6zRI	Fkbp4	FK506 binding protein 4	-0.4563	12.8722	-3.7423	0.0020	0.0360	-1.4679
oPE5K3u7N_TwP9SXfs	3632451O06Rik	RIKEN cDNA 3632451O06 gene	0.3505	9.4434	3.7418	0.0020	0.0361	-1.4691
3n0VeT_4top,Sv146g	Cd72	CD72 antigen	0.4753	8.8432	3.7405	0.0020	0.0361	-1.4715
TfInyLTrXRpHvnmdrE	Ccar1	cell division cycle and apoptosis regulator 1	-0.4553	11.1598	-3.7386	0.0021	0.0362	-1.4753
HaU0_oIilX635AfzlU	Gm10125	predicted gene 10125	0.5384	10.6763	3.7383	0.0021	0.0362	-1.4758
rSgKigpijkqeyehx0s	Plxnd1	plexin D1	0.4263	10.5156	3.7381	0.0021	0.0362	-1.4764
uXqStLw6,oj0c103sU	Mycbp	c-myc binding protein	0.3253	10.6466	3.7380	0.0021	0.0362	-1.4765
rHekX9EEk8SL5Ck9go	Arg2	arginase type II	-0.3815	9.0193	-3.7335	0.0021	0.0365	-1.4853
lVIueIuzielxev0,pc	Aqr	aquarius	-0.1533	8.6071	-3.7331	0.0021	0.0365	-1.4861
WIATeV9zfBJ78f8DAE	Efhd1	EF hand domain containing 1	0.3135	8.7610	3.7291	0.0021	0.0367	-1.4941
i7d1HZ6th6pO9f6AZs	Ormdl3	ORM1-like 3 (S, cerevisiae)	0.3163	12.0037	3.7289	0.0021	0.0367	-1.4944
Q6jV33ru3ghBBLtdEw	Slc11a1	solute carrier family 11 (proton-coupled divalent metal ion transporters) member 1	0.5353	11.3956	3.7279	0.0021	0.0368	-1.4963
xh,RuroK90GfpfqjB0	Polr3g	polymerase (RNA) III (DNA directed) polypeptide G	-0.1718	8.7231	-3.7277	0.0021	0.0368	-1.4968
H04PCZ7v46reoeRHtI	Nup93	nucleoporin 93	-0.3620	10.4703	-3.7270	0.0021	0.0368	-1.4982
ZVJ59fv0uxd3DnrpD0	Gprasp1	G protein-coupled receptor associated sorting protein 1	-0.6030	12.6491	-3.7268	0.0021	0.0368	-1.4985
9lIMBULSJO57SL_qEk	Arhgef25	Rho guanine nucleotide exchange factor (GEF) 25	0.2369	8.7438	3.7251	0.0021	0.0368	-1.5018
lNiNfadVCmeQqOC6fg	Cdca8	cell division cycle associated 8	-0.5507	9.8001	-3.7251	0.0021	0.0368	-1.5019
uin0zr,u1PXX22DwJ4	Smarca5-ps	SWI/SNF related matrix associated actin depenent ragulator of chromatin subfamily a member 5 pseudogene	-0.5808	10.7974	-3.7223	0.0021	0.0370	-1.5074
NHUrUKDUOV33p97iVY	Il27ra	interleukin 27 receptor alpha	0.2708	9.1342	3.7218	0.0021	0.0370	-1.5085
TVV_Pnd6jjQsgtDATk	Msrb1	methionine sulfoxide reductase B1	0.4882	9.5511	3.7197	0.0021	0.0371	-1.5125
l4YrJRFGUUfpTBAd5M	Uba7	ubiquitin-like modifier activating enzyme 7	0.3587	10.3574	3.7194	0.0021	0.0371	-1.5130
lU9Op_sl960XS17p3w	Wnt5a	wingless-type MMTV integration site family member 5A	0.7224	10.4107	3.7183	0.0021	0.0372	-1.5153
KXfTV90,WLRczQ6nhE	Mpv17l2	MPV17 mitochondrial membrane protein-like 2	0.5732	10.4028	3.7171	0.0021	0.0372	-1.5177
WUw1xVL9XBQqa5MmEI	Hcn1	hyperpolarization-activated cyclic nucleotide-gated K+ 1	-0.2322	8.6707	-3.7169	0.0021	0.0372	-1.5181
QeeeleUUR910u06UhE	AU021092	expressed sequence AU021092	0.5436	9.4565	3.7166	0.0021	0.0372	-1.5186

Probe ID	Gene symbol	Gene name	Log_2FC	Average expression	t	P, Value	Adj,P,Val	B
NpjCE,vvSo,rDupeR0	Glud1	glutamate dehydrogenase 1	0.4023	9.9814	3.7146	0.0022	0.0373	-1.5225
T_J9uMCgLer999SDVo	Cpa3	carboxypeptidase A3 mast cell	0.1923	8.6339	3.7136	0.0022	0.0374	-1.5245
3UXknpTWQYYonQQnvo	Hist1h2af	histone cluster 1 H2af	-0.5316	14.8584	-3.7098	0.0022	0.0376	-1.5319
cdR46ByiLf77qI7l0k	Rfc2	replication factor C (activator 1) 2	-0.3523	10.9751	-3.7087	0.0022	0.0376	-1.5341
ZpR4Ow,iV,udHAEKNE	Il10rb	interleukin 10 receptor beta	0.5617	9.4105	3.7086	0.0022	0.0376	-1.5343
0I5Lg2oCSLqSKikle8	Unk	unkempt homolog (Drosophila)	-0.2124	9.2819	-3.7086	0.0022	0.0376	-1.5344
HCWNZ1EtdJ_h6TVBDs	Arpc1a	actin related protein 2/3 complex subunit 1A	0.3621	11.1428	3.7069	0.0022	0.0377	-1.5377
6pfhXgosUoKCAojofo	Srxn1	sulfiredoxin 1 homolog (S, cerevisiae)	0.3207	8.8237	3.7066	0.0022	0.0377	-1.5382
cLqxnuXuuGuvImOeBA	Htatip2	HIV-1 tat interactive protein 2 homolog (human)	0.5871	10.7702	3.7063	0.0022	0.0377	-1.5388
QdeXF0tMXe7kufTry8	Slc25a45	solute carrier family 25 member 45	0.5640	10.0527	3.7057	0.0022	0.0377	-1.5401
0SXnDonnVeAgjnv1Co	Nop2	NOP2 nucleolar protein	-0.2719	9.3432	-3.7049	0.0022	0.0378	-1.5417
re360XoFZ0p_BFvOqI	Pwp2	PWP2 periodic tryptophan protein homolog (yeast)	-0.3057	9.7074	-3.7037	0.0022	0.0378	-1.5439
TMlehqI7LqS13C6Dpw	Pycrl	pyrroline-5-carboxylate reductase-like	-0.4181	10.6247	-3.7021	0.0022	0.0379	-1.5471
iCoKL1S1QNLlEnldrk	Cd248	CD248 antigen endosialin	0.1842	8.5667	3.7013	0.0022	0.0380	-1.5488
0kKBrE5lLolgVKi6Us	Timm21	tranlocase of inner mitochondrial membrane 21	-0.3717	11.0851	-3.6999	0.0022	0.0380	-1.5514
K27KzVK44qPqgU6lyU	Ramp1	receptor (calcitonin) activity modifying protein 1	0.3544	9.7862	3.6987	0.0022	0.0381	-1.5538
uimigoQ2_beK0rrTcU	Cygb	cytoglobin	0.4729	12.4059	3.6967	0.0022	0.0382	-1.5578
62V02Imo4LGKGU1L00	Ptp4a3	protein tyrosine phosphatase 4a3	0.3054	9.4114	3.6953	0.0022	0.0383	-1.5606
9Cvo2lolf11LYh,wV4	Dab2ip	disabled 2 interacting protein	0.3761	10.3667	3.6943	0.0022	0.0383	-1.5625
BHUJru1ebl,soV,kYE	Hoxa5	homeobox A5	0.2871	8.8561	3.6933	0.0023	0.0383	-1.5644
Nmh10YORErfSov4e18	Dmkn	dermokine	0.3754	9.7087	3.6932	0.0023	0.0383	-1.5646
WUoafcChDgBcidF9NU	Plxdc1	plexin domain containing 1	0.6866	9.7876	3.6931	0.0023	0.0383	-1.5648
oVSxVuKwveNHkL_K0k	Ypel2	yippee-like 2 (Drosophila)	0.3235	9.8762	3.6928	0.0023	0.0383	-1.5654
TSU7eF9UeIBE70,O40	Pex14	peroxisomal biogenesis factor 14	0.3316	10.3637	3.6927	0.0023	0.0383	-1.5655
3cTpAVTXu,9cH_lIFM	Wls	wntless homolog (Drosophila)	0.4799	10.4790	3.6926	0.0023	0.0383	-1.5657
9lJU0FW9fPn3r_id6k	Abcf2	ATP-binding cassette sub-family F (GCN20) member 2	-0.4784	11.5978	-3.6923	0.0023	0.0383	-1.5664
6gUhOfV3V4ySP45cec	Vcan	versican	-0.4301	9.1275	-3.6918	0.0023	0.0383	-1.5673
Zaf30n_61clpxc5bEU	Fam115c	family with sequence similarity 115 member C	0.4329	9.4126	3.6907	0.0023	0.0383	-1.5695
BN4uJ_O72Ode1Tv830	Lrtm1	leucine-rich repeats and transmembrane domains 1	0.1708	8.6069	3.6899	0.0023	0.0384	-1.5711
0UgpNU5eCicF0iy0KU	Cracr2b	calcium release activated channel regulator 2B	0.1906	8.7063	3.6864	0.0023	0.0386	-1.5779
WSKKX6b5yj5tL,Xv5E	Mid1ip1	Mid1 interacting protein 1 (gastrulation specific G12-like (zebrafish))	-1.0042	11.7650	-3.6858	0.0023	0.0386	-1.5792

Probe ID	Gene symbol	Gene name	Log_2FC	Average expression	t	P, Value	Adj,P,Val	B
3R5QKJd3s4fnqQIr4k	Cluap1	clusterin associated protein 1	-0.2284	9.9305	-3.6816	0.0023	0.0389	-1.5875
cUUr5FLOg0v8V7kjDo	Pkp2	plakophilin 2	-0.3566	10.6155	-3.6809	0.0023	0.0389	-1.5889
uaRUstO6KOCnWnCCV8	Ctnna3	catenin (cadherin associated protein) alpha 3	-0.1785	8.5986	-3.6806	0.0023	0.0389	-1.5895
QkkHjaY0jxKR1N1y9k	Tnfrsf19	tumor necrosis factor receptor superfamily member 19	0.1945	8.5792	3.6801	0.0023	0.0389	-1.5904
otLujo,vlO5H_o,7D4	Cdk2	cyclin-dependent kinase 2	-0.3804	11.6845	-3.6738	0.0023	0.0394	-1.6028
Q5Jale1daSRl3wpa4c	G0s2	G0/G1 switch gene 2	0.3409	9.3834	3.6737	0.0023	0.0394	-1.6030
r15qhfuba4yoDAHlV0	Lat2	linker for activation of T cells family member 2	0.3046	8.9769	3.6729	0.0023	0.0394	-1.6045
EfV77x3_iBXn3J6Fng	Hipk1	homeodomain interacting protein kinase 1	0.3195	9.0528	3.6723	0.0024	0.0394	-1.6058
9j6,Hp0AJdQnDjirkY	Neto2	neuropilin (NRP) and tolloid (TLL)-like 2	-0.3052	8.8423	-3.6722	0.0024	0.0394	-1.6059
cDSAtZeCPagkjp1ijU	Mar-02	membrane-associated ring finger (C3HC4) 2	0.3176	10.0941	3.6714	0.0024	0.0394	-1.6074
WCBOi6XdKeEuSRTSBo	Dnajc2	DnaJ (Hsp40) homolog subfamily C member 2	-0.5173	10.6543	-3.6700	0.0024	0.0395	-1.6102
rrf,E43397iXpc3un4	Tcl1b4	T cell leukemia/lymphoma 1B 4	-0.2730	8.8360	-3.6689	0.0024	0.0396	-1.6124
ZpJu3XS3pz7jf1TlCl	Slc25a15	solute carrier family 25 (mitochondrial carrier ornithine transporter) member 15	-0.5158	9.7658	-3.6671	0.0024	0.0397	-1.6159
Hh3g1R2iC,B3pstFlo	Cd14	CD14 antigen	0.2071	8.9474	3.6670	0.0024	0.0397	-1.6162
rWg7XRtx97pBFVJ,r0	Pold2	polymerase (DNA directed) delta 2 regulatory subunit	-0.5582	10.6268	-3.6669	0.0024	0.0397	-1.6165
ip790kNblKbp1KX9R0	Rwdd1	RWD domain containing 1	-0.2346	9.6039	-3.6662	0.0024	0.0397	-1.6177
uV0eiE0U6L8p_SEX4k	Prmt7	protein arginine N-methyltransferase 7	-0.4200	11.5908	-3.6659	0.0024	0.0397	-1.6183
orHq1,d7R2u0ujDu70	Gpc1	glypican 1	0.6389	11.8512	3.6653	0.0024	0.0397	-1.6195
xuyJlv4OeUKtXs3D1U	Erc2	ELKS/RAB6-interacting/CAST family member 2	0.1902	8.7523	3.6650	0.0024	0.0397	-1.6201
uVBXzVDDCFD6TllhTs	Spag5	sperm associated antigen 5	-0.4250	9.8839	-3.6627	0.0024	0.0398	-1.6247
3EklyB4Z,LpW3kiUDc	Clip2	CAP-GLY domain containing linker protein 2	0.2907	9.0821	3.6595	0.0024	0.0400	-1.6309
lll66Ki7yo6Cl5fH94	Mfsd7c	major facilitator superfamily domain containing 7C	0.4640	9.4091	3.6594	0.0024	0.0400	-1.6311
QBVbvJM1UltSiellOU	St8sia5	ST8 alpha-N-acetyl-neuraminide alpha-28-sialyltransferase 5	0.2236	8.7461	3.6576	0.0024	0.0401	-1.6347
9LEc,v6seO3ColEWuo	Gpr182	G protein-coupled receptor 182	0.1880	8.6033	3.6576	0.0024	0.0401	-1.6347
TgVVNQonuJPHldRG,k	Cenpm	centromere protein M	-0.3150	9.2594	-3.6569	0.0024	0.0402	-1.6361
Kh,QoCB2gX,pcTqom4	Ugt1a7c	UDP glucuronosyltransferase 1 family polypeptide A7C	0.1810	8.5334	3.6540	0.0024	0.0404	-1.6418
lQQJ0h_h1hvghzwXXk	Lig1	ligase I DNA ATP-dependent	-0.5892	10.1080	-3.6526	0.0024	0.0404	-1.6445
lS6h4cxMXfy7ve4Z50	Pigx	phosphatidylinositol glycan anchor biosynthesis class X	-0.2660	12.2355	-3.6511	0.0025	0.0405	-1.6476

Probe ID	Gene symbol	Gene name	Log_2FC	Average expression	t	P, Value	Adj,P,Val	B
QV46vnm7aB03Uoeygg	Lhfp	lipoma HMGIC fusion partner	0.4935	9.3175	3.6499	0.0025	0.0406	-1.6497
Ed4n9VeUf_E,R7k,yg	Insm1	insulinoma-associated 1	-0.2445	8.6760	-3.6492	0.0025	0.0406	-1.6512
K6TQf5wr3vu4omrumk	Gimap1	GTPase IMAP family member 1	0.2726	9.1335	3.6482	0.0025	0.0406	-1.6532
xVdg5prpUo,PtxNSXM	Alox5ap	arachidonate 5-lipoxygenase activating protein	0.3335	10.1541	3.6473	0.0025	0.0406	-1.6549
rqJR8oHXsdNfMlLv4o	Evx1	even skipped homeotic gene 1 homolog	-0.4070	8.9973	-3.6472	0.0025	0.0406	-1.6551
QkihhJ97ruLChPpEik	Tex9	testis expressed gene 9	-0.2204	8.9606	-3.6470	0.0025	0.0406	-1.6555
oIs5Olfcw17o545,qE	Brdt	bromodomain testis-specific	-0.4678	9.1312	-3.6469	0.0025	0.0406	-1.6557
BLfXdfv,Af_SPExg98	Slc3a2	solute carrier family 3 (activators of dibasic and neutral amino acid transport) member 2	0.3654	8.7892	3.6451	0.0025	0.0408	-1.6592
Wp,v5,4ISeKan6ddiI	Cotl1	coactosin-like 1 (Dictyostelium)	0.3296	10.5689	3.6444	0.0025	0.0408	-1.6606
QXjpdGhEh9S05ihJdM	Tmem63b	transmembrane protein 63b	0.5217	10.5396	3.6441	0.0025	0.0408	-1.6612
fRdutd9qlR9dLA_U18	Sf3b4	splicing factor 3b subunit 4	-0.3514	10.6407	-3.6426	0.0025	0.0409	-1.6642
9Us7nuunjfO7Rf5elE	Aldh4a1	aldehyde dehydrogenase 4 family member A1	0.5443	11.1779	3.6425	0.0025	0.0409	-1.6644
EA0YBB9V7O71QnWZX4	Ndufaf4	NADH dehydrogenase (ubiquinone) 1 alpha subcomplex assembly factor 4	-0.4814	11.1557	-3.6421	0.0025	0.0409	-1.6652
xleuLrfIEteXjH3sJU	Hsd11b1	hydroxysteroid 11-beta dehydrogenase 1	0.6188	9.1173	3.6414	0.0025	0.0409	-1.6665
QR54yrhXhAG,cXfVqE	Casp1	caspase 1	0.5333	9.7712	3.6397	0.0025	0.0410	-1.6700
QdXIddXoDoXoqnoIsc	Prim2	DNA primase p58 subunit	-0.3849	9.5511	-3.6390	0.0025	0.0410	-1.6714
3_Cjv0g56HvTF2fKOg	Ncald	neurocalcin delta	0.4549	9.5339	3.6375	0.0025	0.0411	-1.6742
BunH2AgpEoJP3w9FXE	Ncoa4	nuclear receptor coactivator 4	0.3153	9.0645	3.6365	0.0025	0.0412	-1.6763
9H_29K5KKUEO6KWdIE	Tnc	tenascin C	0.1880	8.5197	3.6355	0.0025	0.0412	-1.6782
BpSbx34eChIqRUDX8U	F13a1	coagulation factor XIII A1 subunit	0.3463	9.2088	3.6346	0.0025	0.0412	-1.6799
Ze4NxIIqrSniuvuF6M	Trit1	tRNA isopentenyltransferase 1	-0.2241	9.9425	-3.6345	0.0025	0.0412	-1.6802
KQkrooiUwkk3JSkvQo	Olfm1	olfactomedin 1	0.3086	9.4874	3.6340	0.0025	0.0412	-1.6810
HOKcUlFFUCIKUKnmh8	Rrp1b	ribosomal RNA processing 1 homolog B (S, cerevisiae)	-0.4579	9.4639	-3.6303	0.0026	0.0415	-1.6883
BUHkp9jxV7iXnk_eV4	Ldha	lactate dehydrogenase A	-0.5151	12.9951	-3.6297	0.0026	0.0415	-1.6895
uX_7XI_HxETJcidL,I	Zfand3	zinc finger AN1-type domain 3	0.3634	12.0201	3.6293	0.0026	0.0415	-1.6904
QVSrjEuUgQKeo6cY7E	Saraf	store-operated calcium entry-associated regulatory factor	0.4617	10.5128	3.6275	0.0026	0.0416	-1.6938
Hb70j3WsCYCUn_cw54	Rassf3	Ras association (RalGDS/AF-6) domain family member 3	0.4568	9.4818	3.6272	0.0026	0.0416	-1.6944
E9N5B7hbiIN591CtU	Pla2g1b	phospholipase A2 group IB pancreas	-0.4119	9.0890	-3.6267	0.0026	0.0416	-1.6954
Q5JYlUp9f3xT3s59Ro	Rbfox3	RNA binding protein fox-1 homolog (C, elegans) 3	-0.2199	8.8688	-3.6267	0.0026	0.0416	-1.6956
inFP,QLXphgu6ous6I	Ggct	gamma-glutamyl cyclotransferase	-0.3630	10.1205	-3.6260	0.0026	0.0417	-1.6969
39tVhSU9KOiP,5SQW4	Gm5065	predicted gene 5065	-0.2812	8.8631	-3.6246	0.0026	0.0417	-1.6997
3hCT1OkSZ1Xnt,FS_4	Rab8a	RAB8A member RAS oncogene family	0.4764	9.5120	3.6237	0.0026	0.0417	-1.7013

Probe ID	Gene symbol	Gene name	Log_2FC	Average expression	t	P, Value	Adj,P,Val	B
W17107X2Wox0FPF030	Alox5ap	arachidonate 5-lipoxygenase activating protein	0.3175	10.0305	3.6235	0.0026	0.0417	-1.7017
lVJ91KDAzXd9L9NIXQ	Lipa	lysosomal acid lipase A	0.4402	10.1080	3.6231	0.0026	0.0417	-1.7025
0nc6CA5dzurAq8XeTk	Nfib	nuclear factor I/B	0.5536	10.1385	3.6230	0.0026	0.0417	-1.7027
HnElNcHl0g0dC99R2s	Ccl9	chemokine (C-C motif) ligand 9	0.2992	9.4308	3.6224	0.0026	0.0418	-1.7040
NV4ooGd,8OEtJ3o8Vl	Vapb	vesicle-associated membrane protein associated protein B and C	0.3350	9.6794	3.6211	0.0026	0.0418	-1.7065
QgaN73R7hXQ931IO9I	Timm21	tranlocase of inner mitochondrial membrane 21	-0.4453	12.1003	-3.6211	0.0026	0.0418	-1.7066
oUuo767U67hPAhSgl4	Hus1	Hus1 homolog (S, pombe)	-0.2077	10.3256	-3.6201	0.0026	0.0419	-1.7086
onrknpTogJ4fp67rEg	Mat2a	methionine adenosyltransferase II alpha	-0.3975	12.6083	-3.6186	0.0026	0.0420	-1.7114
QggkspyTxEPf5xROF4	Tcf12	transcription factor 12	0.2087	9.2632	3.6181	0.0026	0.0420	-1.7123
lyid_6tSITNeqHiirg	Haghl	hydroxyacylglutathione hydrolase-like	0.3207	10.7214	3.6176	0.0026	0.0420	-1.7134
ZOkieX1t3_LUl0VC14	C4a	complement component 4A (Rodgers blood group)	0.4602	9.0881	3.6165	0.0026	0.0421	-1.7157
ibu0j_YoRf4c4fo9V4	Gprasp1	G protein-coupled receptor associated sorting protein 1	-0.5849	10.6417	-3.6152	0.0026	0.0421	-1.7182
B,n0e97u_ooQrWPe3U	Cp	ceruloplasmin	0.1780	8.6367	3.6149	0.0026	0.0421	-1.7188
urTbua6QQTyyUEn0ok	Sdsl	serine dehydratase-like	0.3637	10.4009	3.6149	0.0026	0.0421	-1.7188
HoJRqF1STYgLRehH1M	Rcan2	regulator of calcineurin 2	0.4001	9.0007	3.6107	0.0027	0.0424	-1.7270
cU4ifRpeSUiHfYTdQs	Mtbp	Mdm2 transformed 3T3 cell double minute p53 binding protein	-0.4140	9.5114	-3.6105	0.0027	0.0424	-1.7274
Z5ej51eJ2qDnuhdSF4	Ccdc85b	coiled-coil domain containing 85B	0.4722	10.0090	3.6090	0.0027	0.0425	-1.7303
WiruJiBI1FfdcrKNJ0	Emp2	epithelial membrane protein 2	0.4499	10.0233	3.6090	0.0027	0.0425	-1.7303
HV9hdVUEXeCU,zge04	Ybx2	Y box protein 2	-0.2922	9.0736	-3.6082	0.0027	0.0425	-1.7320
0V3g30,5GB34kLV_KM	Vstm2b	V-set and transmembrane domain containing 2B	0.2574	9.1171	3.6062	0.0027	0.0426	-1.7358
fDg_V_,4BucNDn6ui0	Cpa3	carboxypeptidase A3 mast cell	0.2460	8.6280	3.6056	0.0027	0.0427	-1.7370
B_Ieu3v021ShGkDgtI	Cd74	CD74 antigen (invariant polypeptide of major histocompatibility complex class II antigen-associated)	0.7302	10.5925	3.6052	0.0027	0.0427	-1.7379
fpE9k,oG3nSqXt4ue4	Cdc20	cell division cycle 20	-0.4710	9.5518	-3.6050	0.0027	0.0427	-1.7383
30VUeIeMTGXki8JOUs	B2m	beta-2 microglobulin	0.4547	13.5909	3.6021	0.0027	0.0429	-1.7438
WU5Ad0SQ7gifhC39AM	Sparc	secreted acidic cysteine rich glycoprotein	0.4218	9.3232	3.6017	0.0027	0.0429	-1.7447
ZfbdJL1FSCUk9QJAnU	Cp	ceruloplasmin	0.3630	9.3318	3.5986	0.0027	0.0431	-1.7507
NdN3VOtVNLeju3iasQ	Hmha1	histocompatibility (minor) HA-1	0.1819	8.7648	3.5986	0.0027	0.0431	-1.7508
EgZyRIn5TIl7gbfSBY	Sub1	SUB1 homolog (S, cerevisiae)	0.3262	9.7026	3.5971	0.0027	0.0432	-1.7538
QA57CW61NUvly5_q9Q	Aox3	aldehyde oxidase 3	0.6436	9.6829	3.5966	0.0027	0.0432	-1.7547
Qk3riHKgeqTPQlCJSU	Cacnb3	calcium channel voltage-dependent beta 3 subunit	0.4387	9.6126	3.5958	0.0027	0.0432	-1.7562
BXvrdgR0Ezj52NH8jI	4833439L19Rik	RIKEN cDNA 4833439L19 gene	0.7259	10.2459	3.5952	0.0027	0.0432	-1.7574

Probe ID	Gene symbol	Gene name	Log_2FC	Average expression	t	P, Value	Adj,P,Val	B
clDeCN,5Kgq447dB9E	Omt2b	oocyte maturation beta	-0.2864	8.9225	-3.5948	0.0028	0.0432	-1.7582
0lpxFCiLoS5EjMjg50	Creld2	cysteine-rich with EGF-like domains 2	-0.6266	11.1006	-3.5946	0.0028	0.0432	-1.7586
TV3IjxxTk4Pv,50xXs	Ifi47	interferon gamma inducible protein 47	0.3433	9.0121	3.5936	0.0028	0.0433	-1.7607
90KIC6796T21Untl4o	Rhobtb1	Rho-related BTB domain containing 1	-0.5202	9.8146	-3.5924	0.0028	0.0433	-1.7629
leHf1_X,x4k7AXWoaU	Ilf3	interleukin enhancer binding factor 3	-0.2814	9.4708	-3.5922	0.0028	0.0433	-1.7634
0hrtuv6DvDzZIoXrIo	Bcl7a	B cell CLL/lymphoma 7A	-0.3716	10.0395	-3.5909	0.0028	0.0434	-1.7659
Nm2NQS5LD9yX,ieEX0	Mfsd6	major facilitator superfamily domain containing 6	0.4444	10.1881	3.5908	0.0028	0.0434	-1.7660
lR,rVp1SXiOVREIq68	Gfpt2	glutamine fructose-6-phosphate transaminase 2	-0.3269	9.5617	-3.5892	0.0028	0.0435	-1.7693
ElloBpJQ0osQLdyeYk	Palld	palladin cytoskeletal associated protein	0.3501	9.1512	3.5884	0.0028	0.0435	-1.7708
QV5HqSKEhygl78tDA0	Prodh	proline dehydrogenase	-0.4192	9.4048	-3.5863	0.0028	0.0436	-1.7749
NdWr_l01On56Eg85J4	Farsb	phenylalanyl-tRNA synthetase beta subunit	-0.5206	12.0718	-3.5862	0.0028	0.0436	-1.7751
WVnVHN6n_HU6M8ACyA	Tnfsf12Tnfsf13	Tnfsf12-Tnfsf13 readthrough transcript	0.4997	10.5807	3.5862	0.0028	0.0436	-1.7751
QE_lulXqhiEK9F7Qug	Hfe	hemochromatosis	0.2602	8.8764	3.5834	0.0028	0.0438	-1.7806
Be1TmFO6GP0K54JhHA	Pacs2	phosphofurin acidic cluster sorting protein 2	0.3455	10.9255	3.5830	0.0028	0.0438	-1.7814
l_7UOeK151oDAZYRdU	Tmem53	transmembrane protein 53	0.4109	10.7302	3.5828	0.0028	0.0438	-1.7817
QXS1PXfn1QRwUJd6pQ	Strn4	striatin calmodulin binding protein 4	-0.2875	10.0538	-3.5823	0.0028	0.0438	-1.7827
rsHKB14leuLrflEteU	Hsd11b1	hydroxysteroid 11-beta dehydrogenase 1	0.4823	8.9914	3.5817	0.0028	0.0438	-1.7840
QUfrTHlLPiAdFljSSg	Ank3	ankyrin 3 epithelial	-0.2139	8.9081	-3.5816	0.0028	0.0438	-1.7841
36VlhFp6VNznBlJP6U	Plec	plectin	0.3478	9.1011	3.5812	0.0028	0.0438	-1.7849
xURo0eKR47KVd5Bh9c	Tnc	tenascin C	0.9964	11.2496	3.5812	0.0028	0.0438	-1.7850
3f1e9MpKJ7IoP,0xR4	Wipf1	WAS/WASL interacting protein family member 1	0.3942	9.4035	3.5796	0.0028	0.0439	-1.7881
QXkj97k257gXeOFcC8	Hat1	histone aminotransferase 1	-0.5037	12.9017	-3.5789	0.0028	0.0440	-1.7894
0,MF3t9XiV9PeJ7KUo	Ptbp1	polypyrimidine tract binding protein 1	-0.3644	12.7824	-3.5776	0.0028	0.0441	-1.7921
cl6Dfy3BggKuyhNXTU	Ptprz1	protein tyrosine phosphatase receptor type Z polypeptide 1	-0.2285	8.6302	-3.5768	0.0029	0.0441	-1.7937
EfX3kEpurRqdnb3f3k	Naca	nascent polypeptide-associated complex alpha polypeptide	-0.2435	11.6025	-3.5767	0.0029	0.0441	-1.7938
rFaKtEKBJJHSEs0hCl	6030419C18Rik	RIKEN cDNA 6030419C18 gene	0.2878	8.7333	3.5763	0.0029	0.0441	-1.7946
HX4FKDoV1I5SxApESQ	Wdr59	WD repeat domain 59	-0.3527	9.7038	-3.5754	0.0029	0.0441	-1.7964
3BKvfBFBTn3XI5ehUQ	Sirpb1a	signal-regulatory protein beta 1A	0.2178	8.6513	3.5736	0.0029	0.0442	-1.7999
lNcF_WVwSNILkXuV2Y	Slc25a18	solute carrier family 25 (mitochondrial carrier) member 18	0.5453	10.2249	3.5730	0.0029	0.0442	-1.8011
op6l_11F50DufUUFIl	Sptb	spectrin beta erythrocytic	0.2130	8.7025	3.5730	0.0029	0.0442	-1.8011
r_ifGql90KH3eUWPwc	Acaa2	acetyl-Coenzyme A acyltransferase 2 (mitochondrial 3-oxoacyl-Coenzyme A thiolase)	0.3666	12.0013	3.5717	0.0029	0.0443	-1.8036
cRdJ2C9fvJ7n7Psd0U	Cytip	cytohesin 1 interacting protein	0.2392	8.9532	3.5713	0.0029	0.0443	-1.8045

Probe ID	Gene symbol	Gene name	Log_2FC	Average expression	t	P, Value	Adj,P,Val	B
WgeNkdFQleAOkgrCCc	Gm3579	predicted gene 3579	0.1586	8.7067	3.5700	0.0029	0.0444	-1.8070
ToCFUGaCkrEN3ESSOk	Ascc1	activating signal cointegrator 1 complex subunit 1	-0.2270	9.8747	-3.5690	0.0029	0.0444	-1.8090
WlRz4PSycz50OX6S18	Naip1	NLR family apoptosis inhibitory protein 1	0.1624	8.5681	3.5684	0.0029	0.0444	-1.8102
rndOQO5ffLIKXodnXU	Plekha1	pleckstrin homology domain containing family A (phosphoinositide binding specific) member 1	-0.2764	9.0498	-3.5684	0.0029	0.0444	-1.8102
WlUWlDkeI1IUjYohAA	Gpr183	G protein-coupled receptor 183	0.1728	8.5925	3.5679	0.0029	0.0444	-1.8112
cAV10g8t2_0,seUDLQ	Megf10	multiple EGF-like-domains 10	0.6607	9.0093	3.5678	0.0029	0.0444	-1.8113
idMdKFc1cHXlWIQI1A	Fhdc1	FH2 domain containing 1	-0.4688	10.6445	-3.5639	0.0029	0.0448	-1.8191
TiZ_0VJ7kKHOAGGCG4	Trappc3	trafficking protein particle complex 3	0.4187	8.9575	3.5629	0.0029	0.0448	-1.8210
ceBJEI6uraqc0KUe6w	S100a16	S100 calcium binding protein A16	0.3834	9.0059	3.5611	0.0029	0.0450	-1.8246
Z6dF3x1pwCFwigL5Vw	Enpp2	ectonucleotide pyrophosphatase/phosphodiesterase 2	0.2732	8.6772	3.5604	0.0029	0.0450	-1.8259
WKpUt0kkhHexL,9DV4	Pcbp4	poly(rC) binding protein 4	0.3908	10.4709	3.5603	0.0029	0.0450	-1.8260
ohFhl3lRXNzn3d5tFE	Ddx39b	DEAD (Asp-Glu-Ala-Asp) box polypeptide 39B	-0.5068	12.3517	-3.5595	0.0030	0.0450	-1.8278
9QqLHtypxus17teQKs	Mrps18b	mitochondrial ribosomal protein S18B	-0.3382	11.2610	-3.5591	0.0030	0.0450	-1.8285
HXenoTnnL3v6df9zUo	Rab29	RAB29 member RAS oncogene family	0.3537	10.0531	3.5577	0.0030	0.0451	-1.8312
WO3oZrCSppCnZlClCE	Hist1h2ah	histone cluster 1 H2ah	-1.0137	13.7111	-3.5574	0.0030	0.0451	-1.8318
Q2oDh2PmoR7pooG2WQ	Ankrd35	ankyrin repeat domain 35	0.1754	8.7130	3.5573	0.0030	0.0451	-1.8320
W_qfdbXaZ_gsaN,,do	Brca1	breast cancer 1	-0.1835	8.7128	-3.5543	0.0030	0.0453	-1.8379
WnkU_,iezhDkWqzoVM	Nudt21	nudix (nucleoside diphosphate linked moiety X)-type motif 21	-0.4328	11.7751	-3.5539	0.0030	0.0453	-1.8386
rnNPp0x3dVaQRELUh4	Jun	jun proto-oncogene	0.4250	9.5408	3.5535	0.0030	0.0453	-1.8394
W3qBeecK4eyCC4IbSY	BC055324	cDNA sequence BC055324	-0.3112	8.9560	-3.5534	0.0030	0.0453	-1.8396
3SV6oJwpIo0guwJSXg	Cdc25a	cell division cycle 25A	-0.1683	8.5878	-3.5532	0.0030	0.0453	-1.8400
ThK6M3OL2KUl6txKt0	Prf1	perforin 1 (pore forming protein)	0.4931	10.3914	3.5520	0.0030	0.0453	-1.8424
fXUFSHSFff30Vxf3cs	Csrp1	cysteine and glycine-rich protein 1	0.4749	12.1704	3.5519	0.0030	0.0453	-1.8425
3Vd7uUInpdj0K_dPEs	Samd10	sterile alpha motif domain containing 10	-0.2379	9.1432	-3.5518	0.0030	0.0453	-1.8427
TbE59ZN5EOnpKyFKU0	Txnl4a	thioredoxin-like 4A	-0.4268	11.7019	-3.5489	0.0030	0.0456	-1.8485
xrSLKq50k3UKBq61ww	Tbrg4	transforming growth factor beta regulated gene 4	-0.4462	9.9156	-3.5474	0.0030	0.0457	-1.8514
0rl0jk6bv6pIgAxN1Q	Mpped1	metallophosphoesterase domain containing 1	-0.1747	8.6293	-3.5457	0.0030	0.0458	-1.8548
WClOxPhFipF,KWiaec	Rad51	RAD51 homolog	-0.4680	9.2150	-3.5439	0.0030	0.0458	-1.8584
iHuTRwpXtX16qWeTQw	Mef2b	myocyte enhancer factor 2B	-0.2853	8.9977	-3.5438	0.0030	0.0458	-1.8585
QKB14leuLrfIEteXjE	Hsd11b1	hydroxysteroid 11-beta dehydrogenase 1	0.4610	8.9894	3.5438	0.0030	0.0458	-1.8586
3iSEzieOa5egh_l0qI	Nup85	nucleoporin 85	-0.4296	10.7788	-3.5438	0.0030	0.0458	-1.8586
3_X6oXUB0PN6Fco0S4	Top1	topoisomerase (DNA) I	-0.3319	10.3060	-3.5431	0.0031	0.0458	-1.8599
cJChQ1t706J64Xul,U	Mrps31	mitochondrial ribosomal protein S31	-0.3962	12.0858	-3.5431	0.0031	0.0458	-1.8600

Probe ID	Gene symbol	Gene name	Log_2FC	Average expression	t	P, Value	Adj,P,Val	B
Q,QBCHT_73NqgUuXzo	Bmpr1b	bone morphogenetic protein receptor type 1B	-0.9484	10.4304	-3.5419	0.0031	0.0459	-1.8624
cnnvI4nnEgq8afqt6g	Sec61a2	Sec61 alpha subunit 2 (S, cerevisiae)	-0.2540	9.0197	-3.5416	0.0031	0.0459	-1.8628
ojo7q3TZD2uMH5,1V0	Stip1	stress-induced phosphoprotein 1	-0.3309	11.3704	-3.5414	0.0031	0.0459	-1.8633
BdihoCF7qBf53lv_yE	Acot11	acyl-CoA thioesterase 11	0.2005	8.7768	3.5410	0.0031	0.0459	-1.8640
lUqeetzv9d7n3F33Rs	Abcc10	ATP-binding cassette sub-family C (CFTR/MRP) member 10	0.2155	8.9835	3.5408	0.0031	0.0459	-1.8645
cBz8M6jO9Vw17H1eD0	Tmem55b	transmembrane protein 55b	0.4206	9.5834	3.5393	0.0031	0.0460	-1.8674
iq13vg6IpH67_ueyV4	Slit2	slit homolog 2 (Drosophila)	0.1676	8.6013	3.5391	0.0031	0.0460	-1.8679
EdSoog7uepzqJTvSI8	Myzap	myocardial zonula adherens protein	0.1959	9.1995	3.5375	0.0031	0.0461	-1.8709
EqL09KBecINpelVIRg	Prmt5	protein arginine N-methyltransferase 5	-0.3118	9.4117	-3.5343	0.0031	0.0464	-1.8772
rpypwlKU0fzR4vJFUE	Pank1	pantothenate kinase 1	0.5309	9.6012	3.5335	0.0031	0.0464	-1.8787
ua,R04qnaNfft0OG5M	Eif4e3	eukaryotic translation initiation factor 4E member 3	-0.3617	11.0495	-3.5313	0.0031	0.0465	-1.8831
0JH553RIIe1LlQSeWs	Gpr137c	G protein-coupled receptor 137C	-0.2663	8.9020	-3.5313	0.0031	0.0465	-1.8832
9JVSBZSGmH1ISK7i5Q	Bai2	brain-specific angiogenesis inhibitor 2	0.1873	8.5947	3.5302	0.0031	0.0466	-1.8852
iH62u,MJM51OR3SKgo	D430042O09Rik	RIKEN cDNA D430042O09 gene	0.3234	10.8793	3.5299	0.0031	0.0466	-1.8859
9Vr_SGGJw02H_EP_5o	Capn2	calpain 2	0.2833	10.1285	3.5294	0.0031	0.0466	-1.8869
uZzlTreN3jxNXAgeLg	Rnaseh2b	ribonuclease H2 subunit B	-0.5051	10.9063	-3.5286	0.0031	0.0466	-1.8883
cwfDTnievrfi3cVyKg	Fbln2	fibulin 2	0.4616	9.5146	3.5285	0.0031	0.0466	-1.8887
T7roo4QLqRYfnYoojQ	Eef1d	eukaryotic translation elongation factor 1 delta (guanine nucleotide exchange protein)	-0.2653	13.7552	-3.5282	0.0031	0.0466	-1.8892
fULuVF5O4KqCOnNB98	Samd14	sterile alpha motif domain containing 14	0.4606	10.6376	3.5234	0.0032	0.0471	-1.8986
lWCYpEA7gF,rTmXu48	Myh2	myosin heavy polypeptide 2 skeletal muscle adult	-0.1451	8.6063	-3.5222	0.0032	0.0471	-1.9009
NhzhPxCTeV0DhDlLlQ	Zmat1	zinc finger matrin type 1	-0.5929	10.1956	-3.5213	0.0032	0.0472	-1.9028
QRFd5H54nXQXnoSgJA	Gatb	glutamyl-tRNA(Gln) amidotransferase subunit B	-0.2018	9.0101	-3.5206	0.0032	0.0472	-1.9042
EXio0qKd8wq4o6UDlQ	Slc9a7	solute carrier family 9 (sodium/hydrogen exchanger) member 7	-0.1713	8.8912	-3.5196	0.0032	0.0473	-1.9060
fclQKwvns10S_3k1Kg	Ss18	synovial sarcoma translocation Chromosome 18	-0.3234	12.2503	-3.5188	0.0032	0.0473	-1.9076
6eoBC7hOilCaSuSliQ	Rab13	RAB13 member RAS oncogene family	0.2781	8.9330	3.5172	0.0032	0.0474	-1.9107
utf5UVEVT3JH_TRvjI	Plscr4	phospholipid scramblase 4	0.4413	10.0857	3.5156	0.0032	0.0476	-1.9140
0FOkB_NeHk8gAlF_98	AU021092	expressed sequence AU021092	0.5368	9.0465	3.5145	0.0032	0.0476	-1.9162
Hp59dAV2uiCh4n0SBE	Vrtn	vertebrae development associated	-0.4122	8.9521	-3.5128	0.0032	0.0478	-1.9195
xg26kQafE6RWCf5qiA	Irak4	interleukin-1 receptor-associated kinase 4	0.1695	8.7070	3.5117	0.0033	0.0478	-1.9217
9p9lQuIlE3xP3e_DaA	Rspo2	R-spondin 2 homolog (Xenopus laevis)	-0.4053	9.0745	-3.5114	0.0033	0.0478	-1.9222

Probe ID	Gene symbol	Gene name	Log_2FC	Average expression	t	P, Value	Adj,P,Val	B
iBxJWDWox32mbnwXF0	Eif4e2	eukaryotic translation initiation factor 4E member 2	-0.2675	11.7661	-3.5104	0.0033	0.0479	-1.9242
KFuY6JpB3SQjgmoeH0	Znrf1	zinc and ring finger 1	-0.2655	9.2215	-3.5099	0.0033	0.0479	-1.9252
6fA0cRs,3xWX0YkXXs	Ooep	oocyte expressed protein	-0.6811	12.8317	-3.5084	0.0033	0.0480	-1.9281
Hpej3t_x68RadB2oJA	Fam3c	family with sequence similarity 3 member C	-0.5278	12.0097	-3.5082	0.0033	0.0480	-1.9284
fqfkbR3re9NuvRKkK4	Cdk2	cyclin-dependent kinase 2	-0.4218	10.5359	-3.5072	0.0033	0.0481	-1.9305
xhJNSRX4Ve41tS0AFI	Rrp1b	ribosomal RNA processing 1 homolog B (S, cerevisiae)	-0.6411	10.8921	-3.5066	0.0033	0.0481	-1.9316
BoTX28XPVblAIYSU2o	Imp4	IMP4 U3 small nucleolar ribonucleoprotein homolog (yeast)	-0.1975	10.0957	-3.5058	0.0033	0.0482	-1.9331
fted3_,UKUP8663pxM	Prcp	prolylcarboxypeptidase (angiotensinase C)	0.4540	11.4175	3.5048	0.0033	0.0482	-1.9353
TSh1u7NLup10sKCKJ0	Ccp110	centriolar coiled coil protein 110	-0.4061	9.9202	-3.5044	0.0033	0.0482	-1.9359
KhcoXXqi3wr,3wM,Ik	Gabpa	GA repeat binding protein alpha	-0.1486	8.8600	-3.5018	0.0033	0.0484	-1.9410
3ep05xy53qVLhTkX0U	Slc41a3	solute carrier family 41 member 3	0.2505	8.9601	3.4997	0.0033	0.0486	-1.9451
QOXgVnC1nVlWCCq1CA	Hist1h2bn	histone cluster 1 H2bn	0.6934	9.6653	3.4976	0.0033	0.0488	-1.9493
cbaeAK91OuMhBpMuCk	Prdx5	peroxiredoxin 5	0.3675	11.4914	3.4970	0.0034	0.0488	-1.9504
cb0l1JuL31KDORJ0dk	Ppil1	peptidylprolyl isomerase (cyclophilin)-like 1	-0.3862	9.9569	-3.4968	0.0034	0.0488	-1.9510
oJO_p0RvXpY6fejh10	Tagln	transgelin	0.3793	9.8208	3.4958	0.0034	0.0489	-1.9530
xVAtOoDe7vNSLn0rCU	Ccdc91	coiled-coil domain containing 91	0.2466	9.4372	3.4941	0.0034	0.0490	-1.9562
9t0VzUl1QEqUGNw9Yg	Hoxd9	homeobox D9	0.4759	10.3906	3.4931	0.0034	0.0491	-1.9581
3kqKBhi7nSTL5ecS3g	Pomp	proteasome maturation protein	0.2779	13.4545	3.4921	0.0034	0.0491	-1.9601
KktVTsFOliUiJ,_RTk	Olfm1	olfactomedin 1	0.4120	10.1979	3.4900	0.0034	0.0493	-1.9643
9XkoqECni70blJKdSA	Ralgps2	Ral GEF with PH domain and SH3 binding motif 2	-0.3594	9.5194	-3.4885	0.0034	0.0494	-1.9671
EJkE7ec6Bv1sE6EIqU	Arpc1a	actin related protein 2/3 complex subunit 1A	0.3443	11.6272	3.4872	0.0034	0.0495	-1.9697
uquihfZpAztFdNxFBw	Gstp1	glutathione S-transferase pi 1	0.4997	11.3330	3.4863	0.0034	0.0496	-1.9715
KRxe6FaCkl8SqKX29l	Hnrnpf	heterogeneous nuclear ribonucleoprotein F	-0.5449	10.4946	-3.4829	0.0035	0.0499	-1.9782
ZlJRpy5j7NwP14qu,8	Sorbs1	sorbin and SH3 domain containing 1	0.2182	8.8071	3.4825	0.0035	0.0499	-1.9789
BBXQcRpWfSWvQASIhQ	Polr2d	polymerase (RNA) II (DNA directed) polypeptide D	-0.2480	10.3850	-3.4810	0.0035	0.0500	-1.9819
iTkRGxORFkRITieoTs	Nin	ninein	-0.3130	9.7103	-3.4808	0.0035	0.0500	-1.9823

Appendix C: Functional annotation cluster for 9-week up-regulated genes

Functional annotation cluster 1 of up-regulated genes

Total number of genes: 214

Enrichment score: 5.95

Category	Term	Gene counts	Gene official names	P Value	Bonferroni	Benjamini
SP_PIR_KEYWORDS	Signal	148	RARRES2, GABRB3, FAM20A, LRTM1, TGFB3, MEGF10, MMP2, B2M, NRCAM, WNT4, TMEM9B, CD44, GRIN2B, SBSN, TGFBI, ROBO4, BC028528, CPA3, LGI3, HTRA3, SPON2, WNT6, PQLC3, SPON1, PTPRK, WNT10A, WNT10B, DDRGK1, C4A, C4B, SCUBE2, SPARCL1, DEFB36, H2-DMB1, LHFP, CERCAM, 3632451O06RIK, H2-DMB2, NCAM1, UGT1A10, LYNX1, BACE1, VSIG8, PRCP, HSD17B11, WNT5A, TWSG1, ENPP2, 3110057O12RIK, CCL9, HFE, TIMP2, FXYD5, AU021092, PVRL2, TEK, ENTPD5, BAI2, OLFM1, BMP1, SLAMF9, ADAM23, SECTM1A, ECM1, THSD7B, EMILIN1, CD55, SFRP1, THSD1, CXCL16, SFRP4, PON2, H2-T23, ANTXR2, ENG, IL27RA, IGFBP6, H2-D1, GM6484, BCAM, SPINK8, SRPX, UGT1A7C, GSN, UGT1A6B, SLC24A3, UGT1A6A, RSPO3, DMKN, LBP, RAMP1, LOXL1, GPC1, NT5E, DPEP1, DPEP2, DHCR24, H2-K1, ICAM1, EGFL7, LEPREL2, CAR12, SDK1, MMP15, WLS, MMP14, FCRLS, SLIT2, SLIT3, TNFRSF9, CTSK, SERPINA3N, PLXDC1, PRF1, CD248, TNC, COL3A1, PF4, ISLR, LY6A, LY6E, LRG1, PRRG2, IL10RB, PTN, TNFRSF19, COL8A1, QSOX1, COL8A2, DPT, LY6C1, VSTM2B, PLA2G15, TNXB, LIPA, FZD1, H2-AB1, SPARC, KLK1, CLEC11A, COL5A1, NBL1, FBLN2, ITPRIPL2, SULF1, C1RL, CP, H2-DMA, IGFBP2, IGFBP4, CD14, VLDLR	2.98E-10	1.08E-07	1.08E-07
UP_SEQ_FEATURE	Signal peptide	148	RARRES2, GABRB3, FAM20A, LRTM1, TGFB3, MEGF10, MMP2, B2M, NRCAM, WNT4, TMEM9B, CD44, GRIN2B, SBSN, TGFBI, ROBO4, BC028528, CPA3, LGI3, HTRA3, SPON2, WNT6, PQLC3, SPON1, PTPRK, WNT10A, WNT10B, DDRGK1, C4A, C4B, SCUBE2, SPARCL1, DEFB36, H2-DMB1, LHFP, CERCAM, 3632451O06RIK, H2-DMB2, NCAM1, UGT1A10, LYNX1, BACE1, VSIG8, PRCP, HSD17B11, WNT5A, TWSG1, ENPP2, 3110057O12RIK, CCL9, HFE, TIMP2, FXYD5, AU021092, PVRL2, TEK, ENTPD5, BAI2, OLFM1, BMP1, SLAMF9, ADAM23, SECTM1A,	6.00E-08	8.83E-05	8.83E-05

Category	Term	Gene counts	Gene official names	P Value	Bonferroni	Benjamini
			ECM1, THSD7B, EMILIN1, CD55, SFRP1, THSD1, CXCL16, SFRP4, PON2, H2-T23, ANTXR2, ENG, IL27RA, IGFBP6, H2-D1, GM6484, BCAM, SPINK8, SRPX, UGT1A7C, GSN, UGT1A6B, SLC24A3, UGT1A6A, RSPO3, DMKN, LBP, RAMP1, LOXL1, GPC1, NT5E, DPEP1, DPEP2, DHCR24, H2-K1, ICAM1, EGFL7, LEPREL2, CAR12, SDK1, MMP15, WLS, MMP14, FCRLS, SLIT2, SLIT3, TNFRSF9, CTSK, SERPINA3N, PLXDC1, PRF1, CD248, TNC, COL3A1, PF4, ISLR, LY6A, LY6E, LRG1, PRRG2, IL10RB, PTN, TNFRSF19, COL8A1, QSOX1, COL8A2, DPT, LY6C1, VSTM2B, PLA2G15, TNXB, LIPA, FZD1, H2-AB1, SPARC, KLK1, CLEC11A, COL5A1, NBL1, FBLN2, ITPRIPL2, SULF1, C1RL, CP, H2-DMA, IGFBP2, IGFBP4, CD14, VLDLR			
SP_PIR_KEYWORDS	Glycoprotein	160	HGSNAT, S100A4, SYT1, ADCY2, GABRB3, FAM20A, LRTM1, F13A1, TGFB3, AQP1, MEGF10, MMP2, S1PR2, NRCAM, WNT4, CD44, GRIN2B, ROBO4, BC028528, LGI3, SPON2, WNT6, SPON1, TOR1AIP2, PTPRK, WNT10A, WNT10B, C4A, C4B, SCUBE2, SPARCL1, H2-DMB1, MRGPRF, CERCAM, 3632451O06RIK, SAG, NCAM1, UGT1A10, LYNX1, AGTR1A, SLC37A2, BACE1, HSD11B1, PRCP, EMP2, WNT5A, ERMP1, TWSG1, GCNT2, ENPP1, ENPP2, 3110057O12RIK, TMEM63A, HFE, CD72, FXYD5, CD74, SLCO2A1, TMEM63B, B3GNT8, SLC11A1, UPK1B, PVRL2, TEK, ENTPD5, BAI2, AI464131, ENTPD2, OLFM1, BMP1, SLAMF9, ADAM23, ACER2, SECTM1A, ECM1, THSD7B, EMILIN1, GGT5, CD55, FAM198B, SFRP1, THSD1, CXCL16, ST8SIA5, SFRP4, PON2, H2-T23, ANTXR2, ENG, SLC46A1, IL27RA, NDST1, IGFBP6, H2-D1, BCAM, TSPAN11, UGT1A7C, UGT1A6B, SLC24A3, UGT1A6A, RSPO3, DMKN, NIPAL2, LBP, DPP6, GPC1, NT5E, DPEP1, DPEP2, H2-K1, ICAM1, PTGER2, LEPREL2, CAR12, SDK1, SLC3A2, MMP15, ST6GALNAC2, SLIT2, SLIT3, TNFRSF9, CTSK, SERPINA3N, BVES, TNFSF13B, PLXDC1, SGCB, GPR182, PRF1, GPR183, CD248, TNC, COL3A1, GPR65, PLVAP, PF4, ISLR, LY6A, LY6E, SORBS1, IL10RB, TNFRSF19, QSOX1, LY6C1, TMC6, PLA2G15, LIPA, FZD1, H2-AB1, SPARC, KLK1, TSPAN17, CLEC11A, CSGALNACT1, FBLN2, SLC6A8, SULF1, C1RL, CP, H2-DMA, IGFBP2, IGFBP4, CD14, VLDLR	1.52E-07	5.50E-05	2.75E-05

Category	Term	Gene counts	Gene official names	P Value	Bonferroni	Benjamini
SP_PIR_KEYWORDS	Disulfide bond	118	GABRB3, TGFB3, MEGF10, MMP2, B2M, NRCAM, CD44, TGFBI, ROBO4, CPA3, SPON2, SPON1, PTPRK, C4A, C4B, SCUBE2, SPARCL1, DEFB36, SAG, NCAM1, LYNX1, AGTR1A, BACE1, CX3CR1, VSIG8, SRXN1, ERMP1, ENPP1, ENPP2, CCL9, HFE, CD72, TIMP2, CD74, PVRL2, TEK, BAI2, ENTPD2, OLFM1, BMP1, ADAM23, SLAMF9, S100A11, THSD7B, EMILIN1, CD55, THSD1, SFRP1, CXCL16, ST8SIA5, SFRP4, PON2, ANTXR2, H2-T23, NDST1, IGFBP6, H2-D1, PRDX5, BCAM, SPINK8, SRPX, GSN, RSPO3, DPP6, NT5E, RAMP1, DPEP1, DPEP2, H2-K1, ICAM1, PTGER2, EGFL7, CAR12, SDK1, SLC3A2, MMP15, MMP14, PALLD, ST6GALNAC2, SLIT2, SLIT3, TNFRSF9, CTSK, TNFSF13B, SGCB, GPR182, PRF1, GPR183, CD248, TNC, COL3A1, GPR65, PF4, ISLR, LY6A, LY6E, PRRG2, IL10RB, PTN, TNFRSF19, GLRX, DPT, LY6C1, VSTM2B, FZD1, H2-AB1, SPARC, KLK1, CLEC11A, NBL1, PTP4A3, FBLN2, C1RL, CP, IGFBP2, H2-DMA, CD14, IGFBP4, VLDLR	3.83E-07	1.38E-04	2.77E-05
UP_SEQ_FEATURE	Disulfide bond	116	GABRB3, TGFB3, MEGF10, MMP2, B2M, NRCAM, CD44, TGFBI, ROBO4, CPA3, SPON2, SPON1, PTPRK, C4A, C4B, SCUBE2, SPARCL1, DEFB36, SAG, NCAM1, LYNX1, AGTR1A, BACE1, CX3CR1, VSIG8, SRXN1, ERMP1, ENPP1, ENPP2, CCL9, HFE, CD72, TIMP2, CD74, PVRL2, TEK, BAI2, OLFM1, BMP1, ADAM23, SLAMF9, S100A11, THSD7B, EMILIN1, CD55, THSD1, SFRP1, CXCL16, ST8SIA5, SFRP4, PON2, ANTXR2, H2-T23, NDST1, IGFBP6, H2-D1, PRDX5, BCAM, SPINK8, SRPX, GSN, RSPO3, DPP6, RAMP1, DPEP1, DPEP2, H2-K1, ICAM1, PTGER2, EGFL7, CAR12, SDK1, SLC3A2, MMP15, MMP14, PALLD, SLIT2, ST6GALNAC2, SLIT3, TNFRSF9, CTSK, TNFSF13B, SGCB, GPR182, PRF1, GPR183, CD248, TNC, COL3A1, GPR65, PF4, ISLR, LY6A, LY6E, PRRG2, IL10RB, PTN, TNFRSF19, GLRX, DPT, LY6C1, VSTM2B, FZD1, H2-AB1, SPARC, KLK1, CLEC11A, NBL1, PTP4A3, FBLN2, C1RL, CP, IGFBP2, H2-DMA, CD14, IGFBP4, VLDLR	9.51E-06	0.0139	0.0069
GOTERM_CC_FAT	Extracellular region	87	RARRES2, FAM20A, F13A1, IL18, IGFBP6, TGFB3, GM6484, MMP2, SPINK8, B2M, WNT4, GSN, SBSN, DMKN, RSPO3, TGFBI, BC028528, LGI3, HTRA3, LBP, CASP1, SPON2, WNT6, GPC1, LOXL1, SPON1, WNT10A, WNT10B, DDRGK1, C4A, EGFL7, SCUBE2, C4B, SPARCL1, DEFB36, MMP15, MMP14, SLIT2,	1.09E-05	0.0030	6.06E-04

Category	Term	Gene counts	Gene official names	P Value	Bonferroni	Benjamini
			SLIT3, SERPINA3N, TNFSF13B, CFL1, HSD17B11, WNT5A, PRF1, TWSG1, ENPP1, ENPP2, TNC, 3110057O12RIK, COL3A1, CCL9, PF4, TIMP2, ISLR, AU021092, PRRG2, PTN, TNFRSF19, COL8A1, ENTPD2, COL8A2, QSOX1, OLFM1, DPT, PLA2G15, BMP1, TNXB, ADAM23, LGALS7, SPARC, ECM1, SECTM1A, CLEC11A, COL5A1, EMILIN1, NBL1, SFRP1, FBLN2, CXCL16, SULF1, SFRP4, C1RL, PON2, CP, IGFBP2, IGFBP4, VLDLR			
SP_PIR_KEYWORDS	Secreted	72	RARRES2, FAM20A, F13A1, IL18, IGFBP6, TGFB3, GM6484, MMP2, SPINK8, B2M, WNT4, GSN, SBSN, RSPO3, DMKN, TGFBI, BC028528, LGI3, HTRA3, LBP, SPON2, WNT6, GPC1, LOXL1, SPON1, WNT10A, WNT10B, DDRGK1, C4A, EGFL7, C4B, SPARCL1, DEFB36, SLIT2, SLIT3, SERPINA3N, TNFSF13B, HSD17B11, WNT5A, PRF1, TWSG1, ENPP2, TNC, 3110057O12RIK, COL3A1, CCL9, PF4, TIMP2, ISLR, AU021092, TNFRSF19, PTN, COL8A1, COL8A2, QSOX1, DPT, PLA2G15, ADAM23, LGALS7, SPARC, ECM1, SECTM1A, CLEC11A, COL5A1, EMILIN1, NBL1, SFRP1, FBLN2, SFRP4, C1RL, CP, IGFBP2, IGFBP4	2.03E-05	0.0073	9.18E-04
UP_SEQ_FEATURE	Glycosylation site:N-linked (GlcNAc...)	144	HGSNAT, S100A4, SYT1, ADCY2, GABRB3, FAM20A, LRTM1, F13A1, TGFB3, AQP1, MEGF10, MMP2, NRCAM, S1PR2, WNT4, CD44, GRIN2B, ROBO4, BC028528, LGI3, WNT6, SPON1, TOR1AIP2, PTPRK, WNT10A, WNT10B, C4A, C4B, SCUBE2, SPARCL1, H2-DMB1, MRGPRF, CERCAM, 3632451O06RIK, NCAM1, UGT1A10, AGTR1A, SLC37A2, BACE1, PRCP, HSD11B1, EMP2, WNT5A, ERMP1, TWSG1, GCNT2, ENPP1, ENPP2, 3110057O12RIK, TMEM63A, HFE, CD72, CD74, SLCO2A1, TMEM63B, B3GNT8, SLC11A1, PVRL2, TEK, ENTPD5, BAI2, AI464131, ENTPD2, OLFM1, BMP1, SLAMF9, ADAM23, ACER2, SECTM1A, ECM1, THSD7B, EMILIN1, GGT5, CD55, FAM198B, SFRP1, THSD1, ST8SIA5, SFRP4, PON2, H2-T23, ANTXR2, ENG, SLC46A1, NDST1, IL27RA, H2-D1, BCAM, TSPAN11, UGT1A7C, UGT1A6B, SLC24A3, RSPO3, UGT1A6A, NIPAL2, LBP, DPP6, GPC1, NT5E, DPEP1, DPEP2, H2-K1, ICAM1, PTGER2, LEPREL2, CAR12, SDK1, SLC3A2, MMP15, ST6GALNAC2, SLIT2, SLIT3, TNFRSF9, CTSK, SERPINA3N, BVES, TNFSF13B, PLXDC1, SGCB, GPR182, PRF1, GPR183, TNC, GPR65, PLVAP, ISLR,	0.0011	0.8167	0.1910

Category	Term	Gene counts	Gene official names	P Value	Bonferroni	Benjamini
			LY6E, IL10RB, TNFRSF19, QSOX1, TMC6, PLA2G15, LIPA, FZD1, H2-AB1, SPARC, KLK1, TSPAN17, CSGALNACT1, FBLN2, SLC6A8, SULF1, C1RL, CP, H2-DMA, IGFBP4, CD14, VLDLR			

Functional annotation cluster 2 of up-regulated genes

Total number of genes: 53

Enrichment score: 5.83

Category	Term	Gene counts	Gene official names	P Value	Bonferroni	Benjamini
GOTERM_CC_FAT	Extracellular matrix	29	WNT5A, TNC, COL3A1, TGFB3, TIMP2, MMP2, WNT4, TGFBI, PTN, WNT6, COL8A1, SPON2, ENTPD2, GPC1, LOXL1, COL8A2, SPON1, DPT, WNT10A, WNT10B, TNXB, SPARCL1, SPARC, MMP15, MMP14, ECM1, COL5A1, EMILIN1, FBLN2	1.08E-06	3.00E-04	3.00E-04
GOTERM_CC_FAT	Extracellular region part	52	IL18, TGFB3, MMP2, WNT4, DMKN, TGFBI, LBP, WNT6, SPON2, GPC1, LOXL1, SPON1, WNT10A, WNT10B, C4A, EGFL7, SCUBE2, C4B, SPARCL1, MMP15, MMP14, SLIT2, SLIT3, TNFSF13B, WNT5A, TWSG1, ENPP1, TNC, COL3A1, CCL9, PF4, TIMP2, PTN, COL8A1, QSOX1, COL8A2, ENTPD2, OLFM1, DPT, TNXB, BMP1, SPARC, ECM1, COL5A1, EMILIN1, FBLN2, CXCL16, SULF1, C1RL, CP, IGFBP2, IGFBP4, VLDLR	1.22E-06	3.39E-04	1.70E-04
GOTERM_CC_FAT	Proteinaceous extracellular matrix	28	WNT5A, TNC, COL3A1, TIMP2, MMP2, WNT4, TGFBI, PTN, WNT6, COL8A1, SPON2, ENTPD2, GPC1, LOXL1, COL8A2, SPON1, DPT, WNT10A, WNT10B, TNXB, SPARCL1, SPARC, MMP15, MMP14, ECM1, COL5A1, EMILIN1, FBLN2	1.59E-06	4.41E-04	1.47E-04
SP_PIR_KEYWORDS	Extracellular matrix	22	WNT5A, WNT10A, WNT10B, TNXB, SPARCL1, TNC, COL3A1, SPARC, TIMP2, MMP2, ECM1, COL5A1, EMILIN1, WNT4, FBLN2, TGFBI, WNT6, COL8A1, SPON2, COL8A2, DPT, SPON1	2.25E-06	8.14E-04	1.36E-04

Functional annotation cluster 3 of up-regulated genes

Total number of genes: 62

Enrichment score: 3.26

Category	Term	Gene counts	Gene official names	P Value	Bonferroni	Benjamini
GOTERM_BP_FAT	Antigen processing and presentation of peptide antigen	13	H2-K1, H2-D1, HFE, H2-DMB1, H2-AB1, CD74, H2-DMB2, B2M, SLC11A1, GM8909, TAP2, H2-T23, H2-DMA	2.35E-10	4.44E-07	4.44E-07
GOTERM_BP_FAT	Immune response	39	MFSD6, GPR183, ENPP1, ENPP2, IL18, H2-D1, CCL9, HFE, PF4, CD74, B2M, SLC11A1, KLHL6, TAP2, OASL2, H2-T10, LBP, SPON2, DHX58, H2-K1, IRAK1, ICAM1, C4A, C4B, H2-DMB1, H2-AB1, H2-DMB2, PSMB8, CD55, LAT2, GM8909, TNFSF13B, CX3CR1, IRF8, C1RL, POMP, H2-T23, H2-DMA, GBP3, CD14	3.98E-08	7.53E-05	3.76E-05
GOTERM_BP_FAT	Antigen processing and presentation	16	H2-K1, ICAM1, H2-D1, HFE, H2-DMB1, H2-AB1, H2-DMB2, CD74, PSMB8, B2M, SLC11A1, GM8909, TAP2, H2-T23, H2-T10, H2-DMA	4.83E-08	9.12E-05	3.04E-05
SP_PIR_KEYWORDS	Immune response	22	H2-K1, GPR183, MFSD6, C4A, C4B, H2-D1, H2-DMB1, HFE, H2-AB1, PSMB8, CD74, B2M, CD55, LAT2, GM8909, TAP2, POMP, C1RL, H2-T23, H2-DMA, SPON2, CD14, DHX58	2.00E-07	7.22E-05	1.81E-05
GOTERM_BP_FAT	Antigen processing and presentation of exogenous peptide antigen	8	H2-K1, TAP2, H2-DMB1, H2-AB1, H2-DMA, CD74, H2-DMB2, B2M	3.66E-06	0.0068	0.0017
GOTERM_CC_FAT	MHC protein complex	11	H2-K1, GM8909, H2-D1, H2-DMB1, HFE, H2-T10, H2-AB1, H2-T23, H2-DMA, H2-DMB2, B2M	5.81E-06	0.0016	4.02E-04
SP_PIR_KEYWORDS	MHC I	6	H2-K1, GM8909, H2-D1, HFE, H2-T23, B2M	1.00E-05	0.0036	5.20E-04
UP_SEQ_FEATURE	Domain: Ig-like C1-type	8	H2-K1, H2-D1, H2-DMB1, HFE, H2-AB1, H2-T23, H2-DMA, B2M	1.16E-05	0.0169	0.0056
GOTERM_BP_FAT	Antigen processing and presentation of exogenous antigen	8	H2-K1, TAP2, H2-DMB1, H2-AB1, H2-DMA, CD74, H2-DMB2, B2M	1.55E-05	0.0288	0.0058
UP_SEQ_FEATURE	Region of interest: Connecting peptide	8	H2-K1, H2-D1, H2-DMB1, HFE, H2-AB1, H2-T23, H2-DMA, CRYBA4	2.63E-05	0.0379	0.0096
INTERPRO	Immunoglobulin C1-set	12	H2-K1, SIRPB1A, GM8909, H2-D1, H2-DMB1, HFE, H2-T10, H2-AB1, H2-T23, H2-DMA, H2-DMB2, B2M	3.42E-05	0.0299	0.0299
SMART	IGc1	12	H2-K1, SIRPB1A, GM8909, H2-D1, H2-DMB1, HFE, H2-T10, H2-AB1, H2-T23, H2-DMA, H2-DMB2, B2M	1.05E-04	0.0198	0.0198
GOTERM_BP_FAT	Antigen	6	H2-K1, GM8909, H2-D1, HFE, H2-	1.16E-04	0.1964	0.0240

Category	Term	Gene counts	Gene official names	P Value	Bonferroni	Benjamini
	processing and presentation of peptide antigen via MHC class I		T23, B2M			
INTERPRO	Immunoglobulin/major histocompatibility complex, conserved site	12	H2-K1, NRCAM, GM8909, H2-D1, H2-DMB1, HFE, H2-T10, H2-AB1, H2-T23, H2-DMA, H2-DMB2, B2M	1.59E-04	0.1319	0.0683
KEGG_PATHWAY	Viral myocarditis	12	H2-K1, ICAM1, PRF1, CD55, H2-D1, H2-DMB1, H2-T10, H2-AB1, H2-T23, H2-DMA, H2-DMB2, SGCB	2.04E-04	0.0307	0.0307
UP_SEQ_FEATURE	Region of interest: Alpha-2	5	H2-K1, H2-D1, HFE, H2-T23, H2-DMA	3.20E-04	0.3756	0.0899
UP_SEQ_FEATURE	Region of interest: Alpha-1	5	H2-K1, H2-D1, HFE, H2-T23, H2-DMA	3.20E-04	0.3756	0.0899
KEGG_PATHWAY	Allograft rejection	9	H2-K1, PRF1, H2-D1, H2-DMB1, H2-T10, H2-AB1, H2-T23, H2-DMA, H2-DMB2	5.01E-04	0.0738	0.0252
KEGG_PATHWAY	Graft-versus-host disease	9	H2-K1, PRF1, H2-D1, H2-DMB1, H2-T10, H2-AB1, H2-T23, H2-DMA, H2-DMB2	5.01E-04	0.0738	0.0252
KEGG_PATHWAY	Antigen processing and presentation	11	H2-K1, TAP2, H2-D1, H2-DMB1, H2-T10, H2-AB1, H2-T23, H2-DMA, CD74, H2-DMB2, B2M	6.61E-04	0.0961	0.0249
KEGG_PATHWAY	Type I diabetes mellitus	9	H2-K1, PRF1, H2-D1, H2-DMB1, H2-T10, H2-AB1, H2-T23, H2-DMA, H2-DMB2	8.82E-04	0.1262	0.0266
GOTERM_BP_FAT	Antigen processing and presentation of exogenous peptide antigen via MHC class II	5	H2-DMB1, H2-AB1, H2-DMA, CD74, H2-DMB2	0.0011	0.8851	0.1432
GOTERM_BP_FAT	Antigen processing and presentation of peptide antigen via MHC class II	5	H2-DMB1, H2-AB1, H2-DMA, CD74, H2-DMB2	0.0011	0.8851	0.1432
INTERPRO	MHC class II, alpha/beta chain, N-terminal	4	H2-DMB1, H2-AB1, H2-DMA, H2-DMB2	0.0019	0.8206	0.2177
KEGG_PATHWAY	Autoimmune thyroid disease	9	H2-K1, PRF1, H2-D1, H2-DMB1, H2-T10, H2-AB1, H2-T23, H2-DMA, H2-DMB2	0.0021	0.2779	0.0528
GOTERM_BP_FAT	Antigen processing and presentation of peptide or polysaccharide antigen via MHC class II	5	H2-DMB1, H2-AB1, H2-DMA, CD74, H2-DMB2	0.0022	0.9862	0.1930

Category	Term	Gene counts	Gene official names	P Value	Bonferroni	Benjamini
GOTERM_CC_FAT	MHC class I protein complex	7	H2-K1, GM8909, H2-D1, HFE, H2-T10, H2-T23, B2M	0.0022	0.4690	0.0679
GOTERM_CC_FAT	Multivesicular body	4	H2-AB1, H2-DMA, CD74, H2-DMB2	0.0025	0.5027	0.0674
UP_SEQ_FEATURE	Region of interest: Alpha-3	4	H2-K1, H2-D1, HFE, H2-T23	0.0025	0.9775	0.3442
GOTERM_CC_FAT	MHC class II protein complex	4	H2-DMB1, H2-AB1, H2-DMA, H2-DMB2	0.0035	0.6226	0.0672
SP_PIR_KEYWORDS	MHC II	4	H2-DMB1, H2-AB1, H2-DMA, H2-DMB2	0.0038	0.7503	0.0830
KEGG_PATHWAY	Cell adhesion molecules (CAMs)	13	H2-K1, ICAM1, CLDN5, H2-D1, H2-DMB1, H2-AB1, H2-DMB2, NCAM1, NRCAM, PVRL2, H2-T23, H2-T10, H2-DMA	0.0040	0.4624	0.0746
PIR_SUPERFAMILY	Class II histocompatibility antigen	4	H2-DMB1, H2-AB1, H2-DMA, H2-DMB2	0.0040	0.7009	0.3312
GOTERM_BP_FAT	Chaperone mediated protein folding requiring cofactor	4	H2-DMB1, H2-DMA, CD74, H2-DMB2	0.0049	0.9999	0.3051
INTERPRO	MHC class I, alpha chain, alpha1 and alpha2	6	H2-K1, GM8909, H2-D1, HFE, H2-T10, H2-T23	0.0071	0.9982	0.4110
GOTERM_BP_FAT	'*De novo*' posttranslational protein folding	4	H2-DMB1, H2-DMA, CD74, H2-DMB2	0.0079	0.9999	0.3483
GOTERM_BP_FAT	'*De novo*' protein folding	4	H2-DMB1, H2-DMA, CD74, H2-DMB2	0.0079	0.9999	0.3483
INTERPRO	MHC class I, alpha chain, C-terminal	3	H2-K1, GM8909, H2-D1	0.0083	0.9994	0.4127
PIR_SUPERFAMILY	Class I histocompatibility antigen	5	H2-K1, GM8909, H2-D1, H2-T10, H2-T23	0.0085	0.9211	0.3983
INTERPRO	MHC class I-like antigen recognition	6	H2-K1, GM8909, H2-D1, HFE, H2-T10, H2-T23	0.0149	0.9999	0.4877
INTERPRO	MHC class II, beta chain, N-terminal	3	H2-DMB1, H2-AB1, H2-DMB2	0.0168	0.9999	0.4967
KEGG_PATHWAY	Intestinal immune network for IgA production	6	TNFSF13B, TGFB3, H2-DMB1, H2-AB1, H2-DMA, H2-DMB2	0.0297	0.9901	0.2990
SP_PIR_KEYWORDS	Heterodimer	5	H2-K1, H2-D1, H2-AB1, H2-T23, B2M	0.0324	0.9999	0.3111
INTERPRO	Immunoglobulin-like	27	H2-D1, HFE, BCAM, B2M, ISLR, SIRPB1A, NRCAM, TEK, PVRL2, ROBO4, H2-T10, H2-K1, VSTM2B, PTPRK, ICAM1, SLAMF9, SDK1, H2-DMB1, H2-AB1, PALLD, FCRLS, H2-DMB2, NCAM1, GM8909, VSIG8, H2-T23, H2-DMA	0.0391	1	0.6481
GOTERM_CC_FAT	Late endosome	5	SLC11A1, H2-AB1, H2-DMA, CD74, H2-DMB2	0.0548	0.9999	0.4517

Category	Term	Gene counts	Gene official names	P Value	Bonferroni	Benjamini
INTERPRO	Immunoglobulin-like fold	27	F13A1, H2-D1, HFE, BCAM, B2M, ISLR, SIRPB1A, NRCAM, TEK, PVRL2, ROBO4, H2-T10, H2-K1, VSTM2B, PTPRK, ICAM1, SDK1, H2-DMB1, H2-AB1, PALLD, FCRLS, H2-DMB2, NCAM1, GM8909, VSIG8, H2-T23, H2-DMA	0.0720	1	0.7082
KEGG_PATHWAY	Asthma	4	H2-DMB1, H2-AB1, H2-DMA, H2-DMB2	0.0899	0.9999	0.5319
GOTERM_BP_FAT	Protein folding	5	H2-DMB1, H2-DMA, QSOX1, CD74, H2-DMB2	0.5422	1	0.9866

Functional annotation cluster 4 of up-regulated genes

Total number of genes: 40

Enrichment score: 2.83

Category	Term	Gene counts	Gene official names	P Value	Bonferroni	Benjamini
SP_PIR_KEYWORDS	Lipoprotein	36	WNT5A, 5430435G22RIK, SYT1, PALM, RAB3D, RAB5C, RAB1B, SLA, S1PR2, LY6A, KRAS, SRPX, RAB43, LY6E, RRAS, GPC1, NT5E, DPEP1, DPEP2, LY6C1, RAB8A, NCALD, RFTN2, NCAM1, CD55, LAT2, RAB31, LYNX1, PTP4A3, PLSCR4, AGTR1A, RAB15, RAB13, CD14, TRAPPC3, VLDLR	1.27E-04	0.0449	0.0050
UP_SEQ_FEATURE	Propeptide: Removed in mature form	18	LY6C1, PSMB10, RAB8A, PSMB8, LY6A, ACTG2, CD55, LYNX1, SRPX, KRAS, LY6E, RRAS, RAB13, NT5E, GPC1, DPEP1, CD14, DPEP2	0.0010	0.7766	0.2210
SP_PIR_KEYWORDS	GPI-anchor	11	LY6A, LY6C1, NCAM1, CD55, LYNX1, LY6E, GPC1, NT5E, DPEP1, CD14, DPEP2	0.0045	0.8073	0.0874
GOTERM_CC_FAT	Anchored to membrane	15	LY6C1, PALM, RAB5C, RFTN2, NCAM1, LY6A, CD55, LYNX1, LY6E, CP, GPC1, NT5E, DPEP1, CD14, DPEP2	0.0082	0.8999	0.1423

Functional annotation cluster 5 of up-regulated genes

Total number of genes: 31

Enrichment score: 2.75

Category	Term	Gene counts	Gene official symbols	P Value	Bonferroni	Benjamini
SP_PIR_KEYWORDS	Cell adhesion	24	ICAM1, ADAM23, TNC, PCDHB3, FLOT2, SDK1, EFS, BCAM, CERCAM, MEGF10, EMILIN1, CTNNA2, NRCAM, NCAM1, CD44, PVRL2, TGFBI, COL8A1, SPON2, COL8A2, ENG, PARVA, DPT, SPON1	0.0014	0.3978	0.0413
GOTERM_BP_FAT	Cell adhesion	31	PPARD, TNC, CLDN5, BCAM, SOX9, MEGF10, NRCAM, CD44, SORBS1, PVRL2, TGFBI, TEK, COL8A1, SPON2, COL8A2, SPON1, DPT, ICAM1, TNXB, ADAM23, FLOT2, PCDHB3, SDK1, EFS, CERCAM, COL5A1, EMILIN1, CTNNA2, NCAM1, ENG, PARVA	0.0019	0.9762	0.1877
GOTERM_BP_FAT	Biological adhesion	31	PPARD, TNC, CLDN5, BCAM, SOX9, MEGF10, NRCAM, CD44, SORBS1, PVRL2, TGFBI, TEK, COL8A1, SPON2, COL8A2, SPON1, DPT, ICAM1, TNXB, ADAM23, FLOT2, PCDHB3, SDK1, EFS, CERCAM, COL5A1, EMILIN1, CTNNA2, NCAM1, ENG, PARVA	0.0020	0.9775	0.1811

Appendix D: Functional annotation cluster for 9-week down-regulated genes

Functional annotation cluster 1 of down-regulated genes

Total number of genes: 134

Enrichment score: 22.04

Category	Term	Gene counts	Gene official symbols	P Value	Bonferroni	Benjamini
GOTERM_CC_FAT	Non-membrane-bounded organelle	134	PRC1, CEP78, KNTC1, AURKC, CBX3, PDLIM1, AURKA, AURKB, MRPS31, WDR74, TOP1, SIN3B, CDCA8, ANK1, SIN3A, MAK16, INCENP, PRIM2, RPP30, MRPL38, GNL2, IMP4, RPS27A, GNL3, GTPBP4, SGOL2, MYH2, SGOL1, KRT12, RRP9, CTNNA3, MRTO4, RSL1D1, TNS4, RCL1, UXT, KDM2B, MAD2L1, NOP2, MRPS18B, SPAG5, RFC2, MYBBP1A, NUP43, BLM, LMNB2, TIPIN, BANF1, SPC24, SPC25, PPAN, NPM2, EIF3L, MNS1, RPL4, NUDC, TRP53, NIN, MYO1B, MYO1E, NDC80, BRCA1, DOCK4, PEO1, TMPO, MYH10, KIF23, CLSPN, KIF22, TAF1A, GAR1, MYBPC3, GTSE1, RPS3, PRMT3, KIF2C, SAP30, RRP1B, HIST2H2AC, RANBP1, CDK5RAP2, CIRH1A, TOP2A, CDC6, KIF11, POLR1E, NOL8, KIF15, POLR1A, MRPS5, NUSAP1, NUP85, MID1IP1, MCM2, CDK2, RAD51, SS18, APITD1, NOL10, BUB1B, NUP107, MAPRE1, POLR2H, HIST1H2AF, USP2, HIST1H2AD, POLA2, IVNS1ABP, RPA2, CENPA, KIF4, AATF, KIF21A, RFPL4, ZWILCH, H1FOO, GEMIN4, MYO5C, MSH6, CENPM, RRP12, TRIM28, CENPP, KIF18B, BIRC5, ILF3, SMC2, PWP2, SMC4, CCNB1, NOP58, HIST1H2AH, HIST1H2AK, NOP56, MPHOSPH6	1.35E-23	4.55E-21	4.55E-21

Category	Term	Gene counts	Gene official symbols	P Value	Bonferroni	Benjamini
GOTERM_CC_FAT	Intracellular non-membrane-bounded organelle	134	PRC1, CEP78, KNTC1, AURKC, CBX3, PDLIM1, AURKA, AURKB, MRPS31, WDR74, TOP1, SIN3B, CDCA8, ANK1, SIN3A, MAK16, INCENP, PRIM2, RPP30, MRPL38, GNL2, IMP4, RPS27A, GNL3, GTPBP4, SGOL2, MYH2, SGOL1, KRT12, RRP9, CTNNA3, MRTO4, RSL1D1, TNS4, RCL1, UXT, KDM2B, MAD2L1, NOP2, MRPS18B, SPAG5, RFC2, MYBBP1A, NUP43, BLM, LMNB2, TIPIN, BANF1, SPC24, SPC25, PPAN, NPM2, EIF3L, MNS1, RPL4, NUDC, TRP53, NIN, MYO1B, MYO1E, NDC80, BRCA1, DOCK4, PEO1, TMPO, MYH10, KIF23, CLSPN, KIF22, TAF1A, GAR1, MYBPC3, GTSE1, RPS3, PRMT3, KIF2C, SAP30, RRP1B, HIST2H2AC, RANBP1, CDK5RAP2, CIRH1A, TOP2A, CDC6, KIF11, POLR1E, NOL8, KIF15, POLR1A, MRPS5, NUSAP1, NUP85, MID1IP1, MCM2, CDK2, RAD51, SS18, APITD1, NOL10, BUB1B, NUP107, MAPRE1, POLR2H, HIST1H2AF, USP2, HIST1H2AD, POLA2, IVNS1ABP, RPA2, CENPA, KIF4, AATF, KIF21A, RFPL4, ZWILCH, H1FOO, GEMIN4, MYO5C, MSH6, CENPM, RRP12, TRIM28, CENPP, KIF18B, BIRC5, ILF3, SMC2, PWP2, SMC4, CCNB1, NOP58, HIST1H2AH, HIST1H2AK, NOP56, MPHOSPH6	1.35E-23	4.55E-21	4.55E-21
GOTERM_CC_FAT	Chromosome	53	KIF22, CLSPN, KNTC1, AURKC, CBX3, AURKB, SAP30, TOP1, CDCA8, SIN3B, SIN3A, INCENP, HIST2H2AC, PRIM2, TOP2A, SGOL2, SGOL1, NUP85, MCM2, CDK2, RAD51, MAD2L1, APITD1, SPAG5, RFC2, BUB1B, NUP107, NUP43, HIST1H2AF, BLM, HIST1H2AD, TIPIN, POLA2, BANF1, SPC24, SPC25, RPA2, CENPA, NPM2, ZWILCH, H1FOO, TRP53, MSH6, CENPM, CENPP, TRIM28, NDC80, BIRC5, SMC2, BRCA1, SMC4, HIST1H2AH, HIST1H2AK, TMPO	4.14E-21	1.40E-18	6.98E-19

Functional annotation cluster 2 of down-regulated genes

Total number of genes: 86

Enrichment score: 19.47

Category	Term	Gene Counts	Gene official symbols	P Value	Bonferroni	Benjamini
GOTERM_BP_FAT	Cell cycle	80	GAS2L3, E2F1, E2F2, CLSPN, PRC1, DBF4, AURKC, KNTC1, AURKA, AURKB, CCNE2, CDCA8, CDC45, MCM7, SIN3A, INCENP, PSMC3IP, MTBP, CDCA2, RANBP1, CDCA5, DNAJC2, CABLES1, CCAR1, CDCA3, CDC7, CDC6, CDK1, KIF11, SGOL2, LIG1, SGOL1, LIG3, SKP2, NUSAP1, ESPL1, MCM2, MCM3, CDK4, ESCO2, CDK2, RAD51, MCM6, UHRF1, MAD2L1, TIMELESS, SPAG5, BUB1B, MAPRE1, RUVBL1, NUP43, DHH, MRE11A, TIPIN, MLF1, SPC24, SPC25, NCAPH, MNS1, ZWILCH, H1FOO, NUDC, TFDP1, TRP53, NASP, BRCA2, BIRC5, NDC80, CDC20, CDC25C, SMC2, BRCA1, CDC25A, SMC4, CCNB1, CHAF1A, CDK20, CHAF1B, TXNL4A, MYH10	3.74E-27	6.80E-24	6.80E-24
SP_PIR_KEYWORDS	Cell cycle	67	E2F1, E2F2, CLSPN, PRC1, DBF4, AURKC, KNTC1, AURKA, AURKB, CCNE2, KIF2C, CDCA8, CDC45, MCM7, INCENP, MTBP, CDCA2, CDCA5, CABLES1, CCAR1, CDCA3, CDC7, CDC6, CDK1, KIF11, SGOL2, LIG1, SGOL1, LIG3, NUSAP1, MCM2, MCM3, CDK4, ESCO2, CDK2, MCM6, UHRF1, MAD2L1, TIMELESS, SPAG5, BUB1B, MAPRE1, RUVBL1, NUP43, TIPIN, MLF1, SPC24, SPC25, NCAPH, ZWILCH, NUDC, TFDP1, TRP53, NASP, CDC20, NDC80, BIRC5, CDC25C, SMC2, BRCA1, CDC25A, SMC4, CCNB1, CHAF1A, CDK20, CHAF1B, TXNL4A	1.24E-26	4.27E-24	2.14E-24
GOTERM_BP_FAT	Cell division	52	PRC1, KNTC1, AURKB, CCNE2, TOP1, CDCA8, CDC45, CDCA7, INCENP, CDCA2, CDCA5, TOP2A, CABLES1, CDCA3, CDC7, CDK1, CDC6, KIF11, LIG1, SGOL2, SGOL1, LIG3, NUSAP1, CDK4, MCM5, CDK2, MAD2L1, TIMELESS, SPAG5, BUB1B, MAPRE1, RUVBL1, NUP43, TIPIN, SPC24, SPC25, NCAPH, AATF, ZWILCH, NUDC, BRCA2, CDC20, NDC80, BIRC5, CDC25C, SMC2, CDC25A, SMC4, CCNB1, CDK20, TXNL4A, MYH10	2.32E-24	4.22E-21	2.11E-21

Category	Term	Gene Counts	Gene official symbols	P Value	Bonferroni	Benjamini
SP_PIR_KEYWORDS	Cell division	48	PRC1, KNTC1, TIPIN, AURKB, SPC24, CCNE2, SPC25, KIF2C, CDCA8, CDC45, NCAPH, CDCA7, INCENP, CDCA2, ZWILCH, CDCA5, CABLES1, NUDC, CDCA3, CDC7, CDC6, CDK1, KIF11, SGOL2, LIG1, SGOL1, LIG3, NUSAP1, NDC80, CDC20, BIRC5, CDC25C, CDK4, SMC2, MCM5, CDK2, CDC25A, SMC4, CCNB1, MAD2L1, TIMELESS, SPAG5, BUB1B, RUVBL1, MAPRE1, NUP43, CDK20, TXNL4A	2.81E-23	9.66E-21	3.22E-21
GOTERM_BP_FAT	Cell cycle process	56	GAS2L3, DBF4, KNTC1, AURKB, CDCA8, SIN3A, INCENP, PSMC3IP, MTBP, CDCA2, RANBP1, CDCA5, DNAJC2, CABLES1, CDCA3, CDK1, CDC6, KIF11, SGOL2, SGOL1, SKP2, NUSAP1, ESPL1, CDK2, RAD51, MAD2L1, TIMELESS, SPAG5, BUB1B, MAPRE1, RUVBL1, NUP43, DHH, MRE11A, TIPIN, MLF1, SPC24, SPC25, NCAPH, MNS1, ZWILCH, H1FOO, NUDC, TFDP1, BRCA2, CDC20, NDC80, BIRC5, CDC25C, SMC2, CDC25A, BRCA1, SMC4, CCNB1, TXNL4A, MYH10	1.29E-20	2.35E-17	5.86E-18
GOTERM_BP_FAT	Cell cycle phase	51	DBF4, KNTC1, AURKB, CDCA8, SIN3A, INCENP, PSMC3IP, CDCA2, MTBP, RANBP1, CDCA5, DNAJC2, CABLES1, CDCA3, CDK1, CDC6, KIF11, SGOL2, SGOL1, SKP2, NUSAP1, ESPL1, CDK2, RAD51, MAD2L1, TIMELESS, SPAG5, BUB1B, MAPRE1, RUVBL1, NUP43, MRE11A, TIPIN, SPC24, SPC25, NCAPH, MNS1, ZWILCH, H1FOO, NUDC, TFDP1, BRCA2, CDC20, NDC80, BIRC5, CDC25C, SMC2, CDC25A, SMC4, CCNB1, TXNL4A	1.94E-20	3.52E-17	5.87E-18
GOTERM_BP_FAT	Mitotic cell cycle	43	DBF4, KNTC1, TIPIN, AURKA, AURKB, SPC24, SPC25, CDCA8, NCAPH, SIN3A, INCENP, MTBP, CDCA2, ZWILCH, DNAJC2, CDCA5, CABLES1, NUDC, TFDP1, CDCA3, CDC6, CDK1, KIF11, SGOL1, SKP2, NUSAP1, NDC80, CDC20, BIRC5, CDC25C, SMC2, CDK2, CDC25A, SMC4, CCNB1, MAD2L1, TIMELESS, SPAG5, BUB1B, RUVBL1, MAPRE1, NUP43, TXNL4A	2.54E-19	4.61E-16	6.58E-17
SP_PIR_KEYWORDS	Mitosis	36	TIPIN, KNTC1, AURKB, SPC24, KIF2C, SPC25, CDCA8, NCAPH, INCENP, CDCA2, ZWILCH, CDCA5, NUDC, CDCA3, CDC6, CDK1, KIF11, SGOL1, NUSAP1, BIRC5, NDC80, CDC20, CDC25C, SMC2, CDC25A, CDK2, SMC4, CCNB1, MAD2L1, TIMELESS, SPAG5, BUB1B, RUVBL1, MAPRE1, NUP43, TXNL4A	1.52E-18	5.24E-16	8.74E-17

Category	Term	Gene Counts	Gene official symbols	P Value	Bonferroni	Benjamini
GOTERM_BP_FAT	M phase	44	MRE11A, KNTC1, TIPIN, AURKB, SPC24, SPC25, CDCA8, NCAPH, INCENP, PSMC3IP, CDCA2, MNS1, RANBP1, ZWILCH, H1FOO, CDCA5, NUDC, CDCA3, CDC6, CDK1, KIF11, SGOL2, SGOL1, NUSAP1, BRCA2, NDC80, CDC20, BIRC5, ESPL1, CDC25C, SMC2, CDK2, CDC25A, SMC4, RAD51, CCNB1, MAD2L1, TIMELESS, SPAG5, BUB1B, RUVBL1, MAPRE1, NUP43, TXNL4A	1.17E-17	2.13E-14	2.66E-15
GOTERM_BP_FAT	Nuclear division	35	TIPIN, KNTC1, AURKB, SPC24, SPC25, CDCA8, NCAPH, INCENP, CDCA2, ZWILCH, CDCA5, NUDC, CDCA3, CDC6, CDK1, KIF11, SGOL1, NUSAP1, BIRC5, NDC80, CDC20, CDC25C, SMC2, CDC25A, CDK2, SMC4, CCNB1, MAD2L1, TIMELESS, SPAG5, BUB1B, RUVBL1, MAPRE1, NUP43, TXNL4A	2.19E-16	4.03E-13	4.49E-14
GOTERM_BP_FAT	Mitosis	35	TIPIN, KNTC1, AURKB, SPC24, SPC25, CDCA8, NCAPH, INCENP, CDCA2, ZWILCH, CDCA5, NUDC, CDCA3, CDC6, CDK1, KIF11, SGOL1, NUSAP1, BIRC5, NDC80, CDC20, CDC25C, SMC2, CDC25A, CDK2, SMC4, CCNB1, MAD2L1, TIMELESS, SPAG5, BUB1B, RUVBL1, MAPRE1, NUP43, TXNL4A	2.19E-16	4.03E-13	4.49E-14
GOTERM_BP_FAT	M phase of mitotic cell cycle	35	TIPIN, KNTC1, AURKB, SPC24, SPC25, CDCA8, NCAPH, INCENP, CDCA2, ZWILCH, CDCA5, NUDC, CDCA3, CDC6, CDK1, KIF11, SGOL1, NUSAP1, BIRC5, NDC80, CDC20, CDC25C, SMC2, CDC25A, CDK2, SMC4, CCNB1, MAD2L1, TIMELESS, SPAG5, BUB1B, RUVBL1, MAPRE1, NUP43, TXNL4A	5.32E-16	1.01E-12	1.01E-13
GOTERM_BP_FAT	Organelle fission	35	TIPIN, KNTC1, AURKB, SPC24, SPC25, CDCA8, NCAPH, INCENP, CDCA2, ZWILCH, CDCA5, NUDC, CDCA3, CDC6, CDK1, KIF11, SGOL1, NUSAP1, BIRC5, NDC80, CDC20, CDC25C, SMC2, CDC25A, CDK2, SMC4, CCNB1, MAD2L1, TIMELESS, SPAG5, BUB1B, RUVBL1, MAPRE1, NUP43, TXNL4A	7.91E-16	1.41E-12	1.28E-13

Functional annotation cluster 3 of down-regulated genes

Total number of genes: 59

Enrichment score: 17.91

Category	Term	Gene counts	Gene official symbols	P Value	Bonferroni	Benjamini
GOTERM_BP_FAT	DNA metabolic process	58	CLSPN, KIF22, DBF4, MCM10, CCNE2, TOP1, CDC45, MCM7, SIN3A, PRMT7, PRIM2, PSMC3IP, DNAJC2, CCNO, TOP2A, CDC6, DTL, LIG1, LIG3, MCM2, MCM3, MCM4, ESCO2, MCM5, MCM6, RAD51, EYA3, UHRF1, RFC2, RRM2, RRM1, AICDA, RUVBL2, RUVBL1, BLM, UNG, MRE11A, HUS1, TIPIN, POLA2, BANF1, RPA3, RPA2, FEN1, TRP53, MSH6, FOXL2, RAD51AP1, NASP, BRCA2, RAD54L, BRCA1, POLD3, PEO1, POLD2, RAD54B, CHAF1A, CHAF1B	1.23E-20	2.24E-17	7.47E-18
GOTERM_BP_FAT	DNA replication	36	BLM, DBF4, TIPIN, POLA2, MCM10, RPA3, CCNE2, TOP1, RPA2, CDC45, SIN3A, MCM7, PRIM2, DNAJC2, FEN1, CDC6, DTL, LIG1, NASP, LIG3, BRCA2, MCM2, MCM3, MCM4, BRCA1, MCM5, MCM6, RAD51, POLD3, PEO1, RFC2, RRM2, RRM1, POLD2, CHAF1A, CHAF1B	1.59E-20	2.88E-17	5.76E-18
SP_PIR_KEYWORDS	DNA replication	27	BLM, DBF4, POLA2, MCM10, RPA3, RPA2, CDC45, MCM7, PRIM2, CDC6, DTL, LIG1, NASP, LIG3, MCM2, MCM3, MCM4, MCM5, MCM6, POLD3, PEO1, RFC2, RRM2, POLD2, RRM1, CHAF1A, CHAF1B	2.92E-19	1.01E-16	2.01E-17
KEGG_PATHWAY	DNA replication	16	LIG1, POLA2, MCM2, MCM3, RNASEH2B, MCM4, MCM5, MCM6, RPA3, POLD3, RPA2, MCM7, RFC2, PRIM2, POLD2, FEN1	4.09E-14	5.56E-12	5.56E-12

Functional annotation cluster 4 of down-regulated genes

Total number of genes: 54

Enrichment score: 12.57

Category	Term	Gene counts	Gene official symbols	P Value	Bonferroni	Benjamini
GOTERM_CC_FAT	Chromosome	53	KIF22, CLSPN, KNTC1, AURKC, CBX3, AURKB, SAP30, TOP1, CDCA8, SIN3B, SIN3A, INCENP, HIST2H2AC, PRIM2, TOP2A, SGOL2, SGOL1, NUP85, MCM2, CDK2, RAD51, MAD2L1, APITD1, SPAG5, RFC2, BUB1B, NUP107, NUP43, HIST1H2AF, BLM, HIST1H2AD, TIPIN, POLA2, BANF1, SPC24, SPC25, RPA2, CENPA, NPM2, ZWILCH, H1FOO, TRP53, MSH6, CENPM, CENPP, TRIM28, NDC80, BIRC5, SMC2, BRCA1, SMC4, HIST1H2AH, HIST1H2AK, TMPO	4.14E-21	1.40E-18	6.98E-19
GOTERM_CC_FAT	Chromosomal part	46	KIF22, HIST1H2AF, BLM, HIST1H2AD, KNTC1, AURKC, TIPIN, CBX3, POLA2, AURKB, SPC24, SAP30, RPA2, SPC25, CDCA8, SIN3B, SIN3A, CENPA, NPM2, HIST2H2AC, INCENP, PRIM2, ZWILCH, H1FOO, TRP53, MSH6, CENPM, SGOL2, SGOL1, CENPP, TRIM28, NUP85, NDC80, BIRC5, MCM2, CDK2, RAD51, MAD2L1, APITD1, SPAG5, RFC2, BUB1B, HIST1H2AH, HIST1H2AK, NUP107, TMPO, NUP43	7.48E-19	2.52E-16	8.41E-17
GOTERM_CC_FAT	Chromosome, centromeric region	24	CENPM, SGOL2, SGOL1, CENPP, AURKC, KNTC1, CBX3, BIRC5, NDC80, NUP85, AURKB, SPC24, SPC25, CDCA8, SIN3A, MAD2L1, APITD1, SPAG5, CENPA, INCENP, BUB1B, NUP107, ZWILCH, NUP43	1.06E-13	3.57E-11	5.94E-12
GOTERM_CC_FAT	Condensed chromosome, centromeric region	17	CENPM, SGOL2, SGOL1, KNTC1, CBX3, NDC80, NUP85, SPC24, SPC25, MAD2L1, CENPA, SPAG5, INCENP, BUB1B, NUP107, ZWILCH, NUP43	1.05E-11	3.55E-09	3.55E-10
GOTERM_CC_FAT	Condensed chromosome	21	CENPM, SGOL2, SGOL1, KNTC1, CBX3, NDC80, NUP85, CDK2, BRCA1, RAD51, SPC24, SPC25, MAD2L1, SPAG5, CENPA, INCENP, BUB1B, NUP107, ZWILCH, NUP43, TOP2A	3.28E-11	1.11E-08	1.01E-09
SP_PIR_KEYWORDS	Kinetochore	17	CENPM, SGOL2, SGOL1, KNTC1, NDC80, NUP85, SPC24, SPC25, KIF2C, MAD2L1, CENPA, SPAG5, INCENP, BUB1B, NUP107, ZWILCH, NUP43	3.32E-11	1.14E-08	1.43E-09
GOTERM_CC_FAT	Kinetochore	15	CENPM, KNTC1, NDC80, NUP85, SPC24, SPC25, SIN3A, MAD2L1, CENPA, SPAG5, INCENP, BUB1B, NUP107, ZWILCH, NUP43	2.31E-09	7.77E-07	5.55E-08
GOTERM_CC_FAT	Condensed chromosome kinetochore	14	CENPM, KNTC1, NDC80, NUP85, SPC24, SPC25, MAD2L1, CENPA, SPAG5, INCENP, BUB1B, NUP107, ZWILCH, NUP43	2.92E-09	9.83E-07	6.55E-08

Functional annotation cluster 5 of down-regulated genes

Total number of genes: 82

Enrichment score: 10.53

Category	Term	Gene counts	Gene official symbols	P Value	Bonferroni	Benjamini
GOTERM_CC_FAT	Nuclear lumen	73	E2F1, E2F2, TAF1A, GAR1, EZH2, PPARG, ASCC1, PDLIM1, WDR74, TOP1, SAP30, GTF2E2, CDCA8, SIN3A, MAK16, RRP1B, RBM8A, HEY2, RPP30, CIRH1A, GNL2, IMP4, TOP2A, GNL3, GTPBP4, ELP2, POLR1E, NOL8, ZFP326, POLR1A, NUSAP1, PRPF3, RRP9, CDK4, CDK2, MRTO4, RSL1D1, RCL1, KDM2B, NOP2, NRM, NOL10, RUVBL2, RANGRF, RUVBL1, MYBBP1A, POLR2H, POLR2F, LMNB2, POLR2D, PPAN, HNRNPF, NUDT21, EIF3L, AATF, RFPL4, GEMIN6, GEMIN4, TFDP1, TRP53, RRP12, TRIM28, ILF3, RNPS1, PWP2, PPIH, SALL4, PPP1R8, DCP1A, NOP58, NOP56, HNRNPH1, MPHOSPH6	1.06E-15	3.74E-13	9.35E-14
GOTERM_CC_FAT	Nucleolus	41	POLR2H, TAF1A, GAR1, WDR74, PPAN, TOP1, CDCA8, SIN3A, MAK16, RRP1B, EIF3L, RPP30, AATF, CIRH1A, GNL2, RFPL4, IMP4, TOP2A, GEMIN4, GNL3, TRP53, GTPBP4, RRP12, POLR1E, NOL8, TRIM28, POLR1A, NUSAP1, ILF3, RRP9, PWP2, MRTO4, RSL1D1, RCL1, KDM2B, NOP2, NOL10, NOP58, NOP56, MPHOSPH6, MYBBP1A	2.27E-15	7.48E-13	1.50E-13
GOTERM_CC_FAT	Membrane-enclosed lumen	82	E2F1, E2F2, TAF1A, GAR1, EZH2, PPARG, ASCC1, PDLIM1, WDR74, TOP1, SAP30, GTF2E2, CDCA8, SIN3A, MAK16, RRP1B, PTGES, RBM8A, TIMM9, HEY2, RPP30, MRPL38, CIRH1A, GNL2, IMP4, TOP2A, CCAR1, GNL3, GTPBP4, ELP2, POLR1E, NOL8, ZFP326, POLR1A, NUSAP1, PRPF3, RRP9, CDK4, CDK2, MRTO4, RSL1D1, RCL1, KDM2B, NOP2, NRM, NOL10, RUVBL2, RANGRF, RUVBL1, MYBBP1A, PRODH, POLR2H, POLR2F, ME2, LMNB2, CHCHD4, POLR2D, PPAN, HNRNPF, NUDT21, EIF3L, AATF, RFPL4, GEMIN6, GEMIN4, TFDP1, TRP53, RRP12, RARS2, TRIM28, ILF3, RNPS1, PWP2, PEO1, PPIH, SALL4, PPP1R8, DCP1A, NOP58, NOP56, HNRNPH1, MPHOSPH6	1.46E-13	4.92E-11	7.03E-12

Category	Term	Gene counts	Gene official symbols	P Value	Bonferroni	Benjamini
GOTERM_CC_FAT	Intracellular organelle lumen	78	E2F1, E2F2, TAF1A, GAR1, EZH2, PPARG, ASCC1, PDLIM1, WDR74, TOP1, SAP30, GTF2E2, CDCA8, SIN3A, MAK16, RRP1B, RBM8A, HEY2, RPP30, MRPL38, CIRH1A, GNL2, IMP4, TOP2A, GNL3, GTPBP4, ELP2, POLR1E, NOL8, ZFP326, POLR1A, NUSAP1, PRPF3, RRP9, CDK4, CDK2, MRTO4, RSL1D1, RCL1, KDM2B, NOP2, NRM, NOL10, RUVBL2, RANGRF, RUVBL1, MYBBP1A, PRODH, POLR2H, POLR2F, ME2, LMNB2, POLR2D, PPAN, HNRNPF, NUDT21, EIF3L, AATF, RFPL4, GEMIN6, GEMIN4, TFDP1, TRP53, RRP12, RARS2, TRIM28, ILF3, RNPS1, PWP2, PEO1, PPIH, SALL4, PPP1R8, DCP1A, NOP58, NOP56, HNRNPH1, MPHOSPH6	1.48E-12	4.99E-10	6.23E-11
GOTERM_CC_FAT	Organelle lumen	78	E2F1, E2F2, TAF1A, GAR1, EZH2, PPARG, ASCC1, PDLIM1, WDR74, TOP1, SAP30, GTF2E2, CDCA8, SIN3A, MAK16, RRP1B, RBM8A, HEY2, RPP30, MRPL38, CIRH1A, GNL2, IMP4, TOP2A, GNL3, GTPBP4, ELP2, POLR1E, NOL8, ZFP326, POLR1A, NUSAP1, PRPF3, RRP9, CDK4, CDK2, MRTO4, RSL1D1, RCL1, KDM2B, NOP2, NRM, NOL10, RUVBL2, RANGRF, RUVBL1, MYBBP1A, PRODH, POLR2H, POLR2F, ME2, LMNB2, POLR2D, PPAN, HNRNPF, NUDT21, EIF3L, AATF, RFPL4, GEMIN6, GEMIN4, TFDP1, TRP53, RRP12, RARS2, TRIM28, ILF3, RNPS1, PWP2, PEO1, PPIH, SALL4, PPP1R8, DCP1A, NOP58, NOP56, HNRNPH1, MPHOSPH6	1.70E-12	5.72E-10	6.35E-11
GOTERM_CC_FAT	Nucleoplasm	37	E2F1, POLR2H, E2F2, POLR2F, TAF1A, GAR1, PPARG, EZH2, ASCC1, PDLIM1, POLR2D, SAP30, TOP1, GTF2E2, RBM8A, HNRNPF, HEY2, NUDT21, EIF3L, GEMIN6, GEMIN4, GNL3, TFDP1, ELP2, TRIM28, PRPF3, RNPS1, CDK4, CDK2, PPIH, SALL4, PPP1R8, DCP1A, RANGRF, RUVBL2, RUVBL1, HNRNPH1	3.71E-05	0.0124	6.25E-04
GOTERM_CC_FAT	Nucleoplasm part	30	E2F1, POLR2H, E2F2, POLR2F, TAF1A, GAR1, EZH2, PPARG, ASCC1, PDLIM1, POLR2D, SAP30, GTF2E2, RBM8A, HEY2, NUDT21, GEMIN6, GEMIN4, TFDP1, ELP2, PRPF3, RNPS1, CDK4, CDK2, PPIH, SALL4, PPP1R8, DCP1A, RUVBL2, RUVBL1	5.86E-04	0.1792	0.0075